INSIGHTS INTO LEUKEMOGENESIS USING A MN1-INDUCED LEUKEMIA MODEL

by

Courteney Kwok-Wynne Lai

B.Sc., The University of British Columbia, 2009

B.A., The University of British Columbia, 2009

A THESIS SUBMITTED IN PARTIAL FULFILLMENT OF

THE REQUIREMENTS FOR THE DEGREE OF

DOCTOR OF PHILOSOPHY

in

THE FACULTY OF GRADUATE AND POSTDOCTORAL STUDIES

(Experimental Medicine)

THE UNIVERSITY OF BRITISH COLUMBIA

(Vancouver)

March 2017

Abstract

Acute myeloid leukemia (AML) spans a wide array of distinct clinical entities and likely molecular determinants. Despite early treatment success, many aspects of leukemogenesis remain poorly understood, including determinants of leukemic phenotype and identity, and genes and pathways critical to leukemic stem cell (LSC) function.

Meningioma 1 (MN1) is a transcriptional co-factor that is an independent prognostic marker for normal karyotype AML, with high expression linked to poor survival and resistance to treatment by ATRA-induced differentiation. MN1 is also a potent and sufficient oncogene in murine leukemia, able to block differentiation and promote LSC self-renewal through transformation of cells at the common myeloid progenitor level. Using this single-hit oncogenic model, MN1 overexpression was exploited to gain further insight into the leukemic process.

The objective of this thesis work was to identify and better understand key regulators in LSC function. Sixteen MN1 structural variants were generated to investigate if the leukemic properties of increased proliferation and self-renewal, arrested hematopoietic differentiation, *in vivo* leukemogenic activity, and resistance to all-trans retinoic acid-induced differentiation could be localised to specific protein regions. Functional assays revealed that the MN1 C-terminus is critical for blocking myeloid and lymphoid differentiation and ATRA resistance while the N-terminus is essential for leukemogenicity, proliferation and self-renewal, and arrested erythro-megakaryocyte differentiation, demonstrating that these leukemic properties can be attributed to specific and largely distinct regions.

To identify key genes and pathways underlying leukemic activity, the phenotypic heterogeneity of MN1 leukemic cells was functionally assessed, revealing leukemic and non-leukemic subsets. Gene expression profiling of these subsets was combined with previously-published datasets

comparing wildtype leukemic MN1 and mutant versions with varying leukemogenic activity to identify candidate genes critical to leukemia. Through functional analysis of leukemic properties, Hlf and HoxA9 were identified as critical to *in vitro* proliferation, self-renewal, and impaired myeloid differentiation in MN1 leukemia. Furthermore, this work identifies Meis2 as a novel player in MN1-induced leukemia, with essential roles in proliferation, self-renewal, differentiation, and apoptosis.

Together, these models provide a platform to unravel the basis for dysregulated gene expression associated with leukemia and to probe the cellular and molecular determinants of leukemogenesis.

Preface

The work presented in this thesis was completed as part of the requirements for a Doctorate of Philosophy in the Experimental Medicine program of the department of Medicine at the University of British Columbia under the supervision of Dr. R. Keith Humphries (Terry Fox Laboratory, Vancouver, BC) and Dr. Samuel A. Aparicio (Molecular Oncology, BC Cancer Agency Research Centre, Vancouver, BC). The investigations presented in this thesis, except for the parts stated below, were designed, performed, analysed, and written by Courteney Lai, under the supervision of Dr. R. Keith Humphries.

The studies described in Chapter 2 of this thesis work were designed by Courteney Lai with and under the supervision of Drs. Michael Heuser and R. Keith Humphries. Most experiments, analysis and interpretation of data, and writing the manuscript were also performed by Courteney Lai. Research students in the laboratory (Sarah Vollett, Stephen Fung, Malina Leung, Grace Lin, and Justin Smrz) assisted Courteney Lai and Dr. Michael Heuser with contributions to cloning, CFC assays, and flow cytometric analysis; the latter two students under my supervision. Courteney Lai performed and analysed the *in vitro* growth kinetics assays and designed the ATRA cytotoxicity assays with Dr. Michael Heuser. Drs. Florian Kuchenbauer, Bob Argiropoulos, and Eric Yung, Malina Leung, and Christy Brookes assisted Courteney Lai and Dr. Michael Heuser with blood and bone marrow analysis of transplanted mice. Dr. Daniel Starzcynowski performed CFU-Mk experiments. Courteney Lai prepared and performed confocal microscopy at the Imaging Facility at the Child and Family Research Institute (Vancouver, BC). Drs. Michael Heuser, Yeonsook Moon, Gyeongsin Park, Philip Beer, and Andrew Weng provided independent pathological analysis of prepared animal samples. Drs. Adrian Schwarzer (Hannover Medical School, Hannover, Germany), Ashish Sharma (Hannover

Medical School, Hannover, Germany), and Eric Yung performed gene expression and pathway analysis.

A version of the Chapter 2 has been published as a first-author publication, written by Courteney Lai under the supervision of Drs. Michael Heuser and R. Keith Humphries:

> Lai CK, Moon Y, Kuchenbauer F, Starzcynowski DT, Argiropoulos B, Yung E, Beer P, Schwarzer A, Sharma A, Park G, Leung M, Lin G, Vollett S, Fung S, Eaves CJ, Karsan A, Weng AP, Humphries RK, Heuser M. (2014). Cell fate decisions in malignant hematopoiesis: leukemia phenotype is determined by distinct functional domains of the MN1 oncogene. PLoS One 9(11):e112671.

The studies presented in Chapter 3 were predominantly designed and conducted by Courteney Lai. Initial experimental design and discussion were performed in collaboration with Dr. Gudmundur Norddahl, as well as transplantation and blood and bone marrow analysis of transplanted mice from *in vivo* MN1 heterogeneity experiments and early gene expression analysis of subpopulations. Dr. Tobias Maetzig designed the shRNA lentiviral vector, with Dr. Gudmundur Norddahl and Patty Rosten designed and gave advice on cloning of shRNA vectors, and with Dr. Gudmundur Norddahl assisted with production of lentivirus. *In vitro* assays were conducted by Courteney Lai with assistance from Tanner Lohr, as a research student in the laboratory under my supervision. Lea Sanchez-Milde, Tanner Lohr, and Niklas von Krosigk assisted with blood and bone marrow analysis of transplanted mice as undergraduate co-op students under my partial supervision. Samples for Agilent gene expression array were prepared by Courteney Lai, Dr. Gudmundur Norddahl, and Patty Rosten. The array was performed by Anne Haegert (Vancouver Prostate Research Centre, Vancouver, BC) and analysis performed by Courteney Lai and Anne Haegert with assistance from Robert Bell (Vancouver Prostate Research Centre, Vancouver, BC) and Shawn Anderson (Vancouver Prostate Research Centre, Vancouver, BC). Patty Rosten provided expertise in the design and execution of molecular methods

including preparation for RNA for Agilent gene expression array, cloning, PCR, and qRT-PCR. Gene expression analysis of de novo and therapy-associated AML and MDS patients from the in-house dataset was performed by Rod Docking (Karsan Lab, Genome Sciences Centre, Vancouver, BC) and statistical analysis of AML patients from Valk dataset was performed by Dr. Michael Heuser. All studies performed in-house with primary samples from AML and MDS patients were approved by the University of British Columbia Clinical Research Ethics Board, certificate number H13-02687. Samples were initially collected under certificate number H04-61292 or H09-01779 and sequenced under certificate number H11-01484. The data presented in Chapter 3 will be used to prepare a manuscript for publication in a peer-reviewed journal.

David Ko, Wenbo Xu, and Gayle Thornbury of the Flow Core Laboratory in the Terry Fox Laboratory, BC Cancer Agency were important resources for flow cytometric analysis and sorting described in thesis. All mice were bred and maintained in the Animal Resource Centre (ARC) of the British Columbia Cancer Agency as approved by the University of British Columbia Animal Care Committee (the Institutional Animal Care and Use Committee, IACUC). Experimental studies conducted in accordance with the policies and guidelines of the University of British Columbia Animal Care Committee under experimental protocol numbers A04-0380, A09-0009 and A13-0063, and all efforts were made to minimise suffering. All Humphries laboratory members contributed advice and ongoing discussion.

Table of Contents

List of Tables

List of Figures

List of Symbols

α	alpha
β	beta
Δ	delta
µ	micro
ac	acetylation
C	Celsius
cGy	centigray
CT	threshold cycle
dl	decilitre
g	grams
H	histone
K	lysine
kDa	kiloDalton
L	litre
m	murine
M	molar
me	methylation
mm^3	cubic millimetres
n	nano
BM	Bone marrow
CTL	control
Dist	distal
For	forward
iso	isoform
miR	microRNA
n.d.	Not determined
n.s.	Not significant
PB	Peripheral blood

Prox	proximal
RBC	Red blood cell
Rev	reverse
Spl	spleen
WBC	White blood cell

%	percent
^{o}	degrees
§	Engraftment in peripheral blood at the indicated timepoint or at death in cases where a mouse was sacrificed before that timepoint
†	All mice had been sacrificed at this timepoint due to disease
*	$P<0.05$
**	$P<0.01$
±	plus/minus

List of Abbreviations

5FU	5-Fluorouracil
7-AAD	7-aminoactinomycin D
ABL	Abelson urine leukemia viral oncogene homolog 1
ALL	Acute lymphoid leukemia
AML	Acute myeloid leukemia
AML-MDS	Acute myeloid leukemia progressed from myelodysplastic syndrome
AP1	Activator protein 1
APC	Allophycocyanin
APL	Acute promyelocytic leukemia
ATRA	All-trans retinoic acid
BAALC	Brain and acute leukemia, cytoplasmic
B-ALL	B-cell acute lymphoblastic leukemia
BCR	Breakpoint cluster region
BrdU	5-bromo-2'-deoxyuridine
BSA	Bovine serum albumin
CBF	Core-binding factor
Ccl9	Chemokine (C-C motif) ligand 9
CD	Cluster of differentiation
cDNA	Complementary deoxyribonucleic acid
CBF-SMMHC	Core binding factor-smooth muscle myosin heavy chain
C/EBPα	CCAAT/enhancer binding protein α
CFC	Colony forming cell
CFU	Colony forming unit
CFU-S	Colony-forming unit-spleen
ChIP	Chromatin immunoprecipitation
CLP	Common lymphoid progenitor
CML	Chronic myelogenous leukemia
CMP	Common myeloid progenitor
DABCO	1,4-Diazabicyclo(2,2,2)octane
DAPI	4,6-Diamidino-2-phenylindole

DAVID	Database for Annotation, Visualisation and Integrated Discovery
DMEM	Dulbecco's Modified Eagle's Medium
DMSO	Dimethyl sulfoxide
DNA	Deoxyribonucleic acid
DNMT	DNA methyltransferase
DOT1L	DOT-like histone H3K79 methyltransferase
DTT	Dithiothreitol
EAR	Eosinophil-associated, ribonuclease A family
ECL	Enhanced chemiluminescence
ECP	Eosinophil cationic protein
EDTA	Ethylenediaminetetraacetate acid
ERK	Extracellular signal-regulated kinase
ETO	Eight-Twenty One
ETS	E26 transformation-specific
EVI1	Ecotropic viral integration site 1
EZH2	Enhancer of zeste homolog 2
FACS	Fluorescence-activated cell sorting
FBS	Fetal bovine serum
FDR	False discovery rate
FLT3	FMS-like tyrosine kinase-3
gag	Group-specific antigen
GFP	Green fluorescent protein
GMP	Granulocyte-macrophage progenitor
GPR	G-protein receptor
GSEA	Gene set enrichment analysis
HA	Hemagglutinin
HES	Hairy and enhancer of split
HLF	Hepatic leukocyte factor
HOX	Homeobox
HRP	Horseradish peroxidase
HSC	Hematopoietic stem cell
HSC-R	Hematopoietic stem cell-related

IC_{50}	50% Inhibitory concentration
IDH1	Isocitrate dehydrogenase 1
Ig	Immunoglobulin
IL	Interleukin
Indel	Inversion-deletion
IRES	Internal ribosomal entry site
Irf8	Interferon regulatory factor 8
KLF	Krüppel-like factor
LIC	Leukemia-initiating cell
LMPP	Lymphocyte-primed multipotent progenitor
LPS	Lipopolysaccharide
LSC	Leukemic stem cell
LSC-R	Leukemic stem cell-related
LSK	Lineage-negative sca-1 positive c-Kit positive
LTR	Long terminal repeat
MEF2C	Myocyte enhancer factor 2C
meKO2	Modified monomeric Kusabira Orange 2
mRNA	Messenger RNA
MDS	Myelodysplastic syndrome
MEIS	Myeloid ectropic viral integration site
MEP	Megakaryocyte-erythroid progenitor
MILE	Microarray Innovations in LEukemia
MLL	Mixed lineage leukemia
MLL1	Mixed lineage leukemia 1
MN1	Meningioma (disrupted in balanced translocation) 1
MOPS	3-(N-morpholino)propanesulfonic acid
MSV	Moloney sarcoma virus
mRNA	Messenger ribonucleic acid
ND13	Nucleoporin 98-HOXD13 fusion protein
NES	Normalised enrichment score
NPM1	Nucleophosmin 1
NUP	Nucleoporin

PBS	Phosphate-buffered saline
PBX	Pre-B-cell leukemia transcription factor
PCR	Polymerase chain reaction
PE	Phycoerythrin
PML-RARα	Promyelocytic leukemia/retinoic acid receptor alpha
PMSF	Phenylmethane sulfonyl fluoride
pol	Polymerase
qRT-PCR	Quantitative real-time polymerase chain reaction
RA	Retinoic acid
RAC3	Ras-related C3 botulinum toxin substrate 3
RAR	Retinoic acid receptor
RARE	Retinoic acid response element
RMA	Robust multi-array
ROS	Reactive oxygen species
RNA	Ribonucleic acid
RSV	Rous sarcoma virus
RUNX1	Runt-related transcription factor 1
RXR	Retinoid X receptor
SCF	Stem cell factor
SD	Standard deviation
SDS	Sodium dodecyl sufate
SEM	Standard error of the mean
SFFV	Spleen focus-forming virus
shRNA	Small hairpin RNA
SMMHC	Smooth muscle myosin heavy chain
STAT	Signal transducer and activator of transcription
T-ALL	T-cell acute lymphoblastic leukemia
TALE	Three-amino acid loop extension
tAML	Therapy-related acute myeloid leukemia
TBS	Tris-buffered saline
TCGA	The Cancer Genome Atlas
TET	Tet methylcytosine dioxygenase

tMDS	Therapy-related myelodysplastic syndrome
TPM	Transcripts per million
VSV-g	Glycoprotein G of the Vesicular stomatitis virus

Acknowledgements

I would like to express my gratitude to my supervisor, Dr. Keith Humphries, for his unwavering support and dedication as my supervisor and mentor throughout my PhD. Thank you for creating and fostering such a collaborative and supportive environment to do amazing science. Your passion, integrity, generosity, and critical thinking have shaped my growth both as a scientist and an individual, and will continue to be an inspiration.

I would also like to thank Dr. Sam Aparicio, who served as a secondary supervisor, for his support, insight, and the freedom to explore my interests over the years. In addition, I would like to thank the members of my Supervisor Committee, Dr. Hugh Brock and Dr. Andrew Weng, for their advice, suggestions, and critiques, which were always appreciated and invaluable to my education.

Thank you to Dr. Michael Heuser, who saw my potential as an undergraduate student and encouraged and supported my scientific pursuits. Your expertise has been highly influential, and your advice and mentorship have had an immeasurable impact on development as a scientist.

I would like to thank the Humphries lab members, past and present, for their knowledge, patience, encouragement, and camaraderie throughout the years. In particular, I would like to thank Drs. Florian Kuchenbauer, Eric Yung, Tobias Berg, Suzan Imren, Bob Argiropoulos, Ping Xiang, Jens Ruschmann, Tobias Maetzig, Gudmundur Norddahl, Michelle Miller, and especially Patty Rosten for the wonderful discussions, scientific critiques, and planning/scheming, for nurturing my enthusiasm, and for making the lab such a fun place to be.

Thank you to the GrasPods executives, past and present, and to everyone in the Terry Fox Laboratory. This is a special place that attracts motivated, passionate, and wonderful people.

I am grateful for generous funding from the University of British Columbia (UBC), Canadian Institute for Health Research (CIHR), Terry Fox Research Institute (TFRI), Stem Cell Network (SCN), BC Cancer Agency Research Centre, and UBC Faculty of Medicine.

Thank you to all my friends, who have been endlessly supportive and patient over the years. I am lucky to have you all in my life.

My heartfelt thanks to my parents and my brother David for their tremendous support and encouragement throughout my life. Your guidance and support have made it possible for me to pursue my interests and succeed. Thank you for always being there for me.

To my parents,

Who taught me to work hard and aim high

Chapter 1: Introduction

1.1 Thesis overview: Using the MN1 overexpression oncogenic model as an approach to study AML

The mammalian hematopoietic system is composed of multiple cell types, each of which perform specific functions. These cells form an organised system that is tightly regulated in large part through transcriptional and epigenetic events that orchestrate a myriad of cellular processes including proliferation, differentiation, maturation, maintenance of deoxyribonucleic acid (DNA) integrity, and cell survival. Perturbation of one or more of these cellular processes can lead to an imbalance of the system that can confer a competitive advantage to specific cells and, ultimately, transformation to a leukemic state. The ways in which the regulatory mechanisms may become perturbed and thereby lead to pre-leukemic and leukemic states are not yet fully understood. Contributing to our poor understanding are the large number of genes that have been linked to the leukemic process and the relative difficulty in deciphering their functional roles.

Overexpression of meningioma (disrupted in balanced translocation) 1 (MN1) has emerged as a prominent player in leukemogenesis since its initial identification as an independent negative prognostic factor for patients with acute myeloid leukemia (AML) with normal karyotype. Subsequent studies in the murine model further revealed that overexpression of human MN1 is potently leukemogenic and capable of inducing an aggressive AML as a single-hit oncogene through promoting leukemic cell self-renewal and blocking myeloid differentiation. In this thesis work, I sought to exploit the MN1 model of leukemogenesis to provide further insight into leukemic transformation through two major lines of investigation. In the first, described in Chapter 2, I carried out a functional dissection of the relationship between regions of the MN1

oncoprotein and its leukemogenic properties. In a second line of investigation, described in Chapter 3, I sought to identify key genes and pathways that underlie the leukemic properties of MN1 by examining the hierarchical nature of MN1 leukemia and associated gene expression signatures within this hierarchy as well as gene signatures associated with mutant forms of MN1 with differential leukemogenic activity. This latter work led to the discovery that a homeobox (Hox) transcription co-factor, myeloid ectropic viral integration site 2 (Meis2), plays a critical role in MN1 growth and proliferation, self-renewal, differentiation block, and ability to evade apoptosis, suggesting that Meis2 may be a core component in MN1-induced leukemogenesis. The following sections of this chapter provide an overview of key concepts related to leukemia, MN1, and additional relevant factors that underpin this work.

1.2 The hematopoietic system is organized in a hierarchical structure governed by tightly regulated self-renewal and differentiation capabilities

The diverse cells of the hematopoietic system work together to provide immune responses, protection against foreign pathogens, wound healing capabilities, control of bleeding and transport of nutrients and oxygen within the body. These heterogeneous cells are organised in a hierarchical structure, with mature, specialised cells – broadly characterised into myeloid and lymphoid lineages – populating the base. These mature cells arise from smaller populations of progenitor cells, characterised by increased differentiation potential and self-renewal ability which, in turn, arise from the hematopoietic stem cell (HSC) at the apex of this hierarchy[1] (Figure 1.1). HSCs are characterised by their ability to differentiate, generating all the mature functional blood cell types in the hematopoietic system, and their ability to self-renew,

generating daughter cells that retain both of these functional characteristics[1]. The mechanisms by which this hierarchy of hematopoietic cells is established and maintained remains a major area of interest. Additionally, there is increasing interest in the ways in which dysregulation of the processes that regulate normal hematopoiesis may occur and ultimately lead to the clonal emergence of leukemic populations.

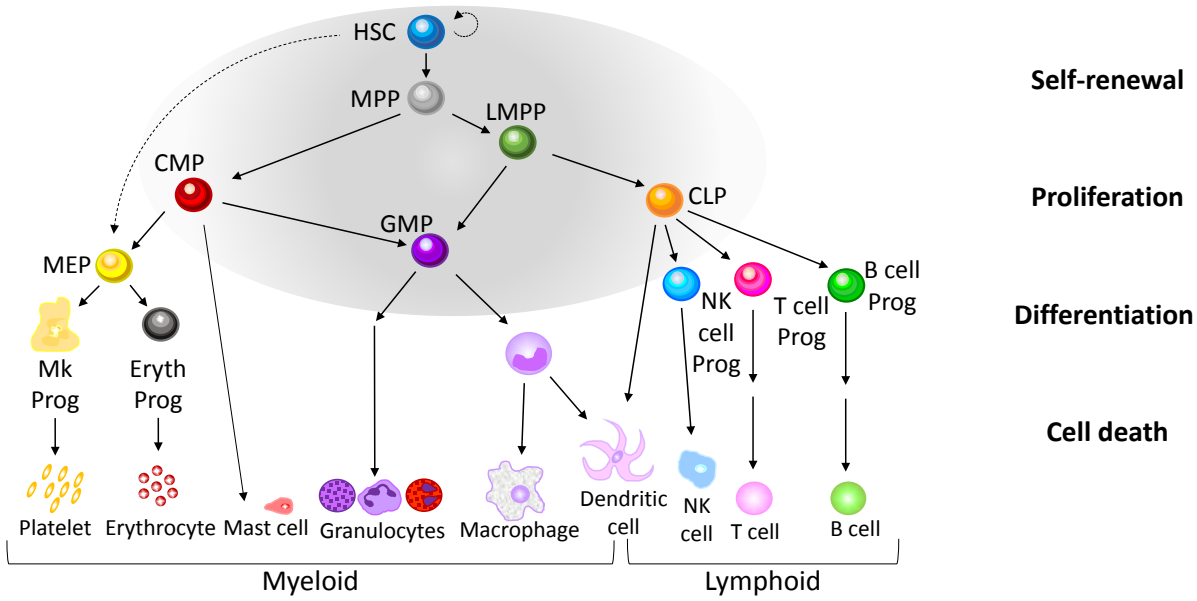

Figure 1.1 The hematopoietic system is organised in a tightly-regulated hierarchical structure.

The hematopoietic system is organised in a hierarchical structure. It is populated at the base by mature, specialised cells, broadly divided into myeloid and lymphoid lineages, which arise through processes of differentiation from their respective progenitor cells which, in turn, arise from the HSC compartment, characterised by multilineage differentiation capacity and high self-renewal abilities. The mechanisms that regulate this hierarchy – self-renewal, proliferation, differentiation, and cell death – are tightly controlled to maintain the balance and distribution of the hematopoietic system.

1.3 Key concepts of leukemia

1.3.1 Leukemia as an aberrant form of normal hematopoiesis

Leukemia is a progressive malignancy characterised by impaired maturation ability and increased production of immature cells of the blood and the blood-forming tissues. Most leukemias involve leukocytes and can be broadly classified into myeloid and lymphoid leukemias, reflecting the range of hematopoietic differentiation capabilities and the myriad of ways in which this process may be distorted[2, 3]. A broad subcategory within myeloid-restricted leukemia is AML, a heterogeneous spectrum of clonal and rapidly fatal disorders characterised by an accumulation of undifferentiated myeloid cells which typically show enhanced proliferation, impaired or blocked differentiation ability, and dysregulated apoptosis.

Contrary to the often-homogeneous appearance of the bulk of leukemic cells in each patient, there is now considerable evidence that, like normal hematopoietic cells, leukemic cells are also organized in a hierarchical manner, with the leukemic stem cell (LSC) at the apex. In support of a leukemic hierarchy, early studies revealed that only a small proportion of murine lymphoma cells can establish disease in transplanted mice[4] and only a small subset of AML cells display *in vitro* clonogenic activity[5]. Subsequent studies using immunodeficient mice as recipients of human AML cells revealed that only a small fraction of AML blast cells have leukemia-initiating activity. In many instances, these cells can be isolated from the majority of leukemic cells based on differential expression of a variety of surface markers that also distinguish normal hematopoietic cells with stem cell properties[6, 7]. Together, these findings support a leukemic model in which only a subset of leukemic cells, often low in frequency, have stem cell-like abilities of long-term self-renewal and proliferation that maintain the leukemic state[7, 8]. Recent

studies demonstrate that the concept of leukemic hierarchy may be more plastic than originally believed, with the LSC occupying one or more cell compartments and potentially including multiple progenitor cell types[9, 10]. Furthermore, work from multiple groups suggest that, depending on the genetic background of the leukemia, LSCs may not always exist as a rare subpopulation, with evidence of a high frequency of LSCs in the AML mixed lineage leukemia (MLL) translocation model MLL-AF9[11] and co-overexpression model of HOXA9 and MEIS1 (HOXA9-MEIS1)[12]. Nevertheless, there is substantial evidence that leukemia, like normal hematopoiesis, constitutes a hierarchical population of cells with LSC at the apex. This recognition has, in turn, prompted key questions, including the possible origin of leukemic stem cells and the basis for their perturbed properties.

1.3.2 Leukemic stem cells may have diverse origins in hematopoietic cells

The overlap between LSC and HSC properties with respect to their self-renewal and sustained proliferative potential has driven key questions regarding the hematopoietic cell compartment from which the LSC arises. Given the high degree of overlap between key LSC and HSC properties, perhaps most notably that of self-renewal capability, one hypothesis is that LSC originate directly from the HSC. Alternatively, the LSC might arise from progenitor cells later in the hematopoietic hierarchy through reactivation of key stem cell properties. Tests of the transforming potential of oncogenes in specific hematopoietic subpopulations provide evidence for both scenarios. In support of an HSC origin for leukemia, oncogenic fusion of the break point cluster region gene (BCR) and a portion of the Abelson tyrosine kinase gene (ABL) associated with chronic myelogenous leukemia (CML), termed BCR-ABL, has leukemia-initiating activity

when transduced into populations enriched for HSCs, but not progenitor populations[10, 13-16]. Gene expression profiling studies also provide support for a HSC origin for leukemias, as evidenced by a high degree of overlap between LSC gene signatures obtained from studying a wide array of leukemias and normal HSC signatures[6, 10]. In contrast, the identification of the common myeloid progenitor (CMP) as the origin of the CCAAT/enhancer binding protein α (C/EBPα) leukemia-initiating cell (LIC)[17], the ability of the mixed-lineage leukemia 1 (MLL1) and eleven nineteen leukemia (ENL) fusion murine leukemia (MLL-ENL), MOZ-TIF2, and MLL-AF9 fusion proteins to induce AML in granulocytic-macrophage progenitors (GMPs)[18-20], and the LSC with lymphoid characteristics described in the murine CALM/AF10-positive leukemia model[21] demonstrate that the target cell of transformation may be restricted to progenitor populations. Still other data suggests that LSCs exist across a spectrum of hematopoietic cell compartments, as demonstrated by the coexistence of lymphoid-primed multipotent progenitor (LMPP)-like and GMP-like LSCs in human AML cells[9] and the identification of LSCs in hematopoietic compartments characterized by the cluster of differentiation markers CD34 and CD38 ($CD34^+CD38^-$ and $CD34^+CD38^+$)[22].

Existing evidence suggests that both models may be correct and, as demonstrated by *in vivo* murine leukemic models, that the leukemic cell of origin may vary depending on the type of leukemia and the nature of the underlying genetic changes[23] (Figure 1.2). Thus, the MN1-induced model of leukemia is of particular interest, as available evidence indicates that a relatively narrow differentiation range of cells, from the HSC to the GMP compartments, are susceptible to its potent leukemogenic activity, as will be discussed in subsequent sections of this chapter.

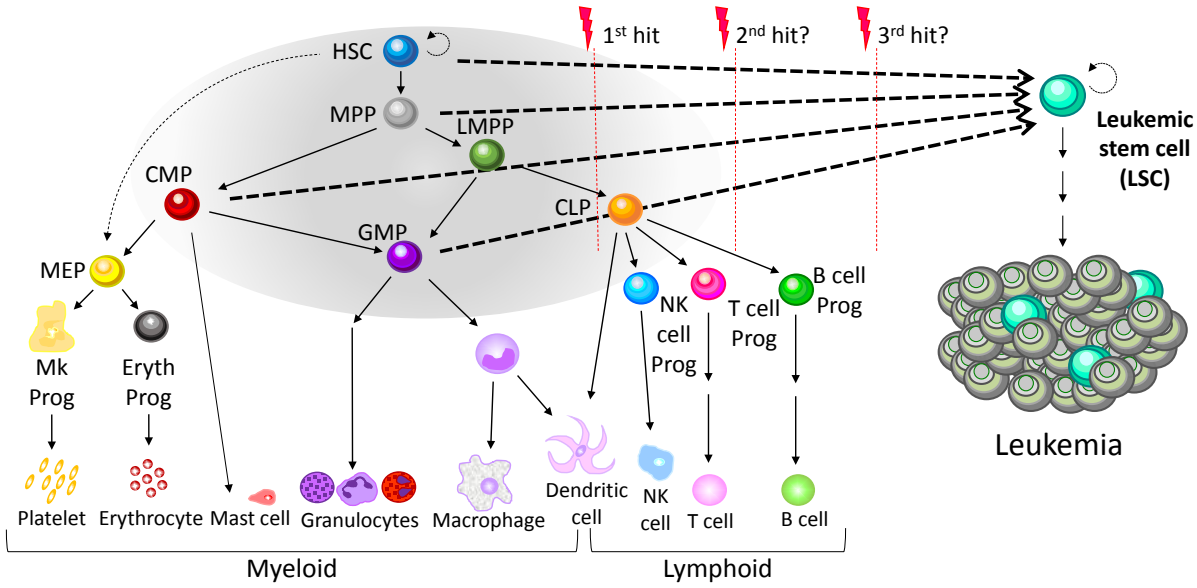

Figure 1.2 LSCs can exist across a spectrum of hematopoietic compartments.

Available evidence indicates that LSCs may originate from transformed HSCs or progenitors that regain key stem cell properties. These LSC subsets may be influenced by their cell of origin, the nature of genetic hit(s) encountered during leukemic transformation and progression, and the chronology of the acquisition of these hits.

1.4 Mechanisms of AML leukemogenesis

1.4.1 Cytogenetic abnormalities are commonly associated with leukemia

Cytogenetic studies were paramount to early understanding of leukemia as a genetic disorder, as the identification and analysis of chromosomal translocation breakpoints led to the discovery of multiple genes critical to leukemic transformation[24]. One of the first discoveries of cytogenetic studies was the predominance of t(9;22), known as the Philadelphia chromosome, in CML[25]. This translocation generates a fusion oncogene known as BCR-ABL. Subsequent studies established BCR-ABL as the initiating mutation in CML[26] and identified the consequent constitutively active tyrosine kinase signaling as central to the transformation ability of BCR-ABL[27], leading to the development of tyrosine kinase inhibitors to treat this disease[28-31].

Similarly, discovery that the chromosomal translocation promyelocytc leukemia/retinoic acid receptor alpha (PML-RARα; t(15;17)(q22;q12)) occurs in 95% of the AML subtype acute promyelocytic leukemia (APL)[32] facilitated elucidation of the molecular mechanisms by which PML-RARα induces APL[33] and the manner in which all-trans retinoic acid (ATRA)-induced differentiation therapy relieves transcriptional repression in APL[34]. Examination of numerous translocations identified in hematopoietic malignancies has revealed recurrent translocation partners. Intriguingly, many of these recurrent partners are known transcription factors, such as MLL1 with over 60 identified translocation partners in both acute myeloid and lymphoid leukemia (ALL)[35], Runt-related transcription factor 1 (RUNX1) with over 30 partners[36], and nucleoporin 98 (NUP98) with at least 29 identified partners, pointing to the important role of transcription factors in malignant states[37]. Study of the genes involved in such translocations has identified a range of transcription factors and transcriptional co-factors essential to hematopoiesis and leukemia, including MN1, which will be the focus of this thesis.

1.4.2 Aberrant gene expression is frequently associated with AML

The advent of high-throughput gene expression analysis and its application to leukemia has also highlighted dysregulated expression not associated with overt mutations in deregulated genes[38]. Notable examples include the frequent overexpression of multiple HOX genes and HOX co-factors such as MEIS1 in a wide array of leukemias[39-44]. Indeed, one of the first extensive studies of gene expression in AML identified overexpression of HOXA9 as one of the most important predictors of poor prognosis[39]. In a similar manner, overexpression of MN1, a transcription co-

factor that is a major focus of this thesis, was identified as strong independent marker of poor prognosis in cytogenetically normal AML some ten years ago[45].

1.4.3 Leukemogenesis is a multistep process representing the accumulation of genetic hits

Next generation sequencing capabilities have also enabled whole genome, exome and messenger ribonucleic acid (mRNA) sequencing to be applied to the study of leukemia, and this in turn has led to an explosion of detailed characterisation of the genetic and expression abnormalities in leukemia. The increased precision and resolution afforded by these technologies has allowed identification of fusion genes not evident by cytogenetics and a deeper, more nuanced understanding of the evolution of AML in patients, including the discovery of pre-leukemic cells, gene signatures associated with malignant states, and recognition and identification of mutation acquisition order[23, 38].

Through the study of frequently mutated genes, one can appreciate how the accumulation of mutations in leukemic cells leads to multiple dysregulated cellular pathways, a multistep mutational process that is intrinsic to the leukemogenic process. Although early models of leukemogenesis described two mutational classifications involving impaired cell differentiation and activation of pro-proliferation pathways[46, 47], detailed sequencing studies of leukemia, particularly AML, have provided further insight into both the frequency and complexity of gene mutations.

In a seminal study from the Cancer Genome Atlas Research Network, sequencing of the genomes of 200 patients with AML revealed that de novo AML genomes have, on average, 13 coding gene mutations per genome, considerably fewer than other adult cancers[48]. Of these 13

mutations only 5 on average for each patient were among those recurrently mutated in AML. These and other studies have led to a proposed nine categories of functionally related genes involved in AML (Table 1.1). This classification, and the exclusivity of mutations in multiple genes within the same category, suggests that despite the relatively large total number of distinct genes that have been implicated in leukemia, there are likely a limited number of genes or core processes that are disrupted and underlie leukemia. This concept compels further interest in the development and study of specific models such as the MN1 model of AML employed in this thesis, as knowledge gleaned from understanding MN1 leukemia may have generalizable relevance to a wider spectrum of AML.

Table 1.1 Categories of Gene Mutations

Simplified and reproduced with permission from The Cancer Genome Atlas (TCGA),[48] Copyright Massachusetts Medical Society.

Category	Examples (frequent sub-categories of mutations)
Transcription factor fusions	PML-RARα; MYH11-CBFB; RUNX1-RUNX1T1; PICALM-MLLT10
NPM1	
Tumour suppressors	TP53; WT1; PHF6
DNA methylation	DNMT3A; DNMT3B; DNMT1; TET1; TET2; IDH1; IDH2
Activated signaling	FLT3; KIT; other tyrosine kinases; serine-tyrosine kinases; KRAS/NRAS, PTPs
Myeloid transcription factors	RUNX1; C/EBPα; other myeloid transcription factors
Chromatin modifiers	MLL-X fusions, MLL-PTD; NUP98-NSD1; ASXL1; EZH2; KDM6A; other modifiers
Cohesin	
Splicesome	

1.5 TALE family homeobox genes in AML

1.5.1 HOX transcription factors are frequently upregulated in leukemia

Among genes frequently aberrantly expressed in leukemia are members of the HOX family of proteins, comprised of 39 genes organised into four gene clusters and 13 paralogs in mammals[49]. The HOX gene family, characterised by a 60-amino acid DNA-binding motif known as the homeodomain[49], was first identified through its critical roles in Drosophila development[50]. Many HOX genes are expressed in normal human and murine hematopoiesis with the striking

characteristic that their expression is largely confined to primitive cells[41, 51-54]. Indeed, expression levels of several Hox genes are inversely correlated with progression down the hematopoietic hierarchy, with the highest levels found in the most primitive HSCs[54]. Furthermore, several HOX genes, including several within the Hox A and B clusters are implicated in the regulation of normal HSC self-renewal, maintenance, and proliferation. While knockout of individual Hox gene generally has limited effects, likely due to compensatory expression of other Hox genes and overlapping functions, deletion of multiple Hox A or B cluster genes results in major impairments in hematopoietic stem cell function and hematopoietic development[55-57]. Conversely, engineered overexpression of a range of Hox genes leads to enhanced self-renewal and/or blocked differentiation, and may have leukemogenic activity. A striking example includes marked enhancement of HSC self-renewal both *in vivo* and *in vitro* without overt leukemogenic effects following overexpression of HoxB4[58-60]. In contrast is the leukemogenic activity induced by HoxA9 overexpression[61-64], consistent with HOXA9 overexpression as a poor prognostic marker in AML[39]. Subsequent studies have identified upregulation of many different HOX genes and their co-factors in multiple leukemic subsets, with high HOX gene expression associated with poor prognosis[65] and poor response to treatment[39]. Furthermore, translocations involving MLL, an upstream regulator of HOX genes, are one of the most frequently occurring translocations in leukemia[40] and directly upregulate Hox gene expression and block normal downregulation of Hox expression[66-68]. Additionally, HoxA9 is essential to maintenance of leukemic properties driven by MLL translocations[69], providing further support for the key role of Hox overexpression in leukemogenesis.

Engineered overexpression and fusion proteins have demonstrated functional roles for Hox proteins in self-renewal, blocking differentiation, and leukemogenesis[70, 71]. Overexpression of

either HoxA9 or HoxA10 can immortalize murine bone marrow cells and block terminal differentiation of progenitor cells *in vitro*[72, 73] while inducing a myeloproliferative disorder and/or AML *in vivo*[62, 73]. Similarly, fusion proteins of NUP98 and multiple HOX genes spanning paralog groups 3 through 13 have demonstrated abilities to immortalize murine bone marrow progenitor cells[61, 74, 75], block progenitor cell differentiation[61, 74-76], and induce AML[61, 75]. These effects are further exacerbated in the context of Meis1 overexpression[61, 77, 78], which is highly relevant to the MN1 model, as will be elaborated on in this chapter.

1.5.2 The transcription factor MEIS1 plays a critical role in leukemogenesis

MEIS1 is a homeodomain-containing HOX co-factor characterised by a three-amino acid loop extension (TALE) between the alpha-helices in its 63-amino acid-long homeodomain. It was first described as a common viral integration site in the BXH-2 model of myeloid leukemogenesis[79] and plays roles in hematopoietic, angiogenic, and eye development[80]. Work from our group and others has established Meis1 as a critical player in adult hematopoiesis, with loss of expression tied to profound impairments at the HSC and progenitor levels, including megakaryocyte-erythroid progenitors (MEPs)[81-83], *in vivo* repopulating ability,[82, 83] and the reduction of reactive oxygen species (ROS) levels in support of these properties[81-83] .

Perhaps most intriguing, however, is the role of MEIS1 in leukemia. MEIS1 is frequently upregulated in primary AML and ALL samples[41-44] and plays key roles in self-renewal, blocking differentiation, and leukemogenesis in conjunction with members of its collaborating Hox and pre-B-cell leukemia transcription factor (Pbx) families[12, 84]. Although overexpression of wildtype Meis1 alone shows no transforming ability in the murine model, co-overexpression of Meis1 and

HoxA9 show collaborative effects, decreasing the latency and increasing the penetrance of HoxA9-induced AML[68, 77, 78, 85]. In contrast, HoxA9 transactivation domains are essential for activation of the Meis1 gene signature in the HoxA9-Meis1 overexpression model[84], demonstrating the key roles of Hox genes and their co-factors in leukemogenesis. Similarly, Wong and colleagues demonstrated the essential role of Meis1 in leukemic transformation, measured by self-renewal, differentiation ability, and disease progression and latency, with Meis1 directly regulating MLL-mediated leukemia in a rate-limiting manner, emphasising the critical role of Meis1 as a collaborator in Hox-induced leukemogenesis[86].

Of the three members of the MEIS subfamily of HOX co-factors, MEIS1, MEIS2, and MEIS3, MEIS1 was the only member that had been implicated in leukemia at the time this thesis was initiated. Similarly, among the other TALE subfamily of PBX genes, Pbx1 has garnered the most attention for its collaborating roles in leukemogenesis[87, 88], although Pbx2 and Pbx3 have shown relevancy in leukemia, particularly MLL-induced AML[86] and in preventing ubiquitination of Meis1 in Hox-induced AML[89]. As will be seen in this thesis, a broader range of Meis family members play crucial roles in leukemogenesis.

Together, these data point to important roles of many Hox genes, Meis1, PBX family genes in a wide range of leukemias. Adding further interest are recent findings showing a strong relationship of these genes to the potent leukemogenic function of MN1, as will be described in the following section.

1.6 MN1 overexpression as a model for AML

1.6.1 Discovery of MN1 and its linkage to leukemia

MN1 was first identified as part of the sporadic balanced translocation t(4;22)(p16;q11) in a patient with meningioma[90]. Shortly after, MN1 was identified as a translocation partner of the E26 transformation-specific (ETS) transcription factor family member TEL in the balanced t(12;22)(p13;q11) found in patients with AML and myelodysplastic syndrome (MDS). The fusion protein contains nearly all of MN1 combined with the DNA-binding domain of TEL[91, 92] and spurring huge interest in MN1 in the context of AML.

Located on human chromosome 22, MN1 encodes a 136 kDa protein that, while highly conserved in vertebrates, shows no homology to other proteins[93]. Although largely devoid of annotated protein domains, MN1 contains two proline-glutamine regions and a 28-residue glutamine stretch encoded by iterations of CAG and CAA triplets[94, 95]. At the time this thesis was initiated, little was known about the relationship between the structure of MN1 and its leukemic properties. However, as glutamine- and proline-rich regions are associated with transcriptional activation[96-98], MN1 was thought to have a putative role in transcriptional activation and regulation. This was supported by the observation that deletion of much of the MN1 sequence in the MN1-TEL protein abrogates its transforming ability in colony-forming cell (CFC) assays[92]. In addition, MN1-TEL is capable of moderately activating the retroviral long terminal repeat region (LTR) in the murine sarcoma viral (MSV) vector[92], and MN1 alone strongly activates this LTR[95], together highlighting the transcriptional activation abilities of MN1. Initial studies of MN1 transcriptional activation focused on its role in retinoic acid receptor-retinoid X receptor (RAR-RXR) mediated transcription. PML-RARα demonstrates that fusion proteins involving

altered transcription factors can alter the balance between transcriptional activation and repression through the altered recruitment of activators and repressors, and evidence suggests that MN1-TEL functions in a similar manner to block myeloid differentiation[95]. Early studies revealed that MN1 can recognize putative retinoic acid response element (RARE) sequences, classical RAR-RXR binding sites[95] and that overexpression of MN1 can both enhance and inhibit RAR/RXR-induced gene expression[99]. However, we now appreciate that RAR-RXR binding represents but one component of MN1 activity.

1.6.2 Overexpression of MN1 is a poor prognostic marker in cytogenetically normal AML

Subsequent to its identification as a TEL fusion partner in hematopoietic malignancies, overexpression of MN1 was identified in a subset of patients with AML and ALL[45]. Gene expression profiling shows aberrant upregulation of MN1 in a broad spectrum of human AMLs, including inv(16)[100, 101], AMLs overexpressing the transcription factor ectropic viral integration site 1 (EVI1)[102], or AML overexpressing cytoplasmic (BAALC)[103, 104], de novo AML[105], and AMLs without nucleophosmin 1 (NPM1) mutations[45]. Similarly, approximately 50% of pediatric patients with de novo AML show elevated MN1 expression, suggesting that deregulated MN1 represents a specific subset of AML[106].

Consistent with this idea, MN1 is an independent negative prognostic marker for AML with normal karyotype, with high expression associated with poor prognosis, decreased survival, shorter relapse-free survival[45, 107], and poor response to induction therapy[45]. Recent reports of retroviral gene insertional activation of MN1 in a patient who underwent gene therapy patient and subsequently developed AML further highlights the potential leukemogenic ability of

MN1[108]. Additionally, patients with high MN1 expression show resistance to the differentiation-inducing agent ATRA, such that high expression negates benefits conferred by the addition of ATRA to maintenance chemotherapy in older patients with non-APL AML[109]. High expression of MN1 has also be associated with progression of MDS to secondary AML and thus reinforcing the likely functional importance of MN1 in leukemogenesis[110].

1.6.3 Overexpression of MN1 in murine models induces AML through promotion of cell self-renewal and blocking myeloid differentiation

MN1 is expressed in limited cell types in the body, most notably playing roles in cranial bone development and the hematopoietic system. In the murine system, Mn1 regulates the expression of Tbx22 in the posterior region of the developing palate and is necessary for late stage palate development and maturation and normal function of cranial osteoblasts[111]. Consequently, Mn1 knockout mice lack several cranial bones, display cleft palate defects, and die shortly after birth[112]. In the hematopoietic system, Mn1 is expressed at low-to-undetectable levels in HSCs and primitive progenitor cells, particularly $CD34^+$ cells[45] and at the highest levels in the GMP compartment[106]. In contrast, MN1 expression is downregulated upon *in vitro* differentiation of $CD34^+$ cells,[45] suggesting that it plays a role in maintaining the immature states of progenitor cells.

Overexpression of the human coding sequence of MN1 has yielded insights into its roles in dysregulation of the hematopoietic system, particularly in proliferation, self-renewal, and differentiation of hematopoietic cells. Retrovirally engineered overexpression of MN1 in murine bone marrow renders cells capable of inducing extremely rapid, fully-penetrant AML in

transplanted mice[109]. This AML is both serially transplantable and has no apparent requirement for collaborating mutations[109], emphasizing the leukemia-initiating ability of this oncogene. Overexpression of MN1 also enhances proliferation and self-renewal of murine hematopoietic bone marrow *in vitro*, as evidenced by the efficient generation of cytokine-dependent polyclonal cell lines and the ability of MN1-transduced cells to outgrow their untransduced counterparts[109]. Consistent with these observations, MN1 overexpression decreases cell cycle transit time and enhances cell viability of human $CD34^+$ cells[113], providing a competitive advantage to MN1-transduced cells. In contrast, loss of MN1 expression in human leukemic cells impairs their proliferative and clonogenic ability, as measured by CFC assays[114].

In addition, MN1 blocks myeloid differentiation. In preleukemic murine bone marrow cell lines immortalized by the NUP98-HOXD13 (ND13) fusion protein, overexpression of MN1 increases c-Kit expression, decreases Gr-1 and CD11b expression, and promotes a general reacquisition of an immunophenotype consistent with an immature state[109]. Conversely, activation of MN1 downstream targets through the fusion of the transactivation domain VP16 results in a more mature immunophenotype, characterised by increased numbers of terminally differentiated macrophage colonies in the CFC assay, increased Gr-1^+ and $CD11b^+$ expression, and decreased c-Kit^+ expression *in vitro*[115]. Such findings are consistent with the role of wildtype MN1 in repression of genes responsible for myeloid differentiation[109, 115].

1.6.4 MN1 collaborates with other proteins and pathways to enhance its leukemic ability

1.6.4.1 MN1 acts as a transcriptional co-factor

MN1 was initially classified as a potential tumour suppressor, due to its disrupted expression as part of the t(4;22) fusion protein identified in a patient with meningioma and its protein sequence that indicates a role in transcriptional regulation[94, 95]. However, the absence of a consensus DNA binding sequence suggests it acts as a transcriptional coactivator[92]. This is supported by work from van Wely and colleagues who identified MN1 as a transcriptional coactivator of p300 and Ras-related C3 botulinum toxin substrate 3 (RAC3), suggesting that the TEL partner of the MN1-TEL fusion is responsible for exerting the repressor effects originally observed[95]. Additionally, MN1 shows synergy with RAC3, achieving even higher induction of transcription in the presence of ATRA[95] and providing further support for the role of MN1 as a transcriptional co-factor.

1.6.4.2 MN1 cooperates with chromosomal fusions common to AML

Work from murine models has helped to inform observations in human hematopoietic malignancies and contributed to the present view of MN1 as a cooperative partner in AML. As previously described, MN1 confers strong transcription-activating potential on TEL in the chromosome translocation MN1-TEL[92], resulting in the immortalization of myeloid cells and AML in mice[116, 117]. A subset of patients with inv(16), which encodes the core binding factor-smooth muscle myosin heavy chain (CBF-SMMHC) fusion protein, show upregulated MN1[106]. In addition, co-expression of MN1 with MLL-ENL enhances leukemic transformation *in vivo*, enhances the GMP immunophenotype characteristic of MLL-ENL, and significantly reduces

disease latency compared to MN1 or MLL-ENL alone, illustrating that MN1 can synergise with MLL-ENL[114]. Additionally, MN1 can act as a cooperative partner in other leukemias, including those characterised by RUNX1 mutations[118] or fusion proteins including CALM-AF10[119] and MLL-AF9[120], providing further evidence of its ability to co-activate transcriptional pathways specific to multiple leukemias.

1.6.4.3 MN1 collaborates with the ND13 fusion protein in AML

A retroviral insertional mutagenesis screen to elucidate potential collaborators of the t(2;11)(q31;p15) translocation, also known as the fusion protein NUP98-HOXD13 (ND13) identified in patients with MDS or AML[121], revealed common insertion sites near Mn1 and Meis1[122]. Studies of a ND13 transgenic mouse model[75, 123, 124] previously showed impaired hematopoietic potential and MDS development, which frequently progresses to AML after a long latency[75, 123, 124]. As common insertion sites, Meis1 and Mn1 were considered candidate genes that may subsequently become dysregulated in the pre-leukemic state, leading to leukemia initiation[122]. Subsequently, work from our laboratory demonstrated that MN1 can collaborate with HoxA9 or ND13, with co-expression resulting in a marked increase in *in vitro* leukemia-initiating cell expansion potential, in part due to the combined ability of MN1 to enhance signal transducer and activator of transcription (STAT) signalling and stem cell self-renewal[125]. Building on these findings, our laboratory has recently generated a forward genetic model of AML using co-transduction of ND13 and MN1 in human cord blood cells[126]. Characterisation of this stepwise transformation model showed that MN1 overexpression expands human cord blood cells *in vitro* and induces myeloproliferation in transplanted mice, but requires dysregulated

HOX gene expression to induce AML and activation of underlying stem cell gene expression signatures[126].

1.6.5 Elucidating targets and pathways of MN1 leukemia

1.6.5.1 MN1 and RAR-RXR signaling

As mentioned above, there has been considerable interest in the way MN1 acts on retinoic acid (RA) signaling. This was based, in part, on early retroviral enhancer work, illustrated by the ability of MN1 to recognize putative RARE sequences that are known RAR/RXR binding sites[95], and on the observation that patients with high MN1 expression respond poorly to induction therapy[45]. Further studies into the role of MN1 overexpression in blocking myeloid differentiation exploited the resistance of MN1 cells to ATRA-induced differentiation, as engineered MN1 overexpression induces a 3230-fold increase in the 50% inhibitory concentration (IC_{50}) of the normally ATRA-sensitive ND13 cells[109] and impairs ATRA-induced granulocyte and monocyte differentiation of the HL-60 and U927 AML cell lines[113]. In addition, transcriptional activation of downstream MN1 targets through the fusion of the VP16 domain re-sensitises MN1 cells to ATRA, with MN1-VP16 cells differentiating into mature granulocytes upon treatment with 1μM ATRA, and upregulation of the RARα target genes C/EBPα and PU.1 and the cell cycle arrest gene p21[109]. Furthermore, fusion of the VP16 domain to MN1 also results in a shift in cell immunophenotype, moving from the CMP-dominated distribution characteristic of MN1 leukemic cells to a GMP-dominant immunophenotype[109]. This significantly blunts the leukemic activity and induces a more phenotypically mature leukemia[109,

[115], providing further evidence of the effects of MN1 overexpression on RAR-RXR signaling and subsequent myeloid differentiation.

1.6.5.2 MN1 and C/EBPα

Beyond RAR/RXR signaling, only a limited number of genes and pathways key to the leukemic activity of MN1 have been elucidated, a matter that will be explored further in Chapter 3 of this thesis. However, the small number of genes and pathways identified thus far have yielded insight into the multifaceted and overlapping ways they contribute to the leukemic phenotype.

As previously described, Kandilci and Grosveld demonstrated that overexpression of MN1 enhances the growth and survival ability of $CD34^+$ cells and impairs myeloid differentiation in primary hematopoietic cells and AML cell lines[113]. These functional changes are accompanied by downregulation of C/EBPα and its downstream targets miR223 and p21, suggesting that C/EBPα may be negatively regulated by MN1[113]. Furthermore, ectopic overexpression of C/EBPα is sufficient to override the MN1-induced partial myeloid differentiation block and suppress the enhanced colony formation in the CFC assay driven by MN1 overexpression, revealing C/EBPα as a downstream target of MN1[113].

1.6.5.3 MN1 and STAT signaling

Overexpression of MN1 in the ND13 AML model increases LIC frequency by 33-fold and the expansion potential by 132-fold *in vitro* compared to MN1 alone[125]. GM-CSF stimulation in both the MN1+ND13 and MN1+HOXA9 co-transduction models increases proliferation *in vitro*, suggesting that STAT signaling plays a key role in MN1 leukemic activity[125]. This is supported

by increased phosphorylation of STAT5, STAT3, STAT1, extracellular signal-regulated kinase 1 (ERK1), and ERK2 in both MN1+ND13 and MN1+HOXA9 AML models[125]. Transduction of Stat5b- or Stat1-knockout murine bone marrow with MN1 and HOXA9 reduces the expansion potential by 86-fold and 28-fold, respectively, demonstrating a relationship between STAT signaling and self-renewal in the context of MN1[125]. Furthermore, patients with high MN1 and HOXA9 expression are correlated with AML with complex karyotype or loss of chromosome 5 or 7 and are associated with strong activation of STAT signaling, suggesting that dysregulated STAT signaling plays a role in more aggressive AML subtypes, such as AML modeled by MN1[125]. In contrast, while certain pathways activated by extrinsic signals, such as FMS-like tyrosine kinase-3 (FLT3) and c-Kit signaling, are downregulated upon MN1 overexpression, they may function to regulate the myeloid bias of the MN1 phenotype while being dispensable for MN1-induced leukemogenesis[127]. Together, these data suggest that while FLT3, STAT, and ERK signaling are not essential for MN1-induced leukemic activity, they are important collaborators that contribute to the self-renewal, proliferative, and immunophenotypic phenotypes of MN1 leukemia.

1.6.5.4 MEIS1 and HOX transcriptional pathways are critical to MN1 transformation

Recent data suggests that HOX and MEIS transcription factors also play significant roles in MN1 leukemia. Interestingly, although Mn1 is expressed at its highest levels in the GMP compartment of the hematopoietic system, it is the CMP compartment with which MN1 leukemic gene expression profiles cluster most closely[128], suggesting that MN1 overexpression induces a change in gene expression to induce a transformation-permissive state in CMP cells[128].

Furthermore, CMPs are the target cells of transformation for MN1-induced leukemia, as only single CMP clones immortalized by MN1 can be serially replated *in vitro* and rapidly induce transplantable leukemias with similar immunophenotype and LIC frequency to bulk MN1-transduced cells[128]. In contrast, MEPs cannot be transformed by MN1, and less than one-quarter of single-transduced HSCs yield highly proliferative clones[128]. However, these clones failed to induce leukemia *in vivo*, demonstrating that HSCs are not susceptible to MN1-induced transformation[128]. Similarly, only 1% of single-sorted GMPs proliferate *in vitro* after MN1 transduction, and bulk transduction fails to produce colonies in the CFC assay or engraft *in vivo*[128]. Gene expression profiling in MN1, CMP, and GMP cells revealed that 75% of differentially expressed genes between normal CMPs and GMPs – including Meis1, Flt3, myocyte enhancer factor 2C (Mef2c), HoxA9, and HoxA10 – are regulated in the same direction as MN1 cells compared to myeloid cells[128]. Subsequent to this observation, double transduction of GMPs with MN1 and MEIS1 or HOXA9 were found to support colony formation in CFC assays[128]. Furthermore, mice transplanted with purified GMP cells engineered to co-overexpress MN1, MEIS1, and either HOXA9 or HOXA10 rapidly succumb to leukemia with similar disease latency and immunophenotypic profiles as MN1-CMP leukemic mice, suggesting that transcriptionally active MEIS1 and HOXA programs are required to support MN1 leukemogenic transformation[128]. Strikingly, chromatin immunoprecipitation sequencing (ChIP-Seq) identified co-localisation of MN1 and MEIS1 peaks at over 500 gene regulatory regions, while transcriptional repression of MEIS1 target genes inhibits MN1 leukemia, providing further support for the role of MEIS1 in MN1 leukemic transformation and initiation[128]. From this data, putative direct target genes of MN1 and MEIS1 were identified that show co-occupancy of MN1

and MEIS1 at 18.1% and 17.1% of their target genes, respectively, establishing a MN1/MEIS1 signature of genes differentially expressed in the leukemic state[128].

1.6.5.5 MLL and DOT1L may play important roles in MN1 leukemogenesis

Recent work from the Bernt group demonstrates that the histone H3K79 methyltransferase DOT1-like (Dot1L) and MLL1 are important factors in MN1- and HOX-expressing leukemias[129]. Gene expression comparisons of the CMP/MN1 gene signature show strong enrichment in DOT1L-dependent genes in both normal lineage-negative sca-1 positive c-Kit positive (LSK) cells and DOT1L-dependent genes in MLL-AF9 leukemia, suggesting an overlap in core transcriptional pathways between MN1 and MLL-AF9 leukemias[129]. Functionally, Dot1l deletion in MN1-transduced CMPs leads to decreased colony numbers and size in serial replating CFC assays, increased CD11b expression, increased apoptosis, and decreased cycling, effectively disrupting MN1-induced effects[129]. Dot1l or Mll1 deletion also abrogates the leukemic gene expression program, including downregulation of 3' HoxA genes HoxA7, HoxA9, HoxA10, and HoxA11, and impair MN1-mediated leukemogenesis[129]. Interestingly, human leukemias with high expression of MN1 and HOXA9 respond to DOT1L inhibitors, as observed by changes in apoptosis, growth, cell cycle, and HOXA9 expression, providing evidence for a cooperative role of chromatin regulation of gene expression in MN1 leukemia[129]. Given that HoxA family genes and Meis1 are critical targets of MLL1 fusions such as MLL-ENL[68], that Meis1 is essential and rate-limiting to MLL leukemias[86], and that MLL-AF9 leukemia requires DOT1L[130], these data highlight interest in the relationship between Hox genes, Meis1, and MN1.

1.6.5.6 MN1 and immune response and regulation

Recent work from Sharma and colleagues identified immune response and immune regulation as key pathways targeted by MN1[115]. Previous work had established that ectopic overexpression of MN1 blocks myeloid differentiation and increases resistance to ATRA by more than 3000-fold[109]. However, *in vitro* assays demonstrate that fusion of the transcriptional activation domain VP16 re-sensitises MN1 to ATRA[109, 115]. Consistent with these observations, RARα target genes C/EBPα and PU.1 and cell cycle gene p21 are upregulated upon ATRA treatment in MN1VP16 cells, suggesting that despite their immortalizing ability, MN1VP16 cells are susceptible to myeloid differentiation[109]. Gene expression profiling to identify downstream targets of MN1 revealed that 38% of the top 60 differentially expressed gene sets belong to immune response and immune regulation pathways and, surprisingly, many of these immune response function genes are directly targeted by MN1 and MEIS1 but not RARα[115]. Of note, these genes include interferon regulatory factor 8 (Irf8) and its downstream target chemokine (C-C motif) ligand 9 (Ccl9), both of which are downregulated in MN1 compared to MN1VP16 cells[115]. In addition, lipopolysaccharide (LPS) stimulation induces significantly higher levels of hydrogen peroxide in MN1VP16 cells compared to MN1 cells, suggesting that the increased phagocytic activity seen in MN1VP16 cells occurs by upregulation of immune response pathways[115]. Engineered overexpression of Irf8 and Ccl9 in MN1-ransduced cells decreases cell cycling, engraftment, and numbers of leukocytes and increase hemoglobin and platelets four weeks post-transplant[115]. Furthermore, Irf8 and Ccl9 overexpression inhibit leukemic development and increase leukemic latency, respectively, in two murine models, suggesting that these genes act, at least in part, cell autonomously in the MN1 model[115]. Similarly, overexpression of IRF8 in AML xenograft

models shows anti-tumour activity resulting in significantly smaller tumour volumes[115]. This work identifies novel MN1 target genes that, upon reversal of their aberrant expression, are capable of arresting MN1-induced leukemogenesis and, thus, acting as potential therapeutic targets.

1.7 Thesis objectives

The overall objective of this thesis was to identify and better understand key regulators in LSC function. As the oncogene MN1 plays a critical role in the abnormal proliferation, self-renewal, and differentiation seen in leukemia, I exploited the MN1 murine model to gain further insight into this process.

As overexpression of human MN1 is sufficient to induce AML in the murine model, I hypothesised that the leukemic properties of increased proliferation and self-renewal, arrested hematopoietic differentiation, and resistance to ATRA-induced differentiation could be localised to specific regions of the MN1 protein. As described in Chapter 2 of this thesis, I generated mutant MN1 constructs involving deletion of regions approximately 200 amino acids in length to delineate the functional domains of MN1. Through functional analysis of these MN1 mutants, the properties of proliferation and self-renewal, inhibition of differentiation, and ATRA resistance, and leukemogenesis could be ascribed to structurally distinct regions of MN1[131].

Chapter 3 of this thesis work centred on attempts to identify key genes and pathways underlying leukemia. I exploited the phenotypic heterogeneity inherent in the MN1-induced leukemic model to identify genes differentially expressed between leukemic and non-leukemic MN1 subsets. I combined these data with previously-published MN1 gene expression datasets to generate a

shortlist of genes potentially critical to MN1-induced leukemogenesis. Through a loss-of-function approach, I investigated the roles of several genes upregulated in MN1 leukemic populations to determine their role on *in vitro* and *in vivo* measurements of leukemic activity, providing powerful insight into key genes in MN1 leukemia and identifying Meis2 as a novel critical player in leukemogenesis.

Chapter 2: Cell fate decisions in malignant hematopoiesis: Leukemia phenotype is determined by distinct functional domains of the MN1 oncogene

2.1 Introduction

The postulated requirement for induction of leukemogenesis has long been the combination of class I and II mutations[132], although recent insights into the genetic composition of AML cells has revealed additional pathogenetic mechanisms including changes in epigenetic regulation. On average, 13 coding genes are mutated per AML genome[48], suggesting that several events are required for leukemogenesis. Despite the heterogeneity of cells that can give rise to AML, only a small proportion of AML cells show clonogenic activity in culture and only a small fraction of AML blast cells are able to confer disease to immune-deficient mice[133]. While such disease-propagating or leukemia-initiating cells (LICs) may be rare, they are not necessarily restricted to the most primitive cells within the hematopoietic hierarchy but rather, can include committed progenitor cells such as CMPs or common lymphoid progenitors (CLPs)[9, 11, 17, 21]. The high level of heterogeneity seen in AML and within an individual patient underscores the importance of understanding the molecular mechanisms underlying this disease and the functional consequences for leukemic cells.

While there is a high degree of cellular heterogeneity in an individual leukemia[125], there is striking redundancy of mutated genes in distinct diseases like AML[134], T-lymphoblastic leukemia (T-ALL)[135], and primary myelofibrosis[136], including mutations in DNA methyltransferase 3A (DNMT3A) and several other genes. Explanations for how mutations in the same gene can cause different diseases may include: differing cells of origin[137] or cell-extrinsic signals[138], as illustrated by the ability of the MLL-AF9 fusion gene to cause myeloid

and lymphoid leukemias; the influence of the microenvironment, such as the ability of abnormal stroma cells to induce myelodysplasia in HSCs[139]; and the ability of mutations to change the lineage potential of the oncogene and possibly the phenotype of the disease, as in enhancer of zeste homolog 2 (EZH2) mutations in B-non-Hodgkin lymphoma and myeloid disorders[140, 141]. The MN1 model of leukemogenesis constitutes a simple and ideal model to test this latter hypothesis due to its ability to induce leukemia as a single hit through constitutive overexpression[128].

The ability of MN1 to induce rapid onset leukemia on its own highlights its central regulatory role in hematopoietic transformation. MN1 has been shown to be most highly expressed in murine CMPs, but is downregulated upon differentiation[128] and is capable of enhancing proliferation of human $CD34^+$ cord blood cells[113]. High MN1 expression has been associated with both acute myeloid and lymphoid leukemias[45] as well as other AML characteristics such as inv(16)[106] or overexpression of ectropic viral integration site 1 (EVI-1)[102]. Significantly, it is an independent prognostic factor in patients with AML with normal cytogenetics, associated with shorter relapse-free survival, overall survival, and resistance to ATRA-induced differentiation[45, 103, 107, 109, 142]. As loss of MN1 expression impairs proliferation and significantly decreases clonogenic activity of human leukemic cells, it is a potential therapeutic target in AML[114].

MN1 rapidly induces leukemia in mice[106, 109]. Work from our lab demonstrated that MN1 is capable of transforming single CMP cells as the cell of origin[128]. Significantly, GMPs require co-overexpression of *Meis1* for *in vitro* transformation, and the additional co-overexpression of HOXA9 or HOXA10 to induce leukemia *in vivo*[128]. Loss of MEIS1 expression abrogates leukemic activity in MN1 cells, suggesting that, combined with co-localization of MN1 and MEIS1 at a large proportion of MEIS1 target sites, MEIS1 and its co-factor HOXA9 are essential

to MN1 leukemogenesis[128]. In addition, MN1 cells are arrested at an immature stage of myelopoiesis and are highly resistant against ATRA[109], a potent inducer of myeloid differentiation, although ectopic CEBPα expression, which MN1 is thought to repress, can abrogate the leukemogenic activity of MN1[113].

The work presented in Chapter 2 of this thesis tests the hypothesis that multiple functions are encoded in the MN1 protein and can be localized to different regions. Thus, delineation and localisation of these functions at a structural level will provide insight into the key mechanisms required for leukemic transformation by a single central regulator such as MN1. Despite the established role of MN1 overexpression in leukemia, little is known about the protein itself. The MN1 protein is highly conserved between different species, but largely lacks recognised protein domains excepting two proline-glutamine stretches and a single 28 residue-long glutamine stretch. Here, known properties of MN1 leukemia were systematically localised using both *in vitro* and extensive *in vivo* studies to specific physical regions of wildtype MN1 through a detailed structure-function analysis of MN1. I demonstrated that the proliferative ability and self-renewal activity, and the inhibition of megakaryocyte/erythroid, myeloid, and lymphoid differentiation are localised to distinct regions within MN1 and provide evidence that different mutations of a single oncogene can induce distinct diseases such as myeloid and lymphoid leukemia and myeloproliferative disease.

2.2 Materials and methods

2.2.1 Retroviral vectors and vector production

Retroviral vectors for expression of MN1[109] and NUP98HOXD13 (ND13)[75] have been previously described. Primers were designed to ensure that the N- and C-termini of the final construct were flanked by *Not*I sites for each MN1 mutant truncation construct, then subcloned into the expression vector pSF91[143] upstream of the internal ribosomal entry site (IRES) and the enhanced green fluorescent protein (GFP) gene. MN1 Strategy 1 constructs were generated through polymerase chain reaction (PCR) amplification of the N- (proximal) and C-terminal (distal) regions of the construct with *Hind*III sites at the internal sites, which were then subcloned into the pSF91-IRESeGFP vector. The pSF91 vector carrying only the IRES-enhanced GFP cassette served as a control. Constructs were validated by sequencing and correct expression and transmission were confirmed by quantitative real-time PCR (qRT-PCR) and PCR. Primer sequences can be found in Table 2.1. For hemagglutinin (HA)-tagged constructs (used in Western blots and confocal microscopy), full-length and MN1 mutant deletion constructs were cut to ensure the N- and C-termini of the final construct were flanked by *BglII* or *BamHI* (for constructs lacking the N-terminal region) and *NotI* sites, respectively, then subcloned into the MSCV-IRES-GFP expression vector[144] with an HA-tag inserted at the N-terminus of MN1 and the deletion constructs. Helper-free recombinant retrovirus was generated by using supernatants from the transfected ecotropic Phoenix packaging cell line to transduce the ecotropic GP+E86 packaging cell line[145].

Table 2.1 MN1 deletion mutant primer sequences

MN1 Strategy 1 Prox For	TTTAAAGCGGCCGCATGTTTGGGCTGGACCAATTC
MN1 Strategy Dist Rev	TTTAAAGCGGCCGCTCA AGTTAGGGCAGCCACGAATG
MN1Δ2 Prox For	TTTAAAGCGGCCGCATGTTTGGGCTGGACCAATTC
MN1Δ2 Prox Rev	TTTAAAAAGCTTGGCTCGGTTAGGGCTCTGGT
MN1Δ2 Dist For	TTTAAAAAGCTTGCGCAATTCGAGTATCCCATCCA
MN1 Δ4 Dist Rev	TTTAAAAAGCTTCGCCTGCTGCTCGAAGGT
MN1 Δ4 Prox Rev	TTTAAAAAGCTTCGCCTGCTGCTCGAAGGT
MN1 Δ4 Dist For	TTTAAAAAGCTTCAGCGCACCTCGGCCAGT
MN1 Δ5 Prox Rev	TTTAAAAAGCTTGGTGCGCTGGCTGGGCTG
MN1Δ5 Dist For	TTTAAAAAGCTTAAGGCGCTCACGTCGCCA
MN1 Δ6 Prox Rev	TTTAAAAAGCTTTGGCGACGTGAGCGCCT
MN1 Δ6 Dist For	TTTAAAAAGCTTTGCTGCTCCGAGGCGGTCA
MN1 Strategy 2 Rev	TTTAAAGCGGCCGCTCA AGTTAGGGCAGCCACGAATG
MN1Δ1 For	TTTAAAGCGGCCGCATG TCCCACAGTCTGGAGCCA
MN1 Δ1-2 For	TTTAAAGZGGCCGCATGACGCGCAATTCGAGTATC
MN1 Δ1-3 For	TTTAAAGCGGCCGCATGCGAACTTTGAGCGCGAAG
MN1 Δ1-4 For	TTTAAAGCGGCCGCATGTCCTTCAACAAGCCCAGCT
MN1 Δ1-5 For	TTTAAAGCGGCCGCATGGAAAAGGCGCTCACGTC
MN1 Δ1-6 For	TTTAAAGCGGCCGCATGTCCGAGGCGGTCAAGAG
MN1 Strategy 3 For	TTTAAAGCGGCCGCATGTTTGGGCTGGACCAATTC
MN1 Δ7 Rev	TTTAAAGCGGCCGCTCA GGTAGAGTTAGACATGATGC
MN1 Δ2-7 Rev	TTTAAAGCGGCCGCTCA GGATTCCAGGGTGTAGTTGG
MN1 Δ3-7 Rev	TTTAAAGCGGCCGCTCACTGCAGCTGACCCA
MN1 Δ4-7 Rev	TTTAAAGCGGCCGCTCACTGTTGCAGGGACTGGTG
MN1 Δ5-7 Rev	TTTAAAGCGGCCGCTCAGAACCTCTCAAAGAACAC
MN1 Δ6-7 Rev	TTTAAAGCGGCCGCTCACATGTGCTCATAGCCCT

2.2.2 Clonogenic progenitor assays

Colony-forming cells (CFCs) were assayed in methylcellulose (MethoCult M3434 or MegaCult-C, Catalog No. 04964; STEMCELL Technologies, Vancouver, BC, Canada). For each assay, freshly isolated and transduced unsorted bone marrow cells were plated in duplicate in Methocult medium (1000 cells/well). Colonies were evaluated microscopically 10 days after plating using standard criteria. To assay megakaryocyte progenitor frequency, freshly isolated and transduced bone marrow cells were sorted for GFP expression, and $1x10^5$ cells were suspended in MegaCult-C medium containing recombinant human thrombopoietin (50 ng/mL), recombinant human interleukin 6 (IL6) (20 ng/mL), recombinant human IL11 (50 ng/mL), and recombinant mouse IL3 (10 ng/mL), mixed with collagen and dispensed in chamber slides (all from STEMCELL Technologies, Vancouver, BC, Canada). Cultures were incubated at 37°C for 7 days. Slides were stained with acetylthiocholiniodide according to manufacturer's instructions, and colonies were counted manually under a microscope, as previously described[146].

2.2.3 Quantitative real-time RT-PCR

Total ribonucleic acid (RNA) from stored, frozen cell pellets were isolated using TRIZOL reagent (Life Technologies, Burlington, ON, Canada). Total RNA was converted into complementary deoxyribonucleic acid (cDNA) using the SuperScript® VILO cDNA synthesis kit (Life Technologies, Burlington, ON, Canada) using 500ng of total RNA. Quantitative real-time PCR was performed as previously described using the 7900HT Fast Real-Time PCR system (Applied Biosystems, Foster City, CA, USA)[147] and Fast SYBR® Green Master Mix (Life Technologies, Burlington, ON, Canada)[147]. Relative expression was determined with the $2^{-\Delta\Delta CT}$

method using the housekeeping gene transcript *Abl1* to normalize the results. Primers were manufactured by Life Technologies. Primer sequences can be found in Table 2.2.

Table 2.2 MN1 qRT-PCR primer sequences

MN1 qRT-PCR N-term For	GTTTGGGCTGGACCAATTC
MN1 qRT-PCR N-term Rev	TGAACACCCACTTTAAGGCC
MN1 qRT-PCR C-term For	CACTTGCAGTGCCTGTCTGT
MN1 qRT-PCR C-term Rev	CAACAGATTTGGGACATTCG

2.2.4 Western blot analysis

For Western blot analysis, transduced GP+E86 cell lines were generated for each construct. From these cells, $1x10^6$ were lysed with 150µL lysis buffer (50mM Tris-HCl[pH 8], 0.1% Tween-20, 0.1% sodium dodecyl suffate (SDS), 150mM NaCl, 0.5mM ethylenediaminetetraacetate acid (EDTA), 10mM dithiothreitol (DTT), and 1mM phenylmethane sulfonyl fluoride (PMSF)), plus protease inhibitor cocktail (Sigma, Oakville, ON, Canada) and incubated for 20 minutes on ice. NuPage LPS loading buffer (4x) and NuPage Sample Reducing Agent (10x) (Life Technologies, Burlington, ON, Canada) were added and samples were heated for 15 minutes at 95^{o}C. Lysates were loaded onto 4%-12% NuPage Novex BIS-Tris SDS-polyacrylamide gels (Life Technologies, Burlington, ON, Canada) and electroblotted in 3-(N-morpholino)propanesulfonic acid (MOPS) transfer buffer to nitrocellulose membrane (Life Technologies, Burlington, ON, Canada). Rabbit polyclonal anti-HA (Abcam, Cambridge, England) or mouse monoclonal anti-beta-actin (abm, Richmond, BC, Canada) and Mouse TrueBlot ULTRA horseradish peroxidase (HRP)-conjugated anti-mouse (Rockland Inc., Gilbertsville, PA, USA) or goat anti-rabbit

immunoglobulin G (IgG) antibodies (Jackson ImmunoResearch Laboratories Inc., PA, USA) in 1:5000 dilutions of 0.1% Tween-20, 5% bovine serum albumin (BSA), Tris-buffered saline (TBS) were used for protein detection. Proteins were visualised using Clarity Western enhanced chemiluminescence (ECL) Substrate (Bio-Rad, Hercules, CA, USA).

2.2.5 ATRA cytotoxicity assay

To ensure that cells proliferated *in vitro* regardless of the functional status of MN1 mutant variants, MN1 deletion constructs were transduced in bone marrow cells immortalized by retroviral expression of the fusion gene ND13. *In vitro* cytotoxicity assays were performed in Dulbecco's modified Eagle medium (DMEM) supplemented with 15% fetal bovine serum (FBS), 6ng/mL murine IL3, 10ng/mL human IL6, and 20ng/mL murine stem-cell factor (mSCF; all from STEMCELL Technologies, Vancouver, BC, Canada). Cells were seeded at a cell density of $1x10^4$/mL in a 96-well plate, and incubated under light-protective conditions. ATRA (Sigma, Oakville, ON, Canada) was dissolved in dimethyl sulfoxide (DMSO) (Sigma) and added to the culture medium at the specified concentrations as $1/1000^{th}$ of the final volume. After 64 hours, cells were stained with Alamar Blue (Sigma) for 8 hours and fluorescence was measured with a Tecan Safire^2 microplate reader (Life Technologies, Burlington, ON, Canada). Viability was determined as percentage of DMSO-treated cells after background subtraction of fluorescence in wells with medium only. The 50% inhibitory concentration was determined as the concentration of ATRA that reduced cell viability to 50% of DMSO-treated cells.

2.2.6 Mice and retroviral infection of primary bone marrow cells and bone marrow transplantation

Primary mouse bone marrow cells from 5-fluorouracil (5FU)-treated C57BL/6J donor mice were pre-stimulated for 48 hours in DMEM media supplemented with 15% FBS, 6ng/mL murine IL3, 10ng/mL human IL6, and 20ng/mL mSCF. Cells were then transduced by co-cultivation with viral producers for 48 hours, then harvested and plated into CFC media or directly transplanted into lethally irradiated syngeneic recipient mice, as previously described[147]. Recipient mice were exposed to a single dose of 750 to 810 cGy total-body irradiation accompanied by a life-sparing dose of $1x10^5$ freshly isolated bone marrow cells from syngeneic mice, and were monitored daily. Engraftment of transduced cells in peripheral blood was monitored every four weeks by fluorescence-activated cell-sorter (FACS) analysis and quantification of GFP-positive cells. Sick or moribund mice were sacrificed, spleens weighed, and red blood cells and white blood cells were counted using the scil Vet abc blood analyser (Vet Novations, Barrie, ON, Canada). C57BL/6J mice were bred and maintained in the Animal Research Centre of the British Columbia Cancer Agency as approved by the University of British Columbia Animal Care Committee (the Institutional Animal Care and Use Committee, IACUC). Experimental studies were approved by the University of British Columbia Animal Care Committe under experimental protocol numbers A04-0380 and A09-0009, and all efforts were made to minimise suffering.

2.2.7 FACS analysis

Lineage distribution was determined by FACS analysis (FACSCalibur; Becton Dickinson, Mississauga, ON, Canada) as previously described[75]. Monoclonal antibodies used were

phycoerythrin (PE)-labeled Gr-1 (clone Ly6G-6C), B220 (CD45R), CD4, Ter119, and Sca-1 (Ly6A/E) and allophycocyanin (APC)-labeled CD11b, CD8, and c-kit (CD117) (BD Biosciences, Mississauga, ON, Canada).

2.2.8 Bone marrow morphology

Cytospin preparations were stained with Wright-Giemsa stain. Images were visualised using a Nikon Eclipse 80i microscope (Nikon, Mississauga, ON, Canada) and a 20x/0.40 numerical aperture objective, or a 100x/1.25 numerical aperture objective and Nikon Immersion Oil (Nikon). A Nikon Coolpix 995 camera (Nikon) was used to capture images.

2.2.9 Confocal microscopy

Twenty-four hours prior to fixation, micro growth glass cover slips (VWR International, Mississauga, ON, Canada) were coated in Cultrex Poly-L-Lysine (Trevigen, Gaithersburg, MD, USA) and GP+E86 expressing cell lines expressing MN1, MN1Δ1, and MN1Δ5-7 were plated. Cells were fixed in 4% paraformaldehyde in phosphate-buffered saline (PBS) for 10 minutes at room temperature, incubated with a 1:500 dilution of rabbit anti-HA primary antibody followed by a 1:300 dilution of anti-rabbit Alexa eFluor 594 secondary antibody (Life Technologies, Burlington, ON, Canada) and then stained with 4,6-diamidion-2-phenylindole (DAPI) at 1µg/mL (Sigma-Aldrich, St Louis, MO, USA). Slides were then mounted with 1,4-diazabicyclo(2,2,2)octane (DABCO) mounting medium (Sigma-Aldrich, St Louis, MO, USA) and Z-stack photographs were taken 0.13µm apart using a Leica TCS SP5 Confocal microscope (100x objective). Images were captured using LAS AF software (Leica Microsystems, Inc.,

Exton, PA, USA) and deconvoluted using Real-time GPU-based 3D Deconvolution[148] and DeconvolutionLab[149] in ImageJ.

2.2.10 Gene expression profiling and gene set enrichment analysis

RNA was extracted using TRIZOL reagent (Life Technologies, Burlington, ON, Canada) from GFP+ cells that were sorted from mouse bone marrow cells four weeks after transplantation**.** Quality and integrity of the total RNA isolated was controlled by running all samples on an Agilent Technologies 2100 Bioanalyzer (Agilent Technologies, Mississauga, ON). Extracted RNA from MN1, MN1Δ1, and MN1Δ7 leukemia cells and Gr-1^{+}/CD11b^{+} bone marrow cells were hybridized to the Affymetrix GeneChip Mouse 430 2.0 (43.000 probes) microarray (n=2) per the manufacturer's instructions. Experiments were performed at the British Columbia Genome Sciences Centre, Vancouver, Canada. Gene expression can be found at the Gene Expression Omnibus database (GEO accession number GSE46990; http://www.ncbi.nlm.nih.gov/geo/query/acc.cgi?token=zhedbmoeuqcksli&acc=GSE46990). Data were analyzed using R and Bioconductor[150]. Quality was assessed with the ArrayQualityMetrics package[151]. Arrays were preprocessed using robust multi-array (RMA)[152]. Differentially expressed probe sets were calculated with the LIMMA package[153] applying Benjamini-Hochberg multiple testing correction at an false discovery rate (FDR) of 0.05. For gene set enrichment, the Broad Institute Gene Set Enrichment Analysis (GSEA) software package was used[154]. The datasets were collapsed into single genes and rank-ordered by signal to noise ratio. Gene set permutations were used to estimate statistical significance. Analyzed gene ontology sets were obtained from MSigDB v3.1[154]. The gene set enrichment analysis software[154]

(http://www.broad.mit.edu/gsea/index.jsp) was used to compare gene enrichment of Gene Ontology gene sets (dataset C5, available from the Molecular Signature database v3.1[154]) between MN1Δ1 vs MN1 and MN1Δ7 vs. MN1.

2.2.11 Statistical analysis

Comparisons were performed by unpaired T-tests. The two-sided level of significance was set at P less than 0.05. Comparison of survival curves were performed using the Kaplan-Meier method and log-rank test. Statistical analyses were performed with Excel (Microsoft Canada, Mississauga, ON, Canada) and GraphPad Prism 6 (GraphPad Software, La Jolla, CA, USA).

2.3 Results

2.3.1 The N-terminal region of MN1 is required for immortalization of bone marrow cells *in vitro*

To elucidate the relationship between the structure of MN1 and the properties of MN1 leukemia, MN1 deletion mutants were generated in three strategies. I divided wildtype MN1 into seven regions, each approximately 200 amino acids in length and numbered sequentially from the N-terminus. In an internal deletion series (Strategy 1), distinct 200 amino acid regions were deleted (Figure 2.1A). Due to technical difficulties, the vector construct lacking the third region from the N-terminus (MN1Δ3) was unable to be generated and was excluded from further analysis. Progressive N-terminal deletions (Strategy 2) included six mutant constructs in which approximately 200 amino acid-regions were cumulatively deleted starting from the MN1 N-terminus. For progressive C-terminal deletions (Strategy 3), stretches of approximately 200

amino acids were cumulatively deleted starting from the MN1 C-terminus (Figure 2.1A). I validated the size and expression of all mutant constructs at the RNA and protein level and detected the expected protein for all constructs lacking one or two regions and for the constructs MN1Δ1-4, MN1Δ3-7, and MN1Δ5-7 lacking three or more regions. The remaining constructs lacking three or more regions did not, however, yield detectable protein (Figure 2.2).

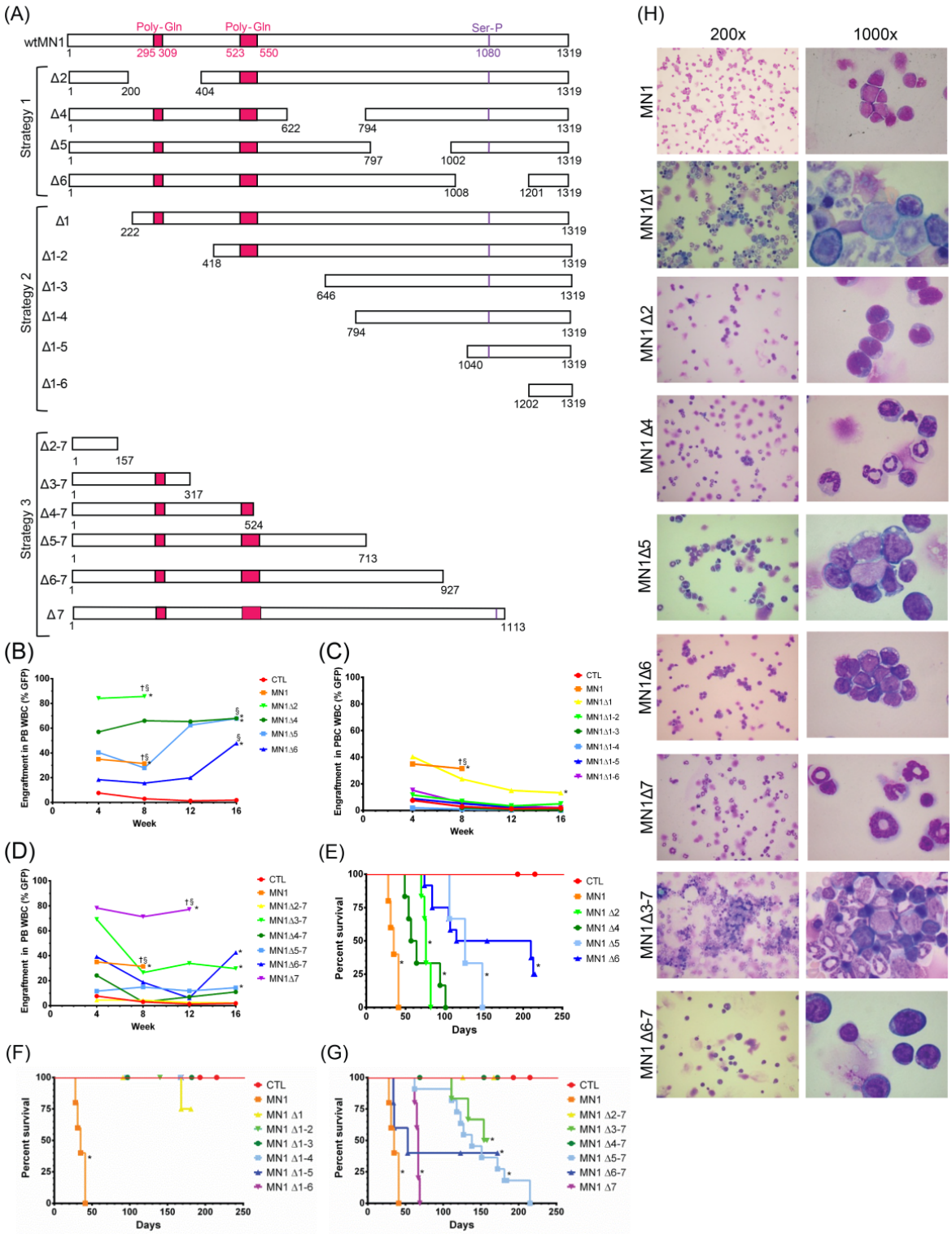

Figure 2.1 The N-terminal region of MN1 is required for its leukemogenic potential

(A) MN1 mutation constructs for structure-function analysis. In Strategy 1 distinct stretches of approximately 200 amino acids were deleted throughout wildtype MN1. In Strategy 2, stretches of approximately 200 amino acids were

cumulatively deleted starting from the MN1 N-terminus. In Strategy 3, stretches of approximately 200 amino acids were cumulatively deleted starting from the MN1 C-terminus. (B-D) Percentage of transgene-positive white blood cells engrafting in peripheral blood of transplanted mice at 4-week intervals. P values are given for the comparison of the indicated construct with CTL-transduced cells. The average engraftment is shown. Number of analysed mice and standard error can be found in Table 2.1. (E-G) Survival of mice receiving transplants of cells transduced with (E) Strategy 1, (F) Strategy 2, and (G) Strategy 3 MN1 deletions. P values are given for the comparison of the indicated construct with CTL-transduced cells. The number of analysed mice is detailed in Table 2.1. (H) Morphology of bone marrow cells at death of diseased mice. The cells were Wright-Giemsa stained. Images were visualised using a Nikon Eclipse 80i microscope (Nikon, Mississauga, ON, Canada) and a 20x/0.40 numerical aperture objective, or a 100x/1.25 numerical aperture objective and Nikon Immersion Oil (Nikon). A Nikon Coolpix 995 camera (Nikon) was used to capture images. § engraftment in peripheral blood at the indicated time point or at death in cases where a mouse died before that time point. † all mice were dead at this timepoint due to disease. * indicates $P<0.05$, ** indicates $P<0.001$.

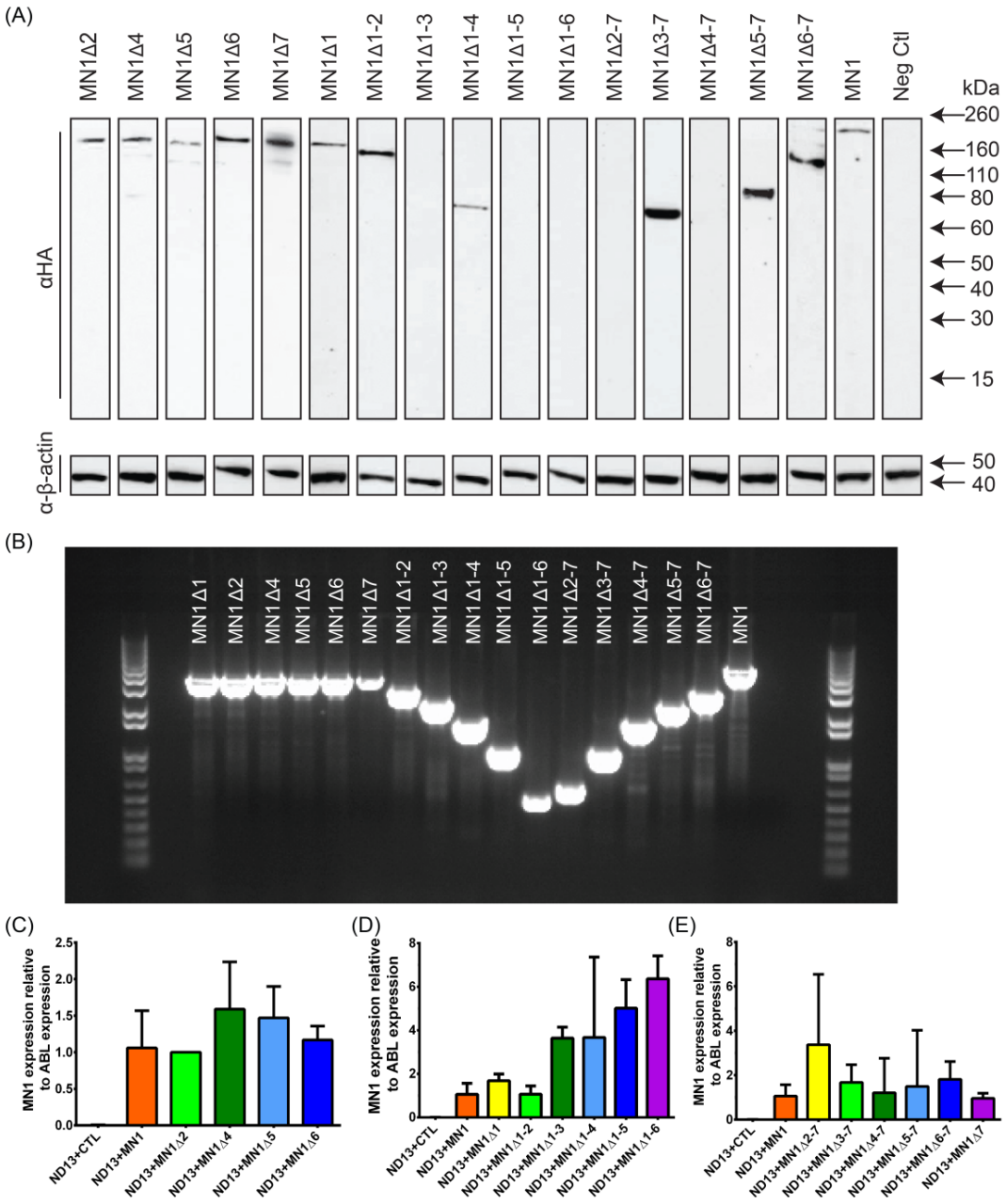

Figure 2.2 Expression levels of MN1 deletion constructs

(A) Western blot analyses of GP-E86 producer cells for the various constucts illustrating the expression and size of protein products of the MN1 deletion constructs compared to full-length MN1. The figure is a composite of multiple gels with each lane representing a single construct stained with either anti-HA or anti-β-actin antibody. (B) Gel electrophoresis with PCR products illustrating the relative size of the MN1 deletion constructs compared to full-

length MN1. (C-E) Expression levels of MN1 deletion constructs measured by qRT-PCR. MN1 deletion constructs were transduced in cells immortalized by NUP98HOXD13 (ND13). Mean ± SD, n=3.

Freshly isolated bone marrow cells were transduced with MN1 mutation constructs or the control vector and plated in CFC medium, and replating ability and proportion of transduced cells (GFP^+) were measured. While GFP-positive cells are lost in control-transduced cells after the second replating, GFP expression is maintained in all internal deletion constructs (Strategy 1) up to the fifth plating, except for MN1Δ6 where no colonies grow after the fourth plating (Figure 2.3A-B). For Strategy 2, involving successive deletions beginning at the N-terminus, only MN1Δ1 retains transforming ability, immortalizing bone marrow cells *in vitro* and competitively outgrowing non-transduced cells. In contrast, all other Strategy 2 constructs show loss of replating ability, with fewer than 50 colonies after the first plating upon additional deletion of regions 2-6 (Figure 2.3C and D). MN1 mutants with cumulative deletions from the C-terminus (Strategy 3) can immortalize bone marrow cells, including MN1Δ3-7, which retains only 317 amino acids, and MN1Δ4-7, which shows colony replating ability despite an inability to detect the protein by Western blot (Figure 2.2). In summary, the N-terminus of MN1 is necessary and sufficient to immortalize bone marrow cells *in vitro* with select regions, such as amino acids 1008-1201, playing a significant role in *in vitro* immortalization.

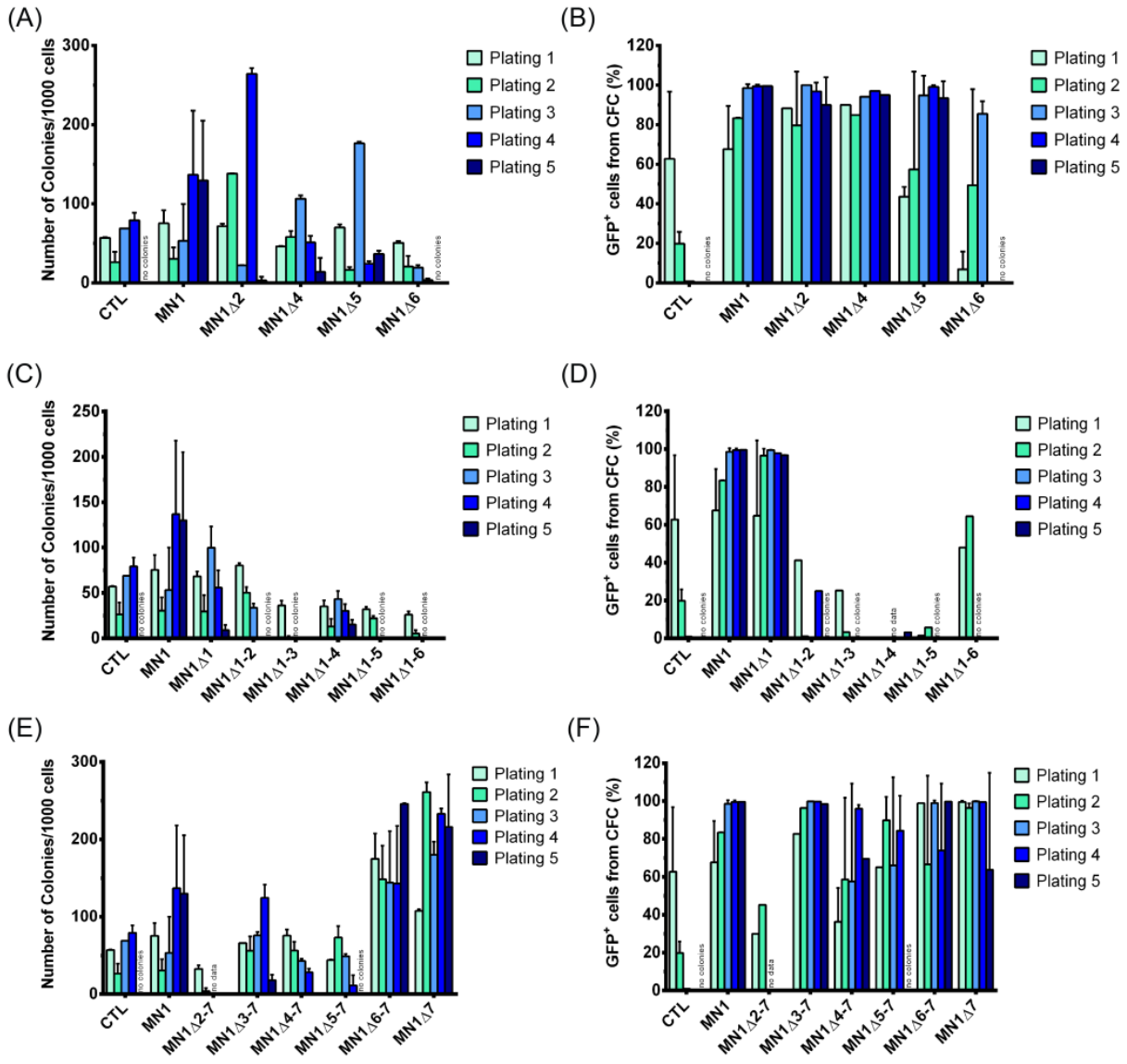

Figure 2.3 Potential of MN1 variants to immortalize bone marrow cells in vitro

Left panels (A, C, E) show number of CFC colonies per plating in methylcellulose under myeloid cytokine conditions. 5-FU pretreated bone marrow cells were transduced with MN1 deletions and were plated after transduction without sorting of cells. Right panels (B, D, F) show percentage of GFP^+ cells at the end of each round of plating.

2.3.2 The N-terminal region of MN1 is required for its leukemogenic potential *in vivo*

MN1-transduced bone marrow cells were transplanted into lethally irradiated mice, and the engraftment in peripheral blood monitored monthly. All mice show engraftment 4 weeks post-transplant (at least 1% of total bone marrow). All internal deletion (Strategy 1) constructs show statistically significant higher engraftment than control mice with increasing engraftment over 16 weeks (lowest engraftment in MN1Δ6 at 18.4 ± 4.5% versus 7.7% for control at week 4 to 38.4 ± 12.0% versus 1.88 ± 0.68% for control at week 16, unpaired t-test, $P<0.05$) (Figure 2.1B). Progressive N-terminal deletion (Strategy 2) constructs also show engraftment at 4 weeks post-transplant, although engraftment levels do not significantly differ from control mice except for MN1Δ1, which shows higher early engraftment levels similar to full-length MN1 (40.4 ± 6.5% versus 35.0 ± 10.2%, unpaired t-test). In addition, engraftment decreases over 16 weeks, suggesting that these constructs, including MN1Δ1 (13.3 ± 3.4% for MN1Δ1 at week 16 versus 31.5 ± 11.6% for MN1 at week 8), have defects in their proliferative and self-renewal capabilities and, thus, are unable to outcompete the co-transplanted normal bone marrow cells (Figure 2.1C and Table 2.3). Of the progressive C-terminal deletions (Strategy 3), MN1Δ7 shows the highest engraftment levels (77.2 ± 11.8%), and MN1Δ6-7 (42.0 ± 15.7%), MN1Δ5-7 (32.7 ± 14.8%) and MN1Δ3-7 (30.0 ± 24.6%) have significantly higher engraftment of transduced cells compared to control cells at 16 weeks (1.9 ± 0.7%) (Figure 2.1D). The MN1 mutations that enhance engraftment and proliferation *in vivo* also induce high white blood cell counts, anemia, and thrombocytopenia (Figures 2.4-2.6; Tables 2.4-2.6).

Table 2.3 Characterisation of mouse phenotype after transplantation with MN1 deletion constructs

Construct	CTL	MN1	MN1 Δ1	MN1 Δ2	MN1 Δ4	MN1 Δ5	MN1 Δ6	MN1 Δ7	MN1 Δ1-2	MN1 Δ1-3	MN1 Δ1-4	MN1 Δ1-5	MN1 Δ1-6	MN1 Δ2-7	MN1 Δ3-7	MN1 Δ4-7	MN1 Δ5-7	MN1 Δ6-7
No. of mice	9	5	5	6	6	3	9	5	3	4	5	5	6	4	7	4	10	5
No. of mice dying from disease	0	5	1	6	6	3	8	5	0	0	0	0	0	0	3	0	9	3
Engraftment in BM at death (% GFP)	0.7 ± 0.5 (2)	31.5 ± 11.6 (5)	7.1 ± 3.0 (4)	85. 7 ± 3.5 (3)	68.0 ± 4.4 (5)	67.8 ± 17.4 (3)	53.7 ± 10.7 (9)	77.2 ± 11.8 (5)	3.5 ± 1.4 (3)	0.4 ± 0.3 (3)	0.2 ± 0.1 (5)	1.3 ± 0.5 (5)	2.2 ± 0.7 (3)	2.2 ± 1.6 (2)	33.8 ± 29.0 (3)	8.2 ± 5.7 (4)	38.4 ± 19.5 (6)	42.0 ± 15.7 (5)
WBC count at death ($x10^3/mm^3$)	8.2 ± 1.8 (2)	66.0 ± 44.0 (2)	5.8 ± 0.5 (4)	23.9 ± 3.1 (4)	176.4 ± 94.4 (3)	12.7 ± 4.9 (3)	4.8 ± 1.0 (8)	197.4 ± 73.8 (5)	n.d.	8.9 ± 1.5 (2)	n.d.	n.d.	n.d.	n.d.	127.6± 118.7 (3)	n.d.	78.0 ± 43.4 (5)	32.8 ± 9.7 (3)
Hemoglobin count at death (g/dl)	13.6 ± 1.4 (2)	2.4 ± 0.2 (2)	8.3 (1)	6.6 ± 2.8 (4)	0.0 (1)	6.4 (1)	2.2 ± 1.3 (4)	7.8 ± 1.8 (5)	n.d.	13.4 ± 0.4 (2)	n.d.	n.d.	n.d.	n.d.	12.0 ± 1.4 (3)	n.d.	8.5 ± 0.5 (5)	2.4 ± 1.2 (3)
Platelet count at death ($x10^3/mm^3$)	1086.0 ± 138.0 (2)	82.0 ± 9.0 (2)	993. 0 (1)	119.3 ± 53.7 (4)	31.0 (1)	115. 0 (1)	27.3 ± 1.3 (4)	280.8 ± 106.3 (5)	n.d.	633.0 ± 68.0 (2)	n.d.	n.d.	n.d.	n.d.	554.0 ± 222.7 (3)	n.d.	317.9 ± 157.0 (5)	76.7 ± 23.1 (3)
Median survival time for diseased mice (days)	N/A	35 (5)	168 (1)	76 (6)	60.5 (6)	126 (3)	106 (8)	67 (5)	N/A	N/A	N/A	N/A	N/A	N/A	133 (3)	N/A	123 (9)	35 (3)
Median observation time for mice not dying from disease	268 (9)	N/A	181 (3)	N/A	N/A	N/A	154 (1)	N/A	140 (3)	139.5 (2)	167 (5)	168 (5)	156. 5 (6)	146. 5 (4)	158 (4)	154 (4)	184 (1)	147.5 (2)
Blast %	n.d.	57 ± 7 (5)	12 ± 3 (5)	39 ± 11 (3)	6 ± 5 (2)	60 ± 9 (2)	92 ± 2 (4)	50 ± 15 (3)	n.d.	n.d.	n.d.	n.d.	n.d.	n.d.	1 ± 0 (2)	n.d.	60 ± 13.5 (2)	85 ± 9 (3)
% Gr-1^+ (BM)	16.7 ± 16.7 (2)	7.3 ± 2.4 (5)	2.2 ± 2.2 (3)	38.5 ± 10.6 (3)	1.1 ± 0.6 (2)	3.1 ± 2.9 (3)	11.3 ± 7.3 (8)	24.5 ± 9.7 (5)	3.9 ± 1.2 (3)	0.0 ± 0.0 (2)	0.4 ± 0.4 (2)	0.7 ± 0.4 (5)	0.5 ± 0.3 (3)	2.4 ± 2.4 (2)	2.7 ± 1.7 (3)	33.0 ± 11.4 (4)	1.1 ± 1.0 (5)	11.1 ± 5.9 (5)
% $CD11b^+$ (BM)	16.7 ± 16.7 (2)	26.1 ± 6.9 (5)	13.0 ± 12.2 (3)	82.2 ± 4.5 (3)	22.1 ± 1.3 (2)	6.9 ± 3.2 (3)	15.9 ± 5.4 (8)	68.0 ± 13.8 (5)	10.1± 6.3 (3)	0.0 ± 0.0 (2)	33.3 (1)	1.2 ± 0.5 (5)	3.0 ± 0.9 (3)	1.5 ± 1.5 (2)	22.4 ± 14.8 (3)	34.2 ± 13.4 (4)	4.4 ± 2.7(5)	12.1 ± 5.8 (5)

Construct	CTL	MN1	MN1 Δ1	MN1 Δ2	MN1 Δ4	MN1 Δ5	MN1 Δ6	MN1 Δ7	MN1 Δ1-2	MN1 Δ1-3	MN1 Δ1-4	MN1 Δ1-5	MN1 Δ1-6	MN1 Δ2-7	MN1 Δ3-7	MN1 Δ4-7	MN1 Δ5-7	MN1 Δ6-7
% Gr-1$^+$CD11b$^+$ (BM)	16.7 ± 16.7 (2)	8.5 ± 2.8 (5)	24.3 ± 19.2 (3)	39.4 ± 10.6 (3)	14.3 ± 12.5 (2)	3.4 ± 3.00 (3)	6.8 ± 2.7 (8)	26.9 ± 10.9 (5)	2.0 ± 1.3 (3)	0.0 ± 0.0 (2)	0.0 (1)	0.1 ± 0.1 (5)	0.1 ± 0.1 (3)	0.0 ± 0.0 (2)	14.6 ± 10.0 (3)	31.6 ± 11.9 (4)	14.0 ± 12.1 (5)	11.1 ± 5.9 (5)
% c-Kit$^+$ (BM)	0.0 ± 0.0 (2)	45.6 ± 12.6 (5)	5.4 ± 5.4 (3)	5.0 ± 2.6 (3)	40.3 ± 29.2 (2)	66.0 ± 4.5 (3)	49.7 ± 11.3 (8)	4.5 ± 2.1 (5)	3.3 ± 2.3 (3)	0.0 ± 0.0 (2)	0.0 (1)	0.5 ± 0.4 (5)	0.3 ± 0.3 (3)	0.0 ± 0.0 (2)	1.7 ± 1.1 (3)	2.8 ± 2.0 (3)	0.6 ± 0.3 (5)	64.0 ± 16.5 (5)
% sca1$^+$ (BM)	44.45 ± 44.45 (2)	24.86 ± 8.61 (5)	44.10 ± 15.23 (3)	6.35 ± 3.25 (3)	9.84 ± 3.47 (2)	40.50 ± 9.75 (3)	31.08 ± 10.23 (8)	10.2 ± 7.6 (5)	72.9± 8.4 (3)	62.5 ± 4.2 (2)	60.0 (1)	78.2 ± 5.7 (5)	56.0 ± 28.0 (3)	76.6 ± 2.7 (2)	25.7 ± 20.2 (3)	55.6 ± 15.7 (3)	38.9 ± 15.8 (5)	43.8 ± 10.2 (5)
% c-Kit$^+$sca1$^+$ (BM)	0.0 ± 0.0 (2)	8.4 ± 3.6 (5)	0.2 ± 0.2 (3)	0.4 ± 0.2 (3)	0.9 ± 0.0 (2)	32.6 ± 10.0 (3)	7.9 ± 4.4 (8)	2.1 ± 2.0 (5)	0.0 ± 0.0 (3)	0.0 ± 0.0 (2)	0.0 (1)	0.2 ± 0.2 (5)	0.0 ± 0.0 (3)	0.7 ± 0.7 (2)	0.1 ± 0.1 (3)	0.6 ± 0.6 (3)	0.6 ± 0.4 (5)	22.5 ± 6.9 (5)
% CD4$^+$ (BM)	20.9 ± 20.9 (2)	0.8 ± 0.3 (5)	35.7 ± 13.8 (3)	2.6 ± 1.1 (3)	7.5 ± 5.8 (2)	1.2 ± 0.7 (3)	6.1 ± 2.1 (8)	0.2 ± 0.1 (5)	43.3± 12.9 (3)	26.8 ± 26.8 (2)	41.7 (1)	25.0 ± 7.8 (5)	6.00 ± 2.4 (3)	18.1 ± 11.4 (2)	4.9 ± 3.1 (3)	19.4 ± 8.3 (3)	36.8 ± 9.9 (5)	2.0 ± 1.5 (5)
% CD8$^+$ (BM)	8.4 ± 8.4 (2)	0.3 ± 0.2 (5)	7.3 ± 4.1 (3)	1.2 ± 0.5 (3)	3.0 ± 0.9 (2)	0.8 ± 0.4 (3)	4.9 ± 3.0 (8)	0.8 ± 0.5 (5)	16.9± 5.9 (3)	13.3 ± 13.3 (2)	16.7 (1)	12.6 ± 3.4 (5)	6.3 ± 1.4 (3)	9.3 ± 5.9 (2)	4.3 ± 2.8 (3)	11.1 ± 3.3 (3)	39.6 ± 16.1 (5)	0.6 ± 0.5 (5)
% CD4$^+$CD8$^+$ (BM)	0.00 ± 0.00 (2)	0.03 ± 0.03 (5)	0.00 ± 0.00 (3)	0.29 ± 0.23 (3)	0.09 ± 0.09 (2)	0.07 ± 0.06 (3)	0.19 ± 0.13 (8)	0.01 ± 0.01 (5)	3.90 ± 3.90 (3)	0.00 ± 0.00 (2)	0.00 (1)	0.20 ± 0.20 (5)	0.00 ± 0.00 (3)	0.48 ± 0.48 (2)	0.02 ± 0.02 (3)	0.00 ± 0.00 (3)	22.70 ± 14.42 (5)	0.23 ± 0.22 (5)
Spleen weight at death (g)	0.06 ± 0.02	0.47 ± 0.02 (2)	n.d.	0.67 ± 0.41 (2)	1.00 ± 0.87 (2)	0.73 ± 0.10 (2)	0.20 ± 0.06 (7)	0.32 ± 0.08 (3)	n.d.	n.d.	n.d.	n.d.	n.d.	n.d.	0.48 (1)	n.d.	0.50 ± 0.22 (3)	0.31 ± 0.07 (3)

Construct		CTL	MN1	MN1 Δ1	MN1 Δ2	MN1 Δ4	MN1 Δ5	MN1 Δ6	MN1 Δ7	MN1 Δ1-2	MN1 Δ1-3	MN1 Δ1-4	MN1 Δ1-5	MN1 Δ1-6	MN1 Δ2-7	MN1 Δ3-7	MN1 Δ4-7	MN1 Δ5-7	MN1 Δ6-7
Secondary Transplants	No. of mice	0	6	5	3	3	0	0	0	0	0	0	0	0	0	7	0	6	4
	No. of mice dying from disease	0	6	0	3	3	0	0	0	0	0	0	0	0	0	7	0	6	4
	Median time of survival (d)	N/A	35 (6)	N/A	35 (3)	65 (3)	N/A	N/A	N/A	N/A	N/A	N/A	N/A	N/A	N/A	58 (7)	N/A	21.5 (6)	30 (4)
	Engraftment in BM at death (% GFP)	N/A	82.8 ± 15.4 (3)	30.1 ± 12.6 (5)	n.d.	62.9 ± 2.0 (3)	N/A	N/A	N/A	N/A	N/A	N/A	N/A	N/A	N/A	87.4 ± 5.3 (3)	N/A	67.5 ± 27.4 (3)	n.d.

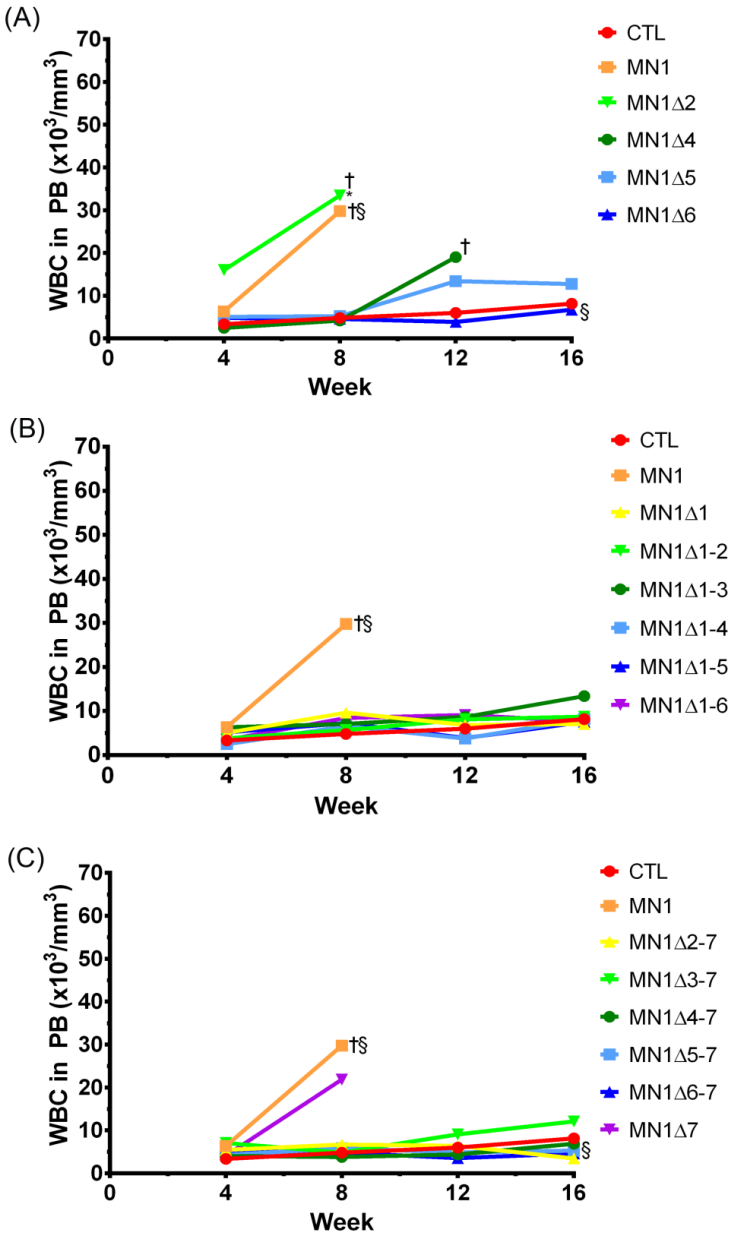

Figure 2.4 White blood cell count in transplanted mice

(A-C) White blood cell count (WBC) in peripheral blood of mice at 4-week intervals after transplantation. MN1 mutation constructs were used from (A) Strategy 1, (B) Strategy 2, and (C) Strategy 3. P values are given for the comparison of the indicated construct with CTL. The average WBC count is shown. Number of analyzed mice and standard error can be found in Table 2.5. § WBC count in peripheral blood at the indicated time point or at death in cases where a mouse died before that time point. † indicates that all mice were dead at this time point due to disease. * indicates $P<0.05$.

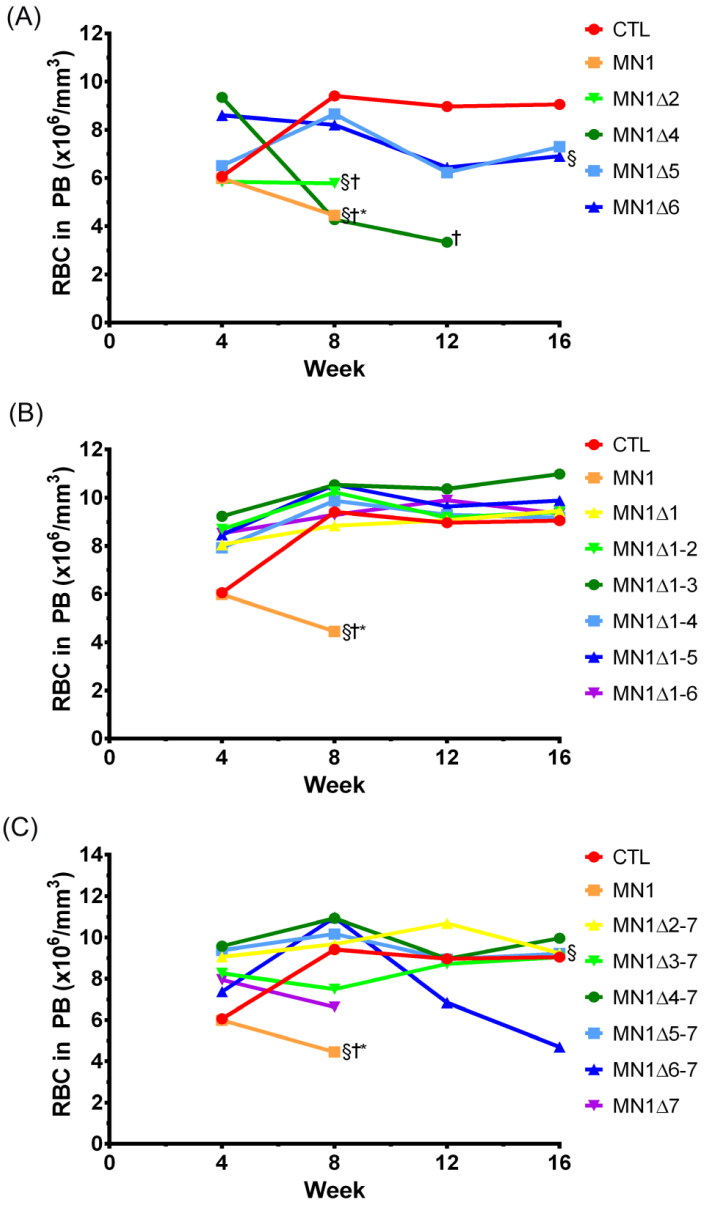

Figure 2.5 Red blood cell count in transplanted mice

(A-C) Red blood cell count (RBC) in peripheral blood of mice at 4 week intervals after transplantation. MN1 mutation constructs were used from (A) Strategy 1, (B) Strategy 2, and (C) Strategy 3. P values are given for the comparison of the indicated construct with CTL. The average RBC count is shown. Number of analyzed mice and standard error can be found in Table 2.5. § RBC count in peripheral blood at the indicated time point or at death in cases where a mouse died before that time point. † indicates that all mice were dead at this time point due to disease. * indicates $P<0.05$.

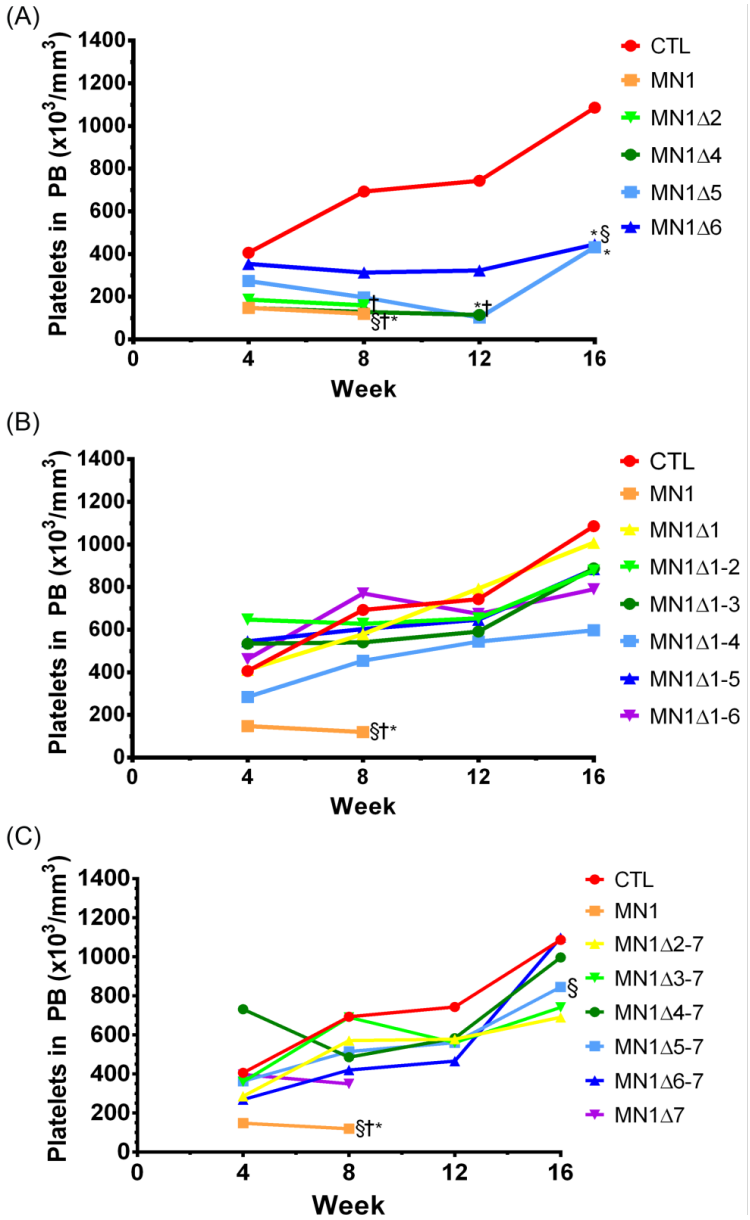

Figure 2.6 Platelet count in transplanted mice

(A-C) Platelet count in peripheral blood of mice at 4 week intervals after transplantation. MN1 mutation constructs were used from (A) Strategy 1, (B) Strategy 2, and (C) Strategy 3. P values are given for the comparison of the indicated construct with CTL. The average platelet count is shown. Number of analyzed mice and standard deviation (SD) can be found in Table 2.5. § Platelet count in peripheral blood at the indicated time point or at death in cases where a mouse died before that time point. † indicates that all mice were dead at this timepoint due to disease. * indicates $P<0.05$.

Table 2.4 *In vivo* engraftment of cells transduced with MN1 deletion constructs

Construct	No of Mice	Engraftment in Peripheral Blood (% GFP)				Engraftment in RBCs (% GFP)			Engraftment in RBCs (% GFP) / WBC (% GFP)		
		Wk 4	Wk 8	Wk 12	Wk 16	Wk 4	Wk 12	Wk 16	Wk 4	Wk 12	Wk 16
CTL	2	7.66	3.01 ± 1.46	1.31 ± 1.06	1.88 ± 0.86	4.94	0.09 ± 0.01	0.08 ± 0.01	0.64	0.07 ± 0.17	0.04 ± 0.03
MN1	5	35.00 ± 10.19	12.61 ± 3.59	n.d.	n.d.	14.13 ± 3.63	n.d.	n.d.	0.40 ± 0.19	n.d.	n.d.
MN1Δ1	5	40.44 ± 6.49	23.64 ± 2.09	15.08 ± 4.23	13.28 ± 3.44	21.67 ± 8.80	81.90 ± 0.40	91.65 ± 0.45	0.54 ± 0.27	5.43 ± 0.84	6.90 ± 1.20
MN1Δ2	3	84.07 ± 1.36	86.45 ± 5.95	n.d.	n.d.	73.73 ± 2.91	n.d.	n.d.	0.88 ± 0.05	n.d.	n.d.
MN1Δ4	5	57.00 ± 7.50	66.04 ± 3.16	57.05 ± 6.05	n.d.	75.55 ± 2.55	n.d.	n.d.	1.33	n.d.	n.d.
MN1Δ5	3	40.43 ± 5.72	27.90 ± 2.89	62.43 ± 15.09	54.65 ± 20.45	32.80 ± 11.24	88.67 ± 3.51	91.60 ± 2.70	0.81 ± 0.20	1.42 ± 0.30	1.68 ± 0.79
MN1Δ6	9	18.42 ± 4.47	15.63 ± 6.31	19.95 ± 6.90	42.40 ± 13.19	47.29 ± 10.29	2.29 ± 1.63	3.11 ± 1.69	2.57 ± 0.48	0.11 ± 0.14	0.16 ± 0.64
MN1Δ7	5	78.30 ± 1.11	71.30 ± 14.64	n.d.	n.d.	14.60 ± 5.61	n.d.	n.d.	0.19 ± 0.07	n.d.	n.d.
MN1Δ1-2	4	11.69 ± 2.37	6.93 ± 1.64	3.47 ± 1.42	3.03 ± 1.24	10.42 ± 0.96	3.62 ± 3.18	3.70 ± 3.65	0.89 ± 0.20	1.04 ± 0.49	1.22
MN1Δ1-3	3	n.d.	2.10 ± 0.91	0.80 ± 0.18	0.19	2.47 ± 1.21	n.d.	n.d.	n.d.	n.d.	n.d.
MN1Δ1-4	5	1.95 ± 0.29	0.99 ± 0.18	0.40 ± 0.16	0.17 ± 0.2	0.15 ± 0.07	n.d.	n.d.	0.08 ± 0.04	n.d.	n.d.
MN1Δ1-5	5	8.05 ± 1.87	4.66 ± 1.00	2.38 ± 0.84	1.29 ± 0.53	0.91 ± 0.34	n.d.	n.d.	0.11 ± 0.20	n.d.	n.d.
MN1Δ1-6	3	15.23 ± 2.36	5.90 ± 1.08	3.50 ± 0.89	2.16 ± 0.74	5.41 ± 1.22	n.d.	n.d.	0.35 ± 0.03	n.d.	n.d.

Construct	No of Mice	Engraftment in Peripheral Blood (% GFP)				Engraftment in RBCs (% GFP)			Engraftment in RBCs (% GFP) / WBC (% GFP)		
		Wk 4	Wk 8	Wk 12	Wk 16	Wk 4	Wk 12	Wk 16	Wk 4	Wk 12	Wk 16
MN1Δ2-7	2	4.47 ± 0.63	4.32 ± 0.49	2.47 ± 0.08	2.19 ± 1.55	2.97 ± 2.77	n.d.	n.d.	0.66 ± 0.73	n.d.	n.d.
MN1Δ3-7	3	69.20 ± 2.87	26.43 ± 7.44	33.88 ± 25.22	29.69 ± 24.60	1.98 ± 0.25	n.d.	n.d.	0.03 ± 0.00	n.d.	n.d.
MN1Δ4-7	4	26.37 ± 8.37	3.00 ± 2.27	7.34 ± 4.83	8.61 ± 2.85	10.67 ± 3.20	1.09	3.42 ± 3.09	0.40 ± 0.18	0.15 ± 0.02	0.40
MN1Δ5-7	8	11.31 ± 3.00	14.91 ± 4.63	13.11 ± 9.71	19.05 ± 9.91	18.17 ± 7.51	3.67 ± 3.58	0.00	1.61 ± 1.13	0.28 ± 0.14	0.00
MN1Δ6-7	5	39.28 ± 6.18	18.75 ± 5.95	6.17 ± 2.02	13.14 ± 5.57	17.56 ± 2.97	15.95 ± 0.45	0.28 ± 0.21	0.45 ± 0.12	2.59 ± 0.87	0.02 ± 0.01

Table 2.5 Peripheral blood counts in mice receiving transplants of cells transduced with MN1 deletion constructs

Construct	No of Mice	WBC (x10^3/mm^3)					RBC (x10^6/mm^3)				
		Wk 4	Wk 8	Wk 12	Wk 16	Wk 20	Wk 4	Wk 8	Wk 12	Wk 16	Wk 20
CTL	2	3.35 ± 0.55	4.80 ± 0.40	6.00 ± 0.60	8.15 ± 1.75	n.d.	6.06 ± 2.96	9.41 ± 0.10	8.97 ± 0.02	9.05 ± 0.77	n.d.
MN1	5	6.34 ± 1.01	n.d.	n.d.	n.d.	n.d.	5.99 ± 1.00	n.d.	n.d.	n.d.	n.d.
MN1 Δ1	5	5.06 ± 0.65	9.62 ± 0.96	6.86 ± 1.34	7.08 ± 0.70	5.42 ± 0.53	8.05 ± 0.92	8.84 ± 0.81	9.07 ± 0.21	9.45 ± 0.42	6.24 ± 0.39
MN1 Δ2	3	16.00 ± 0.61	33.47 ± 13.18	n.d.	n.d.	n.d.	5.85 ± 0.60	5.78 ± 0.94	n.d.	n.d.	n.d.
MN1 Δ4	2	2.50 ± 0.10	4.20 ± 0.60	19.05 ± 3.45	n.d.	n.d.	9.35 ± 0.14	4.28 ± 0.01	3.34 ± 1.20	n.d.	n.d.
MN1 Δ5	3	5.07 ± 0.94	5.23 ± 0.61	13.40 ± 9.46	12.73 ± 4.89	n.d.	6.51 ± 1.90	8.65 ± 1.09	6.22 ± 1.20	7.30 ± 1.27	n.d.
MN1 Δ6	9	4.79 ± 0.58	4.59 ± 0.56	3.88 ± 0.82	6.74 ± 0.52	0.82	8.60 ± 0.71	8.20 ± 0.79	6.44 ± 1.06	6.91 ± 1.45	n.d.
MN1 Δ7	5	4.08 ± 0.40	106.72 ± 58.00	n.d.	n.d.	n.d.	7.95 ± 0.28	6.63 ± 1.37	n.d.	n.d.	n.d.
MN1Δ1-2	4	3.80 ± 0.38	5.68 ± 0.71	8.13 ± 0.50	8.73 ±0.74	n.d.	8.69 ± 0.90	10.23 ± 0.28	9.17 ± 0.35	9.40 ± 0.14	n.d.
MN1Δ1-3	3	6.30 ± 2.42	7.07 ± 0.64	8.67 ± 0.90	13.40	n.d.	9.23 ± 0.04	10.53 ± 0.53	10.37 ± 0.79	10.98	n.d.
MN1Δ1-4	5	2.50 ± 0.29	6.58 ± 0.78	3.78 ± 0.58	8.20 ± 1.39	n.d.	7.93 ± 0.80	9.87 ± 0.81	9.29 ± 0.26	9.17 ± 0.50	n.d.
MN1Δ1-5	5	5.18 ± 1.05	7.24 ± 0.66	3.88 ± 0.85	7.56 ± 0.38	n.d.	8.46 ± 0.41	10.55 ± 0.23	9.63 ± 0.21	9.88 ± 0.41	n.d.
MN1Δ1-6	3	3.50 ± 0.55	8.43 ± 2.06	9.10 ± 0.75	7.67 ± 1.99	n.d.	8.53 ± 0.19	9.29 ± 0.16	9.90 ± 0.09	9.33 ± 0.41	n.d.

Construct	No of Mice	WBC ($x10^3/mm^3$)					RBC ($x10^6/mm^3$)				
		Wk 4	**Wk 8**	**Wk 12**	**Wk 16**	**Wk 20**	**Wk 4**	**Wk 8**	**Wk 12**	**Wk 16**	**Wk 20**
MN1Δ2-7	2	5.45 ± 3.65	6.70 ± 3.00	6.40 ± 1.70	3.45 ± 0.05	n.d.	9.06 ± 0.28	9.67 ± 0.27	10.69 ± 0.04	9.23 ± 0.40	n.d.
MN1Δ3-7	3	7.07 ± 0.87	4.83 ± 0.90	9.07 ± 0.91	12.10 ± 3.20	n.d.	8.26 ± 0.45	7.50 ± 1.61	8.72 ± 0.44	9.04 ± 0.50	n.d.
MN1Δ4-7	4	4.03 ± 0.66	3.80 ± 0.31	4.40 ± 0.71	6.90 ± 0.86	n.d.	9.57 ± 0.43	10.93 ± 0.64	8.97 ± 0.14	9.96 ± 0.26	n.d.
MN1Δ5-7	8	4.29 ± 0.59	5.83 ± 0.78	5.14 ± 0.67	6.63 ± 0.96	3.67 ± 0.27	9.37 ± 0.23	10.17 ± 0.84	8.94 ± 0.49	9.21 ± 0.72	5.64 ± 0.90
MN1Δ6-7	5	5.24 ± 0.81	4.80 ± 0.40	3.55 ± 1.25	4.60 ± 2.40	n.d.	7.37 ± 1.27	10.97 ± 0.55	6.84 ± 1.52	4.69 ± 3.37	n.d.
Construct	**No of Mice**	**Hemoglobin (g/dl)**					**Platelets ($x10^3/mm^3$)**				
		Wk 4	**Wk 8**	**Wk 12**	**Wk 16**	**Wk 20**	**Wk 4**	**Wk 8**	**Wk 12**	**Wk 16**	**Wk 20**
CTL	2	9.60 ± 4.70	13.15 ± 0.35	13.10 ± 0.10	13.55 ± 1.35	n.d.	406.00 ± 232.00	693.00 ± 117.00	743.00 ± 7.00	1086.00 ± 138.00	n.d.
MN1	5	8.94 ±1.50	n.d.	n.d.	n.d.	n.d.	148.00 ±26.13	n.d.	n.d.	n.d.	n.d.
MN1 Δ1	5	12.42 ± 1.33	12.28 ± 0.55	11.98 ± 0.39	12.72 ± 0.69	9.42 ± 0.56	411.20 ± 81.49	579.20 ± 67.90	792.80 ± 79.24	1007.80 ± 126.23	415.40 ± 161.95
MN1 Δ2	3	9.90 ± 0.97	11.47 ± 1.74	n.d.	n.d.	n.d.	186.00 ± 24.58	159.67 ± 54.19	n.d.	n.d.	n.d.
MN1 Δ4	2	13.05 ± 0.25	6.85 ± 0.25	5.65 ± 1.25	n.d.	n.d.	147.00 ± 15.00	128.50 ± 26.50	114.50 ± 79.50	n.d.	n.d.
MN1 Δ5	3	10.00 ± 2.67	11.80 ± 1.42	8.93 ± 1.30	10.20 ± 0.74	n.d.	273.00 ± 69.48	197.00 ± 37.99	102.00 ± 8.50	431.67 ± 343.32	n.d.
MN1 Δ6	9	12.94 ± 1.05	11.42 ± 0.96	8.81 ± 1.71	10.74 ± 1.98	n.d.	353.78 ± 70.56	313.22 ± 63.98	322.89 ± 91.14	445.00 ± 171.72	n.d.

Construct	No of Mice	Hemoglobin (g/dl)					Platelets (x10^3/mm^3)				
		Wk 4	**Wk 8**	**Wk 12**	**Wk 16**	**Wk 20**	**Wk 4**	**Wk 8**	**Wk 12**	**Wk 16**	**Wk 20**
MN1 Δ7	5	12.74 ± 0.38	11.06 ± 2.03	n.d.	n.d.	n.d.	397.60 ± 98.13	349.80 ± 100.31	n.d.	n.d.	n.d.
MN1Δ1-2	4	13.10 ± 1.52	14.18 ± 0.27	13.33 ± 0.52	14.07 ± 0.35	n.d.	647.75 ± 131.82	627.50 ± 38.50	653.67 ± 11.86	877.33 ± 15.38	n.d.
MN1Δ1-3	3	13.73 ± 0.12	15.67 ± 0.76	14.37 ± 0.99	15.60	n.d.	534.00 ± 59.56	540.67 ± 88.91	591.00 ± 57.49	888.00	n.d.
MN1Δ1-4	5	11.98 ± 1.00	15.30 ± 1.46	13.05 ± 0.19	13.50 ± 0.39	n.d.	284.40 ± 58.38	454.60 ± 88.87	544.00 ± 141.55	597.40 ± 141.54	n.d.
MN1Δ1-5	5	12.90 ± 0.56	15.58 ± 0.49	13.06 ± 0.13	14.08 ± 0.28	n.d.	545.20 ± 31.72	603.40 ± 34.92	646.60 ± 64.28	884.20 ± 64.02	n.d.
MN1Δ1-6	3	12.80 ± 0.06	14.07 ± 0.12	13.87 ± 0.09	13.23 ± 0.58	n.d.	461.67 ± 75.50	770.33 ± 148.71	674.33 ± 42.01	789.67 ± 192.61 n.d.	n.d.
MN1Δ2-7	2	13.65 ± 0.75	14.90 ± 0.30	14.85 ± 0.15	13.40 ± 0.60	n.d.	286.00 ± 26.00	570.50 ± 94.50	578.00 ± 87.00	690.00 ± 47.00	n.d.
MN1Δ3-7	3	13.07 ± 0.35	11.60 ± 2.35	12.27 ± 0.45	12.97 ± 0.44	n.d.	360.33 ± 34.23	690.00 ± 68.54	560.33 ± 119.56	740.67 ± 71.51	n.d.
MN1Δ4-7	4	15.18 ± 0.67	15.58 ± 1.23	13.50 ± 0.21	15.15 ± 0.41	n.d.	731.75 ± 147.96	486.00 ± 37.25	582.75 ± 50.43	996.25 ± 69.13	n.d.
MN1Δ5-7	8	14.04 ± 0.40	15.43 ± 1.20	12.32 ± 0.87	13.18 ± 1.18	9.20 ± 1.19	362.38 ± 65.08	514.83 ± 119.93	560.00 ± 56.52	845.25 ± 117.41	174.33 ± 41.07
MN1Δ6-7	5	11.02 ± 1.81	15.50 ± 0.70	10.25 ± 1.85	7.65 ± 5.05	n.d.	269.00 ± 103.45	420.00 ± 181.00	465.65 ± 464.35	1098.00 ± 1071.00	n.d.

Table 2.6 Immunophenotype of GFP-positive cells in peripheral blood of mice receiving transplants of cells transduced with MN1 deletion constructs

Construct			CTL	MN1	MN1 Δ1	MN1 Δ2	MN1 Δ4	MN1 Δ5	MN1 Δ6	MN1 Δ7	MN1 Δ1-2	MN1 Δ1-3	MN1 Δ1-4	MN1 Δ1-5	MN1 Δ1-6	MN1 Δ2-7	MN1 Δ3-7	MN1 Δ4-7	MN1 Δ5-7	MN1 Δ6-7
No of Mice			2	6	2	3	2	3	9	5	4	3	5	5	3	2	3	4	8	5
% Gr-1$^+$	Week	4	0.00	11.78 ± 0.99	17.49 ± 5.42	64.63 ± 2.98	11.37 ± 2.83	33.30 ± 4.76	32.24 ± 9.73	47.84 ± 11.78	10.67 ± 3.25	16.07 ± 10.46	0.72	7.45 ± 3.18	3.32 ± 1.57	n.d.	16.93 ± 3.90	13.93 ± 7.22	10.88 ± 6.84	20.12 ± 11.81
		8	0.54 ± 0.54	1.99 ± 0.99	1.94 ± 0.73	27.95 ± 0.15	20.85 ± 2.25	0.74 ± 0.18	8.60 ± 3.28	41.88 ± 10.73	12.58 ± 7.27	2.78 ± 2.78	n.d.	4.07 ± 0.86	1.12 ± 0.37	2.84 ± 0.39	11.15 ± 8.08	6.68 ± 6.68	n.d.	15.66 ± 14.25
		12	16.65 ± 16.65	n.d.	18.62 ± 11.59	n.d.	0.45 ± 0.04	23.35 ± 8.89	17.35 ± 10.15	n.d.	n.d.	0.00 ± 0.00	0.00	0.29 ± 0.29	0.53 ± 0.22	2.44 ± 2.44	0.59 ± 0.33	18.50 ± 16.27	0.14 ± 0.14	0.00 ± 0.00
		16	n.d.	n.d.	13.61 ± 9.62	n.d.	n.d.	5.89 ± 5.42	0.11	n.d.	3.86 ± 1.15	n.d.	n.d.	n.d.	n.d.	n.d.	33.54 ± 27.66	50.90	7.93 ± 3.08	21.90 ± 11.40
% CD11b$^+$	Week	4	6.82	28.80 ± 4.53	25.04 ± 8.40	78.50 ± 3.50	23.65 ± 4.15	49.80 ± 6.11	35.74 ± 9.65	62.92 ± 12.75	19.33 ± 4.89	25.00 ± 14.43	n.d.	8.60 ± 1.64	8.47 ± 1.15	n.d.	27.80 ± 3.27	20.35 ± 8.86	12.25 ± 7.37	29.54 ± 13.68
		8	4.17 ± 4.17	14.45 ± 4.25	3.25 ± 0.51	83.85 ± 7.25	28.50 ± 2.30	9.04 ± 3.13	10.23 ± 3.04	83.18 ± 5.28	20.42 ± 10.85	0.00 ± 0.00	n.d.	2.97 ± 1.31	1.79 ± 0.46	5.28 ± 2.05	10.39 ± 7.37	11.43 ± 3.38	n.d.	20.47 ± 17.43
		12	19.78 ± 13.53	n.d.	22.63 ± 13.18	n.d.	19.35 ± 1.45	32.07 ± 11.82	24.72 ± 10.80	n.d.	n.d.	1.45 ± 1.45	33.30	0.98 ± 0.57	3.00 ± 0.66	1.45 ± 1.45	18.67 ± 16.66	33.17 ± 16.00	2.70 ± 1.48	18.13 ± 12.77
		16	0.00	n.d.	39.57 ± 20.60	n.d.	n.d.	15.93 ± 8.28	25.80 ± 8.14	n.d.	10.13 ± 6.31	n.d.	n.d.	n.d.	n.d.	n.d.	48.29 ± 42.41	54.70	15.39 ± 2.78	23.25 ± 10.05
% Gr-1$^+$/CD11b$^+$	Week	4	0.00	12.28 ± 0.97	15.18 ± 6.00	65.33 ± 2.90	11.37 ± 2.83	32.80 ± 4.80	20.05 ± 8.73	48.44 ± 12.00	10.30 ± 3.17	11.90 ± 11.90	n.d.	6.08 ± 1.83	3.13 ± 2.21	n.d.	20.25 ± 3.55	11.53 ± 7.88	10.68 ± .77	20.16 ± 11.92
		8	4.44 ± 3.90	1.68 ± 0.17	9.18 ± 5.02	28.80 ± 0.20	20.40 ± 2.70	33.97 ± 17.19	27.04 ± 9.78	45.53 ± 10.55	12.93 ± 7.60	0.00 ± 0.00	n.d.	0.78 ± 0.78	0.61 ± 0.29	1.62 ± 1.62	9.30 ± 7.35	25.81 ± 15.77	n.d.	15.44 ± 14.27
		12	16.65 ± 16.65	n.d.	28.59 ± 16.46	n.d.	23.95 ± 2.85	24.12 ± 9.00	20.82 ± 9.95	n.d.	n.d.	0.00 ± 0.00	0.00	0.17 ± 0.17	0.14 ± 0.11	0.00 ± 0.00	38.77 ± 23.71	18.80 ± 16.57	39.04 ± 13.89	0.00 ± 0.00
		16	0.00	n.d.	18.30 ± 11.29	n.d.	n.d.	4.06 ± 3.21	11.48 ± 3.98	n.d.	2.01 ± 1.27	n.d.	n.d.	n.d.	n.d.	n.d.	37.64 ± 31.76	27.57 ± 14.85	6.35 ± 6.35	21.90 ± 11.40

Construct			CTL	MN1	MN1 Δ1	MN1 Δ2	MN1 Δ4	MN1 Δ5	MN1 Δ6	MN1 Δ7	MN1 Δ1-2	MN1 Δ1-3	MN1 Δ1-4	MN1 Δ1-5	MN1 Δ1-6	MN1 Δ2-7	MN1 Δ3-7	MN1 Δ4-7	MN1 Δ5-7	MN1 Δ6-7
% c-Kit.	Week	4	0.00	20.54 ± 7.76	14.84 ± 14.57	7.00 ± 1.78	0.53 ± 0.53	2.69 ± 0.81	7.27 ± 3.77	4.64 ± 1.89	2.12 ± 0.28	2.08 ± 2.08	n.d.	0.00 ± 0.00	0.35 ± 0.31	n.d.	0.99 ± 0.33	13.90 ± 10.29	0.28 ± 0.17	46.68 ± 17.69
		8	0.24 ± 0.24	71.60 ± 8.80	0.42 ± 0.16	1.30	2.18 ± 2.18	3.93 ± 1.96	19.83 ± 7.33	1.45 ± 0.60	0.10 ± 0.10	0.00	n.d.	0.80 ± 0.80	0.00 ± 0.00	1.07 ± 1.07	0.30 ± 0.25	0.00 ± 0.00	n.d.	2.71 ± 2.47
		12	0.00 ± 0.00	n.d.	1.31 ± 0.61	n.d.	28.95 ± 17.85	36.90 ± 13.84	29.52 ± 9.64	n.d.	n.d.	0.00 ± 0.00	0.00	0.46 ± 0.37	0.27 ± 0.21	0.00 ± 0.00	0.59± 0.34	27.41 ± 26.50	0.18 ± 0.09	14.86 ± 9.14
		16	0.00	n.d.	6.50 ± 5.08	n.d.	n.d.	57.20 ± 17.70	77.60	n.d.	3.34 ± 2.28	n.d.	n.d.	n.d.	n.d.	n.d.	0.00 ± 0.00	2.78 ± 2.00	2.14 ± 1.08	43.96 ± 34.64
% sca1$^+$	Week	4	0.00	40.06 ± 5.00	58.38 ± 15.00	5.61 ± 3.25	34.40 ± 6.00	53.63 ± 2.39	59.59 ± 9.27	24.28 ± 5.72	56.90 ± 4.26	78.13 ± 9.68	n.d.	65.70 ± 17.78	72.40 ± 5.51	n.d.	56.67 ± 8.75	51.74 ± 25.41	55.18 ± 9.59	32.22 ± 9.32
		8	0.24 ± 0.24	7.06 ± 2.79	69.36 ± 9.59	7.04	34.50 ± 9.90	42.47 ± 21.39	31.33 ± 8.59	3.77 ± 1.57	44.65 ± 4.26	66.70	n.d.	86.70 ± 4.20	85.20 ± 1.21	89.45 ± 4.15	68.83 ± 12.40	51.17 ± 15.60	n.d.	64.15 ± 16.15
		12	0.00 ± 0.00	n.d.	44.90 ± 14.69	n.d.	8.64 ± 4.67	33.40 ± 1.19	29.17 ± 11.81	n.d.	n.d.	73.40 ± 11.17	60.00	78.24 ± 5.69	55.97 ± 21.69	76.60 ± 2.70	33.69 ± 22.53	28.73 ± 15.53	25.37 ± 6.21	35.20 ± 2.80
		16	88.90	n.d.	45.93 ± 13.99	n.d.	n.d.	43.10 ± 12.70	53.90 ± 10.57	n.d.	72.87 ± 8.40	n.d.	n.d.	n.d.	n.d.	n.d.	35.27 ± 30.63	55.63 ± 15.68	54.85 ± 8.65	54.70 ± 19.00
% c-Kit$^+$/ sca1$^+$	Week	4	0.00	8.10 ± 3.72	0.67 ± 0.29	0.48 ± 0.13	0.53 ± 0.53	2.16 ± 0.13	4.47 ± 3.12	2.20 ± 1.93	0.28 ± 0.07	0.00 ± 0.00	n.d.	0.00 ± 0.00	0.35 ± 0.31	n.d.	0.78 ± 0.55	1.56 ± 1.17	0.15 ± 0.09	14.62 ± 7.29
		8	0.24 ± 0.24	3.78 ± 1.30	0.39 ± 0.26	0.03	0.00 ± 0.00	5.52 ± 3.36	3.37 ± 1.50	0.20 ± 0.10	0.00 ± 0.00	0.00	n.d.	0.80 ± 0.80	0.16 ± 0.13	0.00 ± 0.00	0.59 ± 0.59	0.00 ± 0.00	n.d.	0.90 ± 0.90
		12	0.00 ± 0.00	n.d.	0.22 ± 0.15	n.d.	2.37 ± 1.45	15.80 ± 5.58	4.99 ± 1.43	n.d.	n.d.	0.00 ± 0.00	0.00	0.21 ± 0.21	0.00 ± 0.00	0.73 ± 0.73	0.08 ± 0.06	0.06 ± 0.06	0.05 ± 0.05	1.09 ± 1.09
		16	0.00	n.d.	0.24 ± 0.24	n.d.	n.d.	16.55 ± 2.55	13.21 ± 8.48	n.d.	0.00 ± 0.00	0.00 ± 0.00	n.d.	n.d.	n.d.	n.d.	0.00 ± 0.00	0.56 ± 0.56	1.36 ± 0.46	12.82 ± 8.58

Construct			CTL	MN1	MN1 Δ1	MN1 Δ2	MN1 Δ4	MN1 Δ5	MN1 Δ6	MN1 Δ7	MN1 Δ1-2	MN1 Δ1-3	MN1 Δ1-4	MN1 Δ1-5	MN1 Δ1-6	MN1 Δ2-7	MN1 Δ3-7	MN1 Δ4-7	MN1 Δ5-7	MN1 Δ6-7
CD4$^+$	**Week**	**4**	5.56	1.52 ± 0.49	11.91 ± 2.50	4.75 ± 0.19	3.21 ± 1.06	4.32 ± 1.86	20.90 ± 6.56	2.76 ± 1.02	9.48 ± 3.51	9.44 ± 3.78	n.d.	18.56 ± 8.93	5.80 ± 2.61	n.d.	20.47 ± 19.01	3.27 ± 2.26	15.62 ± 9.00	0.48 ± 0.36
		8	24.67 ± 17.53	0.62 ± 0.20	23.56 ± 7.56	1.76 ± 0.98	6.37 ± 0.30	5.88 ± 1.56	6.22 ± 2.82	0.26 ± 0.09	29.30 ± 9.28	15.40	n.d.	22.07 ± 17.53	12.05 ± 1.24	13.85 ± 11.15	12.57 ± 3.49	24.54 ± 8.13	n.d.	2.92 ± 0.93
		12	22.75 ± 22.75	n.d.	35.18 ± 13.01	n.d.	7.59 ± 5.72	6.43 ± 2.98	11.12 ± 6.18	n.d.	n.d.	26.80 ± 26.80	41.70	24.99 ± 7.75	5.96 ± 1.82	18.09 ± 11.42	14.60 ± 12.20	27.36 ± 10.62	7.10 ± 2.68	3.39
		16	41.70	n.d.	21.41 ± 11.52	n.d.	n.d.	2.74 ± 0.49	10.48 ± 2.69	n.d.	43.30 ± 12.86	n.d.	n.d.	n.d.	n.d.	n.d.	5.63 ± 4.87	19.37 ± 8.26	22.68 ± 1.97	3.95 ± 3.95

All transplantation groups were fully characterized at time of sacrifice including bone marrow morphology with blast count, immunophenotype of GFP^+ bone marrow cells, spleen weight and (for most constructs) secondary transplantations (Table 2.3). For mice succumbing to hematologic disease, the diagnosis is noted in Table 2.3 and supported by bone marrow morphology (Figure 2.1H). In summary, deletions including the first 221 N-terminal amino acids prevent MN1-induced AML, except one MN1Δ1 mouse that was sacrificed due to low engraftment, low white blood cell count, and a non-elevated blast count (Figure 2.1F). Confocal microscopy of cells expressing MN1Δ1 detects the protein in both the cytoplasm and the nucleus to a similar extent as MN1, suggesting that loss of this region does not impact the ability of the mutant to localize to the nucleus. (Figure 2.7). Deletion of regions 2, 5, 6, or 7 do not affect the ability of MN1 to induce AML, although their loss significantly prolongs disease latency (median disease latency of 76 days for MN1Δ2, 126 days for MN1Δ5, 162.5 days for MN1Δ6, and 67 days for MN1Δ7 versus 35 days for MN1, log-rank Mantel-Cox test, $P<0.05$) (Figure 2.1E). Deletion of region 4 results in a rapid disease onset (median 60.5 days) with low blast count, most likely a myelproliferative disease (Figure 2.1E and G). Combined deletion of regions 6 and 7 (MN1Δ6-7) at the C-terminus induces AML with 60% penetrance (Figure 2.1G). Interestingly, despite showing nuclear localization of the protein by confocal microscopy (Figure 2.7), deletion of regions 5-7 (MN1Δ5-7) at the C-terminus in two independent experiments results in T-lymphoblastic leukemia (see below). The minimal portion of MN1 with biologic function is MN1Δ3-7, corresponding to the 317 amino acids at the N-terminus, which induces a myeloproliferative disease with long latency (median 156 days) and 50% penetrance (Figure 2.1G). In summary, these data suggest that the N-terminus of MN1 is required and sufficient for its proliferation-enhancing function in vivo (see also Table 2.6).

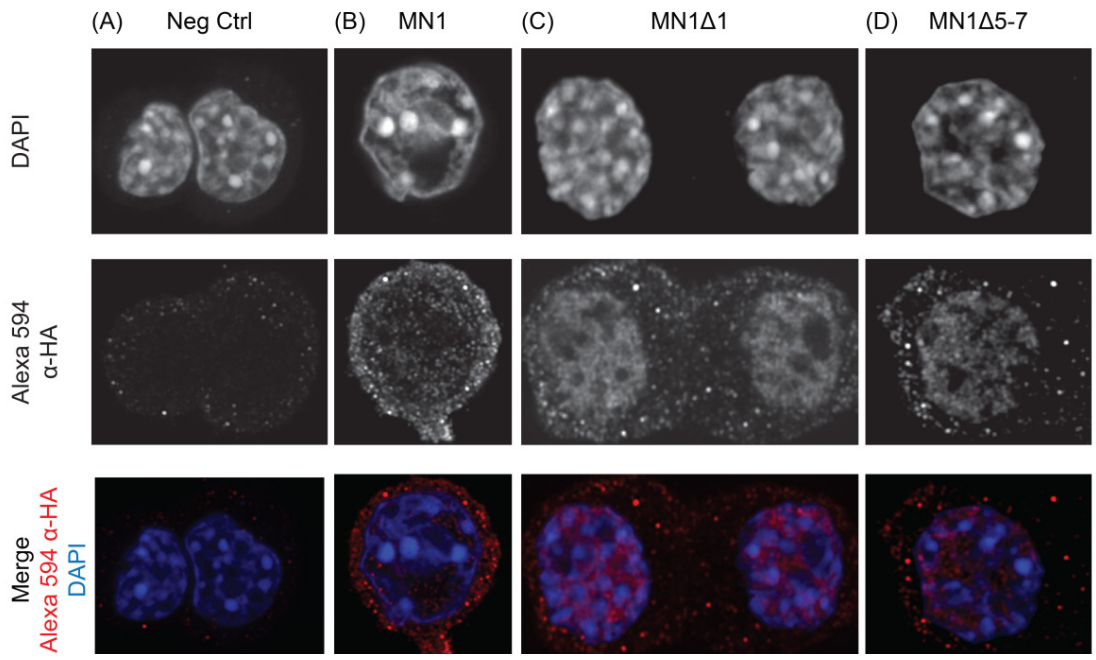

Figure 2.7 Confocal microscopy of MN1-transduced cells

Representative confocal microscopy images of GP+E86 cells transduced with (A) negative control, (B) MN1 tagged with an HA-tag, (C) MN1Δ1 with an HA-tag, and (D) MN1Δ5-7 with an HA-tag stained with (i) DAPI or (ii) anti-HA and (iii) DAPI and anti-HA merged.

Table 2.7 Role of MN1 regions in leukemia cell fate regulation

Phenotype	Required Domain(s)	Dispensable Domain(s)	Deletions likely too large to have any effect
Proliferation/Self-Renewal	1	One of: 3, 4, 5, 6, 7	2-7, 1-2, 1-3,1-4, 1-5, 1-6
Myeloid Differentiation Block	2, 7	One of: 1, 4, 5, 6	
Megakaryocyte/ Erythroid Differentiation Block	1	One of:2, 4, 5, 6, 7, 3-7, 5-7	
ATRA resistance	5, 6, 7	One of: 1, 2, 4	
Lymphoid Differentiation Block	5-7	One of:1, 2, 4	

2.3.3 The N-terminal region of MN1 is required to block megakaryocyte/erythroid differentiation

Peripheral blood analysis of mice transplanted with MN1 mutant-transduced bone marrow shows decreasing red blood cell engraftment in all but two constructs over the 16-week period or the lifetime of the mouse. MN1Δ2 and MN1Δ4 mice have high engraftment levels at 4 weeks corresponding to high engraftment in white blood cells (84.1 ± 1.4% and 57.0 ± 7.5%, respectively, versus 7.7% in control, unpaired t-test, $P<0.05$). Only two constructs, MN1Δ1 and MN1Δ5, show an increase in red blood cell engraftment over time (21.7 ± 8.8% to 91.7 ± 0.5% in MN1Δ1 and 32.8 ± 11.2% to 91.6 ± 2.7% in MN1Δ5, unpaired t-test, $P<0.05$), although the absolute number of red blood cells and hemoglobin does not increase in these mice (Figure 2.8A-C). When comparing the ratio of transgene positive red blood cells to white blood cells, MN1Δ1 and to a lesser extent MN1Δ5 are the only mutant constructs that show higher engraftment in red blood cells than white blood cells; a difference that increases over 16 weeks (ratio 0.7 in MN1Δ1 and 0.9 in MN1Δ5 at week 4 to 1.9 in MN1Δ1 and 1.2 in MN1Δ5 at week 16) (Figure 2.8D-F). To assess the ability of MN1 deletion mutants to support megakaryocyte differentiation, I performed colony-forming unit-megakaryocyte (CFU-Mk) assays of all internally-deleted (Strategy 1) and select N- and C-terminally deleted (Strategy 2 and 3) constructs. Control cells, but not full-length MN1 cells, form few, small CFU-Mk colonies. Like full-length MN1 cells, most MN1 deletion mutants are unable to form CFU-Mk colonies. However, N-terminally deleted (MN1Δ1) cells give rise to 2 to 3-fold more colonies and larger colonies than control-transduced cells, sustained over two replatings (32 versus 8 colonies at first plating, 24 versus 7 colonies at second plating) (Figure 2.8G and H). MN1Δ6-transduced cells also generate a small number of colonies (5 colonies in the first plating) (Figure 2.8G). Together, these experiments

suggest that the ability of MN1 to block erythroid-megakaryocyte differentiation can be localized to the N-terminus, with some contribution of regions 5 and 6 (see also Table 2.6).

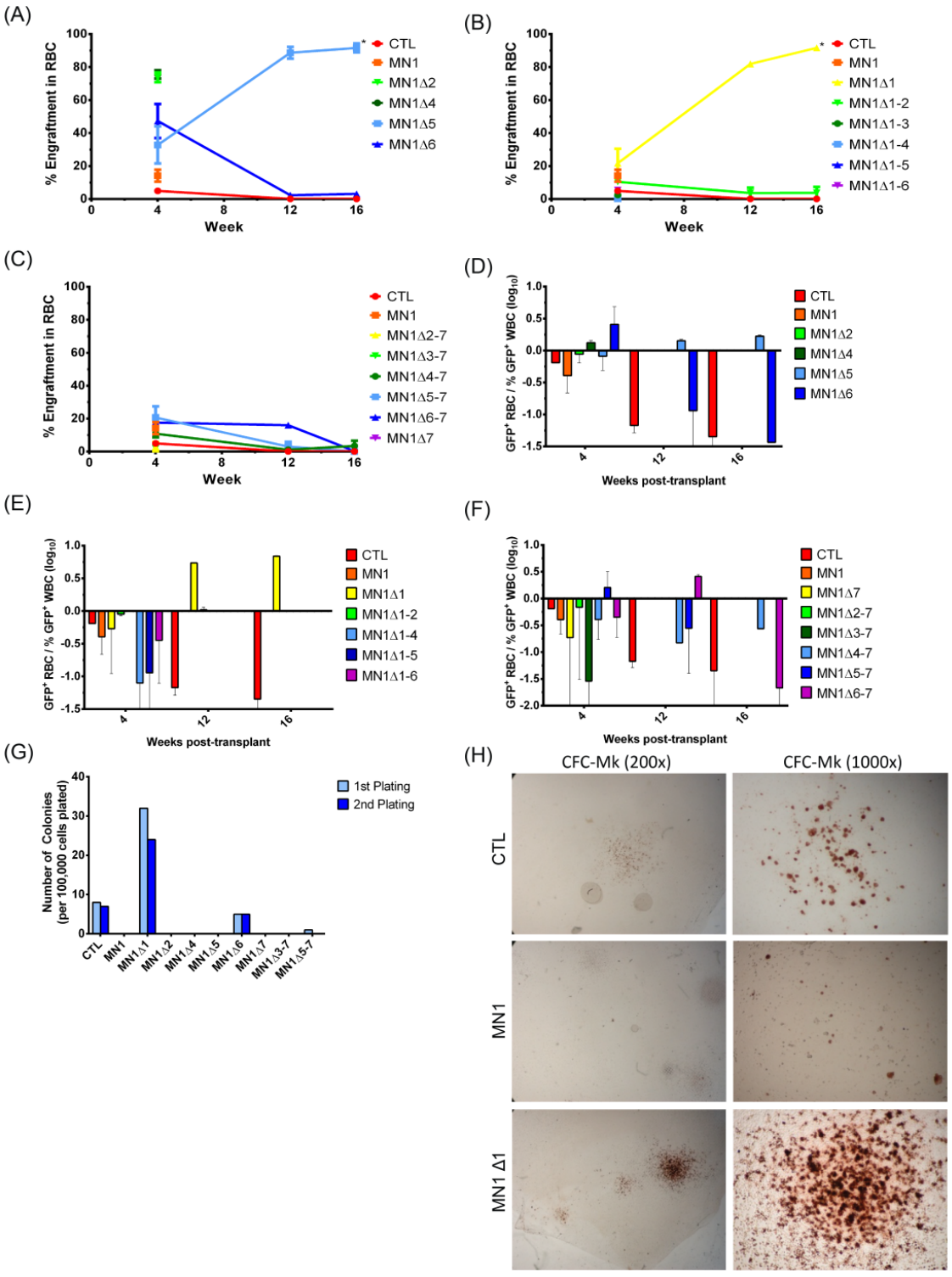

Figure 2.8 The N-terminal region of MN1 is required to block megakaryocyte/erythroid differentiation

(A-C) Percentage of transgene positive red blood cells engrafting in peripheral blood of transplanted mice at 4-week intervals. P values are calculated for the comparison of the indicated construct with CTL-transduced cells. The

number of analysed mice and standard error is detailed in Table 2.3. (D-F) Proportion of red blood cells (RBC) compared to white blood cells (WBC) expressing (D) Strategy 1, (E) Strategy 2, or (F) Strategy 3 MN1 deletion constructs after transplantation. P values are calculated for the comparison of the indicated construct with CTL-transduced cells. The number of analysed mice and standard error is detailed in Table 2.3. (G) Megakaryocyte colony-forming ability of mouse bone marrow cells transduced with MN1 deletion constructs (mean ± SD, n=4). (H) Micrographs of representative CFC-Mk slides at the end of the first plating of bone marrow cells transduced with CTL vector, full-length MN1 or MN1Δ1. Images were visualised using a Nikon Eclipse 80i microscope (Nikon, Mississauga, ON, Canada) and a 20x/0.40 numerical aperture objective, or a 100x/1.25 numerical aperture objective and Nikon Immersion Oil (Nikon). A Nikon Coolpix 995 camera (Nikon) was used to capture images. * indicates $P<0.05$

2.3.4 The C-terminal region of MN1 is required to block myeloid differentiation

To assess the effect of MN1 deletions on resistance to ATRA, ND13 bone marrow cells, previously reported to immortalize cells *in vitro*[75, 124], were transduced with each of the MN1 deletion mutants. ND13 control cells are sensitive to *in vitro* ATRA administration with an IC50 of 0.27 μM. ND13+MN1-transduced cells are highly resistant with an IC_{50} of 32.4 μM, while cells transduced with MN1 alone are even more ATRA resistant with an IC_{50} beyond 100 μM. When distinct regions are internally deleted from MN1 (Strategy1), loss of regions 2 or 4 have no effect on ATRA resistance (IC_{50} greater than 100μM and 44.7μM, respectively). (Figure 2.9A). However, loss of regions 5, 6, or 7 restore ATRA sensitivity of the cells (IC_{50} 0.83μM, 0.94μM, and 0.04μM, respectively) (Figure 2.9B). Progressive N-terminal deletions (Strategy 2) with 2 or more regions deleted from the N-terminus are sensitive to ATRA (IC_{50} less than 0.02μM for all Strategy 2 constructs) (Figure 2.9C-D). Additionally, constructs with cumulative deletions of the C-terminus (Strategy 3) are sensitive to ATRA (IC_{50} less than 0.9μM for all

Strategy 3 constructs) (Figure 2.9E-F), highlighting the importance of the most C-terminal 206 amino acids of MN1 for ATRA resistance. These data suggest that the MN1 C-terminus plays an important role in regulating resistance to ATRA in MN1 cells, with the MN1 N-terminus (amino acids 222-418) being important for maintaining functionality of the MN1 protein.

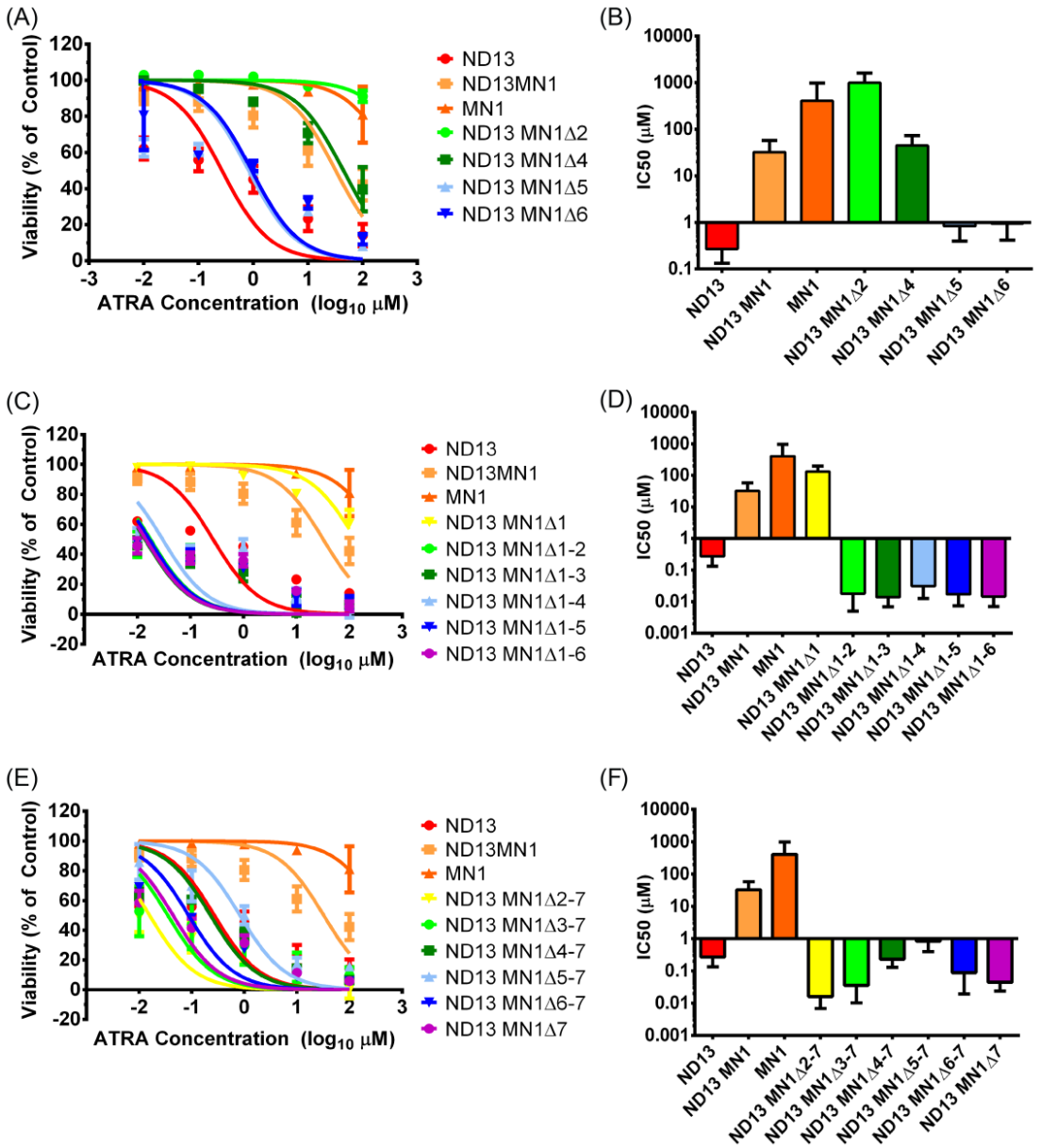

Figure 2.9 The C-terminal region of MN1 is required to block myeloid differentiation

(A-F) *In vitro* sensitivity to ATRA of ND13-immortalized cells that were transduced with MN1 deletion constructs. Dose-response curves are shown in the left panels (A, C, E) and IC_{50} values are shown in the right panels (B, D, F) for each deletion strategy (mean ± SD, n≥6).

I performed gene expression profiling on GFP-positive bulk MN1-, MN1Δ1- and MN1Δ7-transduced bone marrow cells, and normal Gr-1$^+$CD11b$^+$ differentiated myeloid cells sorted from bone marrow. Unsupervised hierarchical clustering shows that bulk C-terminally deleted MN1 cells (MN1Δ7, with an average 26.9% GFP$^+$/Gr-1$^+$/CD11b$^+$ population) cluster with Gr-1$^+$CD11b$^+$ normal myeloid cells, which have low Mn1 expression[128]. Alternatively, N-terminally deleted MN1 cells (MN1Δ1, with an average 24.3% GFP$^+$/Gr-1$^+$/CD11b$^+$ population) cluster with wildtype MN1 cells (Figure 2.10A). Comparison of the 60 most differentially expressed gene ontology gene sets between wildtype MN1 and MN1Δ1 or MN1Δ7 cells show that those related to differentiation and metabolism are overrepresented in MN1Δ7 cells compared to MN1Δ1 cells (Figure 2.10B and Table 2.8). Conversely, gene sets related to signal transduction and cell structure are overrepresented in MN1Δ1 cells (Figure 2.10B and Table 2.9). The most differentially expressed genes in MN1Δ1 compared to MN1 cells are *HOXA9*, *HOXA10* and *MEIS2* (Table located at http://dx.doi.org/10.1371/journal.pone.0112671), which are among the most important genes driving self-renewal of HSCs, and their low expression in MN1Δ1 cells may explain their loss of leukemogenic potential. Several Krüppel-like factors are also upregulated in MN1Δ1 cells, providing a link for their preferential erythroid differentiation. Among the most differentially upregulated genes in MN1Δ7 compared to full-length MN1 cells are 3 members of the eosinophil cationic protein (*Ecp* or *Ear1*, *2*, *3*) and eosinophil peroxidase (Table located at http://dx.doi.org/10.1371/journal.pone.0112671).

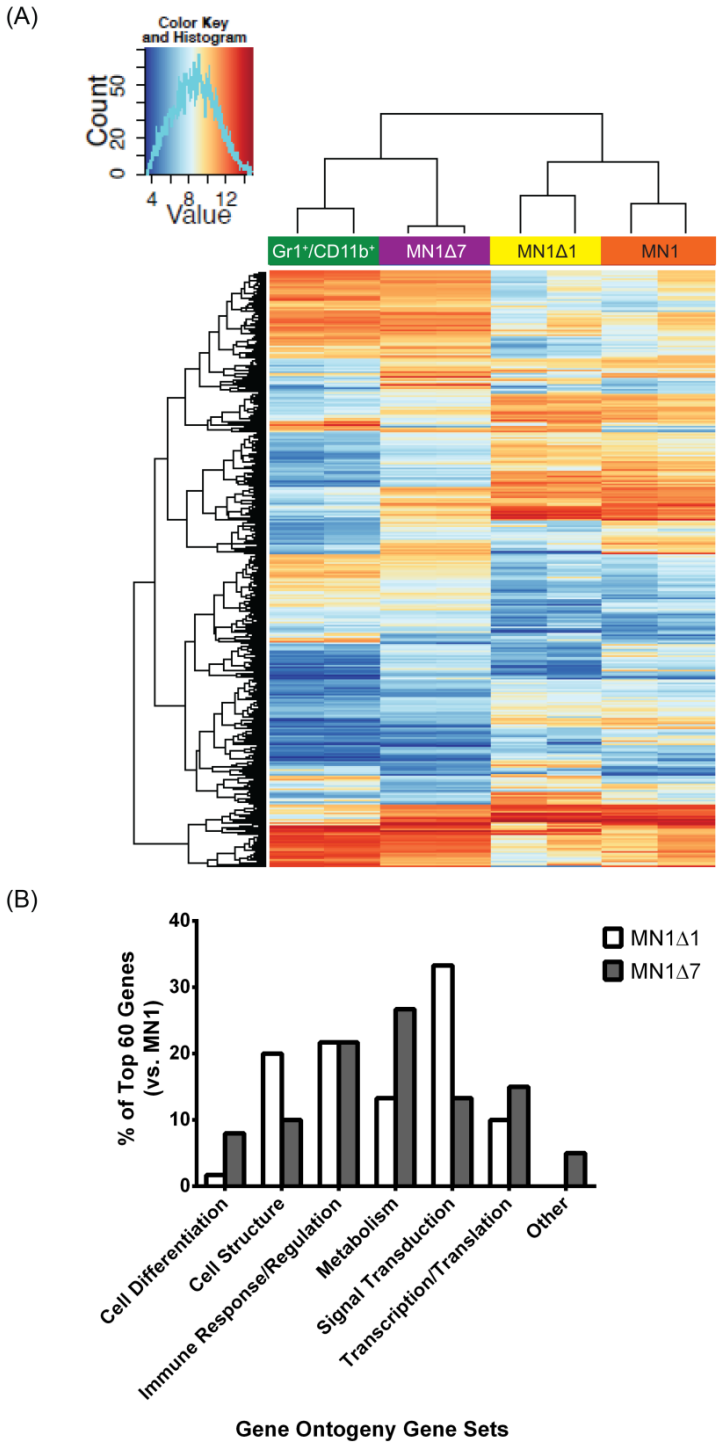

Figure 2.10 Hierarchical clustering of cells with N- and C-terminally deleted MN1

(A) Heat map of differentially regulated pathways for enhanced proliferation and blocked differentiation. (B) Comparison of top 60 enriched gene ontology gene sets for the comparison of MN1Δ1 and MN1Δ7 with full-length MN1.

Table 2.6 Gene ontology gene sets enriched in MN1Δ7 cells compared to MN1 cells

Rank	Gene Sets	Normalised Enrichment Score (NES)	P	Category
1	OXYGEN_AND_REACTIVE_OXYGEN_SPECIES_METABOLIC_PROCESS	1.45	0.0	metabolism
2	REGULATION_OF_NEUROTRANSMITTER_LEVELS	1.44	0.0	signal transduction
3	CHEMOKINE_ACTIVITY	1.40	0.0	immune response / regulation
4	BIOGENIC_AMINE_METABOLIC_PROCESS	1.36	0.0	metabolism
5	G_PROTEIN_COUPLED_RECEPTOR_BINDING	1.35	0.0	signal transduction
6	CYTOKINE_ACTIVITY	1.31	0.0	immune response / regulation
7	VOLTAGE_GATED_CATION_CHANNEL_ACTIVITY	1.31	0.0	signal transduction
8	VOLTAGE_GATED_CHANNEL_ACTIVITY	1.31	0.0	signal transduction
9	VOLTAGE_GATED_POTASSIUM_CHANNEL_ACTIVITY	1.30	0.0	signal transduction
10	LIGAND_DEPENDENT_NUCLEAR_RECEPTOR_ACTIVITY	1.30	0.0	signal transduction
11	REGULATION_OF_BLOOD_PRESSURE	1.30	0.0	Other
12	AMINO_ACID_DERIVATIVE_METABOLIC_PROCESS	1.30	0.0	metabolism
13	EXOCYTOSIS	1.29	0.0	cell structure
14	CHEMOKINE_RECEPTOR_BINDING	1.29	0.0	immune response / regulation
15	HEMATOPOIETIN_INTERFERON_CLASSD200_DOMAIN_CYTOKINE_RECEPTOR_BINDING	1.24	0.0	immune response / regulation
16	HORMONE_METABOLIC_PROCESS	1.23	0.2073922	metabolism
17	TRANSCRIPTION_CO-FACTOR_ACTIVITY	1.22	0.0	transcription/translation
18	AXON_GUIDANCE	1.22	0.0	cell structure
19	GROWTH_FACTOR_ACTIVITY	1.21	0.09128631	immune response / regulation
20	MESODERM_DEVELOPMENT	1.20	0.0	cell differentiation
21	REGULATION_OF_DNA_METABOLIC_PROCESS	1.20	0.26868686	metabolism

Rank	Gene Sets	Normalised Enrichment Score (NES)	P	Category
22	REGULATION_OF_IMMUNE_RESPONSE	1.20	0.09034908	immune response / regulation
23	TRANSLATION	1.19	0.09128631	transcription/translation
24	TRANSCRIPTION_COREPRESSOR_ACTIVITY	1.19	0.0	transcription/translation
25	ANTIOXIDANT_ACTIVITY	1.19	0.19507186	metabolism
26	SODIUM_ION_TRANSPORT	1.19	0.0	signal transduction
27	NEGATIVE_REGULATION_OF_BIOSYNTHETIC_PROCESS	1.19	0.0	metabolism
28	REGULATION_OF_CELL_DIFFERENTIATION	1.18	0.0	cell differentiation
29	NEGATIVE_REGULATION_OF_CELLULAR_BIOSYNTHETIC_PROCESS	1.18	0.0	metabolism
30	RESPONSE_TO_OXIDATIVE_STRESS	1.18	0.178	metabolism
31	NUCLEAR_BODY	1.18	0.0	Other
32	NEGATIVE_REGULATION_OF_CELLULAR_PROTEIN_METABOLIC_PROCESS	1.18	0.0	metabolism
33	ACTIN_FILAMENT_ORGANIZATION	1.18	0.0	cell structure
34	ESTABLISHMENT_AND_OR_MAINTENANCE_OF_CELL_POLARITY	1.18	0.0	cell structure
35	TRANSCRIPTION_FACTOR_BINDING	1.18	0.0	transcription/translation
36	VIRAL_REPRODUCTIVE_PROCESS	1.18	0.0	immune response / regulation
37	SPECIFIC_RNA_POLYMERASE_II_TRANSCRIPTION_FACTOR_ACTIVITY	1.18	0.0	transcription/translation
38	NEGATIVE_REGULATION_OF_PROTEIN_METABOLIC_PROCESS	1.17	0.0	metabolism
39	GLYCOLIPID_METABOLIC_PROCESS	1.17	0.0	metabolism
40	CHROMOSOME	1.17	0.0	cell structure
41	CHROMATIN_ASSEMBLY_OR_DISASSEMBLY	1.17	0.2073922	cell structure
42	ONE_CARBON_COMPOUND_METABOLIC_PROCESS	1.17	0.0	metabolism

Rank	Gene Sets	Normalised Enrichment Score (NES)	P	Category
43	SECRETORY_PATHWAY	1.16	0.09034908	immune response / regulation
44	VIRAL_INFECTIOUS_CYCLE	1.16	0.0	immune response / regulation
45	NEURON_APOPTOSIS	1.16	0.19507186	Other
46	VIRAL_GENOME_REPLICATION	1.16	0.0	immune response / regulation
47	NEGATIVE_REGULATION_OF_CELL_DIFFERENTIATION	1.16	0.0	cell differentiation
48	SKELETAL_MUSCLE_DEVELOPMENT	1.16	0.0	cell differentiation
49	POSITIVE_REGULATION_OF_CYTOKINE_BIOSYNTHETIC_PROCESS	1.15	0.29774126	immune response / regulation
50	VIRAL_REPRODUCTION	1.15	0.0	immune response / regulation
51	NEGATIVE_REGULATION_OF_TRANSLATION	1.15	0.0	transcription/translation
52	TRANSCRIPTION_COACTIVATOR_ACTIVITY	1.15	0.0927835	transcription/translation
53	TRANSCRIPTION_ACTIVATOR_ACTIVITY	1.15	0.0	transcription/translation
54	CYTOKINE_METABOLIC_PROCESS	1.15	0.0	metabolism
55	CYTOKINE_BIOSYNTHETIC_PROCESS	1.15	0.0	metabolism
56	INTERLEUKIN_BINDING	1.15	0.29774126	immune response / regulation
57	STEROID_BIOSYNTHETIC_PROCESS	1.15	0.21560575	metabolism
58	CALCIUM_ION_BINDING	1.14	0.30020705	signal transduction
59	REGULATION_OF_MYELOID_CELL_DIFFERENTIATION	1.14	0.09034908	cell differentiation
60	REGULATION_OF_TRANSLATION	1.14	0.19507186	transcription/translation

Table 2.7 Gene ontology gene sets enriched in MN1Δ1 cells compared to MN1 cells

Rank	Gene Sets	Normalised Enrichment Score (NES)	P	Category
1	SYNAPTOGENESIS	1.53	0.0	cell structure
2	METALLOENDOPEPTIDASE_ACTIVITY	1.27	0.0	signal transduction
3	GLUTATHIONE_TRANSFERASE_ACTIVITY	1.24	0.0	signal transduction
4	PROTEIN_SECRETION	1.24	0.0	cell structure
5	G_PROTEIN_COUPLED_RECEPTOR_BINDING	1.23	0.0	signal transduction
6	VIRAL_REPRODUCTION	1.23	0.0	immune response / regulation
7	SODIUM_ION_TRANSPORT	1.23	0.19411765	signal transduction
8	GTPASE_BINDING	1.22	0.0	signal transduction
9	PROTEIN_AMINO_ACID_DEPHOSPHORYLATION	1.22	0.0	signal transduction
10	CHEMOKINE_RECEPTOR_BINDING	1.22	0.0	immune response / regulation
11	SMALL_GTPASE_BINDING	1.22	0.0	signal transduction
12	DEPHOSPHORYLATION	1.22	0.0	signal transduction
13	VIRAL_REPRODUCTIVE_PROCESS	1.22	0.0	immune response / regulation
14	CHEMOKINE_ACTIVITY	1.21	0.0	immune response / regulation
15	CYTOKINE_ACTIVITY	1.21	0.0	immune response / regulation
16	SECRETION	1.20	0.0	cell structure
17	LYTIC_VACUOLE	1.20	0.20512821	cell structure
18	LYSOSOME	1.20	0.20512821	cell structure
19	IMMUNE_EFFECTOR_PROCESS	1.20	0.18627451	immune response / regulation
20	MICROSOME	1.20	0.0	cell structure
21	VOLTAGE_GATED_CHANNEL_ACTIVITY	1.20	0.19488189	signal transduction

Rank	Gene Sets	Normalised Enrichment Score (NES)	P	Category
22	TRANSCRIPTION_COREPRESSOR_ACTIVITY	1.20	0.0	transcription/translation
23	EXOCYTOSIS	1.20	0.3019608	cell structure
24	ACTIVATION_OF_IMMUNE_RESPONSE	1.20	0.18627451	immune response / regulation
25	RESPONSE_TO_VIRUS	1.20	0.29637095	immune response / regulation
26	VACUOLE	1.20	0.20392157	cell structure
27	VIRAL_GENOME_REPLICATION	1.20	0.08431373	immune response / regulation
28	VESICULAR_FRACTION	1.19	0.0	cell structure
29	VIRAL_INFECTIOUS_CYCLE	1.19	0.0	immune response / regulation
30	MESODERM_DEVELOPMENT	1.19	0.0	cell differentiation
31	SECRETION_BY_CELL	1.19	0.0	immune response / regulation
32	TRANSCRIPTION_REPRESSOR_ACTIVITY	1.18	0.0	transcription/translation
33	TRANSFERASE_ACTIVITY_TRANSFERRING_ALKYL_OR_ARYLOTHER_THAN_METHYLGROUPS	1.18	0.20512821	signal transduction
34	REGULATION_OF_MAP_KINASE_ACTIVITY	1.18	0.08382066	signal transduction
35	UNFOLDED_PROTEIN_BINDING	1.18	0.19215687	signal transduction
36	ACTIN_FILAMENT_ORGANIZATION	1.18	0.18627451	cell structure
37	OXIDOREDUCTASE_ACTIVITY_GO_0016705	1.18	0.29637095	signal transduction
38	ACETYLGLUCOSAMINYLTRANSFERASE_ACTIVITY	1.17	0.286	signal transduction
39	RNA_CATABOLIC_PROCESS	1.17	0.10784314	metabolism
40	CELLULAR_RESPIRATION	1.17	0.39803922	metabolism
41	GLYCOPROTEIN_METABOLIC_PROCESS	1.17	0.20967741	metabolism
42	TRANSCRIPTION_FACTOR_BINDING	1.16	0.0	transcription/translation
43	CARBOXYLESTERASE_ACTIVITY	1.16	0.0	signal transduction

Rank	Gene Sets	Normalised Enrichment Score (NES)	P	Category
44	NEGATIVE_REGULATION_OF_TRANSCRIPTION_DNA_DEPENDENT	1.16	0.0	transcription/translation
45	NEGATIVE_REGULATION_OF_RNA_METABOLIC_PROCESS	1.16	0.0	metabolism
46	SPLICEOSOME	1.16	0.3019608	transcription/translation
47	AEROBIC_RESPIRATION	1.16	0.30392158	metabolism
48	MONOOXYGENASE_ACTIVITY	1.16	0.2882353	signal transduction
49	ONE_CARBON_COMPOUND_METABOLIC_PROCESS	1.16	0.19411765	metabolism
50	ATPASE_ACTIVITY_COUPLED_TO_TRANSMEMBRANE_MOVEMENT_OF_IONS_PHOSPHORYLATIVE_MECHANISM	1.16	0.19411765	signal transduction
51	NEGATIVE_REGULATION_OF_SIGNAL_TRANSDUCTION	1.16	0.10784314	signal transduction
52	PROTEIN_FOLDING	1.16	0.20392157	metabolism
53	AMINO_SUGAR_METABOLIC_PROCESS	1.15	0.0	metabolism
54	INFLAMMATORY_RESPONSE	1.15	0.19723865	immune response / regulation
55	SECRETORY_PATHWAY	1.15	0.08431373	immune response / regulation
56	CARBON_CARBON_LYASE_ACTIVITY	1.15	0.08704454	signal transduction
57	GTPASE_ACTIVITY	1.15	0.08431373	signal transduction
58	CHROMATIN_ASSEMBLY	1.15	0.08431373	cell structure
59	ACTIN_CYTOSKELETON_ORGANIZATION_AND_BIOGENESIS	1.15	0.09467456	cell structure
60	TRANSCRIPTION_CO-FACTOR_ACTIVITY	1.15	0.19411765	transcription/translation

To compare the differentiation potential of cells transduced with different MN1 deletions, I compared the immunophenotype of GFP positive cells in peripheral blood at week 4 post-transplant and in bone marrow at time of sacrifice for all deletion constructs (Figures 2.11-13). Expression of the progenitor cell marker c-Kit inversely correlates with those of the myeloid markers Gr-1 and CD11b. Loss of the C-terminus and unexpectedly, also the loss of region 2, result in increased expression of the myeloid markers Gr-1 (24.5 ± 9.7% in MN1Δ7 and 38.5 ± 10.6% in MN1Δ2 versus 16.7% in control mice and 7.3 ± 2.4% in full-length MN1 mice), and CD11b (68.0 ± 13.8% in MN1Δ7 and 82.2 ± 4.5% in MN1Δ2 versus 16.7% in control mice and 26.1 ± 6.9% in full-length MN1 mice), as well as mature neutrophils (MN1Δ7) and monocytic cells (MN1Δ2) besides blast cells in bone marrow smears of diseased mice (Figure 2.1H and 2.11-2.12). In summary, the C-terminal region is required to block myeloid differentiation and to induce resistance against ATRA, while region 2 prevents myeloid differentiation but is dispensable for ATRA resistance (see also Table 2.6).

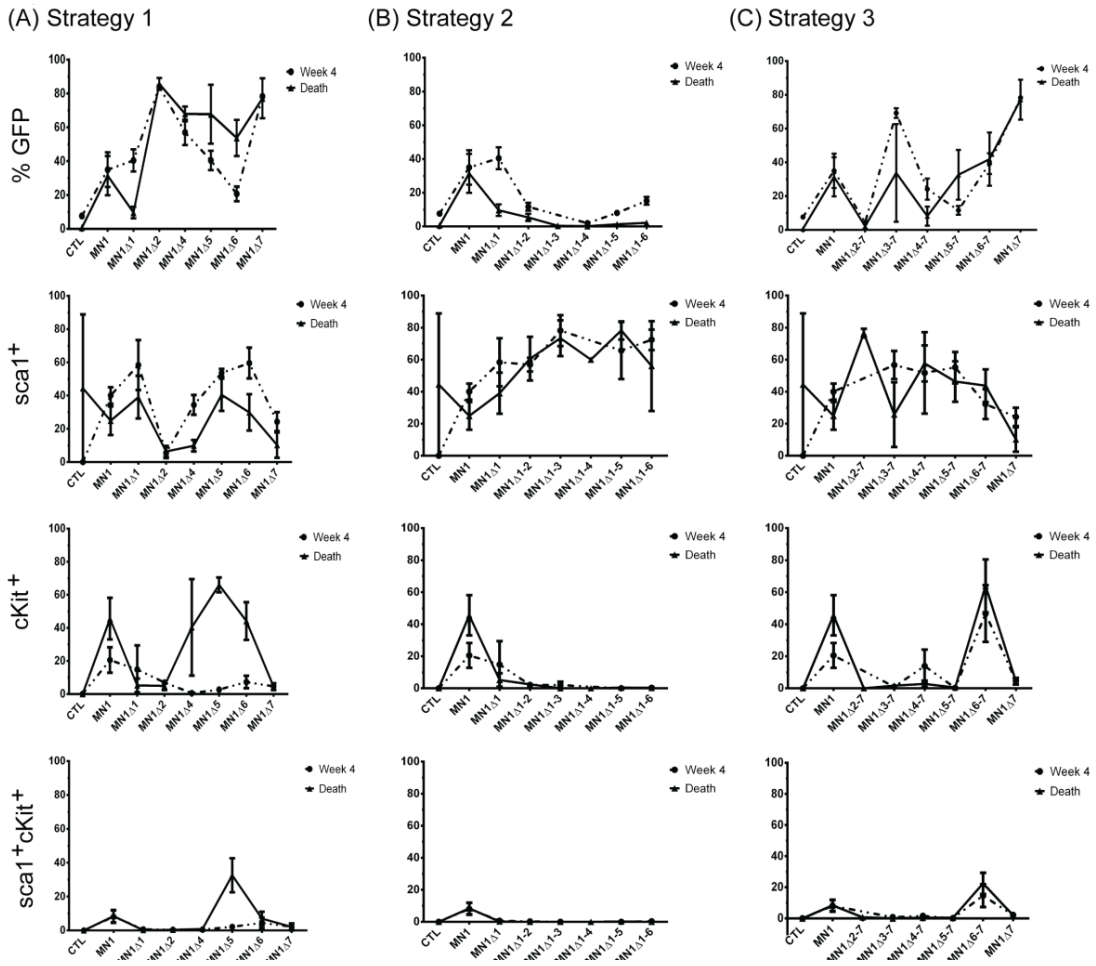

Figure 2.11 Immunophenotype of MN1-transduced cells in transplanted mice – stem and progenitor markers

Percentage of GFP-expressing cells and expression of c-Kit and Sca1 in GFP^+ cells in peripheral blood at 4 weeks and in bone marrow at death of mice receiving transplants of MN1-transduced cells. (A) Strategy 1, (B) Strategy 2, and (C) Strategy 3 MN1 constructs. Mean ± standard error of the mean (SEM). The number of analyzed mice is provided in Table 2.6.

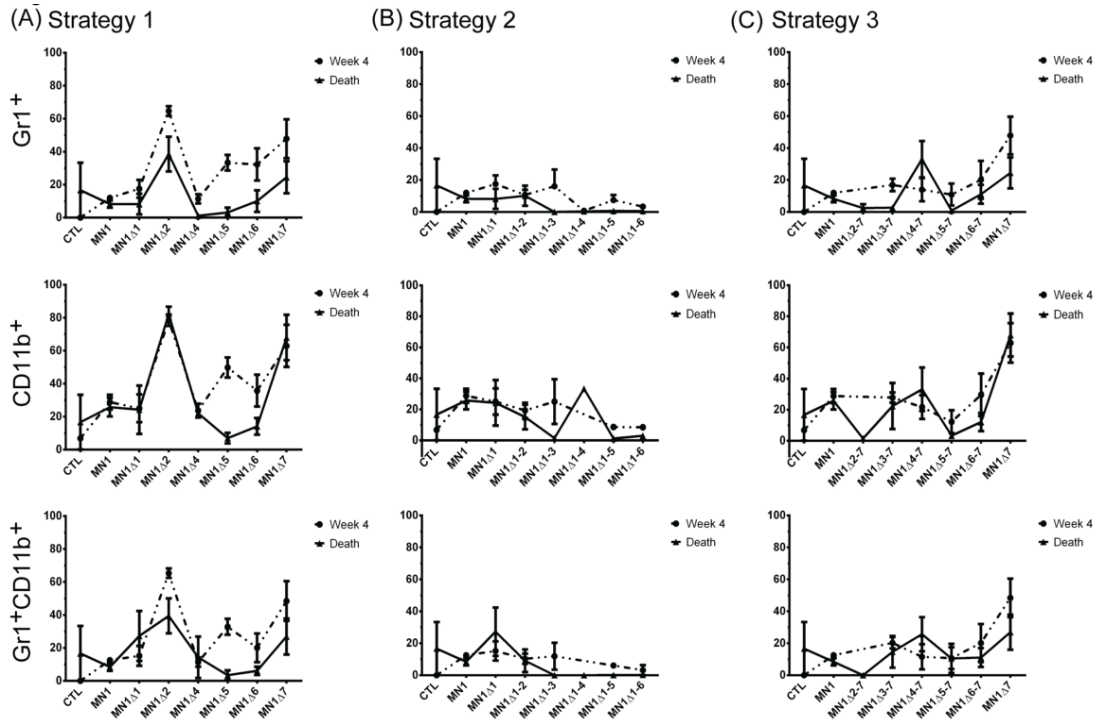

Figure 2.12 Immunophenotype of MN1-transduced cells in transplanted mice – myeloid markers

Expression of myeloid markers in GFP+ cells in peripheral blood at 4 weeks and in bone marrow at death of mice receiving transplants of MN1-transduced cells. (A) Strategy 1, (B) Strategy 2, and (C) Strategy 3 MN1 constructs. Mean ± SEM. The number of analyzed mice is provided in Table 2.6.

2.3.5 A 606 amino-acid C-terminal region of MN1 is required to prevent T-lymphoid differentiation

Combining deletion of the three most C-terminally located regions in MN1Δ5-7 results in delayed onset of leukemia with a median survival of 123 days (versus 35 days with full-length MN1, log-rank Mantel-Cox test, $P<0.05$) (Figure 2.1G and Table 2.3). Interestingly, immunophenotypic analysis reveals 22.7 ± 14.4% CD4/CD8 double positive T cells within the GFP donor cell gate in primary transplantations (versus 0.0 ± 0.0% in control cells and 0.03 ± 0.03% in full-length MN1), and morphologic analysis shows blast cells in diseased mice in two

independent experiments (Figure 2.14A-B), consistent with a diagnosis of T-lymphoblastic leukemia. Furthermore, these cells also induce T-ALL upon secondary transplantation (Figure 2.14C-D). Despite the differences in leukemic phenotype, MN1Δ5-7 also localises to the nucleus (Figure 2.7). In summary, these data suggest that the extended C-terminus of MN1 is required to block lymphoid differentiation and demonstrates the role of MN1 in regulating hematopoietic cell fate (see also Table 2.6 and Figure 2.13).

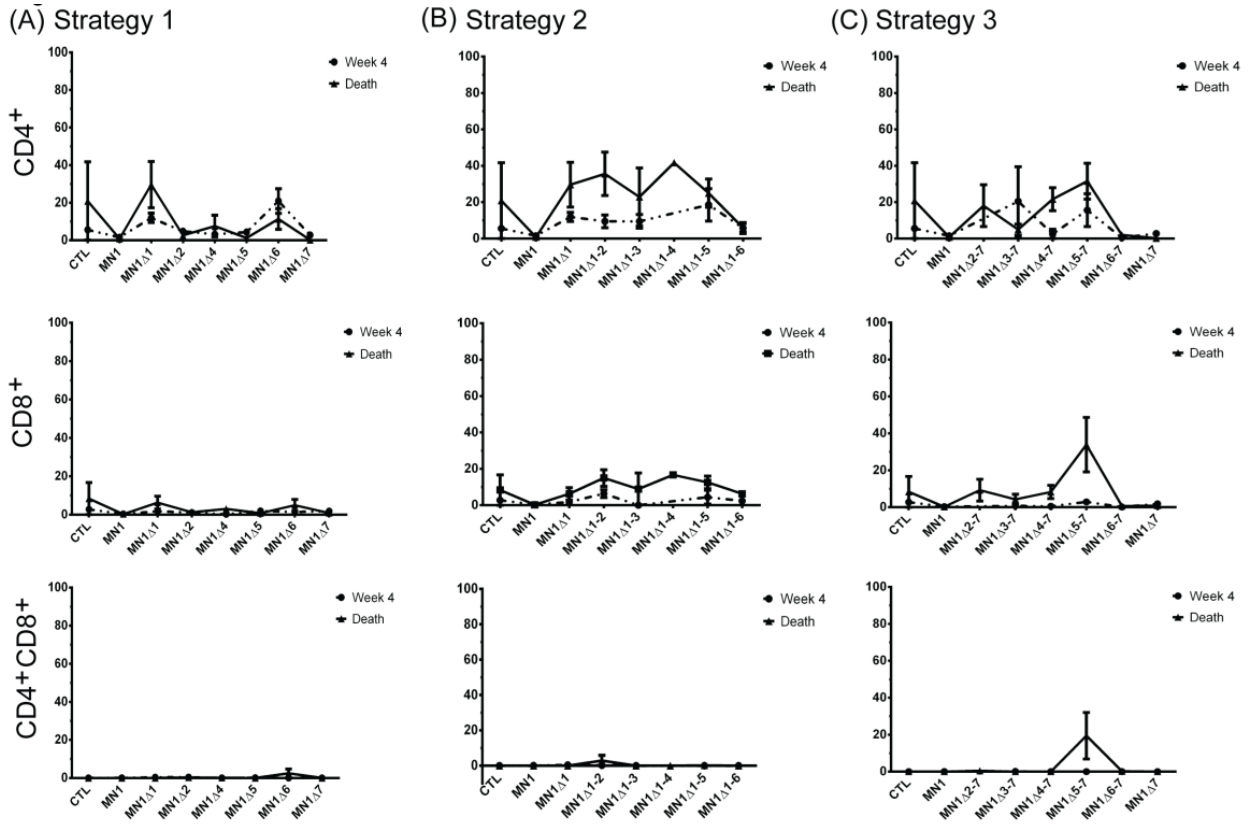

Figure 2.13 Immunophenotype of MN1-transduced cells in transplanted mice – T-cell markers

Expression of T-cell markers in GFP^+ cells in peripheral blood at 4 weeks and in bone marrow at death of mice receiving transplants of MN1-transduced cells. (A) Strategy 1, (B) Strategy 2, and (C) Strategy 3 MN1 constructs. Mean ± SEM. The number of analyzed mice is provided in Table 2.6.

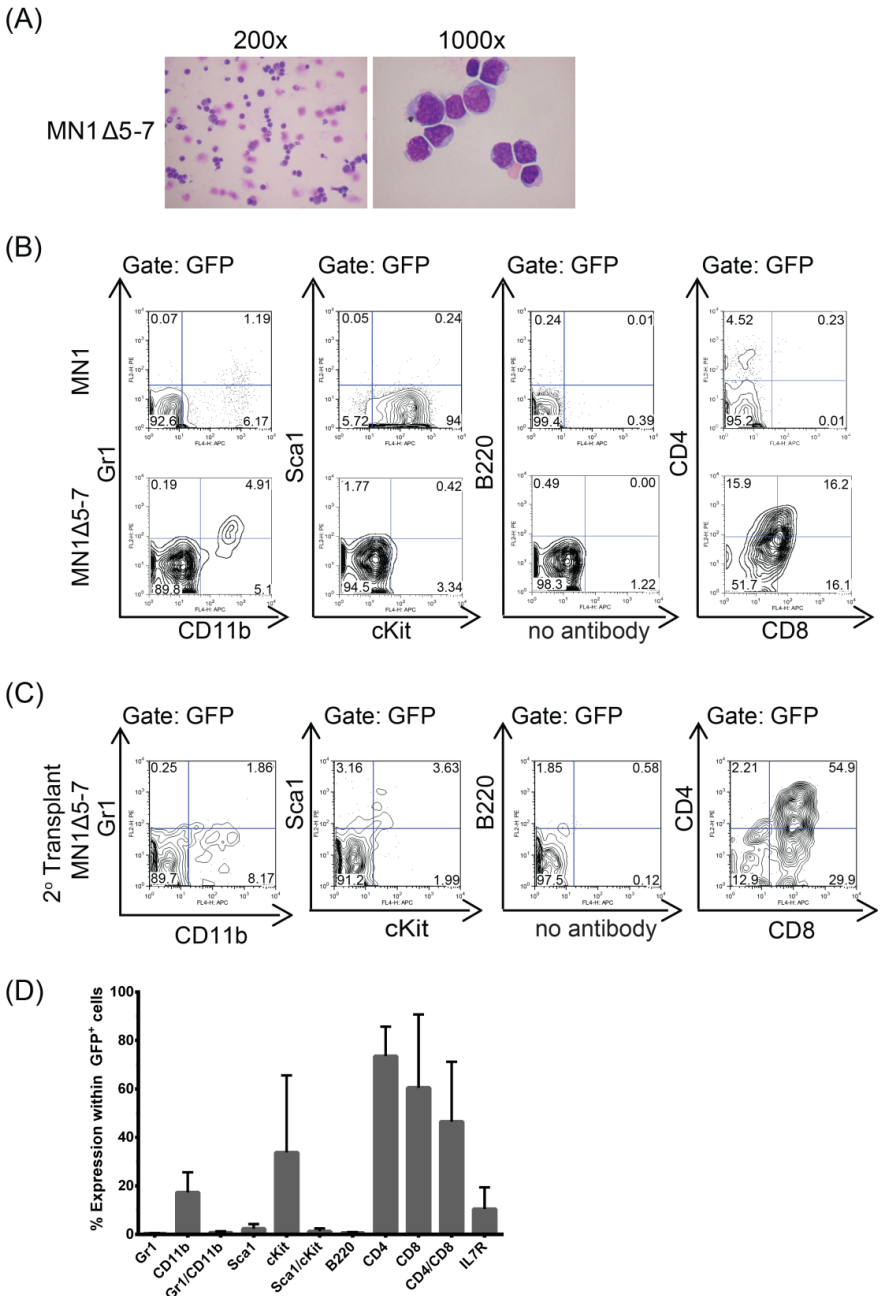

Figure 2.14 A 606 amino-acid C-terminal portion of MN1 prevents T-lymphoid differentiation

(A) Morphology of bone marrow cells from MN1Δ5-7 mice at death, showing a shift in leukemia from AML, as seen in MN1 leukemia, to an ALL leukemia upon loss of the C-terminal domains 5-7. (B) Representative immunophenotype of GFP$^+$ MN1Δ5-7 bone marrow cells compared to wildtype MN1 bone marrow cells at death. (C) Representative immunophenotype of secondary transplants of GFP$^+$ MN1Δ5-7 bone marrow cells at death. (D)

Average cell surface marker expression for secondary transplants of GFP^+ MN1Δ5-7 bone marrow cells at death (mean ± SEM, n=3).

2.4 Discussion

In the work presented in this thesis chapter, the functional properties of MN1 deletion mutants were systematically determined to identify regions that encode the key leukemogenic functions of MN1. These analyses demonstrate that a single gene can induce leukemia by a "double-hit", as the two functions promoting proliferation and inhibiting differentiation are encoded in structurally distinct regions. In addition, the myeloid or lymphoid lineage identity of leukemias can be determined by different mutations of the same oncogene, thus providing a potential explanation for the similar mutation spectrum in phenotypically distinct diseases like AML and T-ALL.

Deletion of the first 221 N-terminal amino acids (MN1Δ1) abolishes the leukemogenicity of MN1 *in vivo*, as evidenced by decreasing white blood cell engraftment in mice over time and failure to develop leukemia. However, the MN1Δ1 mutant provides both growth advantage and retention of ATRA resistance to bone marrow cells *in vitro*. This thesis work reports the novel finding that MN1Δ1-transduced cells preferentially differentiate to the erythroid lineage *in vivo* and have increased megakaryocyte differentiation potential *in vitro*, suggesting that the most N-terminal sequences of MN1 are also critical for blocking megakaryocyte/erythroid differentiation (Figure 2.15). Consistent with the reduced proliferative ability of MN1Δ1 cells, expression levels of HOXA9, HOXA10, and MEIS2 are most differentially downregulated compared to full-length MN1. In addition, JUN and FOS, factors of the activator protein 1 (AP1) complex, are most upregulated together with Krüppel-like factors (KLF) 2, 3, 4 and 6, which play an important role

in erythroid differentiation and bind DNA at CACCC motifs[155-158]. Interestingly, the CACCC motif also serves as a consensus motif for MN1 binding to DNA in an oligonucleotide selection assay[95, 159].

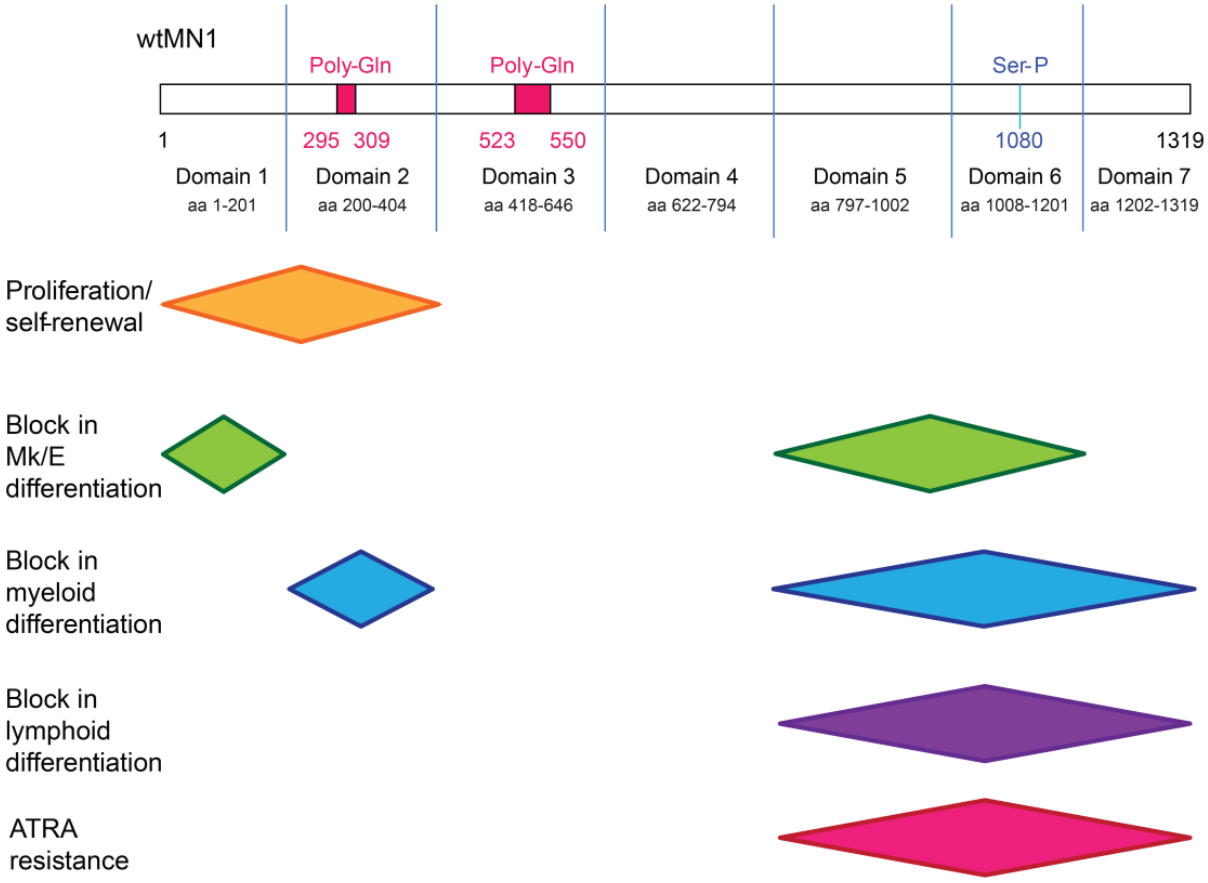

Figure 2.15. Functionally defined regions of MN1

Additional deletion of a region containing the first poly-Gln repeat (MN1Δ1-2) abolishes any functional effect of MN1 *in vitro* and *in vivo*, despite the formation of protein. Conversely, the N-terminal sequence up to amino acid 317 (MN1Δ3-7) is sufficient to induce strong myeloproliferation with high white blood cell counts and splenomegaly with full myeloid differentiation potential, demonstrating that the MN1 N-terminus drives proliferation in MN1

leukemia. MN1 and MEIS1 share a high proportion of their regulatory chromatin sites, and MN1 leukemogenicity is dependent on MEIS1[128]. This work suggests that the N-terminus is required for localization of MN1 to MEIS1 chromatin binding sites. Previous work from van Wely and colleagues demonstrated that MN1 interacts with P300 at amino acids 48 to 256, a region with considerable transcription activation function[95], and the majority of which overlaps with region 1. Future studies will be required to demonstrate if interaction between the MN1 N-terminus and P300 is required for the N-terminal functions promoting proliferation and blocking megakaryocyte/erythroid differentiation.

Several levels of evidence suggested that the MN1 C-terminus is required to inhibit myeloid differentiation (Table 2.6). First, loss of individual regions 5, 6, or 7 restores sensitivity to ATRA *in vitro*. Second, myeloid surface markers Gr-1 and CD11b are most highly expressed in cells transduced with MN1Δ7 *in vivo*. In addition, gene expression profiling shows a close relationship between MN1Δ7 cells and differentiated myeloid cells, and more differentiation-related gene sets are upregulated in MN1Δ7 than in MN1Δ1 cells. Third, cumulative loss of regions 5, 6 and 7 results in loss of myeloid identity (see below). Lastly, cumulative deletion of regions 3 to 7 (MN1Δ3-7) results in a myeloproliferative disease with full differentiation potential to mature neutrophils (Table 2.6). These data suggest that the C-terminal regions (MN1Δ5, 6, 7) are the critical regions mediating resistance to ATRA-cytotoxicity, with some contribution from amino acids 222-418 (Figure 2.15). Recent work by Sharma and colleagues demonstrated that Ccl9 and Irf8 are upregulated in both MN1Δ7 cells and a MN1 model fused to the transcriptional activation domain VP16 (MN1VP16), suggesting that phenotypic similarities between the two models may be rooted in similar underlying gene expression patterns[115]. Van Wely and colleagues showed that MN1 binds to retinoic-acid response elements by an

oligonucleotide selection assay[95] and, combined with the data reported in this chapter, I hypothesised that the MN1 C-terminus directs MN1 to retinoic acid (RA) response elements to regulate transcription. Although retroviral overexpression, as used in this study, is likely to lead to artificially high transcriptional expression of MN1 and the mutants, patients with AML with the highest MN1 expression have similar expression levels to murine MN1-transduced cell lines with the lowest MN1 expression, suggesting that at least some of the cell lines described are comparable to patient data (data not shown). In addition, previous studies have demonstrated that MN1 induces resistance to ATRA-induced differentiation and cell death[109], and that high-level expression of MN1 predicts ATRA resistance in patients with AML, suggesting its future use as a biomarker for ATRA treatment[109, 160].

Deletion of a 606-amino acid fragment from the C-terminus reproducibly induces T-ALL with CD4/CD8-double positive cells in mice. This suggests that the C-terminus of MN1 directs hematopoietic progenitor cells towards the myeloid lineage, but in its absence, allows differentiation towards the T cell lineage. Although this study cannot rule out that T-cell precursors may have been transduced by MN1Δ5-7, resulting in a bias or advantage towards lymphoid differentiation seen in the T-ALLs that developed, this is unlikely as findings were consistent in two independent experiments performed and supported by similar findings by an independent group[161]. Interestingly, mice lacking a portion of this 606-amino acid fragment, namely MN1Δ5 or MN1Δ7, develop AML. This suggests that amino acids 714-797 may be critical for myeloid differentiation, and it is only in their absence that lymphoid differentiation may occur. Kawagoe and Grosveld also described CD4/CD8-double positive T cell lymphomas in mice expressing the MN1-TEL fusion oncoprotein under the control of the RUNX1 promoter[116]. In this fusion protein, the 60 C-terminal amino acids of MN1 are lost due to the

fusion to TEL[91]. As RUNX1 is also expressed in the T-lineage, these data suggest that overexpression of MN1 in T-progenitor cells can promote leukemogenesis, with Neumann and colleagues providing evidence of MN1 overexpression in T-lymphoblastic leukemias[162]. Taken together, these data suggest that the C-terminus of MN1 encoded by amino acids 513-1319 (regions 5-7) instructs progenitor cells to the myeloid lineage and that in its absence, progenitor cells can differentiate to the lymphoid lineage (Table 2.6).

During preparation of the manuscript that provides the basis of this chapter, one other group characterised functional MN1 regions, creating deletion constructs modelled off known MN1 protein domains in U937 cells[161]. Consistent with data reported in this chapter, Kandilci and colleagues report decreased growth and colony-forming ability *in vitro* upon loss of the MN1 N-terminus[161]. In addition, they also show that the loss of MN1 amino acids 570-1273 gives rise to T-cell lymphoma[161]. This deleted region partially overlaps with our MN1Δ5-7 mutant, supporting the idea that the MN1 C-terminus promotes a myeloid-skew to MN1 leukemia. Finally, Kandilci and colleagues also localise ATRA resistance to amino acids 18-458, but not 12-228, with their MN1-transduced U937 cells showing increased CD11b expression after 3 days of treatment[161]. Interestingly, this region partially overlaps with region 2 of our deletion mutants, supporting my observation of increased CD11b expression in peripheral blood of animals transplanted with MN1Δ2. They did not, however, report increased CD11b expression in C-terminal deletions, although this may be attributed to their most C-terminal deletion mutant retaining the 46 most C-terminal amino acids[161]. It is possible that retention of these critical amino acids may abrogate the differentiation effect seen in my complete deletions.

The data presented in this chapter characterises functional regions of the MN1 protein by a systematic mutation analysis and identifies key regions that enhance proliferation and self-

renewal, block myeloid, megakaryocytic/erythroid, and lymphoid differentiation, and induce resistance against ATRA. These data support a critical function of MN1 as a key cell fate regulator in malignant hematopoiesis and provide a powerful new model for further dissection of the molecular events controlling transformation and the resulting leukemic phenotype.

Chapter 3: Discovery of Meis2 as a critical player in leukemogenesis using a MN1 leukemia model

The data presented in Chapter 3 of this thesis will be used in preparation of a manuscript.

3.1 Introduction

The meningioma 1 (MN1) gene was first identified as part of a balanced chromosomal translocation in human meningioma[90] and was subsequently recognised as a partner in the chromosomal translocation MN1-TEL t(12;22)(p13;q11) in de novo AML and MDS[91]. While the MN1-TEL translocation is relatively infrequent, overexpression of MN1 is observed in a broad spectrum of AML and correlates with inv(16) AML[100, 101], AML with overexpression of EVI1[102], AML with high BAALC expression[103, 104], and a subset of patients with ALL[45]. MN1 is also an independent prognostic marker for AML with normal karyotype, with high expression associated with poor prognosis, shorter survival, increased likelihood of relapse, and poor response to treatment. In elderly patients with AML, lower levels of MN1 expression are associated with response to ATRA-induced differentiation[45, 109]. The potential relevance of MN1 expression in a broad range of leukemic settings and its role as a transcriptional co-factor has stimulated investigation of MN1 function to gain insight into key leukemogenic targets and pathways.

In the murine model, overexpression of MN1 induces aggressive, fully-penetrant AML through the promotion of leukemic cell self-renewal, as demonstrated in human $CD34^+$ cells[113], leukemic cells[114], and immature murine hematopoietic cells[106, 109], and the impairment of myeloid differentiation, as demonstrated by immunophenotype[106, 109], resistance to ATRA-induced differentiation[109], and repression of differentiation-promoting transcription factors C/EBPα and

PU.1[113]. MN1-induced murine leukemias most closely resemble CMPs, both immunophenotypically and at a gene expression level. Consistent with this, CMPs are susceptible to transformation by MN1 overexpression in both bulk and at the single-cell level[128]. In contrast to CMPs, both HSCs and GMPs are strongly resistant to transformation by MN1[128]. This resistance appears to be due, at least in part, by the inability of MN1 to trigger or enforce requisite levels of Hox and Meis1, as evidenced by the ability to render GMPs susceptible to MN1 transformation by engineered co-overexpression of MEIS1 and HOXA9 or HOXA10[128]. Adding to these findings, ChIP-Seq analysis reveals a high degree of co-localisation of MN1 with MEIS1 at over 500 MEIS1 binding sites, suggesting that MN1 requires the presence of HOX/MEIS protein complexes for its leukemogenic activity[128].

The potency of MN1 overexpression to drive leukemic transformation and to generate sustained growth of leukemogenic cells *in vitro* provides an attractive platform to search for key functional domains and genes and pathways that underlie its activities[106, 109]. Ours and other groups have utilized this platform for such purposes. As described in the previous chapter, a screen for key functional domains of MN1 identified the N-terminal 202 amino acids as critical to MN1-induced leukemogenic activity. Subsequent analysis of differential gene expression induced by full-length MN1 and this mutant MN1 revealed a number of genes potentially underlying the leukemogenic activity of MN1[131]. Similarly, fusion of the transcriptional activation domain VP16 and transcriptional repression domain M33 to MN1 modulates genes associated with immune response signaling[115]. These models identified Irf8 as a downregulated target of MN1 that contributes to the enhanced proliferation and *in vivo* engraftment and leukemogenicity characteristic of this oncogene[115]. Furthermore, characterization of a forward genetic model of human leukemogenesis through co-overexpression of MN1 and the NUP98HOXD13 fusion in

cord blood cells compared to singly-transduced pre-leukemic cells revealed that the leukemic state coincides with activation of stem cell expression gene signatures characteristic of primary human AML[126].

Previous work has demonstrated that MN1-induced leukemia gives rise to a heterogeneous phenotype[106, 109]. This suggested an additional approach to study the role of MN1 by exploring the relationship of phenotypic heterogeneity to leukemic function and determining if such differences can be correlated with relevant genes and pathways.

This study sought to further explore the observed phenotypic heterogeneity of MN1 leukemic cells to determine if it constituted a functional hierarchy that could be exploited to identify key genes in leukemia. Gene expression comparisons between these cells were combined with data from comparative studies on MN1 variants with demonstrated differential leukemic activity to uncover key genes and pathways associated with MN1 leukemia. Findings include identification of hepatic leukocyte factor (Hlf) and HoxA9 as crucial to *in vitro* proliferation, self-renewal, and blocked myeloid differentiation in MN1-transduced cells. Furthermore, Meis2, a well-known player in limb, eye, cardiac, and neural crest development that has only recently been implicated in AML, was identified as critical to MN1 leukemogenic activity. These findings demonstrate the important role of another MEIS family member in leukemia.

3.2 Materials and methods

Methods already described in Section 2.2 in Chapter 2 of this thesis are not repeated here.

3.2.1 Vector production

The 4-kb full-length cDNA of human MN1 was previously subcloned into the *NotI* site of the pSF91 retroviral vector[143] upstream of the internal ribosomal entry site (IRES) and the enhanced green fluorescent protein (GFP) gene[109] as described in Chapter 2[131], and HA-tagged, as previously described[128].

3.2.2 Lentiviral shRNA vector and virus production

The small hairpin RNA (shRNA) sequences were ordered as 97-mer[163] non-PAGE purified IDT Ultramers (Integrated DNA Technologies, Coralville, IA, USA). Ultramers were amplified with Platinum Taq DNA Polymerase (ThermoFisher Scientific, Carlsbad, CA, USA) to add *XhoI* and *EcoRI* restriction enzyme sites and subcloned using TOPO TA Cloning Kit (ThermoFisher Scientific, Carlsbad, CA, USA). After sequence verification, shRNAs were subcloned into a pRRL.ppt.MeKO2.miR30e lentiviral vector using the *XhoI*/*EcoRI* sites based on a third-generation pRRL.PPT.SF.GFP.pre* lentiviral backbone with a spleen focus-forming virus (SFFV) promotor[164]. Alternatively, shRNA ultramers containing existing *XhoI* or *EcoRI* restriction enzyme sites were amplified using Phusion DNA Polymerase (ThermoFisher Scientific, Carlsbad, CA, USA) and cloned directly into the pRRL.ppt.MeKO2.miR30e lentiviral vector using Gibson Assembly Master Mix (New England Biolabs, Ipswich, MA, USA). Primer amplification sequences are provided in Table 3.1 and shRNA vector schematic is provided in Figure 3.1.

Table 3.1 Primer Sequences for amplification of IDT Ultramers for cloning

Primer Name	Primer Sequence
miRE-Xho-FWD	5'-TGAACTCGAGAAGGTATATTGCTGTTGACAGTGAGCG-3'
miRE-Eco-REV	5'-TCTCGAATTCTAGCCCCTTGAAGTCCGAGGCAGTAGGC-3'
MIR30e Lenti Gibson FWD	5'-TAACCCAACAGAAGGCTCGAGAAGGTATATTGCTGTTGACAGTG-3'
MIR30e Lenti Gibson REV	5'- AAACAAGATAATTGCTCGAATTCTAGCCCCTTGAAGTCCGA-3'

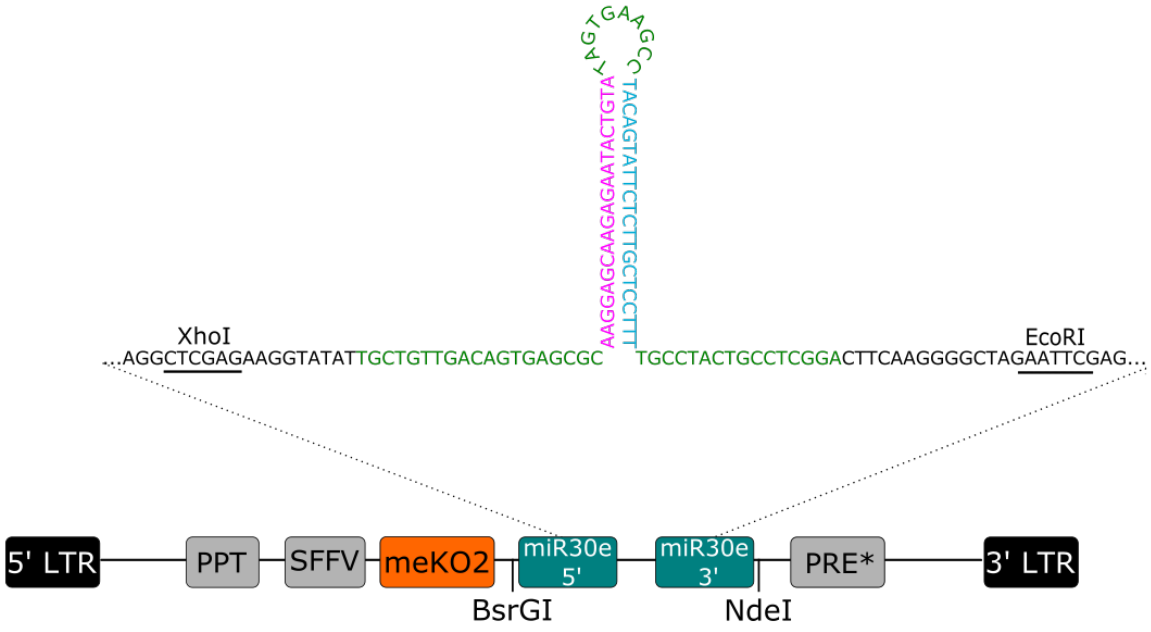

Figure 3.1 Schematic of shRNA lentiviral vector

Coloured sequence indicates 97-mer previously referenced[163]. (magenta = guide sequence, blue = mRNA target sequence) Restriction enzyme recognition sequences are underlined and annotated.

Lentiviruses were produced by seeding $7x10^6$ 293T cells per 10cm dish in Dulbecco's modified Eagle's medium (DMEM; StemCell Technologies Inc., Vancouver, BC, Canada) supplemented with 1/100 100mM sodium pyruvate (ThermoFisher Scientific, Carlsbad, CA, USA), 1/100 penicillin-streptomycin (10,000 U/mL; ThermoFisher Scientific, Carlsbad, CA, USA), and 10% FBS Performance Plus (Gibco/ThermoFisher Scientific, Carlsbad, CA, USA) 24 hours prior to calcium phosphate-mediated transient transfection with 6-10µg lentiviral vector, 6µg Rous sarcoma virus (RSV)-Rev, 9µg lentiviral group-specific antigen/polymerase (gag/pol) and 2µg vesicular stomatitis virus glycoprotein envelope pMD.G (VSV-g). Sixteen hours after transfection, medium was replaced by DMEM supplemented with 1/100 100mM sodium pyruvate, 1/100 penicillin-streptomycin (10,000 U/mL), 10% FBS Performance Plus, and 10mM HEPES (Gibco/ThermoFisher Scientific, Carlsbad, CA, USA). Vector supernatants were harvested 36 hours and 60 hours after transfection, filtered (0.22µM; Argos Technologies, IL, USA) and stored at -80^{o}C.

3.2.3 Lentiviral transduction of MN1 bone marrow cell lines

Lentiviral transduction was performed by seeding 100,000 MN1 bone marrow cells per well in 96-well U-bottom plates (VWR/Falcon, Mississauga, ON, Canada) in DMEM supplemented with 15% FBS, 10ng/mL hIL6, 6ng/mL mIL3, 100ng/mL mSCF, and 5µg/mL protamine sulfate (Sigma-Aldrich, Oakville, ON, Canada) and adding 30µL unconcentrated viral supernatant for shRNAs of interest. After 24 hours transduction, half of the media was removed from each well and the remaining contents were transferred to 48-well plates (Greiner Bio One, Fisher

Scientific, Carlsbad, CA, USA) with additional DMEM supplemented with 15% FBS, 10ng/mL hIL6, 6ng/mL mIL3, and 100ng/mL mSCF. At 48 hours post-transduction, half of well contents was removed and remaining contents were moved to a 6-well plate (VWR/Falcon) with additional DMEM supplemented with 15% FBS, 10ng/mL hIL6, 6ng/mL mIL3, and 100ng/mL mSCF. At 72 hours post-transduction, well contents were collected and prepared for flow cytometric sorting.

3.2.4 In vitro proliferation assays

Cytokine-dependent cell lines were generated from transduced bone marrow cells directly after sorting or from the cKit fraction of bone marrow cells from primary animals with MN1-induced leukemia directly after sorting in DMEM supplemented with 15% FBS, 10ng/mL hIL6, 6ng/mL mIL3, and 100ng/mL mSCF. For *in vitro* growth and proliferation assays, 75,000 cells were sorted using a BD FACSAria or BD FACSAria Fusion (both from BD Biosciences, San Diego, CA, USA) into triplicate wells by flow cytometry three days after shRNA transduction in DMEM media supplemented with 15% FBS, 10ng/mL hIL6, 6ng/mL mIL3, and 100ng/mL mSCF. Cells were maintained at a cell density below $2x10^6$/mL and were counted with the Vi-Cell XR Cell Viability Analyzer (Beckman Coulter, Fullerton, CA, USA). For *in vitro* competitive assays, equal numbers of shRNA-transduced cells and untransduced MN1 cells were seeded in identical media and analysed by flow cytometry.

3.2.5 Cell cycle and apoptosis assays

Cells were sorted into triplicate wells by flow cytometry three days after shRNA- or control-transduction. 50,000 sorted cells were seeded in DMEM media supplemented with 15% FBS, 10ng/mL hIL6, 6ng/mL mIL3, and 100ng/mL mSCF and incubated at 37^{o}C. In addition, 100,000 transduced cells were sorted in triplicate into phosphate buffered saline (PBS) supplemented with 2% FBS for immediate analysis. Cell cycle analysis was performed on day 0, 3, and 7 after sorting using the APC 5-bromo-2'-deoxyuridine (BrdU) flow kit (eBioscience, San Diego, CA, USA) and apoptosis assay was performed 3 and 7 days after transduction (experimental days 0 and 4) using 1x10^{6} unsorted cells and the APC Annexin V apoptosis detection kit. (eBioscience, San Diego, CA, USA) Cell cycle and apoptosis assays were analysed using a FACS LSRFortessa (BD Biosciences, San Jose, CA, USA).

3.2.6 FACS analysis

Cells were prepared for FACS analysis as described in Chapter 2[131]. Monoclonal antibodies used were phycoerythrin (PE)-labeled CD4 (clone H129.19) and CD8 (clone 53-6.7; both BD Biosciences, San Jose, CA, USA), allophycocyanin (APC)/Cy7-, PE/Cy7-, and APC-labeled c-Kit (CD117, clone 2B8), AF700-labeled Gr-1 (Ly6G/6C, clone RB6-8C5; all Biolegend, San Diego, CA, USA), PE/Cy7-labeled CD19 (clone 1D3), and APC-labelled CD11b (clone M1/70; both eBioscience, San Diego, CA, USA). Human cord blood AML ND13+MN1 cells[126] were sorted using PE-labeled G-protein receptor 56 (GPR56) (clone CG4; Biolegend, San Diego, CA, USA) and APC-labeled CD34 (STEMCELL Technologies, Vancouver, BC, Canada).

For isolation of primary murine progenitor and mature cell populations, bone marrow was isolated and suspended in PBS supplemented with 2% FBS and red blood cells were lysed with PharmLyse reagent (BD Biosciences, San Jose, CA, USA) per manufacturer instructions. Cells were blocked for 20 minutes on ice in PBS supplemented with 5% rat sera (STEMCELL Technologies, Vancouver, BC, Canada) and 1μg/1x10^6 Fc receptor (FcR, CD16/32), then washed with PBS supplemented with 2% FBS. Cells to be sorted for GMPs, MEPs, or CMPs were stained directly without blocking. Antibodies used were as previously described[83].

Immunophenotypic analysis of murine cells was performed on stained cells filtered through a 45 μM filter (Argos Technologies, IL, USA) using a BD LSRFortessa (BD Biosciences, San Diego, CA, USA) in the presence of 1μM 4',6-diamidino-2-phenylindole (DAPI, Sigma-Aldrich, Oakville, ON, Canada).

3.2.7 Bone marrow transplantation and monitoring of mice

Bone marrow cells (100,000 of each subpopulation or 50,000 shRNA-transduced cells) accompanied by a life-sparing dose of 1×10^5 freshly isolated bone marrow cells from syngeneic mice were intravenously injected into recipient mice that had been exposed to a single dose of 810 cGy total-body x-ray irradiation, and were monitored daily. Engraftment of transduced cells in peripheral blood was monitored every 2-4 weeks by blood counts with differential red and white blood cell analysis using the scil Vet abc blood analyser (Vet Novations, Barrie, ON, Canada), fluorescence-activated cell-sorter (FACS) analysis, and quantification of GFP-positive cells. Sick or moribund mice were sacrificed, spleens weighed, and red blood cells and white blood cells from cardiac puncture of euthanised mice were counted using the scil Vet abc blood

analyser. C57BL/6J mice were bred and maintained in the Animal Research Centre of the British Columbia Cancer Agency as approved by the University of British Columbia Animal Care Committee (the Institutional Animal Care and Use Committee, IACUC). Experimental studies were approved by the University of British Columbia Animal Care Committee under experimental protocol number A13-0063, and all efforts were made to minimise suffering.

3.2.8 Bone marrow morphology

Cytospin preparations were stained with Wright-Giemsa stain as described in Chapter 2[131]. Images were visualised using a Axioplan2 microscope (Zeiss, Oberkochen, Germany) and a 63x/1.4 numerical aperture objective and Nikon Immersion Oil (Nikon, Mississauga, ON, Canada). Images were captured using OpenLab 5 (Improvision, Coventry, England).

3.2.9 RNA extraction, Agilent gene expression array, and gene set enrichment analysis

RNA was extracted using TRIZOL reagent (Life Technologies, Burlington, ON, Canada) from MN1 cell subpopulations that were sorted from mouse bone marrow cells at time of sacrifice. Cleanup of RNA was performed using the GeneJET RNA Cleanup and Concentration Micro Kit (ThermoFisher Scientific). Gene expression profiling was conducted using the Agilent Mouse GE 8x60K microarray (Agilent Technologies, Mississauga, ON, Canada). Quality and integrity of the total RNA isolated was controlled by running all samples on an Agilent Technologies Bioanalyzer 2100 (Agilent Technologies). Quantile normalization and data analysis were performed using the GeneSpring 1.5.1 software package (Agilent Technologies), applying an unpaired T-test and Benjamini-Hochberg multiple testing correction at an FDR of 0.05.

Experiments were performed at the British Columbia Genome Sciences Centre, Vancouver, BC, Canada.

For gene set enrichment the Broad Institute GSEA software package was used for gene set enrichment analysis[154]. Analyzed gene ontology sets were obtained from MSigDB v3.1[154]. The gene set enrichment analysis software (http://www.broad.mit.edu/gsea/index.jsp) was used to compare MN1 cKit versus MN1 CD11b for gene enrichment of Gene Ontology gene sets (dataset C5, available from the Molecular Signature database v3.1)[154] or gene expression sets from published literature as indicated in the text. Venn diagrams were generated using the BioVenn web application[165].

3.2.10 RNA extraction and cDNA generation

Total RNA was isolated from MN1 cell subpopulations sorted from mouse bone marrow cells at time of sacrifice, sorted shRNA-transduced MN1 bone marrow cell lines 72 hours after transduction, or stored frozen cell pellets and converted into cDNA as described in Chapter 2[131].

3.2.11 Analysis of human patient samples

The in-house gene expression database was generated from RNA-Seq from patients with AML, MDS, therapy-related AML (tAML), therapy-related MDS (tMDS), and AML arising from MDS (AML-MDS). Patients were consented and studies were approved by the BC Cancer Agency Research Ethics Board under protocol number H13-02687. Expression quantification was performed using sailfish (version 0.9.0)[166] from raw read counts and transcripts-per-million (TPM) expression measures. Variant-calling was performed on gene targets with known

relevance to myeloid malignancies using VarScan 2 (version 2.3.9)[167] and all samples were annotated with respect to presence or absence of inversions-deletions (indels) in NPM1. The expression values of HOXA9, MN1, MEIS1, and MEIS2 were subcategorized from the larger expression matrix and for MEIS1 and MN1 divided into high (50%) and low (50%) based on median gene expression. The pheatmap program (version 1.0.8) from R (version 3.3.0) was used to cluster all samples by Euclidean distance.

3.2.12 Statistical analysis

Gene expression analyses and functional assay comparisons were performed by unpaired T-tests and applying a Benjamini-Hochberg test correction at an FDR of 0.05 using GeneSpring 12.0 (Agilent Technologies)[168]. Functional data were evaluated using the two-sided Students t-test with differences with P values less than 0.05 considered statistically significant. Comparison of survival curves were performed using the Kaplan-Meier method and log-rank test, and visualised using GraphPad Prism 6 (GraphPad Software, La Jolla, CA, USA) or using the Bloodspot database[169]. Statistical analyses of patient RNA-Seq data from the in-house dataset were performed using a Welch two-sample t-test using R (version 3.3.1)[170]. Statistical analyses were performed with Excel (Microsoft Canada, Mississauga, ON, Canada), GraphPad Prism 6, and FLOWJO (Tree Star Inc., Ashland, OR, USA) to analyse the FACS plots. P-values of less than 0.05 were considered statistically significant.

3.3 Results

3.3.1 Establishing an experimental framework to explore genes and pathways critical to MN1 leukemia

The overarching goal this thesis was to establish experimental frameworks that would allow further elucidation of genes and pathways relevant to leukemia. Comparisons of functional and gene expression differences in leukemic cells have identified genes, pathways, and molecular signatures associated with LSC activity, as demonstrated by studies of the phenotypic, functional, and gene expression properties of AML cells[6, 10]. To further unravel genes and pathways arising from overexpression of MN1, I made informative comparisons using MN1 models with varying LIC activity. One such comparison is the non-leukemic MN1 variant lacking the N-terminal 202 amino acids (MN1Δ1), described in Chapter 2 of this thesis. Although murine bone marrow retrovirally-transduced with MN1Δ1 shows no leukemic activity *in vivo*, the gene expression profile of these cells clusters more closely to wildtype MN1 leukemic cells as opposed to mature myeloid Gr-1$^+$CD11b$^+$ cells, while showing significant gene expression differences in genes linked to self-renewal, such as HoxA9, HoxA10, Jun, and Fos, and differentiation, including Klf family members (table located at http://dx.doi.org/10.1371/journal.pone.0112671)[131]. Further analysis of a variant lacking the C-terminal 206 amino acids (MN1Δ7), which induces a less-aggressive AML with a more mature phenotype, compared to the full-length MN1 revealed a gene expression profile that clusters more closely to mature myeloid cells, with differentially expressed genes pointing to the immune response pathway, such as Ecp proteins and eosinophil peroxidase, and differentiation-related gene sets (table located at at http://dx.doi.org/10.1371/journal.pone.0112671)[131]. Similarly, gene expression analysis of a MN1 variant fused to the transcriptional activation domain VP16

(MN1VP16), which induces AML with a longer latency and a more mature myeloid phenotype than wildtype MN1, revealed downregulation of key genes involved in the immune response pathway – Ir8 and its downstream target Ccl9 – as critical to MN1 leukemic activity. These gene expression data provided an opportunity to search for overlapping signature genes that may represent genes and pathways key to the leukemogenic activity of MN1. In addition, I further assessed the phenotypic and functional heterogeneity of MN1 leukemia, with the goal to identify subpopulations with differential leukemia-initiating activity to provide value for gene expression profiling and supplement the existing datasets.

3.3.2 Phenotypic heterogeneity of primary murine MN1 leukemic bone marrow cells reflects functional heterogeneity

As described in Chapter 2 and previous literature[109], bone marrow from moribund leukemic MN1 mice is phenotypically heterogeneous, with cells showing variable expression of the immature cell surface markers c-Kit and Sca1 and myeloid markers Gr-1 and CD11b. Here, I sought to determine if this phenotypic heterogeneity was associated with differential LIC content. I generated primary murine leukemias by MN1 overexpression in bone marrow through retroviral gene transfer followed by transplantation of transduced cells. Bone marrow from individual leukemic mice was subfractionated into three populations: c-Kit^{+}CD11b^{-} (abbreviated as the cKit fraction or subpopulation), c-Kit$^{neg\text{-}mid}$CD11b^{+} (abbreviated as the CD11b fraction or subpopulation), and a population lacking expression of either of these markers (abbreviated as the cKit^{neg}CD11b^{neg} fraction or subpopulation) (Figure 3.2A). Functional assessment of the colony-forming ability of these cell subpopulations reveals that the cKit^{neg}CD11b^{neg} and CD11b

fractions are essentially devoid of CFC activity (6.5 ± 1.3 and 0.25 ± 0.25 colonies, respectively) while the cKit fraction has equivalent colony-forming unit (CFU) ability compared to MN1 bulk cells (152.5 ± 19.69 versus 104.3 ± 8.56 colonies per 1000 cells plated, unpaired two-tailed t-test, n.s.) (Figure 3.2B). Colonies derived from the cKit fraction have similar replating ability to bulk MN1 cells over five successive replatings (314,000 ± 87,000 versus 750,000 ± 317,000 cumulative colonies, unpaired two-tailed t-test, P=0.16). In contrast, the $cKit^{neg}CD11b^{neg}$ (52 ± 10.58 cumulative colonies) and CD11b fractions (2 ± 2 cumulative colonies) generate few colonies with replating ability (Figure 3.2B). I transplanted equal numbers of MN1 bulk, cKit, and CD11b cells into secondary recipients to investigate the leukemogenic activity of these subpopulations. Cells from the cKit subpopulation retain full LSC activity, with engraftment levels and median latency of leukemia essentially identical to bulk MN1 cells (38.5 compared to 39.5 days post-transplantation, Mantel-Cox test, n.s.) (Figure 3.2C). Immunophenotyping of bone marrow arising from cKit cells also regenerate the full spectrum of cell types as seen in both primary leukemic cells and bone marrow derived from unfractionated MN1 leukemic cells (Figure 3.2D, Figure 3.3A). Additionally, mice transplanted with MN1 bulk or cKit cells display splenomegaly, elevated white blood cell numbers, and depressed red blood cell and platelet counts compared to CD11b-transplanted mice (unpaired t-test, $P<0.05$ and $P<0.01$) (Figure 3.3B-C). In contrast, mice transplanted with CD11b cells largely fail to develop leukemia after 120 days post-transplant, with the survival curve significantly diverging from that of bulk MN1-transplanted mice ($P<0.01$, Mantel-Cox test) (Figure 3.C). Most CD11b-transplanted mice show no engraftment of GFP^+ donor cells (Figure 3.2D) but contain GFP^- bone marrow containing $CD19^+$ B cells, $CD4^+/CD8^+$ T cells, $CD11b^+$ monocytes, low expression of immature $c\text{-}Kit^+$ cells, and fewer blasts (Figure 3.3.3D-E), normal spleen weights, and normal white blood cell,

red blood cell, and platelet counts (Figure 3.3B-C). These data provide support for functional heterogeneity among MN1 leukemic cells and reveal a hierarchical structure consistent with a stem cell model, with the c-Kit fraction containing leukemia-initiating activity whereas the CD11b subset is severely depleted or absent of such cells.

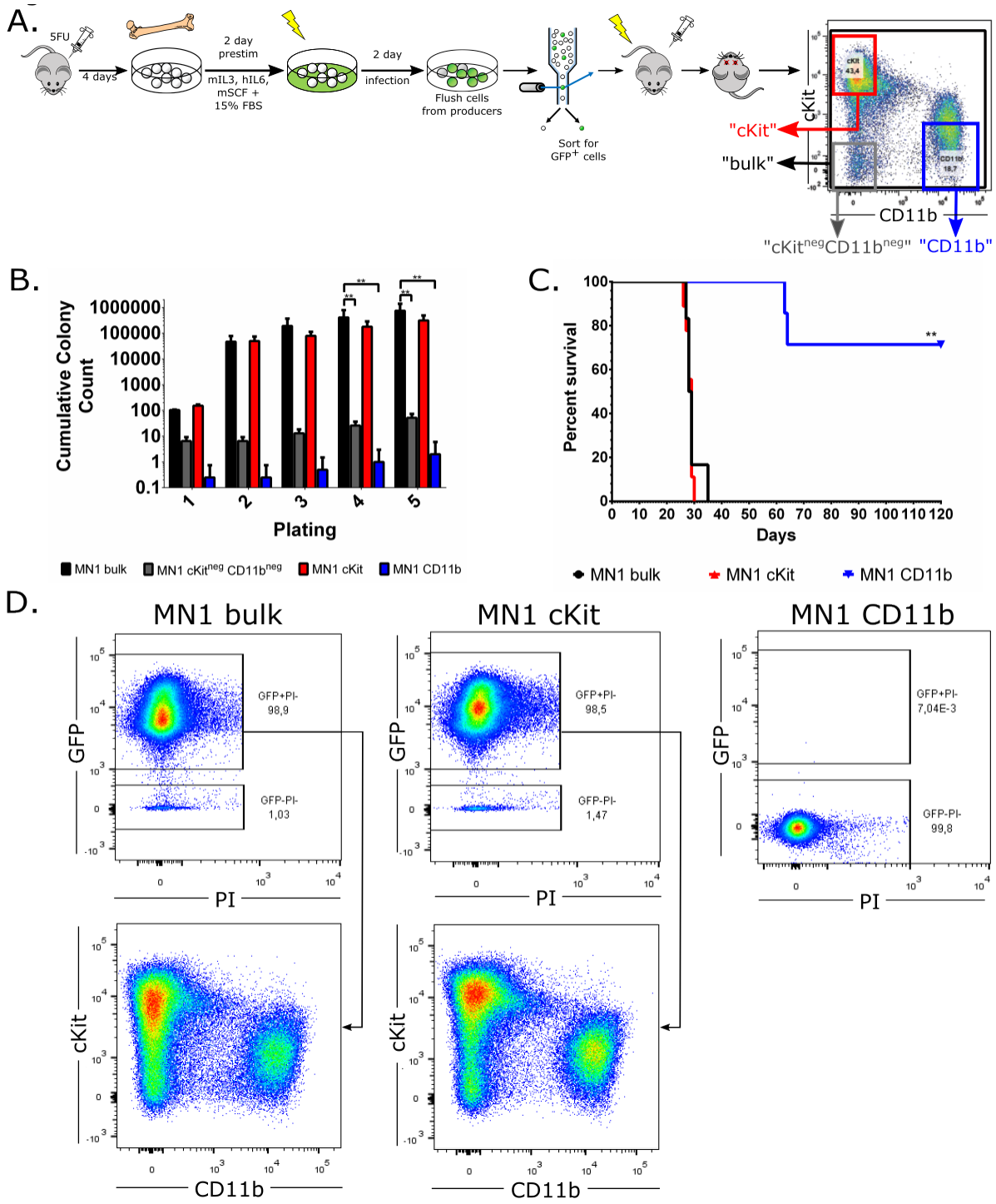

Figure 3.2 Primary murine MN1 leukemic cells can be separated into phenotypically distinct populations that are functionally heterogeneous

(A) Experimental design for generation of MN1-transduced 5FU bone marrow and fractionation of primary bone marrow from moribund mice into three distinct subpopulations based on the cell surface markers c-Kit and CD11b

(c-Kit^{+}CD11b^{-}, "cKit"; c-Kit$^{neg\text{-}mid}$CD11b^{+}, "CD11b"; and c-Kit^{-}CD11b^{-}, "cKit^{neg}CD11b^{neg}") by flow cytometry. (B) Serial replating of sorted MN1 bulk, cKit, CD11b bone marrow cells from moribund MN1 mice, represented as cumulative colony count. Subpopulations from two independent mice, n=2; error bars represent ± SEM; *P<0.05, **P<0.01 (unpaired t-test versus MN1 bulk). (C) Survival curve of mice transplanted with sorted MN1 bulk, cKit, and CD11b bone marrow subpopulations from leukemic mice transplanted with MN1-transduced cells. n=6 for MN1 bulk, n=8 for cKit and CD11b cells; **P<0.01 (Mantel-Cox). (D) Representative flow cytometric analysis of engraftment level and c-Kit and CD11b cell surface markers on bone marrow from moribund mice transplanted with (i) MN1 bulk, (ii) cKit cells, and (iii) CD11b cells.

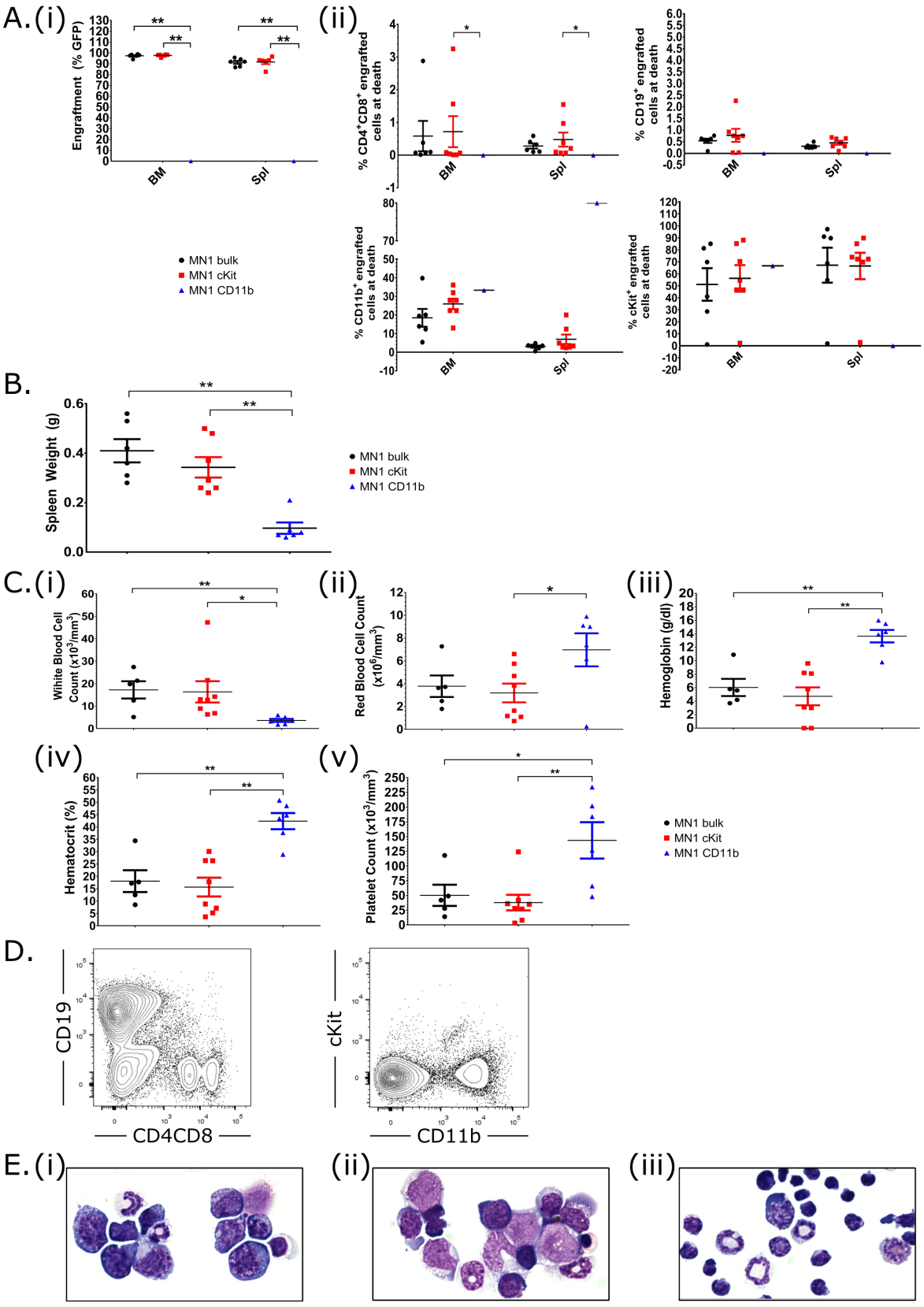

Figure 3.3 Mice transplanted with CD11b cells are functionally devoid of leukemic initiating cell activity

(A) (i) Engraftment and (ii) cell surface marker expression of engrafted $CD4^+CD8^+$, $CD19^+$, $CD11b^+$, and c-Kit^+ cells in bone marrow in moribund/sacrificed secondary mice transplanted with MN1 bulk, cKit, and CD11b cells. n=6 for MN1 bulk, n=8 for cKit, and n=1 for CD11b. Unpaired two-sided t-test in MN1 bulk vs cKit/CD11b. Error bars represent ± SEM; *P<0.05, **P<0.01. (B) Mean spleen weight of mice transplanted with MN1 bulk, cKit, or CD11b cells isolated from leukemic MN1 mice at sacrifice. n=6 for MN1 bulk and CD11b cells, n=8 for cKit cells. Unpaired two-sided t-test in MN1 bulk vs cKit/CD11b. Error bars represent ± SEM; *P<0.05, P<0.01. (C)(i) White blood cell count, (ii) red blood cell count, (iii) hemoglobin measurement, (iv) percent hematocrit, and (v) platelet count in peripheral blood of moribund/sacrifice secondary mice transplanted with MN1 bulk, cKit, or CD11b cells. n=6 for MN1 bulk and CD11b cells, n=8 for cKit cells. Unpaired two-sided t-test in MN1 bulk vs cKit/CD11b. Error bars represent ±SEM; *P<0.05, **P<0.01. (D) Representative flow cytometric analysis on bone marrow from non-leukemic mouse transplanted with CD11b cells. (E) Representative cytospins of bone marrow from moribund/sacrificed mice transplanted with (i) MN1 bulk, (ii) cKit, and (iii) CD11b cells.

3.3.3 Gene expression analysis of primary murine MN1 leukemic cell subpopulations

Having determined that the cKit and CD11b subpopulations contain and are depleted of LIC activity, respectively, I performed Agilent microarray mRNA gene expression profiling on matched subpopulations from three leukemic mice representing two independent transductions. Analysis of this gene expression data reveals 9796 differentially expressed probe sets or 5516 unique annotated genes with a minimum 1.5-fold difference in expression between the cKit and CD11b subpopulations. Of these annotated genes, 3009 are upregulated in the cKit over CD11b subpopulation, 2520 downregulated, and 354 genes show expression differences less than 1.5-fold between the two subpopulations (Figure 3.4A). Unsupervised hierarchical clustering of the top 500 differentially expressed probes reveals a clear separation in gene expression between the two subpopulations (Figure 3.4B). Using gene sets from the Broad Institute MSigDB[154] and previously-reported leukemic[137], HSC-related (HSC-R), and LSC-related (LSC-R) gene

profiles[10], GSEA of the differentially expressed genes reveals that CD11b cells are enriched in genes associated with leukocyte maturation and inflammatory and immune signaling. In contrast, the cKit fraction is enriched in genes associated with leukemic[137], HSC-R, and LSC-R[10] gene signatures (Figure 3.4C). Furthermore 587 genes from the LSC-R gene signature[10] are also differentially expressed between the cKit and CD11b subpopulations, 428 of which are core enrichment genes that contribute to the leading-edge analysis (Table 3.2). Included in this set of LSC-associated genes[10] are several members of the Hox transcription factor family that play key roles in HSC self-renewal, lineage commitment, and maturation, such as HoxA5[171], HoxA7[172], and HoxA9[57, 60, 75], and leukemic properties of transformation, self-renewal, proliferation, and differentiation[39, 63, 64, 74, 173, 174]. The Meis1 upstream regulator, Gfi1b[175], and Meis1 target gene, Trib2[176], are also represented, and are linked to cell differentiation[177] and cell fate[178]. Additionally, among the LSC-associated genes are G-protein receptors including Gpr64 and its downstream target hairy and enhancer of split 1 (Hes1), which are associated with AML development through FLT3 and Notch signaling[179], and Gpr56, which was recently reported to mark cells with high repopulating potential in primary human AML cells[180]. Together, the underlying gene expression is consistent with the cKit subpopulation of MN1 cells having LIC activity and positioned at the top of the MN1 leukemic cell hierarchy. Furthermore, the overlap between genes differentially expressed between the cKit and CD11b subpopulations and genes associated with HSC, leukemic, and LSC signatures provide support for relevance and use of the MN1 model of leukemia to provide insight into genes and pathways relevant to leukemogenesis.

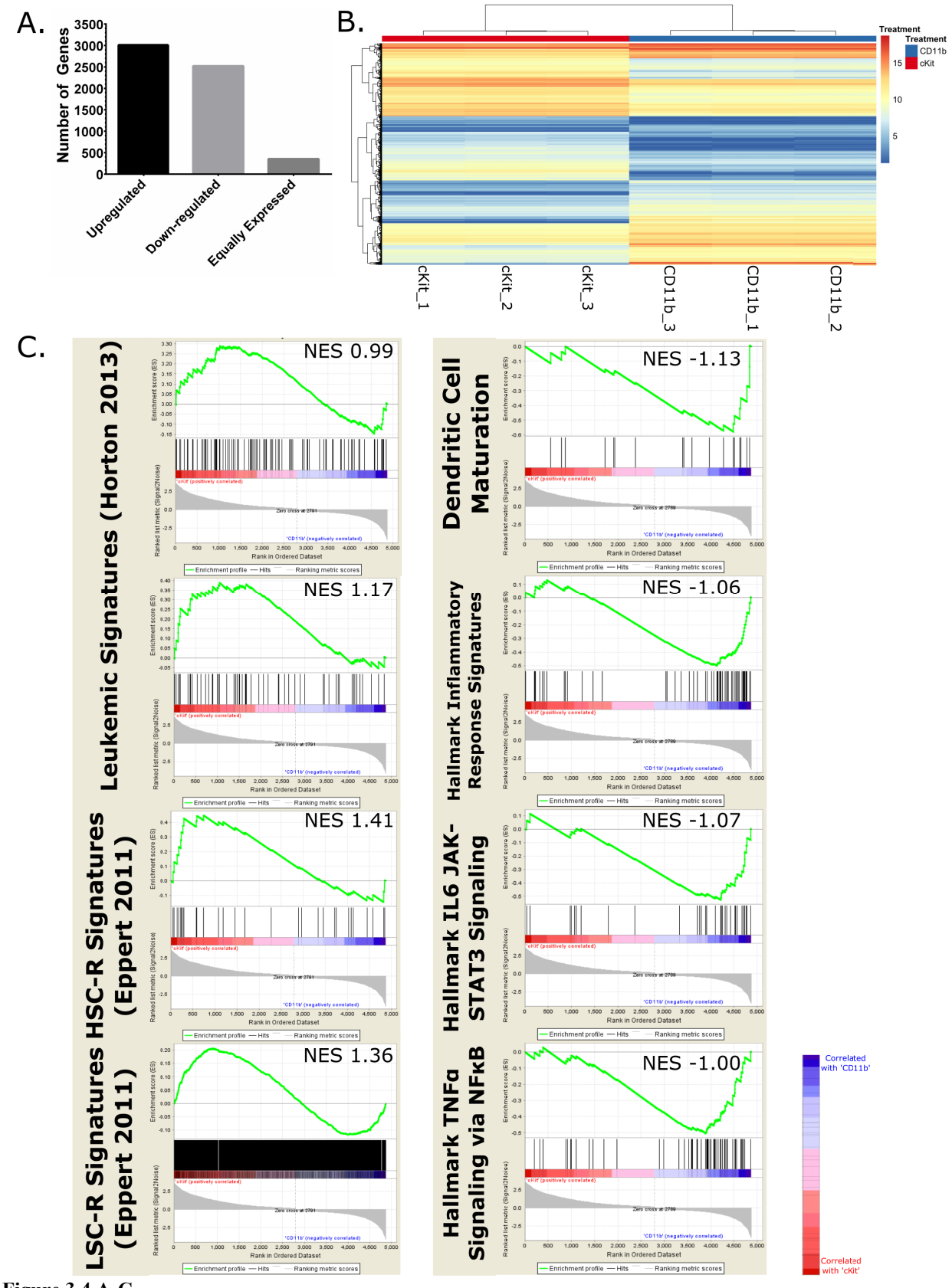
A.
Number of Genes
3500
3000
2500
2000
1500
1000
500
0
Upregulated
Down-regulated
Equally Expressed
B.
Treatment
Treatment
CD11b
cKit
15
10
5
cKit_1
cKit_2
cKit_3
CD11b_3
CD11b_1
CD11b_2
C.
Leukemic Signatures (Horton 2013)
NES 0.99
NES 1.17
LSC-R Signatures HSC-R Signatures (Eppert 2011)
NES 1.41
LSC-R Signatures (Eppert 2011)
NES 1.36
Dendritic Cell Maturation
NES -1.13
Hallmark Inflammatory Response Signatures
NES -1.06
Hallmark IL6 JAK-STAT3 Signaling
NES -1.07
Hallmark TNFα Signaling via NFκB
NES -1.00
Enrichment score (ES)
Ranked list metric (Signal2Noise)
Rank in Ordered Dataset
Enrichment profile
Hits
Ranking metric scores
'cKit' (positively correlated)
'CD11b' (negatively correlated)
Correlated with 'CD11b'
Correlated with 'cKit'

Figure 3.4 A-C

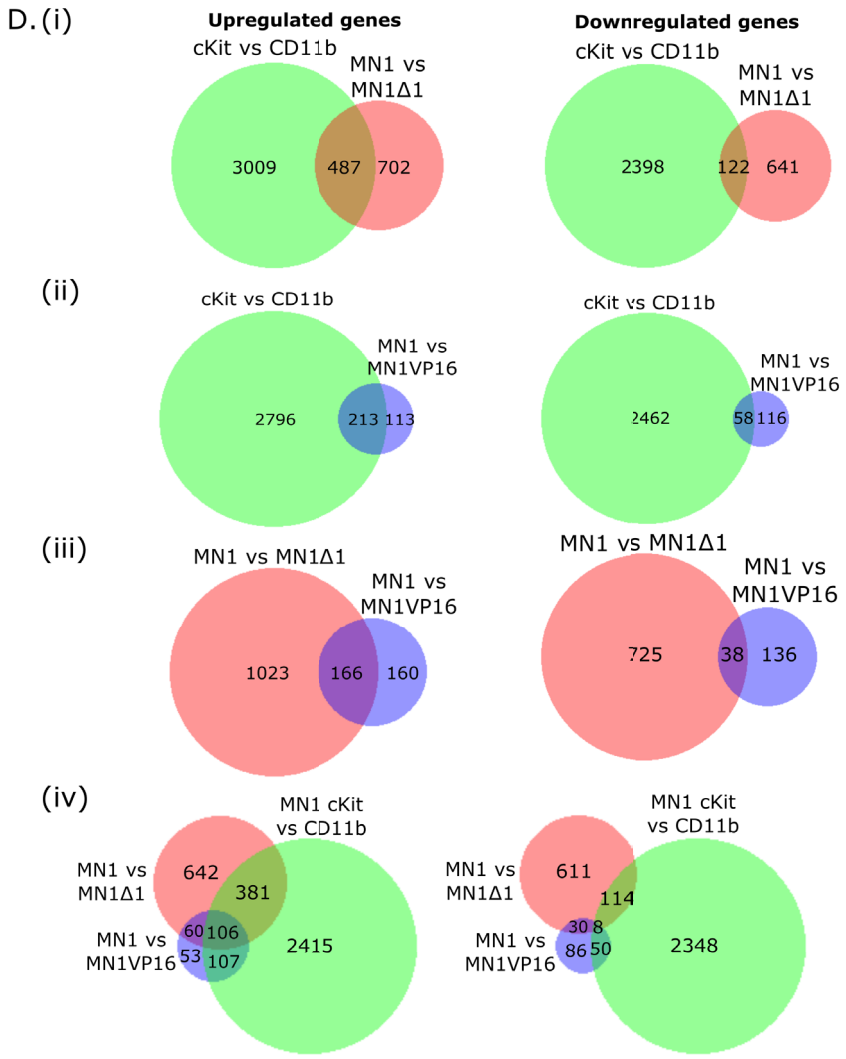

Figure 3.4 Comparisons of gene expression analysis between MN1 populations with varying LIC activity

(A) Categorization of genes upregulated, downregulated, and equally expressed (fold change between -2 and 2) between cKit and CD11b cells in murine Agilent microarray. From three mice representing two independent transductions, unpaired t-test, corrected P value<0.05 (Benjamini-Hochberg correction). (B) Heatmap of unsupervised hierarchical clustering of the top 500 differentially expressed annotated gene between cKit and CD11b cells. From three mice representing two independent transductions, unpaired t-test, fold change ≥1.5, corrected P value<0.05 (Benjamini-Hochberg correction). (C) GSEA of differentially expressed annotated gene sets in cKit vs CD11b cells. NES, normalised enrichment score; FDR, false discovery rate, and P value calculated as previously referenced[154]. (D) Graphical representation of the overlapping differentially-expressed up- and downregulated genes between (i) MN1 cKit versus CD11b cells and MN1 versus MN1Δ1 cells,[131] (ii) MN1 cKit versus CD11b and MN1

versus MN1VP16 cells[115], (iii) MN1 versus MN1Δ1 and MN1 versus MN1VP16, and (iv) up- and downregulated genes between all three datasets.

Table 3.2 Core enrichment genes enriched in cKit subpopulation from LSC-R gene set

Gene Symbol	Gene Name	Rank in Gene List	Rank Metric Score	Running ES
Kcnk5	potassium channel, subfamily K, member 5	4	3.677767	-5.27E-05
Fkbp9	FK506 binding protein 9, 63 kDa	7	3.660452	7.17E-04
Ermap	erythroblast membrane-associated protein (Scianna blood group)	10	3.60553	0.001462
Slamf1	signaling lymphocytic activation molecule family member 1	12	3.575598	0.002609
Twist1	twist homolog 1 (acrocephalosyndactyly 3; Saethre-Chotzen syndrome) (Drosophila)	18	3.51442	0.00207
Rpp40	ribonuclease P 40kDa subunit	19	3.507996	0.003602
Enpep	glutamyl aminopeptidase (aminopeptidase A)	20	3.50609	0.005134
Ppic	peptidylprolyl isomerase C (cyclophilin C)	22	3.496448	0.006246
Bmp7	bone morphogenetic protein 7 (osteogenic protein 1)	24	3.486974	0.007354
Kel	Kell blood group, metallo-endopeptidase	26	3.479464	0.008459
Ehd3	EH-domain containing 3	27	3.473526	0.009976
Galnt6	UDP-N-acetyl-alpha-D-galactosamine:polypeptide N-acetylgalactosaminyltransferase 6 (GalNAc-T6)	28	3.472379	0.011493
Antxr1	anthrax toxin receptor 1	29	3.467808	0.013008
Il7	interleukin 7	34	3.441648	0.012852
Freq	frequenin homolog (Drosophila)	41	3.394625	0.011846
Maob	monoamine oxidase B	42	3.382342	0.013323
Il27Ra	interleukin 27 receptor, alpha	43	3.382281	0.014801
Tpd52L1	tumor protein D52-like 1	47	3.34118	0.015016
Hivep2	human immunodeficiency virus type I enhancer binding protein 2	49	3.32725	0.016054
Kcnb1	potassium voltage-gated channel, Shab-related subfamily, member 1	51	3.31314	0.017086
Zfpm2	zinc finger protein, multitype 2	54	3.287076	0.017693
Ptk2	PTK2 protein tyrosine kinase 2	57	3.280651	0.018296
Rgs6	regulator of G-protein signalling 6	61	3.258554	0.018475
Sdc2	syndecan 2 (heparan sulfate proteoglycan 1, cell surface-associated, fibroglycan)	62	3.255588	0.019897
Plxna3	plexin A3	64	3.252565	0.020903
Cst6	cystatin E/M	66	3.234455	0.021901
St6Galnac5	ST6 (alpha-N-acetyl-neuraminyl-2,3-beta-galactosyl-1,3)-N-acetylgalactosaminide alpha-2,6-sialyltransferase 5	67	3.234139	0.023313
Spag6	sperm associated antigen 6	68	3.233654	0.024726

Gene Symbol	Gene Name	Rank in Gene List	Rank Metric Score	Running ES
Dctd	dCMP deaminase	69	3.227587	0.026135
Scara3	scavenger receptor class A, member 3	70	3.216034	0.02754
Rhobtb3	Rho-related BTB domain containing 3	71	3.212664	0.028943
Actn2	actinin, alpha 2	72	3.203793	0.030343
Dpt	dermatopontin	74	3.192886	0.031322
Tmcc2	transmembrane and coiled-coil domain family 2	75	3.18959	0.032716
Ank3	ankyrin 3, node of Ranvier (ankyrin G)	77	3.174191	0.033687
Copz2	coatomer protein complex, subunit zeta 2	78	3.174171	0.035074
Grap2	GRB2-related adaptor protein 2	82	3.164403	0.035211
Evc	Ellis van Creveld syndrome	83	3.159052	0.036591
Jrk	jerky homolog (mouse)	85	3.150432	0.037552
Lphn1	latrophilin 1	86	3.139913	0.038924
Tceal1	transcription elongation factor A (SII)-like 1	89	3.114946	0.039455
Spag4	sperm associated antigen 4	92	3.105361	0.039982
Serpinb5	serpin peptidase inhibitor, clade B (ovalbumin), member 5	95	3.093118	0.040503
Abhd14A	abhydrolase domain containing 14A	97	3.084771	0.041436
Srgap3	SLIT-ROBO Rho GTPase activating protein 3	98	3.083625	0.042783
Tnfsf4	tumor necrosis factor (ligand) superfamily, member 4 (tax-transcriptionally activated glycoprotein 1, 34kDa)	99	3.081715	0.044129
Prkg1	protein kinase, cGMP-dependent, type I	101	3.078821	0.045059
Homer2	homer homolog 2 (Drosophila)	102	3.074119	0.046401
Aldh1A3	aldehyde dehydrogenase 1 family, member A3	103	3.072142	0.047743
Ptch1	patched homolog 1 (Drosophila)	104	3.065707	0.049082
Maged1	melanoma antigen family D, 1	107	3.058495	0.049589
Stx1A	syntaxin 1A (brain)	108	3.057205	0.050924
Bak1	BCL2-antagonist/killer 1	109	3.049532	0.052256
Bcl11B	B-cell CLL/lymphoma 11B (zinc finger protein)	110	3.0482	0.053587
Fhl2	four and a half LIM domains 2	111	3.046017	0.054918
Trib2	tribbles homolog 2 (Drosophila)	113	3.029953	0.055826
Rpusd2	RNA pseudouridylate synthase domain containing 2	114	3.02988	0.05715
Pkd2	polycystic kidney disease 2 (autosomal dominant)	116	3.028066	0.058057
Txk	TXK tyrosine kinase	117	3.016052	0.059375
Dact1	dapper, antagonist of beta-catenin, homolog 1 (Xenopus laevis)	118	3.015471	0.060692
Mtap	methylthioadenosine phosphorylase	119	3.009978	0.062007
Col6A3	collagen, type VI, alpha 3	120	3.007916	0.06332
Kcns3	potassium voltage-gated channel, delayed-rectifier, subfamily S, member 3	121	3.007712	0.064634
Gsta3	glutathione S-transferase A3	122	3.00756	0.065948
Gpr125	G protein-coupled receptor 125	123	3.003216	0.067259

Gene Symbol	Gene Name	Rank in Gene List	Rank Metric Score	Running ES
Lamb2	laminin, beta 2 (laminin S)	126	2.995081	0.067738
Tmod1	tropomodulin 1	130	2.96626	0.067789
Gimap5	GTPase, IMAP family member 5	131	2.958893	0.069082
Kcns1	potassium voltage-gated channel, delayed-rectifier, subfamily S, member 1	133	2.947241	0.069954
Rtn2	reticulon 2	135	2.939233	0.070823
Lmcd1	LIM and cysteine-rich domains 1	136	2.935858	0.072106
Il4	interleukin 4	138	2.924732	0.072968
Pcdhb6	protocadherin beta 6	140	2.912904	0.073826
Slc22A3	solute carrier family 22 (extraneuronal monoamine transporter), member 3	141	2.903812	0.075094
Inpp4B	inositol polyphosphate-4-phosphatase, type II, 105kDa	143	2.895994	0.075944
Arhgef5	Rho guanine nucleotide exchange factor (GEF) 5	144	2.886074	0.077205
Gspt2	G1 to S phase transition 2	150	2.858265	0.076379
Thbs2	thrombospondin 2	154	2.836447	0.076374
Gypa	glycophorin A (MNS blood group)	157	2.81891	0.076776
Spon2	spondin 2, extracellular matrix protein	158	2.787489	0.077993
Ahsg	alpha-2-HS-glycoprotein	162	2.777627	0.077962
Sytl2	synaptotagmin-like 2	163	2.773229	0.079173
Nap1L3	nucleosome assembly protein 1-like 3	164	2.764999	0.080381
Grtp1	growth hormone regulated TBC protein 1	175	2.699816	0.077413
Hoxa5	homeobox A5	178	2.689551	0.077758
Slc2A10	solute carrier family 2 (facilitated glucose transporter), member 10	179	2.688918	0.078932
Apbb1	amyloid beta (A4) precursor protein-binding, family B, member 1 (Fe65)	180	2.68821	0.080106
Gfra1	GDNF family receptor alpha 1	181	2.687676	0.08128
Sidt1	SID1 transmembrane family, member 1	182	2.686846	0.082454
Sdc1	syndecan 1	183	2.678951	0.083624
Pdzrn4	PDZ domain containing RING finger 4	184	2.673301	0.084792
Hoxa11	homeobox A11	185	2.66401	0.085955
Plxna2	plexin A2	187	2.65597	0.0867
Notch3	Notch homolog 3 (Drosophila)	188	2.643381	0.087855
Rarres1	retinoic acid receptor responder (tazarotene induced) 1	189	2.642308	0.089009
Znf250	zinc finger protein 250	192	2.629672	0.089328
Slc14A1	solute carrier family 14 (urea transporter), member 1 (Kidd blood group)	193	2.62902	0.090476
Sfrp4	secreted frizzled-related protein 4	195	2.616319	0.091204
Efna5	ephrin-A5	196	2.613787	0.092346
Col4A1	collagen, type IV, alpha 1	197	2.613486	0.093487
Stk32B	serine/threonine kinase 32B	198	2.612147	0.094628
Ppy	pancreatic polypeptide	200	2.607424	0.095352
Arhgdig	Rho GDP dissociation inhibitor (GDI) gamma	201	2.601322	0.096489
Il7R	interleukin 7 receptor	207	2.590282	0.095546

Gene Symbol	Gene Name	Rank in Gene List	Rank Metric Score	Running ES
Spats2	spermatogenesis associated, serine-rich 2	209	2.587532	0.096262
Sh2D4A	SH2 domain containing 4A	210	2.587145	0.097392
Efhc2	EF-hand domain (C-terminal) containing 2	211	2.58178	0.098519
Zmat4	zinc finger, matrin type 4	212	2.578244	0.099645
Faah	fatty acid amide hydrolase	214	2.559964	0.100349
Dnaja4	DnaJ (Hsp40) homolog, subfamily A, member 4	215	2.558527	0.101466
Icam4	intercellular adhesion molecule 4 (Landsteiner-Wiener blood group)	217	2.555085	0.102167
Aqp1	aquaporin 1 (Colton blood group)	219	2.552445	0.102868
Fads1	fatty acid desaturase 1	220	2.551557	0.103982
Hoxa2	homeobox A2	221	2.550482	0.105096
Pycr1	pyrroline-5-carboxylate reductase 1	224	2.540827	0.105376
Ccl17	chemokine (C-C motif) ligand 17	225	2.536856	0.106484
Fbn1	fibrillin 1	226	2.526079	0.107588
Crhbp	corticotropin releasing hormone binding protein	230	2.514906	0.107442
Islr	immunoglobulin superfamily containing leucine-rich repeat	231	2.513266	0.108539
Gp5	glycoprotein V (platelet)	232	2.509449	0.109636
Epha3	EPH receptor A3	233	2.509129	0.110731
Zdhhc14	zinc finger, DHHC-type containing 14	234	2.508567	0.111827
Itga9	integrin, alpha 9	236	2.50507	0.112507
Ryk	RYK receptor-like tyrosine kinase	239	2.498112	0.112768
Sorbs3	sorbin and SH3 domain containing 3	241	2.497082	0.113444
Tfpi	tissue factor pathway inhibitor (lipoprotein-associated coagulation inhibitor)	243	2.487834	0.114116
Galnt10	UDP-N-acetyl-alpha-D-galactosamine:polypeptide N-acetylgalactosaminyltransferase 10 (GalNAc-T10)	244	2.486197	0.115202
Mst1R	macrophage stimulating 1 receptor (c-met-related tyrosine kinase)	245	2.484198	0.116287
Myo1E	myosin IE	246	2.481546	0.117371
Kremen2	kringle containing transmembrane protein 2	252	2.46403	0.116373
Fzd1	frizzled homolog 1 (Drosophila)	254	2.463096	0.117034
Fgf3	fibroblast growth factor 3 (murine mammary tumor virus integration site (v-int-2) oncogene homolog)	256	2.455329	0.117692
Pcyt1B	phosphate cytidylyltransferase 1, choline, beta	258	2.45319	0.118349
Srd5A1	steroid-5-alpha-reductase, alpha polypeptide 1 (3-oxo-5 alpha-steroid delta 4-dehydrogenase alpha 1)	260	2.444785	0.119002
Bicd1	bicaudal D homolog 1 (Drosophila)	261	2.440051	0.120067
Gbx2	gastrulation brain homeobox 2	275	2.390867	0.11572
Col5A1	collagen, type V, alpha 1	277	2.377416	0.116343

Gene Symbol	Gene Name	Rank in Gene List	Rank Metric Score	Running ES
P4Ha2	procollagen-proline, 2-oxoglutarate 4-dioxygenase (proline 4-hydroxylase), alpha polypeptide II	279	2.374455	0.116966
Gng3	guanine nucleotide binding protein (G protein), gamma 3	283	2.356436	0.116751
Fads3	fatty acid desaturase 3	286	2.350738	0.116948
Clca3	chloride channel, calcium activated, family member 3	287	2.347204	0.117973
Hdac11	histone deacetylase 11	288	2.341937	0.118996
Arhgef12	Rho guanine nucleotide exchange factor (GEF) 12	290	2.337577	0.119602
Pkp2	plakophilin 2	291	2.334365	0.120622
Prkch	protein kinase C, eta	293	2.333262	0.121226
Lag3	lymphocyte-activation gene 3	294	2.330028	0.122244
Pax6	paired box gene 6 (aniridia, keratitis)	296	2.325394	0.122845
Ntng1	netrin G1	299	2.315787	0.123027
Elovl6	ELOVL family member 6, elongation of long chain fatty acids (FEN1/Elo2, SUR4/Elo3-like, yeast)	301	2.314179	0.123623
Vegfc	vascular endothelial growth factor C	304	2.3097	0.123802
Bag2	BCL2-associated athanogene 2	307	2.30235	0.123978
Hyal1	hyaluronoglucosaminidase 1	308	2.299363	0.124982
Cplx2	complexin 2	309	2.297467	0.125986
Gstm5	glutathione S-transferase M5	320	2.272447	0.122831
Tpm2	tropomyosin 2 (beta)	323	2.266469	0.122991
Sphk1	sphingosine kinase 1	324	2.263917	0.12398
Kif5A	kinesin family member 5A	330	2.244327	0.122886
Mmp15	matrix metallopeptidase 15 (membrane-inserted)	331	2.240406	0.123865
Dpf3	D4, zinc and double PHD fingers, family 3	332	2.239722	0.124843
Smo	smoothened homolog (Drosophila)	333	2.236917	0.12582
Lrrn3	leucine rich repeat neuronal 3	340	2.225912	0.124304
Cdon	Cdon homolog (mouse)	342	2.224627	0.124861
Epor	erythropoietin receptor	343	2.22283	0.125832
Pipox	pipecolic acid oxidase	345	2.216694	0.126385
Phactr1	phosphatase and actin regulator 1	347	2.207392	0.126934
Podxl	podocalyxin-like	348	2.206006	0.127898
St8Sia3	ST8 alpha-N-acetyl-neuraminide alpha-2,8-sialyltransferase 3	350	2.203528	0.128446
Cdh4	cadherin 4, type 1, R-cadherin (retinal)	352	2.200121	0.128992
Chst8	carbohydrate (N-acetylgalactosamine 4-0) sulfotransferase 8	354	2.194276	0.129535
Dpp4	dipeptidyl-peptidase 4 (CD26, adenosine deaminase complexing protein 2)	355	2.190411	0.130492
Akap12	A kinase (PRKA) anchor protein (gravin) 12	358	2.173872	0.130612
F8	coagulation factor VIII, procoagulant component (hemophilia A)	359	2.171253	0.13156
Myog	myogenin (myogenic factor 4)	363	2.162583	0.131261

Gene Symbol	Gene Name	Rank in Gene List	Rank Metric Score	Running ES
Hmgn3	high mobility group nucleosomal binding domain 3	364	2.158252	0.132203
Frzb	frizzled-related protein	369	2.150836	0.131484
Atp4A	ATPase, H+/K+ exchanging, alpha polypeptide	370	2.150695	0.132423
Slc1A3	solute carrier family 1 (glial high affinity glutamate transporter), member 3	371	2.141648	0.133359
Tbc1D16	TBC1 domain family, member 16	373	2.132115	0.133875
Ext1	exostoses (multiple) 1	374	2.129117	0.134805
Auts2	autism susceptibility candidate 2	375	2.127487	0.135734
Dhtkd1	dehydrogenase E1 and transketolase domain containing 1	379	2.115339	0.135414
Cyp11A1	cytochrome P450, family 11, subfamily A, polypeptide 1	381	2.112376	0.135922
Slc11A2	solute carrier family 11 (proton-coupled divalent metal ion transporters), member 2	382	2.111767	0.136844
Gfi1B	growth factor independent 1B (potential regulator of CDKN1A, translocated in CML)	383	2.108537	0.137765
Ablim1	actin binding LIM protein 1	384	2.10812	0.138686
Spink4	serine peptidase inhibitor, Kazal type 4	386	2.101621	0.139189
Snn	stannin	387	2.099162	0.140106
Insl6	insulin-like 6	391	2.086301	0.139773
Arhgef9	Cdc42 guanine nucleotide exchange factor (GEF) 9	393	2.080765	0.140267
Cacnb3	calcium channel, voltage-dependent, beta 3 subunit	394	2.079987	0.141175
Slc2A2	solute carrier family 2 (facilitated glucose transporter), member 2	395	2.079632	0.142084
Lgi2	leucine-rich repeat LGI family, member 2	396	2.076917	0.142991
Pcdhb17	protocadherin beta 17 pseudogene	400	2.07179	0.142651
Adam11	ADAM metallopeptidase domain 11	405	2.061169	0.141893
Npy	neuropeptide Y	406	2.060668	0.142793
Xylb	xylulokinase homolog (H. influenzae)	408	2.059235	0.143277
Chn2	chimerin (chimaerin) 2	409	2.056701	0.144176
Capn5	calpain 5	411	2.048852	0.144656
Itgb1Bp2	integrin beta 1 binding protein (melusin) 2	412	2.044647	0.145549
Leprel2	leprecan-like 2	417	2.041985	0.144782
Prrg4	proline rich Gla (G-carboxyglutamic acid) 4 (transmembrane)	418	2.041589	0.145673
Sv2A	synaptic vesicle glycoprotein 2A	419	2.039979	0.146564
Mmp14	matrix metallopeptidase 14 (membrane-inserted)	420	2.0386	0.147455
Gata2	GATA binding protein 2	422	2.036926	0.14793
Tulp3	tubby like protein 3	425	2.032576	0.147988
Nme4	non-metastatic cells 4, protein expressed in	427	2.029372	0.14846
Dazl	deleted in azoospermia-like	429	2.027832	0.14893
Trpm4	transient receptor potential cation channel, subfamily M, member 4	430	2.022396	0.149814

Gene Symbol	Gene Name	Rank in Gene List	Rank Metric Score	Running ES
Mab21L2	mab-21-like 2 (C. elegans)	432	2.018075	0.15028
Gab1	GRB2-associated binding protein 1	433	2.017377	0.151162
Abi2	abl interactor 2	434	2.013615	0.152041
Avil	advillin	435	2.011125	0.152919
Klk8	kallikrein 8 (neuropsin/ovasin)	440	1.99864	0.152133
Parvb	parvin, beta	442	1.99451	0.15259
Amph	amphiphysin (Stiff-Man syndrome with breast cancer 128kDa autoantigen)	446	1.980931	0.152211
Pmfbp1	polyamine modulated factor 1 binding protein 1	449	1.973385	0.152243
Phlda3	pleckstrin homology-like domain, family A, member 3	451	1.96772	0.152688
Ctf1	cardiotrophin 1	452	1.960433	0.153544
Spock2	sparc/osteonectin, cwcv and kazal-like domains proteoglycan (testican) 2	453	1.96017	0.1544
Calml4	calmodulin-like 4	455	1.956321	0.15484
Abca5	ATP-binding cassette, sub-family A (ABC1), member 5	456	1.953678	0.155693
Nutf2	nuclear transport factor 2	459	1.945858	0.155714
Hoxa7	homeobox A7	460	1.943764	0.156563
Ankh	ankylosis, progressive homolog (mouse)	461	1.942939	0.157411
Ltbp3	latent transforming growth factor beta binding protein 3	462	1.941878	0.158259
Slc29A2	solute carrier family 29 (nucleoside transporters), member 2	463	1.941686	0.159107
Evpl	envoplakin	468	1.933209	0.158293
Ak5	adenylate kinase 5	472	1.923289	0.157889
Emp2	epithelial membrane protein 2	473	1.922762	0.158728
Cx3Cl1	chemokine (C-X3-C motif) ligand 1	477	1.91543	0.158321
Aldh1B1	aldehyde dehydrogenase 1 family, member B1	482	1.914003	0.157498
Abcb4	ATP-binding cassette, sub-family B (MDR/TAP), member 4	483	1.913118	0.158333
Sdpr	serum deprivation response (phosphatidylserine binding protein)	484	1.911973	0.159168
Tbxa2R	thromboxane A2 receptor	485	1.910713	0.160003
Rab36	RAB36, member RAS oncogene family	491	1.907578	0.158762
Frk	fyn-related kinase	492	1.906605	0.159595
Shq1	SHQ1 homolog (S. cerevisiae)	494	1.904075	0.160012
Gucy1B3	guanylate cyclase 1, soluble, beta 3	495	1.903914	0.160843
Osbpl3	oxysterol binding protein-like 3	498	1.897099	0.160842
Rrad	Ras-related associated with diabetes	502	1.891871	0.160424
Galr2	galanin receptor 2	503	1.889025	0.16125
Plek2	pleckstrin 2	504	1.888704	0.162075
Asph	aspartate beta-hydroxylase	505	1.888249	0.162899
Lepre1	leucine proline-enriched proteoglycan (leprecan) 1	506	1.88658	0.163723
Sept4	septin 4	507	1.886403	0.164547

Gene Symbol	Gene Name	Rank in Gene List	Rank Metric Score	Running ES
Itga2B	integrin, alpha 2b (platelet glycoprotein IIb of IIb/IIIa complex, antigen CD41)	508	1.886141	0.165371
Aldh18A1	aldehyde dehydrogenase 18 family, member A1	510	1.885469	0.16578
Crip2	cysteine-rich protein 2	511	1.885073	0.166603
Ddx4	DEAD (Asp-Glu-Ala-Asp) box polypeptide 4	515	1.878402	0.166179
Sec14L2	SEC14-like 2 (S. cerevisiae)	516	1.876455	0.166999
Lass4	LAG1 homolog, ceramide synthase 4 (S. cerevisiae)	517	1.874289	0.167817
Pcgf2	polycomb group ring finger 2	518	1.865287	0.168632
Sall2	sal-like 2 (Drosophila)	520	1.864611	0.169032
Ccr9	chemokine (C-C motif) receptor 9	523	1.859456	0.169014
Lhx2	LIM homeobox 2	527	1.857184	0.168581
Igfbp5	insulin-like growth factor binding protein 5	528	1.856461	0.169392
Ehhadh	enoyl-Coenzyme A, hydratase/3-hydroxyacyl Coenzyme A dehydrogenase	530	1.855575	0.169788
Chrna9	cholinergic receptor, nicotinic, alpha 9	532	1.851791	0.170182
Tmem14A	transmembrane protein 14A	535	1.845862	0.170159
Ndrg2	NDRG family member 2	537	1.844215	0.170549
Efemp2	EGF-containing fibulin-like extracellular matrix protein 2	539	1.83628	0.170937
Dhcr24	24-dehydrocholesterol reductase	545	1.828189	0.169661
Rab26	RAB26, member RAS oncogene family	546	1.825835	0.170459
Bcmo1	beta-carotene 15,15'-monooxygenase 1	547	1.825012	0.171256
Clca2	chloride channel, calcium activated, family member 2	548	1.824314	0.172053
Rgnef	-	555	1.81873	0.170359
Fabp7	fatty acid binding protein 7, brain	557	1.817174	0.170737
Tnni3	troponin I type 3 (cardiac)	558	1.816897	0.171531
Cdh1	cadherin 1, type 1, E-cadherin (epithelial)	559	1.809258	0.172321
Decr1	2,4-dienoyl CoA reductase 1, mitochondrial	560	1.809085	0.173111
Ranbp17	RAN binding protein 17	561	1.804999	0.1739
Ppp1R9A	protein phosphatase 1, regulatory (inhibitor) subunit 9A	564	1.799248	0.173856
St6Gal1	ST6 beta-galactosamide alpha-2,6-sialyltranferase 1	568	1.796942	0.173397
Ckm	creatine kinase, muscle	569	1.795803	0.174181
Rcl1	RNA terminal phosphate cyclase-like 1	573	1.789938	0.173719
Alas2	aminolevulinate, delta-, synthase 2 (sideroblastic/hypochromic anemia)	574	1.788677	0.1745
E2F5	E2F transcription factor 5, p130-binding	575	1.784349	0.175279
Socs2	suppressor of cytokine signaling 2	576	1.78192	0.176058
Lypd3	LY6/PLAUR domain containing 3	577	1.780985	0.176835
Cnot1	CCR4-NOT transcription complex, subunit 1	578	1.780811	0.177613
Epha7	EPH receptor A7	584	1.77038	0.176313
Col5A3	collagen, type V, alpha 3	587	1.765494	0.176254
Egf	epidermal growth factor (beta-urogastrone)	588	1.764671	0.177025
Plscr4	phospholipid scramblase 4	592	1.75934	0.176549

Gene Symbol	Gene Name	Rank in Gene List	Rank Metric Score	Running ES
Kifc3	kinesin family member C3	593	1.756796	0.177316
Inadl	InaD-like (Drosophila)	597	1.752593	0.176838
Nudt6	nudix (nucleoside diphosphate linked moiety X)-type motif 6	598	1.751662	0.177603
Gria3	glutamate receptor, ionotrophic, AMPA 3	609	1.731927	0.174212
Colec11	collectin sub-family member 11	610	1.731277	0.174968
Pvrl1	poliovirus receptor-related 1 (herpesvirus entry mediator C; nectin)	611	1.728881	0.175723
Gpr171	G protein-coupled receptor 171	612	1.728814	0.176478
Ly6D	lymphocyte antigen 6 complex, locus D	613	1.726138	0.177232
Map3K13	mitogen-activated protein kinase kinase kinase 13	614	1.724828	0.177985
Eraf	erythroid associated factor	615	1.723462	0.178738
Fasn	fatty acid synthase	616	1.722491	0.17949
Npl	N-acetylneuraminate pyruvate lyase (dihydrodipicolinate synthase)	617	1.722283	0.180243
Suv39H2	suppressor of variegation 3-9 homolog 2 (Drosophila)	625	1.713752	0.178088
Slc25A15	solute carrier family 25 (mitochondrial carrier; ornithine transporter) member 15	627	1.712387	0.178421
Dyrk3	dual-specificity tyrosine-(Y)-phosphorylation regulated kinase 3	628	1.710062	0.179168
Adrb1	adrenergic, beta-1-, receptor	629	1.707005	0.179913
F2R	coagulation factor II (thrombin) receptor	631	1.704649	0.180243
Cecr5	cat eye syndrome chromosome region, candidate 5	635	1.692547	0.179738
Nr1D2	nuclear receptor subfamily 1, group D, member 2	636	1.690396	0.180476
Gpr56	G protein-coupled receptor 56	637	1.69039	0.181215
Leprel1	leprecan-like 1	638	1.688475	0.181952
Hdhd3	haloacid dehalogenase-like hydrolase domain containing 3	639	1.68696	0.182689
Endog	endonuclease G	641	1.683504	0.18301
Nrip1	nuclear receptor interacting protein 1	643	1.677882	0.183328
Polr3D	polymerase (RNA) III (DNA directed) polypeptide D, 44kDa	644	1.674344	0.184059
Rprm	reprimo, TP53 dependent G2 arrest mediator candidate	645	1.670937	0.184789
Echdc3	enoyl Coenzyme A hydratase domain containing 3	646	1.669694	0.185518
Ccnd2	cyclin D2	650	1.666223	0.185002
Klhl22	kelch-like 22 (Drosophila)	651	1.665784	0.185729
Plod2	procollagen-lysine, 2-oxoglutarate 5-dioxygenase 2	652	1.664043	0.186456
Dpf1	D4, zinc and double PHD fingers family 1	654	1.656173	0.186765
Arhgef16	Rho guanine exchange factor (GEF) 16	656	1.652966	0.187072

Gene Symbol	Gene Name	Rank in Gene List	Rank Metric Score	Running ES
Galnt14	UDP-N-acetyl-alpha-D-galactosamine:polypeptide N-acetylgalactosaminyltransferase 14 (GalNAc-T14)	659	1.650415	0.186963
Elp4	elongation protein 4 homolog (S. cerevisiae)	665	1.633926	0.185603
Icos	inducible T-cell co-stimulator	667	1.632542	0.185901
Tspan6	tetraspanin 6	668	1.626878	0.186612
Taf4B	TAF4b RNA polymerase II, TATA box binding protein (TBP)-associated factor, 105kDa	670	1.622236	0.186906
Ick	intestinal cell (MAK-like) kinase	671	1.62166	0.187614
F2Rl3	coagulation factor II (thrombin) receptor-like 3	672	1.618467	0.188321
Serpini1	serpin peptidase inhibitor, clade I (neuroserpin), member 1	674	1.613836	0.188611
Egr4	early growth response 4	675	1.613745	0.189316
Tgfb3	transforming growth factor, beta 3	677	1.610402	0.189604
Pgr	progesterone receptor	680	1.606331	0.189477
Cd34	CD34 molecule	681	1.604669	0.190177
Slc7A6	solute carrier family 7 (cationic amino acid transporter, y+ system), member 6	682	1.603556	0.190878
Kcnj14	potassium inwardly-rectifying channel, subfamily J, member 14	683	1.602051	0.191578
Clec11A	C-type lectin domain family 11, member A	686	1.59966	0.191447
Rwdd3	RWD domain containing 3	688	1.592822	0.191728
Lcat	lecithin-cholesterol acyltransferase	690	1.591736	0.192008
Aldh5A1	aldehyde dehydrogenase 5 family, member A1 (succinate-semialdehyde dehydrogenase)	691	1.588853	0.192702
Cox6A2	cytochrome c oxidase subunit VIa polypeptide 2	692	1.587799	0.193396
Acy1	aminoacylase 1	696	1.583149	0.192843
Pacrg	PARK2 co-regulated	697	1.582312	0.193534
Cbx2	chromobox homolog 2 (Pc class homolog, Drosophila)	703	1.564045	0.192143
Depdc6	DEP domain containing 6	705	1.559487	0.19241
Cgref1	cell growth regulator with EF-hand domain 1	706	1.559209	0.193091
Six5	sine oculis homeobox homolog 5 (Drosophila)	707	1.558176	0.193771
Bzw2	basic leucine zipper and W2 domains 2	709	1.556531	0.194036
Slc35D1	solute carrier family 35 (UDP-glucuronic acid/UDP-N-acetylgalactosamine dual transporter), member D1	710	1.556035	0.194716
Upk1B	uroplakin 1B	711	1.554783	0.195395
Tuft1	tuftelin 1	714	1.55201	0.195243
Arhgap5	Rho GTPase activating protein 5	715	1.551923	0.195921
Thop1	thimet oligopeptidase 1	717	1.548598	0.196183
Lsamp	limbic system-associated membrane protein	726	1.527721	0.193532
Cdh13	cadherin 13, H-cadherin (heart)	727	1.527607	0.194199
Cpa3	carboxypeptidase A3 (mast cell)	728	1.524448	0.194865

Gene Symbol	Gene Name	Rank in Gene List	Rank Metric Score	Running ES
Mlf1	myeloid leukemia factor 1	731	1.520365	0.1947
Cdc42Ep1	CDC42 effector protein (Rho GTPase binding) 1	733	1.518716	0.194948
Pogk	pogo transposable element with KRAB domain	737	1.507439	0.194362
S100A10	S100 calcium binding protein A10	738	1.505772	0.19502
Pa2G4	proliferation-associated 2G4, 38kDa	740	1.50392	0.195262
Ntrk3	neurotrophic tyrosine kinase, receptor, type 3	741	1.501588	0.195918
Slc19A1	solute carrier family 19 (folate transporter), member 1	742	1.501221	0.196574
Cacna2D1	calcium channel, voltage-dependent, alpha 2/delta subunit 1	744	1.499542	0.196814
Rbpms	RNA binding protein with multiple splicing	745	1.496322	0.197467
Grwd1	glutamate-rich WD repeat containing 1	752	1.491044	0.19563
Sec24D	SEC24 related gene family, member D (S. cerevisiae)	756	1.489627	0.195036
Kiaa0859	KIAA0859	757	1.489441	0.195687
Dhrs2	dehydrogenase/reductase (SDR family) member 2	759	1.485041	0.195921
Xrcc5	X-ray repair complementing defective repair in Chinese hamster cells 5 (double-strand-break rejoining; Ku autoantigen, 80kDa)	761	1.484512	0.196154
Cbx6	chromobox homolog 6	762	1.482795	0.196802
Wbscr16	Williams-Beuren syndrome chromosome region 16	763	1.482513	0.197449
Stau2	staufen, RNA binding protein, homolog 2 (Drosophila)	764	1.482494	0.198097
Rhd	Rh blood group, D antigen	765	1.48178	0.198744
Gnl3	guanine nucleotide binding protein-like 3 (nucleolar)	766	1.474345	0.199388
Cth	cystathionase (cystathionine gamma-lyase)	767	1.472247	0.200031
Ppp3Cc	protein phosphatase 3 (formerly 2B), catalytic subunit, gamma isoform (calcineurin A gamma)	769	1.469461	0.200258
Lefty1	left-right determination factor 1	771	1.463911	0.200483
Plagl1	pleiomorphic adenoma gene-like 1	773	1.458607	0.200705
Fgd1	FYVE, RhoGEF and PH domain containing 1 (faciogenital dysplasia)	774	1.458212	0.201342
Pla2G12A	phospholipase A2, group XIIA	777	1.456694	0.201149
Foxj1	forkhead box J1	779	1.453457	0.201369
Prg3	proteoglycan 3	780	1.452379	0.202003
Pdcd1	programmed cell death 1	785	1.443627	0.200975
Clcn2	chloride channel 2	786	1.442171	0.201605
Actn3	actinin, alpha 3	789	1.435986	0.201402
Traf3Ip2	TRAF3 interacting protein 2	791	1.433766	0.201614
Chrnb1	cholinergic receptor, nicotinic, beta 1 (muscle)	793	1.432202	0.201825
Akap1	A kinase (PRKA) anchor protein 1	796	1.42986	0.20162

Gene Symbol	Gene Name	Rank in Gene List	Rank Metric Score	Running ES
Vpreb1	pre-B lymphocyte gene 1	797	1.429619	0.202244
Ptger3	prostaglandin E receptor 3 (subtype EP3)	798	1.429062	0.202868
Rpp38	ribonuclease P/MRP 38kDa subunit	800	1.428813	0.203077
Col1A2	collagen, type I, alpha 2	801	1.427778	0.203701
Pfkm	phosphofructokinase, muscle	803	1.424468	0.203908
Amacr	alpha-methylacyl-CoA racemase	807	1.419379	0.203284
Rbm9	RNA binding motif protein 9	811	1.413249	0.202657
Pccb	propionyl Coenzyme A carboxylase, beta polypeptide	813	1.412396	0.202859
Icam5	intercellular adhesion molecule 5, telencephalin	816	1.409536	0.202645
Alpk3	alpha-kinase 3	818	1.407974	0.202846
Slc5A3	solute carrier family 5 (inositol transporters), member 3	822	1.406221	0.202215
Cdkl1	cyclin-dependent kinase-like 1 (CDC2-related kinase)	823	1.404388	0.202829
Praf2	PRA1 domain family, member 2	824	1.40372	0.203442
Smyd2	SET and MYND domain containing 2	826	1.401026	0.203639
Mfge8	milk fat globule-EGF factor 8 protein	828	1.400347	0.203836
Gemin4	gem (nuclear organelle) associated protein 4	830	1.399655	0.204033
B4Galt2	UDP-Gal:betaGlcNAc beta 1,4-galactosyltransferase, polypeptide 2	834	1.388761	0.203395
Rnf122	ring finger protein 122	836	1.387191	0.203586
Rab6B	RAB6B, member RAS oncogene family	837	1.386796	0.204192
Smyd5	SMYD family member 5	838	1.385982	0.204797
Mylc2Pl	-	839	1.385347	0.205402
Dkkl1	dickkopf-like 1 (soggy)	842	1.381729	0.205176
Brdt	bromodomain, testis-specific	847	1.374524	0.204117
Gpc3	glypican 3	853	1.360002	0.202638
Irf6	interferon regulatory factor 6	854	1.359336	0.203231
Tnni1	troponin I type 1 (skeletal, slow)	855	1.35596	0.203824
Ifrd2	interferon-related developmental regulator 2	858	1.352972	0.203585
Mtrr	5-methyltetrahydrofolate-homocysteine methyltransferase reductase	859	1.352419	0.204176
Nthl1	nth endonuclease III-like 1 (E. coli)	864	1.346331	0.203105
Gchfr	GTP cyclohydrolase I feedback regulator	865	1.345638	0.203692
Cpox	coproporphyrinogen oxidase	869	1.338897	0.203033
Fzd4	frizzled homolog 4 (Drosophila)	871	1.338109	0.203203
Gadd45Gip1	growth arrest and DNA-damage-inducible, gamma interacting protein 1	873	1.332288	0.20337
F2Rl2	coagulation factor II (thrombin) receptor-like 2	875	1.328476	0.203535
Tgfa	transforming growth factor, alpha	876	1.328144	0.204115
Itga5	integrin, alpha 5 (fibronectin receptor, alpha polypeptide)	877	1.327246	0.204695
Cyp51A1	cytochrome P450, family 51, subfamily A, polypeptide 1	879	1.32352	0.204858
Opn3	opsin 3 (encephalopsin, panopsin)	880	1.322932	0.205436
Srm	spermidine synthase	884	1.319193	0.204768

Gene Symbol	Gene Name	Rank in Gene List	Rank Metric Score	Running ES
Tle6	transducin-like enhancer of split 6 (E(sp1) homolog, Drosophila)	886	1.315562	0.204928
Tsen2	tRNA splicing endonuclease 2 homolog (S. cerevisiae)	887	1.314176	0.205502
Acn9	ACN9 homolog (S. cerevisiae)	888	1.314083	0.206076
H1Fx	H1 histone family, member X	890	1.312318	0.206234
Tsc22D1	TSC22 domain family, member 1	891	1.310828	0.206807
Luzp1	leucine zipper protein 1	892	1.308384	0.207378

3.3.4 Selection of genes potentially relevant to MN1 leukemogenic ability for further analysis

To identify genes that are potentially important contributors to MN1 leukemia, I also compared differentially expressed genes between cKit and CD11b subpopulations to available gene expression profiles of MN1 models with varying LIC activity, specifically those comparing MN1 to MN1Δ1 (as presented in Chapter 2 and in Lai *et al.* PLOS One 2014) and MN1 to MN1VP16[115].

Of the differentially expressed genes in both cKit versus CD11b and MN1 versus MN1Δ1 gene expression analyses, 487 genes are upregulated in both comparisons while 122 genes are mutually downregulated (Figure 3.4Di). Comparing cKit versus CD11b differentially expressed genes with the genes differentially expressed between MN1 and MN1VP16 reveals 213 upregulated genes and 58 downregulated genes in both datasets (Figure 3.4Dii). In addition, comparisons of MN1 versus MN1Δ1 and MN1 versus MN1VP16 differentially expressed genes identify 166 upregulated genes and 38 downregulated genes in both analyses (Figure 3.4Diii). Together, comparisons of genes up- or downregulated in all three datasets identify 106 upregulated and 8 downregulated genes in all three datasets, and 548 genes upregulated and 210 genes downregulated in at least two of the datasets (Figure 3.4Div). From these analyses, we

selected 20 genes for validation and follow-up analysis. Twelve of these genes are differentially expressed in two or more of the MN1 datasets, suggesting they play key roles in MN1 leukemogenicity, and six genes are Meis or Pbx family members, which are crucial collaborators in MN1-induced leukemia and more broadly in leukemia[12, 84, 86, 128] (Figure 3.5A). Validation by qRT-PCR on cKit and CD11b cells isolated from primary MN1 murine leukemias, normal murine CMP cells (the target cell of transformation for MN1 murine leukemia[128]), and unfractionated mouse bone marrow (Table 3.3) demonstrated that gene expression patterns can be separated into three categories: genes overexpressed in the leukemic cKit subpopulation compared to the non-leukemic CD11b subpopulation (Figure 3.5B), genes overexpressed in the CD11b versus cKit subpopulation (Figure 3.5C), and genes that are similarly expressed between the cKit and CD11b subpopulations but overexpressed compared to normal murine CMPs and whole bone marrow (Figure 3.5D).

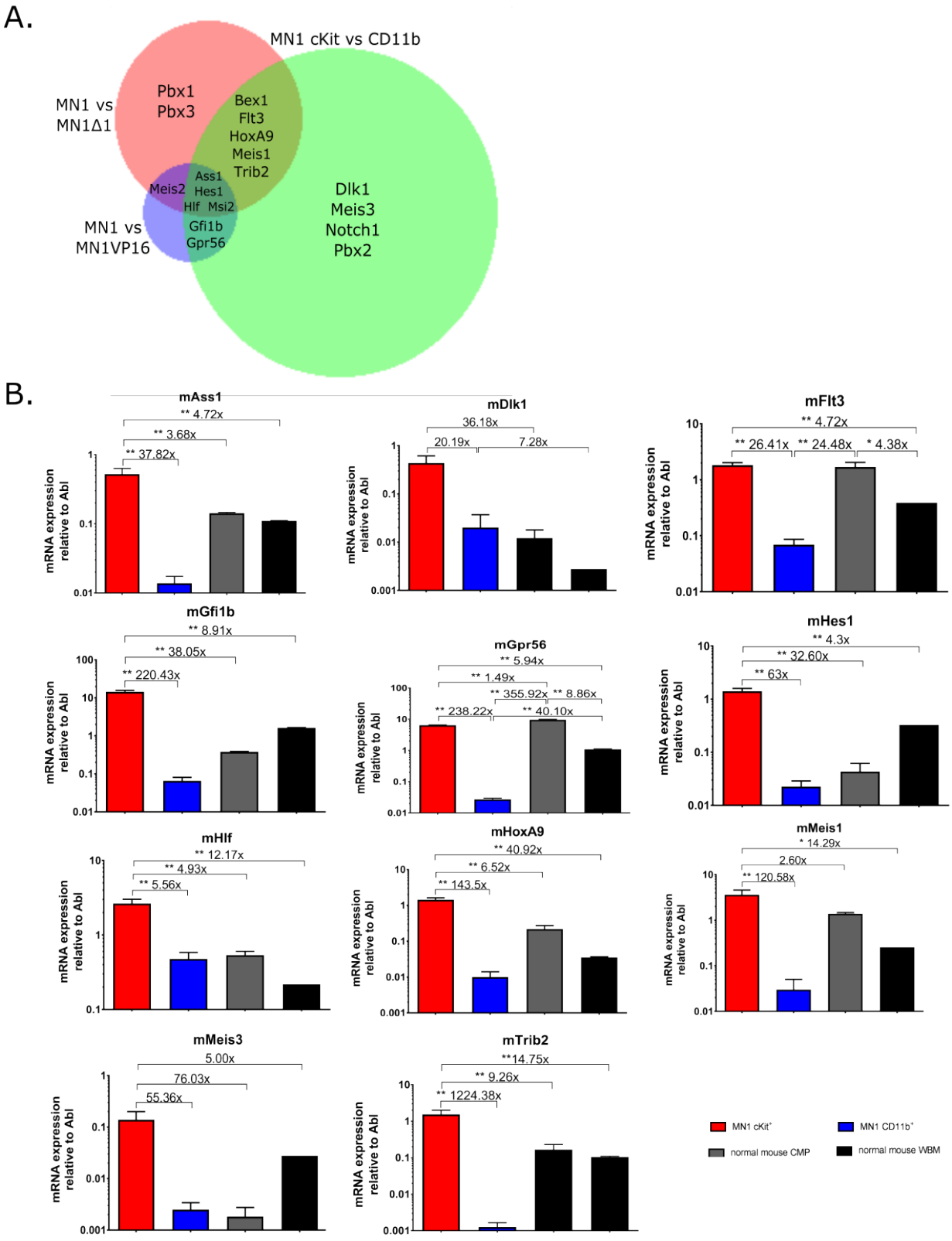
A.
MN1 cKit vs CD11b
MN1 vs MN1Δ1
Pbx1
Pbx3
Bex1
Flt3
HoxA9
Meis1
Trib2
Meis2
Ass1
Hes1
Hlf
Msi2
MN1 vs MN1VP16
Gfi1b
Gpr56
Dlk1
Meis3
Notch1
Pbx2
B.
mAss1
** 4.72x
** 3.68x
** 37.82x
mDlk1
36.18x
20.19x
7.28x
mFlt3
** 4.72x
** 26.41x
** 24.48x
* 4.38x
mGfi1b
** 8.91x
** 38.05x
** 220.43x
mGpr56
** 5.94x
** 1.49x
** 355.92x
** 8.86x
** 238.22x
** 40.10x
mHes1
** 4.3x
** 32.60x
** 63x
mHlf
** 12.17x
** 4.93x
** 5.56x
mHoxA9
** 40.92x
** 6.52x
** 143.5x
mMeis1
* 14.29x
2.60x
** 120.58x
mMeis3
5.00x
76.03x
55.36x
mTrib2
**14.75x
** 9.26x
** 1224.38x
mRNA expression relative to Abl
MN1 cKit+
MN1 CD11b+
normal mouse CMP
normal mouse WBM

Figure 3.5A-B

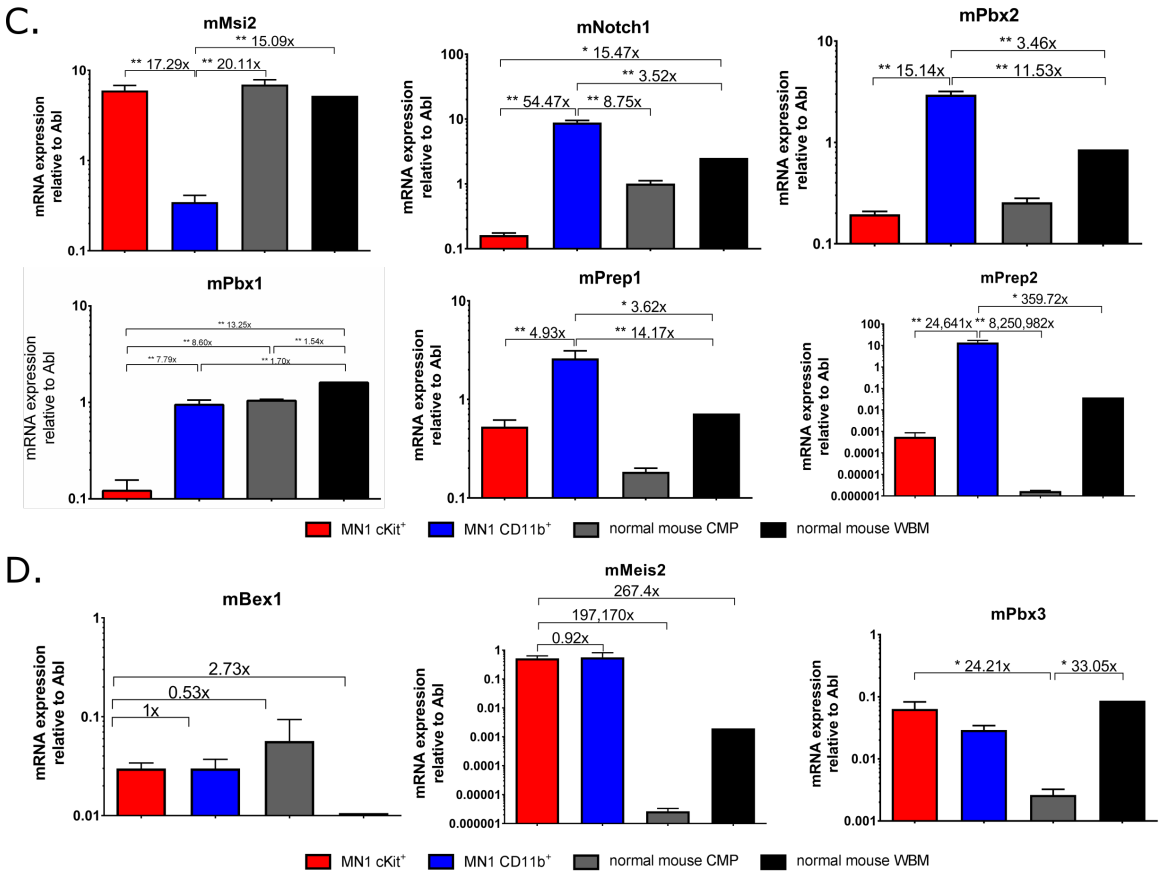

Figure 3.5 Genes differentially expressed between multiple MN1 datasets modeling varying LIC activity reveal different patterns of expression

(A) Comparison of MN1 gene expression datasets representing models with varying LIC activity where shortlisted genes are differentially expressed. (B) Absolute gene expression of candidate genes relative to Abl in cKit, CD11b, CMP, and whole bone marrow (WBM) cells by qRT-PCR, categorized by genes that are upregulated in cKit compared to CD11b cells, (C) genes that are upregulated in CD11b compared to cKit cells, and (D) genes that are expressed equally between cKit and CD11b cells, but are upregulated compared to gene expression levels in CMP and/or WBM. n=3 from four mice transplanted with cells from three independent transductions, one-sided ANOVA; error bars represent ±SEM; *P<0.05, **P<0.01.

Table 3.3 Gene expression fold change between cKit and CD11b subpopulations for shortlisted genes

	Fold Change by Agilent array (cKit vs CD11b)	Corrected P-value	Fold Change by qRT-PCR (cKit vs CD11b)	P-value	MN1 datasets showing differential expression			
					MN1 vs MN1Δ1	MN1 vs MN1VP16	MN1/CMP target genes	MN1/MEIS1 gene signature
Ass1	71.432526	0.015334087	37.8225862	P = 0.0007	✓	✓	✓	✓
	15.086127	0.029829802						
Bex1	228.53189	0.004331606	1	P=0.4670	✓			
	155.63301	0.006342706						
Dlk1	34.331863	0.013690726	21.732158	P = 0.0465				✓
	18.766941	0.017623542						
Flt3	144.99829	0.00346817	26.4095602	P = 0.0002	✓		✓	✓
	136.57591	0.009090904						
	1.937791	0.003277035						
Gfi1b	231.9252	0.001376133	220.429605	P < 0.0001		✓	✓	✓
Gpr56	179.37985	0.002537061	238.223218	P < 0.0001		✓	✓	✓
Hes1	127.094185	0.001167549	63	P<0.0001	✓	✓	✓	✓
Hlf	22.718737	0.002453691	5.55789474	P = 0.0002	✓	✓	✓	✓
HoxA9	7.0063443	0.010332281	143.5	P<0.0001	✓		✓	✓
	2.718716	0.04090069						
Meis1	331.89087	0.004726616	120.583333	P = 0.0065	✓		✓	✓
Meis2	4.048872	0.17273742	-1.081339713	P = 0.0786	✓	✓		
Meis3	3.8576012	0.020275272	55.3581748	P = 0.0724				✓
	-1.9703048	0.2740551						
	-2.4048817	0.017752737						
Msi2	172.28432	0.002811954	17.2876194	P = 0.0002	✓	✓	✓	✓
	24.070248	0.001744282						

	Fold Change by Agilent array (cKit vs CD11b)	Corrected P-value	Fold Change by qRT-PCR (cKit vs CD11b)	P-value	MN1 datasets showing differential expression			
					MN1 vs MN1Δ1	MN1 vs MN1VP16	MN1/CMP target genes	MN1/MEIS1 gene signature
Notch1	-12.560759	0.008162658	-54.47120181	P < 0.0001				✓
	-2.8337083	0.16954324						
Pbx1	-5.5113344	0.05264638	-7.785571379	P < 0.0001	✓			
	-1.5097088	0.60003144						
	-1.4272451	0.65455186						
	-1.0302261	0.3173339						
	-1.5826656	0.06275438						
Pbx2	-4.5434713	0.00666592	-15.1441969	P < 0.0001	✓			
Pbx3	5.0304384	0.0852126	2.18022057	P = 0.0099				✓
	5.708258	0.066381745						
Prep1/Pknox1	-1.4742813	0.18366252	-4.925756296	P = 0.0013				✓
	-1.590051	0.0763324						
Prep2/Pknox2	-722.6323	9.15E-04	-24641.06945	P = 0.0017				✓
Trib2	95.40409	0.004107124	1224.3808	P = 0.0011	✓		✓	✓
	5.377564	0.038642246						

3.3.5 Investigating the functional relevance of selected differentially expressed genes in MN1 leukemic properties

To assess the roles of a selected subset of candidate genes upregulated in leukemic groups (Figure 3.5A) in MN1-induced leukemogenesis, I generated lentiviral shRNAs to induce gene knockdown and perform functional assays for *in vitro* proliferation and competitive growth ability, self-renewal by CFU assay, and differentiation in two independently-derived MN1 cell lines. A 70-72% knockdown of Hlf or 50-63% knockdown of HoxA9 (Figure 3.6A) significantly impairs MN1 growth kinetics compared to Renilla-transduced control cells within 14 days (599,967 ± 11767 cells for shHlf and 416,800 ± 3333 cells for shHoxA9 versus 882,267 ± 1667 cells for control, unpaired t-test $P<0.01$, unpaired t-test) without any evidence of shRNA vector silencing, as measured by expression of the modified monomeric Kusabira Orange 2 (meKO2) fluorochrome (Figure 3.6Bi-ii). Major impairment in growth following Hlf of Hoxa9 knockdown is further evident in *in vitro* competition assays, composed of GFP^+meKO2^+ shRNA-transduced MN1 cells mixed with equal numbers of untransduced GFP^+ MN1 cells. For this assay, each population is tracked by their fluorescence expression and their relative proportions within the total cells calculated. Significant deviations from the starting proportions of 50% (1:1 ratio) suggest differential *in vitro* competitive growth ability due to knockdown of the gene of interest. The contributions of MN1 cells transduced with shHlf or shHoxA9 to the total cell population decreases within four (0.70 ± 0.07 relative to input, Student's t-test, $P<0.05$) and two days (0.79 ± 0.04 relative to input, Student's t-test, $P<0.01$), respectively, consistent with roles for both Hlf and HoxA9 in the leukemic growth properties of MN1 cells (Figure 3.6Biii). In addition, knockdown of Hlf or HoxA9 result in a slight increase in $CD11b^+$ cells after nine days (0.66 ± 0.03% for shHlf, and 1.39 ± 0.08% for shHoxA9 versus 0.25 ± 0.02% for control, unpaired t-test,

P<0.01) (Figure 3.6Ci) accompanied by a slight concordant decrease in c-Kit expression in shHoxA9 cells, providing evidence for a role of HoxA9 in the characteristic myeloid differentiation block seen in MN1 leukemia (Figure 3.6Cii). Knockdown of Hlf or HoxA9 also result in a significant decrease in colony-forming ability in serial replating assays (212 ± 7.75 shHlf colonies and 142 ± 9.13 shHoxA9 colonies versus 300.5 ± 4.79 control colonies; unpaired t-test, P<0.01) (Figure 3.6Di). In addition, flow cytometric analysis of cells from these colonies show no evidence of shRNA vector silencing, as measured by meKO2 expression (unpaired t-test, n.s.) (Figure 3.6Dii). Intriguingly, qRT-PCR analysis of Hlf and HoxA9 gene expression demonstrate evidence of a relationship between Hlf and HoxA9 in MN1 leukemia, with Hlf knockdown resulting in a significant decrease in HoxA9 expression (0.80 ± 0.03 versus 1.91 ± 0.01, unpaired t-test, P<0.05) (Figure 3.6Ei). In contrast, knockdown of HoxA9 has no effect on Hlf expression (0.97 ± 0.01 versus 0.96 ± 0.05, unpaired t-test, n.s.), suggesting that transcriptional pathways of these genes overlap, with Hlf located upstream of HoxA9 (Figure 3.6Eii).

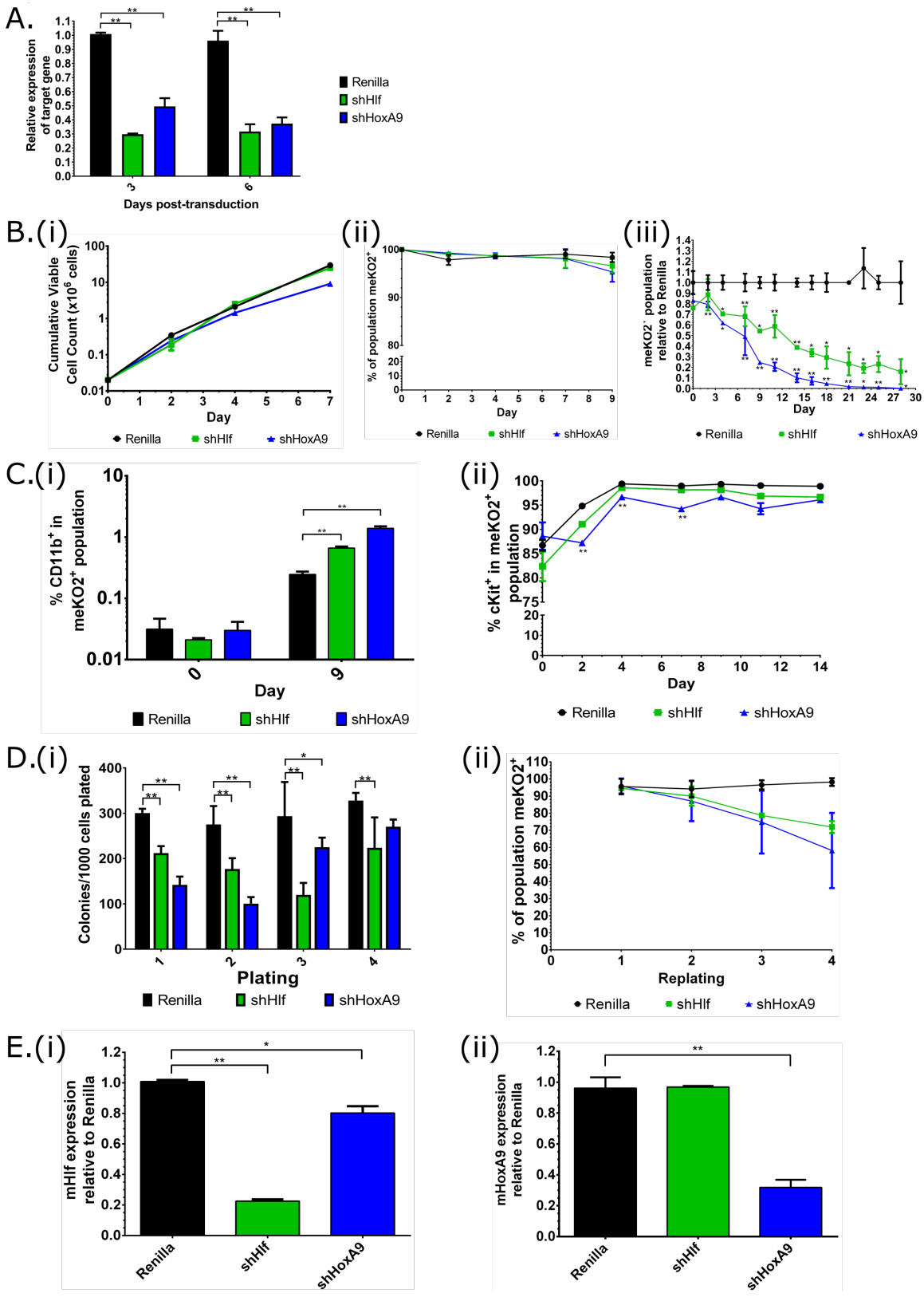

Figure 3.6 Investigating the functional relevance of HoxA9 and Hlf on MN1 leukemic properties

(A) Relative mRNA expression of Hlf, HoxA9 in MN1 cells three and six days after shRNA transduction; n=3 from 2 independent experiments, unpaired t-test in Renilla vs shRNA; error bars represent ±SD; *P<0.05, **P<0.01. (B)(i) Growth kinetics of Renilla-, shHlf- and shHoxA9-transduced MN1 cell line after lentiviral transduction. (ii) Kinetics of meKO2$^+$ expression of Renilla-, shHlf-, or shHoxA9-transduced MN1 cells after flow cytometric purification; n=3 from 2 independent experiments, unpaired t-test in Renilla vs shRNA; error bars represent ±SD; *P<0.05, **P<0.01. (iii) Competitive growth assay containing mixed populations of 50% sorted untransduced MN1 cells and 50% sorted Renilla-, shHlf-, or shHoxA9-transduced (meKO2$^+$) MN1 cells. n=3 from 2 independent experiments, multiple two-sided t-test in Renilla vs shRNA; error bars represent ± SD; *P<0.05, **P<0.01. (C)(i) CD11b expression of Renilla-, shHlf-, and shHoxA9-transduced MN1 cell lines 9 days after lentiviral transduction. (ii) Kinetics of c-Kit$^+$ expression in Renilla-, shHlf-, and shHoxA9-transduced MN1 cells. Sorted meKO2$^+$ cells; n=3 from 4 independent experiments, two-sided t-test in Renilla vs shRNA; error bars represent ± SD; *P<0.05, **P<0.01. (D)(i) Serial colony replating of Renilla- and shHlf- and shHoxA9-transduced MN1 cell lines post-sort, represented per 1000 cells plated. (ii) meKO2+ expression of cells comprising colonies of shRNA-transduced MN1 cells in CFU assay. Sorted meKO2$^+$ cells, n=3 from 4 independent experiments, two-sided t-test; error bars represent ± SD; *P<0.05, **P<0.01. (E) Relative gene expression of mHlf and mHoxA9 upon shRNA knockdown of (i) mHlf and (ii) mHoxA9 in MN1 cells six days post-transduction. Sorted meKO2$^+$ cells, n=3, two-sided t-test. Error bars represent ±SD; *P<0.05, **P<0.01.

The impact of Meis1 knockdown was similarly tested based on its significant upregulation in leukemic MN1 subpopulations shown in this chapter and previous literature[115, 131] and its essential role in MN1 leukemic transformation[128]. Unlike for Hlf and Hoxa9, Meis1 knockdown, 38% knockdown of Meis1, as measured by qRT-PCR analysis of mRNA (Figure 3.7A), results in only mild impairments in cell growth (37,500 ± 2,500 cells versus 283,300 ± 45,600 cells after 14 days, unpaired t-test, P<0.01) and short-term colony-forming ability (214.5 ± 12.4 versus 267 ± 7.05 colonies, unpaired t-test, P<0.05) (Figure 3.7Bi, D). Of note, there is a slight decrease in the proportion of cells transduced with shMeis1 over the 14 days of the growth assay, as evident

by the decrease in meKO2^{+} cells, suggesting a mild negative selective pressure against MN1 cells lacking Meis1 (90.6 ± 0.7% versus 93.1 ± 0.4% at day 14, unpaired t-test, $P<0.05$) (Figure 3.7Bii). However, Meis1 knockdown has no effect on *in vitro* competitive ability, CD11b expression, or c-Kit expression (unpaired t-test, n.s.) (Figure 3.7Biii, C).

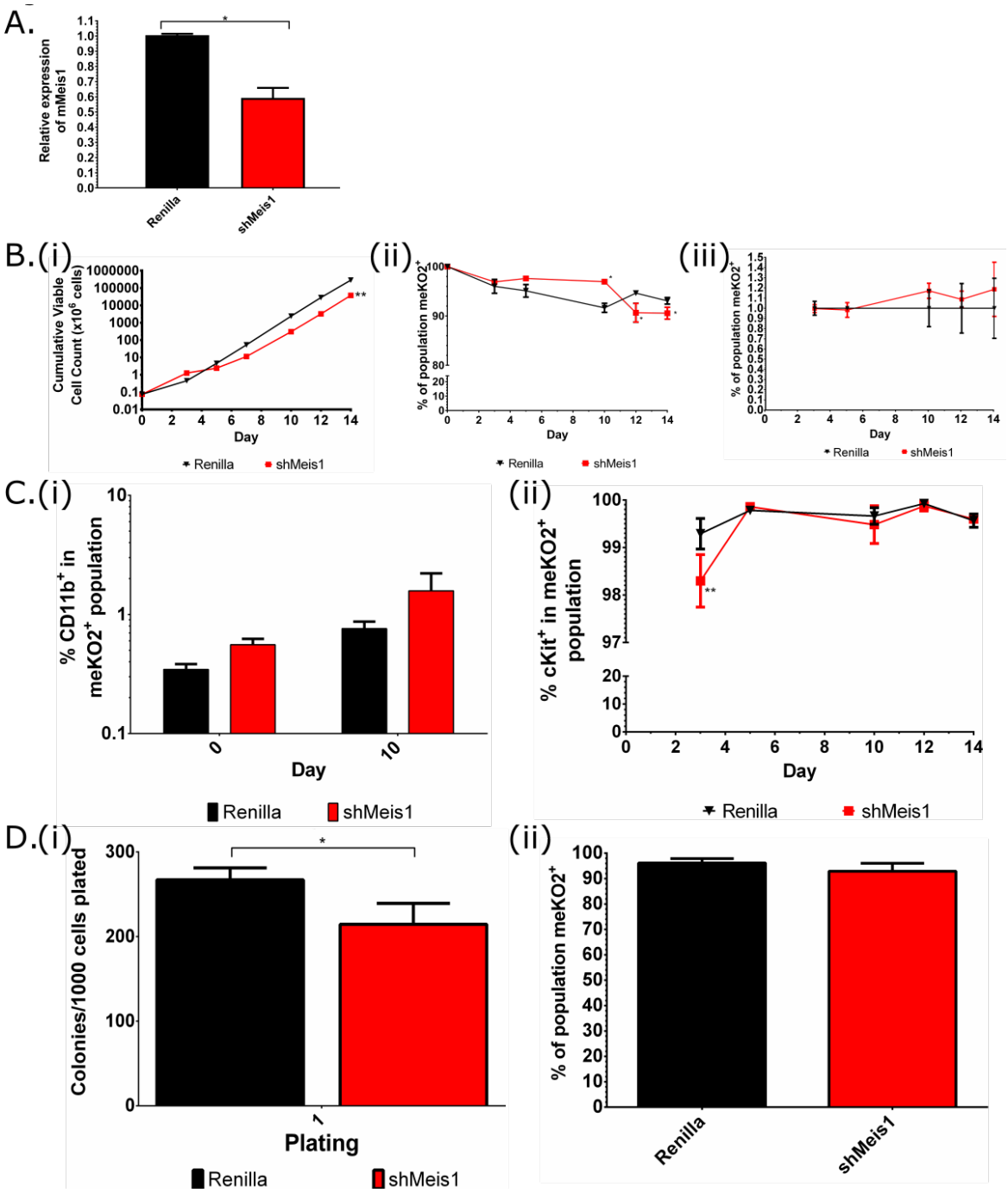

Figure 3.7 Investigating the functional relevance of Meis1 on MN1 leukemic properties

(A) Relative mRNA expression of Meis1 in MN1 cells three days after shRNA transduction. (B)(i) Growth kinetics of Renilla-, Meis1-transduced MN1 cell line after lentiviral transduction. (ii) Kinetics of meKO2$^+$ expression of Renilla- and shMeis1-transduced MN1 cells after flow cytometric purification. (iii) Competitive growth assay containing mixed populations of 50% sorted untransduced MN1 cells and 50% sorted Renilla- or Meis1-transduced

(meKO2$^+$) MN1 cells. n=3 from 2 independent experiments, multiple two-sided t-test in Renilla vs shRNA; error bars represent ± SD; *P<0.05, **P<0.01. (C)(i) CD11b expression of Renilla- and shMeis1-transduced MN1 cell lines 10 days post-sort. (ii) Kinetics of c-Kit$^+$ expression in Renilla- or shMeis1-transduced MN1 cells. Sorted meKO2$^+$ cells; n=3 from 2 independent experiments, multiple two-sided t-test in Renilla vs shMeis1; error bars represent ± SD; *P<0.05, **P<0.01. (D)(i) CFU assay of Renilla- and shMeis1-transduced MN1 cell lines 10 days after lentiviral transduction. (ii) Expression of meKO2$^+$ expression of cells comprising colonies of transduced MN1 cells in CFU assay. Sorted meKO2$^+$ cells; n=4 from 2 independent experiments, represented per 1000 cells plated; multiple two-sided t-test in Renilla vs shRNA. Error bars represent ± SEM; *P<0.05, **P<0.01.

3.3.6 Analysis of the functional role of Meis2 in MN1 leukemia

Given the prevalence of MEIS1 overexpression in AML[41-44], its critical role in MN1 leukemic transformation[128], and its upregulated gene expression in the LIC-containing cKit subpopulation and leukemic MN1 subsets[115, 131], the minimal effect of Meis1 knockdown on *in vitro* leukemic properties described above are surprising. This stimulated closer examination of a possible role for the Meis family member Meis2. Meis2 is significantly upregulated in MN1 cKit and CD11b subpopulations compared to murine CMPs ($2.65x10^{-6}$ ± $6.60x10^{-7}$ relative to Abl, unpaired t-test, P<0.05) and whole bone marrow ($1.95x10^{-3}$ ± 0.00 relative to Abl, unpaired t-test, P<0.05), although it is equally expressed between the cKit and CD11b subsets (0.52 ± 0.11 versus 0.57 ± 0.25 relative to Abl, unpaired t-test, n.s.) (Figure 3.5D). This upregulation of Meis2 in MN1 leukemic cells is of further interest given that Meis2 is normally expressed at significantly lower levels than Meis1 in normal hematopoietic cell compartments (unpaired t-test, P<0.01) (Figure 3.8A). Further highlighting Meis2 is the previous identification of Meis2 as among the top-ranked genes upregulated between both MN1 and MN1Δ1[131] and MN1 and MN1VP16[115]. Moreover, previous work from our laboratory has examined the phenotypic and functional

heterogeneity of a forward genetic model of human leukemia based on co-transduction of human $CD34^+$ cord blood cells with MN1 and the ND13 fusion gene. Intriguingly, MEIS2 is also upregulated in the LIC-containing $CD34^+GPR56^+$ fraction compared to the LIC-depleted $CD34^-GPR56^-$ fraction (Figure 3.8B)[180]. Together, these data suggest that MN1 leukemia is associated with a striking upregulation of Meis2 and this upregulation may play a key role in MN1 leukemia.

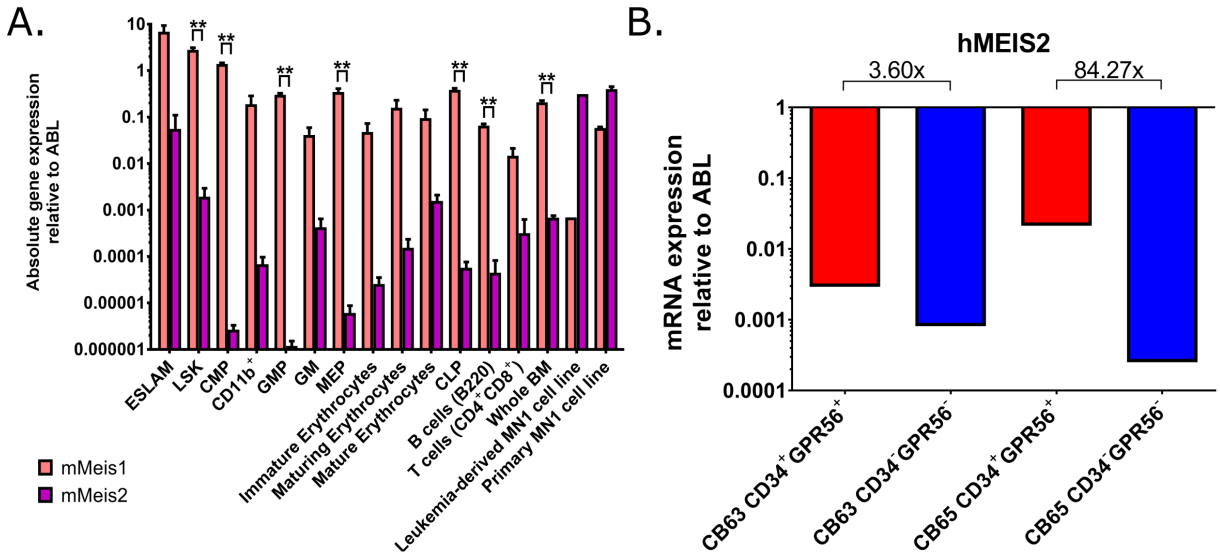

Figure 3.8 Relative expression of Meis2 in normal hematopoietic compartments and human AML cell line models

(A) Gene expression of Meis1 and Meis2 relative to Abl by qRT-PCR in murine hematopoietic compartments. n=3 from 3 independent mice, two-sided t-test; error bars represent ±SEM; **P<0.01. (B) Gene expression of MEIS2 relative to ABL by qRT-PCR in $CD34^+GPR56^+$ compared to CD34-GPR56- fraction of two human AML cord blood models generated through overexpression of NUP98-HOXD13 fusion and MN1 (ND13+MN1). n=1 from 2 independent cell lines.

To explore this possibility further, I tested the effect of Meis2 knockdown on MN1 leukemia using two different MN1 leukemia models. The leukemia-derived MN1 cell line is a leukemic cell line established from the *in vitro* culture of c-Kit$^+$ cells of bone marrow from a moribund mouse transplanted with MN1-transduced cells. The second model involves 5-FU treated murine bone marrow cells that were retrovirally-transduced with MN1 and cultured *in vitro* to establish a primary leukemic MN1 cell line. To functionally assess the impact of Meis2 knockdown, I tested six shRNAs against Meis2 based on work reported by Fellmann and colleagues for knockdown efficacy[163]. Three shRNAs against Meis2 provide gene knockdown ranging from 26-54% as assessed by qRT-PCR analysis of Meis2 mRNA levels three and six days post-transduction (unpaired t-test, $P<0.01$) (Figure 3.9A). In both leukemia models, transduction with each of the three Meis2 shRNAs significantly impairs cell growth, apparent as early as 5 days after plating ($4.13 \pm 0.15 \times 10^6$ average shMeis2-transduced cells versus $8.41 \pm 0.47 \times 10^6$ cells in leukemia-derived cell line, unpaired t-test, $P<0.01$), resulting in an average of 16-fold fewer cells after 14 days across all conditions (Figure 3.9Bi). Cells transduced with shMeis2 also show decreasing levels of the shMeis2 vector over the 14 days of culture, as assessed by meKO2 expression by flow cytometry (average $91.5 \pm 1.9\%$ versus $60.9 \pm 6.3\%$ in leukemia-derived cell line, average $93.4 \pm 1.6\%$ versus $47.2 \pm 7.4\%$ in primary MN1 cell line, unpaired t-test at day 14, $P<0.01$) (Figure 3.9Bii), suggesting that cells with downregulated Meis2 are at a competitive disadvantage and are rapidly eliminated from the population. This is supported by *in vitro* competitive assays, where GFP$^+$meKO2$^+$ shMeis2-transduced MN1 cells are mixed with equal numbers of control GFP$^+$ MN1 cells and the population kinetics tracked by their fluorescence expression. In competitive assays, the contribution of shMeis2-transduced MN1 cells decreases rapidly, with significantly fewer cells than the untransduced counterparts within seven days

(average 29.1 ± 7.6% versus 69.3 ± 1.2% in leukemia-derived cell line, average 8.8 ± 3.8% versus 42.9 ± 0.8% in primary MN1 cell line, unpaired t-test, $P<0.01$) indicative of severe growth impairment in *vitro* (Figure 3.9Biii). To measure the effect of Meis2 knockdown on *in vitro* self-renewal ability, I functionally assayed transduced cells for colony-forming ability. Cells transduced with shMeis2 show significant impairments in colony formation over four successive platings in the CFU assay (unpaired t-test, $P<0.05$ or $P<0.01$), providing evidence for an impairment of *in vitro* self-renewal upon loss of Meis2 (Figure 3.9Ci). In addition, flow cytometric analysis of the cells comprising these colonies demonstrate that the proportion of cells expressing the shRNAs, measured by proportion of meKO2-positive cells, is significantly lower in primary, secondary, tertiary, and quaternary colonies compared to initial levels (7.3 ± 4.1% from one shRNA versus 78 ± 8 % in the leukemia-derived cell line and 6.5 ± 3.5% from one shRNA versus 97.8 ± 0.4% in the primary MN1 cell line at fourth plating, unpaired t-test, $P<0.01$) (Figure 3.9Cii) and thus consistent with the downregulation of Meis2 in MN1 leukemic cells resulting in their rapid removal. Moreover, knockdown of Meis2 leads to increases in CD11b (unpaired t-test, $P<0.01$ for leukemia-derived cell lines; $P<0.05$ for primary MN1 cell lines) (Figure 3.9Di) and, to a lesser degree, Gr-1 expression *in vitro* (data not shown), suggesting that Meis2 also contributes to the myeloid differentiation block. Together, these data suggest that there is a strong negative selection against MN1 cells lacking upregulated Meis2 expression, with knockdown of Meis2 impairing *in vitro* growth, self-renewal ability and survival, and the myeloid differentiation block characteristic of these leukemic cells.

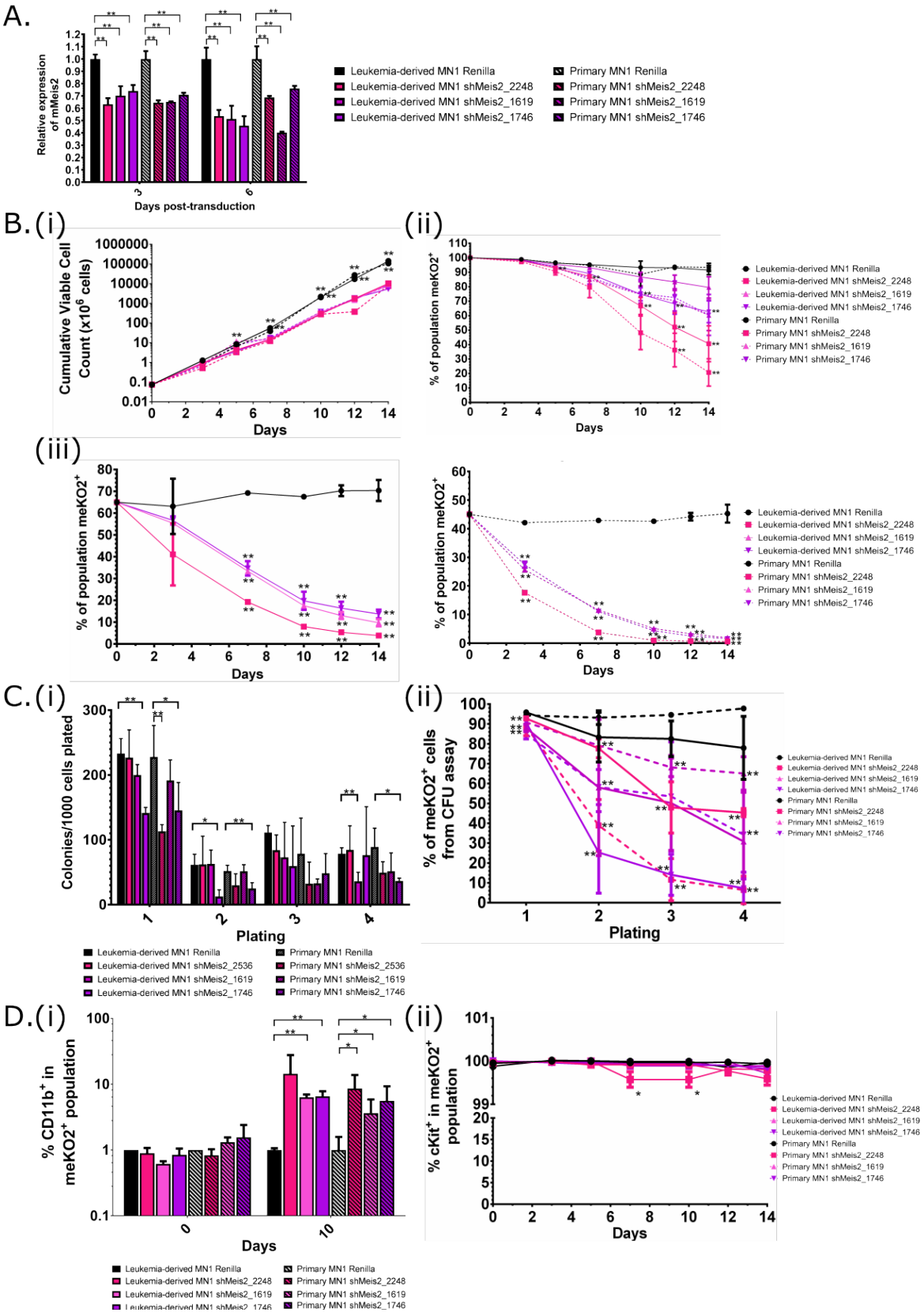

Figure 3.9 Knockdown of Meis2 impairs the functional leukemic properties of MN1 cells

(A) Relative mRNA expression of mMeis2 in MN1 cells three and six days after shRNA transduction. (B)(i) Growth kinetics of Renilla-, shMeis2-transduced MN1 cell line after lentiviral transduction. (ii) Kinetics of meKO2$^+$ expression of Renilla- and shMeis2-transduced MN1 cells after flow cytometric purification. (iii) Competitive growth assay containing mixed populations of 50% sorted untransduced MN1 cells and 50% sorted Renilla- or shMeis2-transduced (meKO2$^+$) MN1 cells. Sorted meKO2$^+$ MN1 cells; n=3 from 3 (shMeis2_2248) or 2 (shMeis2_1619 and shMeis2_1746) independent experiments, multiple two-sided t-test in Renilla vs shRNA; error bars represent ± SEM; *P<0.05, **P<0.01. (C)(i) Serial colony replating of Renilla- and shMeis2-transduced sorted MN1 cell lines, represented per 1000 cells plated. (ii) meKO2+ expression of cells comprising colonies of transduced MN1 cells in CFU assay. Sorted meKO2$^+$ cells, n=4 from 2 independent experiments, multiple two-sided t-test; error bars represent ±SEM; *P<0.05, **P<0.01. (D)(i) CD11b$^+$ expression of Renilla- and shMeis2-transduced leukemia-derived MN1 cell lines 10 days post-sort. (ii) Kinetics of c-Kit$^+$ expression in Renilla- and shMeis2-transduced MN1 cells. Sorted meKO2$^+$ MN1 cells; n=3 from 3 (shMeis2_2248) or 2 (shMeis2_1619 and shMeis2_1746) independent experiments; error bars represent ± SEM; *P<0.05, **P<0.01.

To further investigate the impairment seen in MN1 cell growth and proliferation upon knockdown of Meis2, I investigated the effect of Meis2 downregulation on cell cycle and apoptosis. Studies in other tissues have pointed to a regulatory role for Meis2 at the G2-M cell cycle checkpoints[181] and in S phase.[182] However, BrdU assays do not demonstrate changes in MN1 cell cycle distribution upon knockdown of Meis2 (Figure 3.10A). In contrast, apoptosis assays based on Annexin V binding show significant increases in both early and late apoptosis, with an 8.1 ± 0.3% increase in total apoptotic cells after four days in culture (Figure 3.10B). Concurrently, there is a 5.1 ± 1.1% decrease in the proportion of live cells, suggesting that a negative selective pressure against loss of Meis2 in MN1 cells resulting in the rapid removal of shMeis2-transduced cells from the population (unpaired t-tests, P<0.01) (Figure 3.10B).

Together, these data provide new evidence that Meis2 plays an important role in MN1 leukemic cell growth, competitive ability, self-renewal, and contributes to blocks in myeloid differentiation and apoptosis *in vitro*.

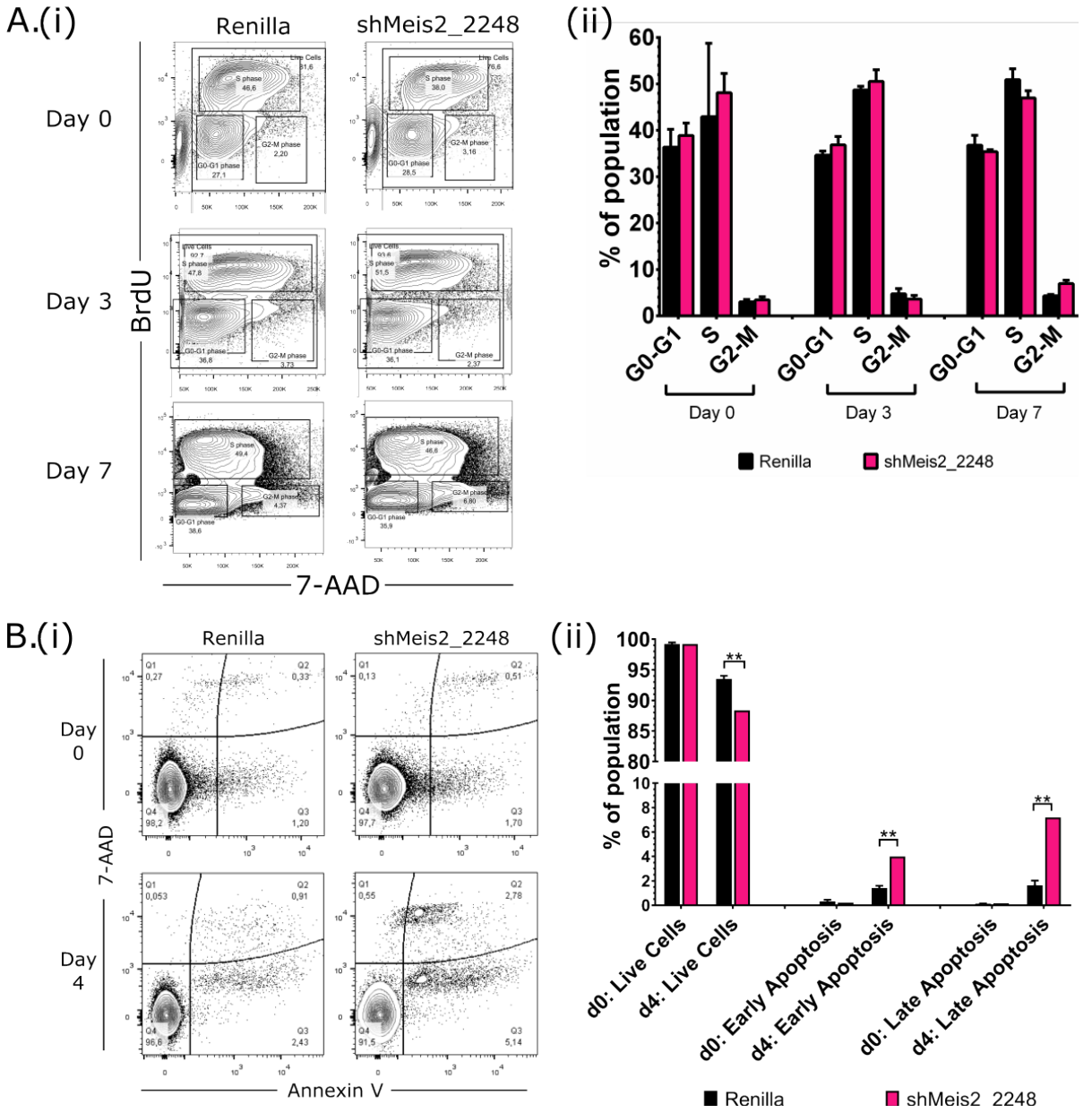

Figure 3.10 Cell cycle and apoptotic analysis of shMeis2-transduced MN1 cells

(A)(i) Representative cell cycle distribution (BrdU incorporation/7-aminoactinomycin D, 7-AAD) flow cytometric analysis in Renilla- and shMeis2-transduced *ex vivo*-derived MN1 cell line at day 0, 3, and 7 post-transduction. (ii) Summary of cell cycle distribution (BrdU incorporation/7-AAD) in Renilla- and shMeis2-transduced *ex vivo*-derived MN1 cell line. meKO2$^+$ sorted cells, n=3 from 3 independent experiments. Error bars represent ± SEM; *P<0.05, **P<0.01. (B)(i) Representative flow cytometric analysis of apoptosis (Annexin V/7-AAD staining) of Renillla- and shMeis2-transduced MN1 cells at 0 and 4 days post-sort. (ii) Annexin V apoptosis assay summary of Renilla- and shMeis2-transduced live, early apoptotic, and late apoptotic MN1 cells at 0 and 4 days post-sort from 3 independent experiments in triplicate. Multiple two-sided t-test in Renilla vs shMeis2_2248. Error bars represent ± SEM; **P<0.01.

3.3.7 Knockdown of Meis2 impairs MN1 leukemic cell engraftment kinetics *in vivo*

To evaluate the role of Meis2 in engraftment and leukemogenicity of MN1 cells, I transplanted 100,000 Renilla- or shMeis2-transduced MN1 leukemic cells into lethally-irradiated recipient mice. Knockdown of Meis2 significantly increases the latency of disease in both MN1 leukemic models, with median latency from 41 to 50 days (Mantel-Cox, P=0.001) in the leukemia-derived MN1 model and 47 to 55 days in the primary MN1 cell line model (Mantel-Cox, P=0.0119) (Figure 3.11A). Analysis of engraftment kinetics by sampling of peripheral blood at biweekly intervals also reveals significant impairments in the ability of shMeis2-transduced cells to engraft (Figure 3.11B) and is thus consistent with the delay in leukemia onset. This is especially prominent in the first six weeks post-transplant, as mice transplanted with shMeis2-transduced cells display lower levels of engraftment four weeks post-transplant (7.1 ± 4.5% engraftment with shMeis2-transduced cells versus 32.5 ± 18.5% engraftment with control cells, unpaired t-test, P<0.01) (Figure 3.11B). Mice transplanted with shMeis2 cells also show modest but insignificant increases in Gr-1$^+$, Gr-1$^+$CD11b$^+$, and CD11b$^+$ cells and decreases in c-Kit$^+$ cells

during the first six weeks post-transplant (all n.s.), suggesting that decreased Meis2 alone is insufficient to relieve the block in myeloid differentiation *in vivo* (Figure 3.12A-D). At the time of sacrifice, engraftment levels had plateaued (Figure 3.11C) and signs of leukemia (high proportion of donor-derived cells, splenomegaly, elevated white blood cell counts, and depressed red blood cell and platelet counts) (Figure 3.12E-F) were essentially identical for mice receiving shMeis2 -transduced MN1 cells versus control MN1 cells.

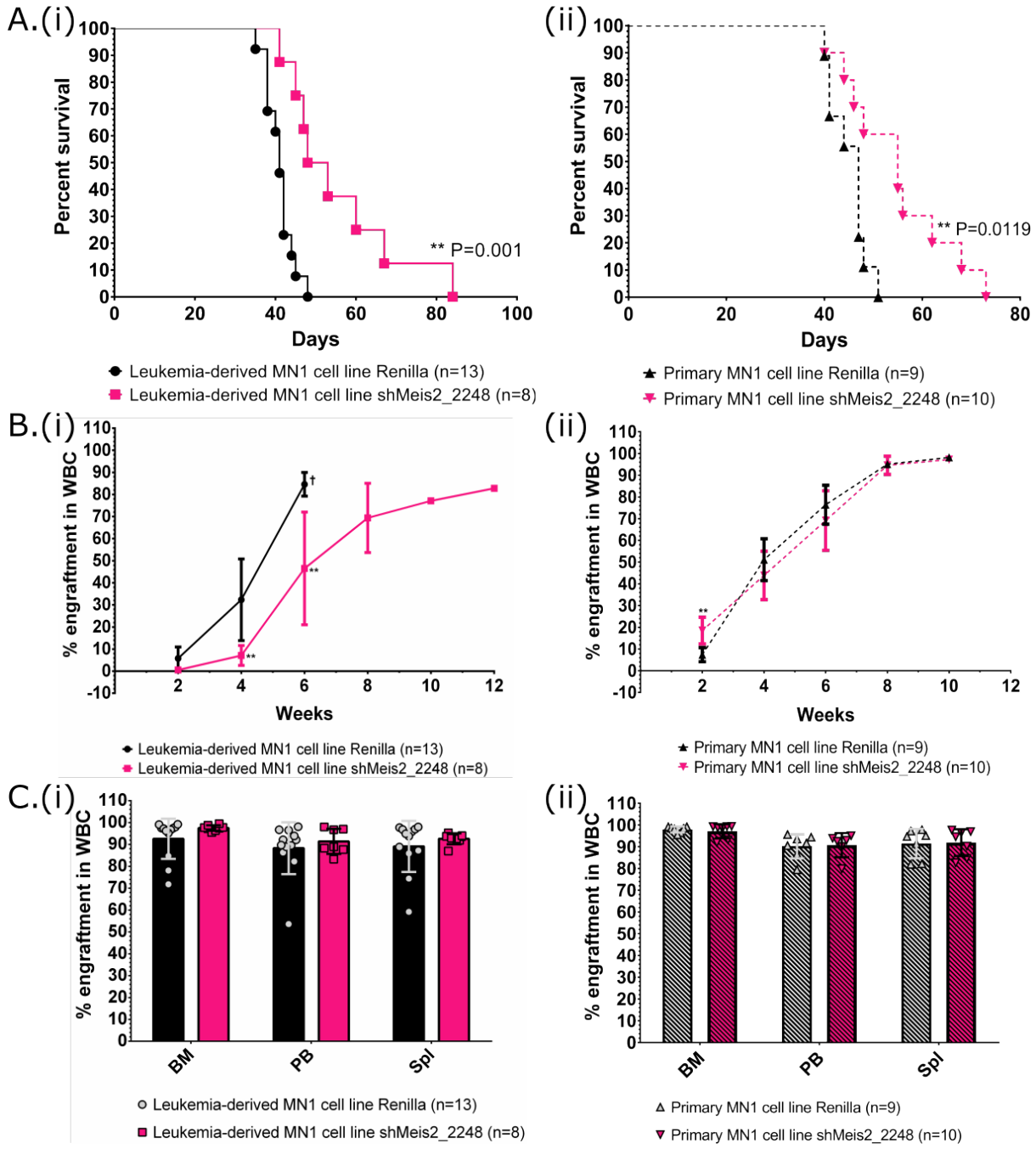

Figure 3.11 Knockdown of Meis2 increases latency and delays engraftment kinetics of MN1 cells

(A) Survival curve of mice transplanted with Renilla- and shMeis2-transduced (i) leukemia-derived and (ii) primary MN1 cell lines. Leukemia-derived: n=13 for Renilla, n=8 for shMeis2; primary: n=9 for Renilla, n=10 for shMeis2; Mantel-Cox. (B) Engraftment kinetics of mice transplanted with Renilla- and shMeis2-transduced (i) leukemia-derived and (ii) primary MN1 cell lines, as determined by bi-weekly peripheral blood analysis. Leukemia-derived:

n=13 for Renilla, n=8 for shMeis2; primary: n=9 for Renilla, n=10 for shMeis2; multiple two-sided t-test in Renilla vs shMeis2_2248; error bars represent ± SD; † indicates all mice were sacrificed after this timepoint due to disease, *P<0.05, **P<0.01. (C) Engraftment of mice transplanted with Renilla- and shMeis2-tranduced (i) leukemia-derived and (ii) primary MN1 cell lines at time of sacrifice determined by peripheral blood analysis. Leukemia-derived: n=13 for Renilla, n=8 for shMeis2; primary: n=9 for Renilla, n=10 for shMeis2; multiple two-sided t-test in Renilla vs shMeis2_2248; error bars represent ± SD; † indicates all mice were sacrificed after this timepoint due to disease; *P<0.05, **P<0.01.

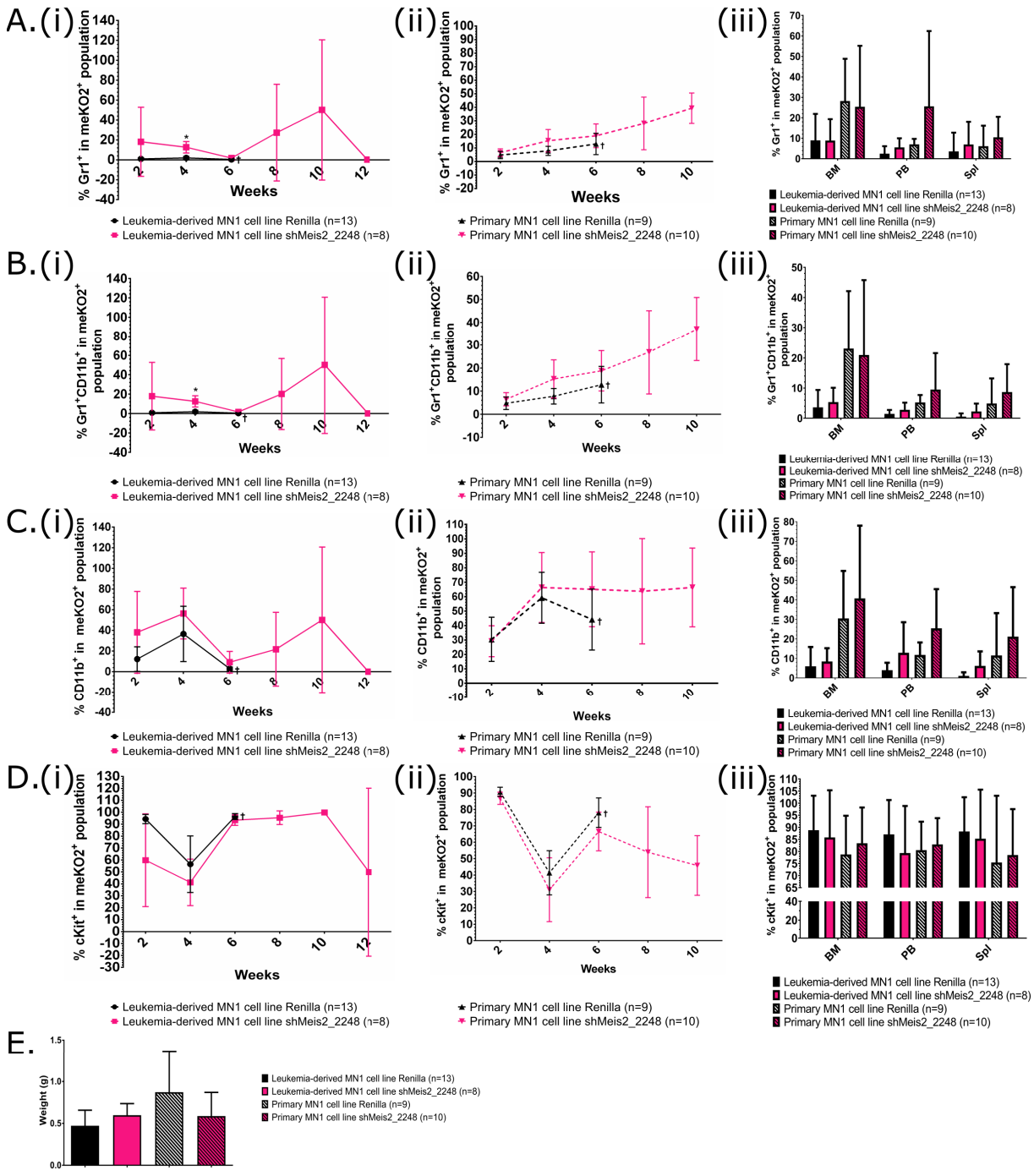

Figure 3.12A-E

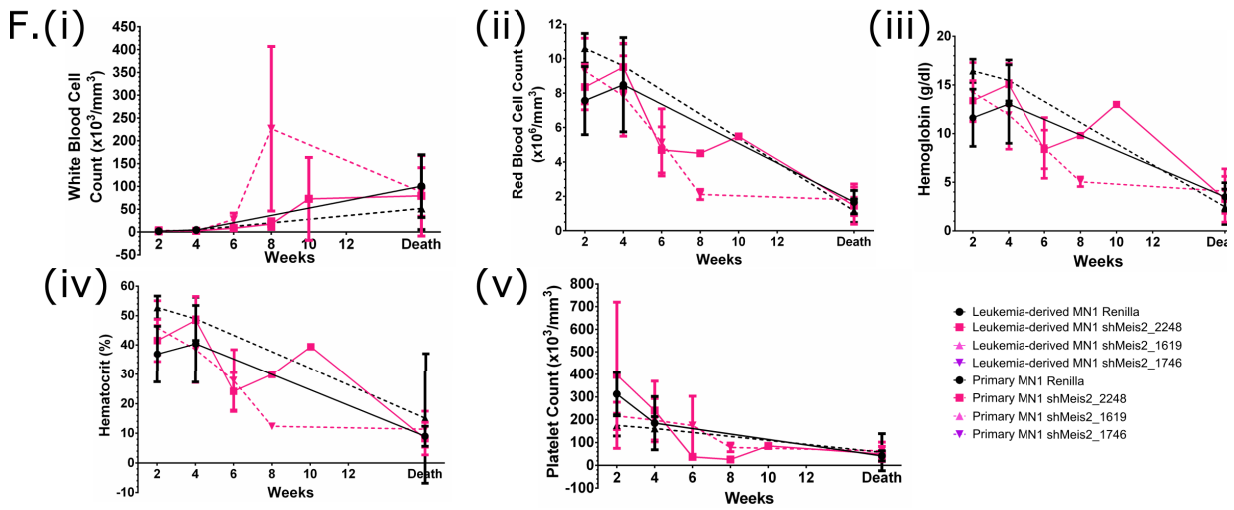

Figure 3.12 Mice transplanted with shMeis2-transduced cells develop leukemia

(A) Kinetics of Gr-1$^+$ expression in meKO2$^+$ engrafted bone marrow of mice transplanted with Renilla- or shMeis2-transduced (i) leukemia-derived- and (ii) primary MN1 cell lines and (iii) in bone marrow, peripheral blood, and spleen cells at sacrifice. (B) Kinetics of Gr-1$^+$CD11b$^+$ expression in meKO2$^+$ engrafted bone marrow of mice transplanted with Renilla- or shMeis2-transduced (i) leukemia-derived and (ii) primary MN1 cell lines and (iii) in bone marrow, peripheral blood, and spleen cells at sacrifice. (C) Kinetics of CD11b$^+$ expression in meKO2$^+$ engrafted bone marrow of mice transplanted with Renilla- or shMeis2-transduced (i) leukemia-derived and (ii) primary MN1 cell lines and (iii) in bone marrow, peripheral blood, and spleen cells at sacrifice. (D) Kinetics of c-Kit$^+$ expression in meKO2$^+$ engrafted bone marrow of mice transplanted with Renilla- or shMeis2-transduced (i) leukemia-derived and (ii) primary MN1 cell lines and (iii) in bone marrow, peripheral blood, and spleen cells at sacrifice. (E) Mean spleen weight of mice transplanted with Renilla- or shMeis2-transduced leukemia-derived or primary MN1 cell lines at sacrifice. (F) Kinetics of (i) white blood cell count, (ii) red blood cell count, (iii) platelet count, (iv) hemoglobin concentration, and (v) hematocrit percentage in peripheral blood of mice transplanted with Renilla- or shMeis2-transduced leukemia-derived and primary MN1 cell lines. Leukemia-derived: n=13 for Renilla, n=8 for shMeis2; primary: n=9 for Renilla, n=10 for shMeis2, two-sided t-test in Renilla vs shMeis2. Error bars represent ± SD; † indicates all mice were sacrificed after this timepoint due to disease, *P<0.05.

Comparisons of the proportion of meKO2-expressing donor-derived cells within engrafted cells shows that 14.0 ± 11.8% of engrafted shMeis2-transduced cells express the shRNA compared to 86.3 ± 15.3% of engrafted Renilla-transduced control cells, demonstrating strong negative selection against cells with downregulated Meis2 (unpaired t-test, $P<0.01$) (Figure 3.13A-B). Furthermore, copy number analysis of mouse bone marrow at time of sacrifice reveals that all mice had equal vector copy numbers, despite lower meKO2 expression in bone marrow from mice transplanted with shMeis2-transduced cells versus those that received Renilla-transduced cells (unpaired t-test $P<0.01$). This suggests that impairments in shMeis2-transduced cells were not due to differences in frequency of vector insertion and provides further evidence for strong negative selection against Meis2 knockdown (Figure 3.13C).

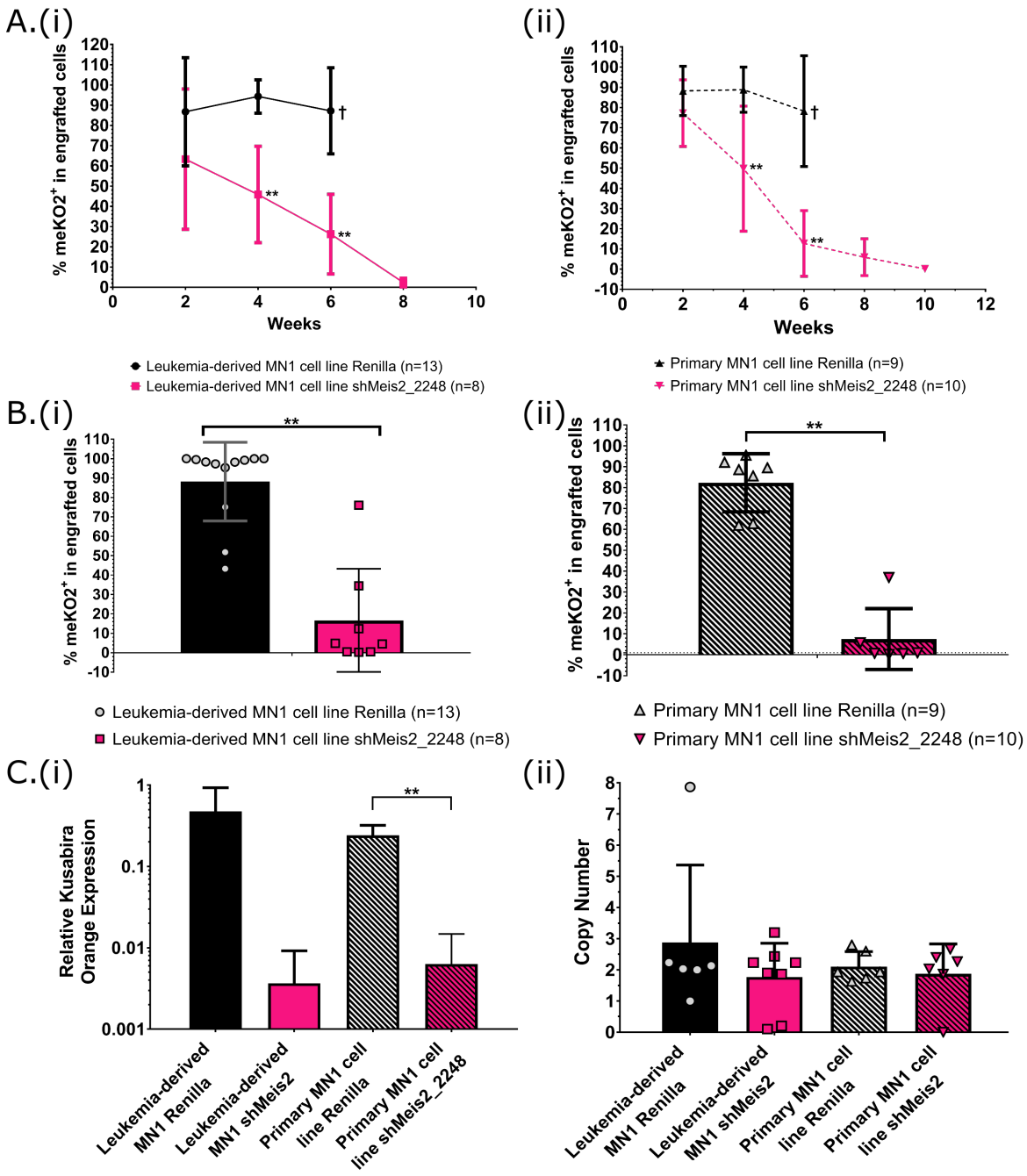

Figure 3.13 Mice transplanted with shMeis2-transduced cells show loss of shRNA expression over time

(A) Proportion of meKO2$^+$ cells within engrafted cells of mice transplanted with Renilla- and shMeis2-transduced (i) leukemia-derived and (ii) primary MN1 cell lines, as determined by bi-weekly peripheral blood analysis. Leukemia-derived: n=13 for Renilla, n=8 for shMeis2; primary: n=9 for Renilla, n=10 for shMeis2. Multiple two-sided t-test in Renilla vs shMeis2_2248. Error bars represent ± SD; † indicates all mice were sacrificed after this timepoint due to disease, *P<0.05, **P<0.01. (B)(i) qRT-PCR of relative meKO2 expression in bone marrow of

mice transplanted with Renilla- or shMeis2-transduced leukemia-derived or primary MN1 cell lines at sacrifice. (ii) qRT-PCR of number of virus copies in bone marrow of mice transplanted with Renilla- or shMeis2-transduced leukemia-derived or primary derived MN1 cell lines at sacrifice. Leukemia-derived: n=6 for Renilla, n=8 for shMeis2; primary: n=6 for Renilla, n=7 for shMeis2, two-sided t-test in Renilla vs shMeis2. Error bars represent ± SD; *P<0.05, **P<0.01.

Together, these data demonstrate that Meis2 is critical to the *in vivo* leukemogenic ability of MN1, as knockdown of Meis2 severely compromises the engraftment kinetics, increases disease latency, and results in in rapid depletion of shMeis2-transduced cells from the population.

3.3.8 Exploring MEIS1, MEIS2, and MN1 expression in human hematopoietic malignancies

At the time these studies were initiated, there was little known association between MEIS2 and leukemia. Having demonstrated the relevance of Meis2 in MN1 leukemogenesis in the MN1 murine model, I investigated if upregulation of MEIS2 could be detected in human hematopoietic malignancies.

Data from the TCGA AML and Leukemia Microarray Innovations in Leukemia (MILE) datasets show significant MEIS2 upregulation in patients with t(8;21) (AML1-eight-twenty one, AML-ETO) compared to all other AML subtypes including AML t(11q23)/MLL, inv(16)/t(16;16), t(15;17) and AMLs with complex karyotypes (Student's t-test, P<0.01 and P<0.001) (Figure 3.14A-B)[169]. In addition, MN1 and MEIS2 are significantly upregulated in AML inv(16) compared to t(11q23)/MLL, and t(15;17) (Student's t-test, P<0.05) (Figure 3.14C)[169]. As high

expression of MN1 is associated with patients with inv(16)[100, 101], there may be a subset of patients expressing inv(16) with both high MN1 and MEIS2 expression.

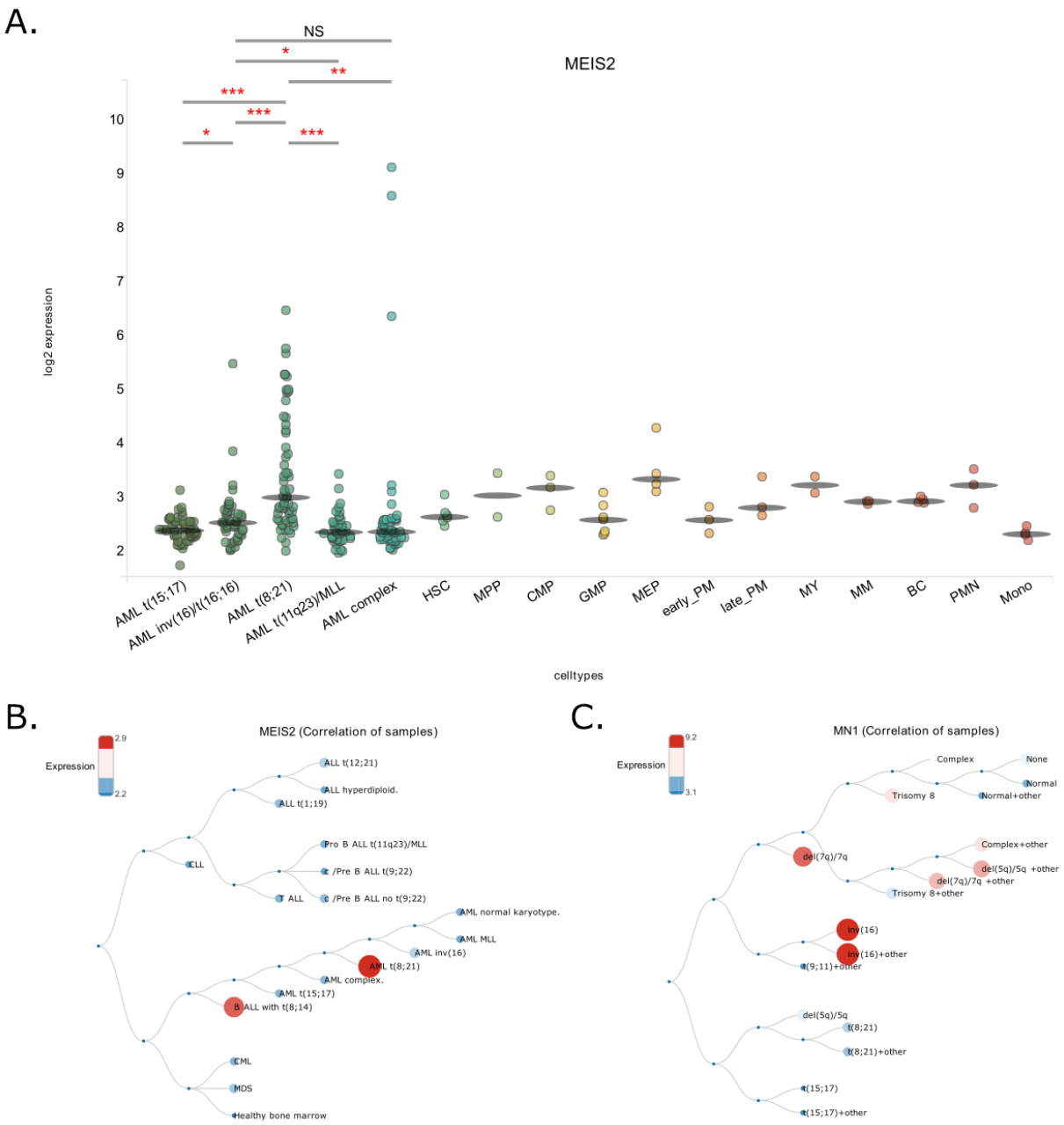

Figure 3.14 MEIS2 and MN1 expression in patients with AML from TCGA AML and Leukemia MILE datasets

(A) MEIS2 expression levels in human AMLs with various genetic aberrations, complex karyotype, and whole bone marrow cells from TCGA. (B) Hierarchical tree showing MEIS2 expression level MEIS2 expression levels in patients from Leukemia MILE dataset. (C) Hierarchical tree showing MN1 expression in patients from TCGA AML dataset. Student's two-tailed t-test, *P<0.05, **P<0.01, ***P<0.001.

Examination of patients with AML or MDS from a small in-house dataset shows higher MEIS1 and HOXA9 expression in patients with AML and low expression of MN1 (Welch's two-sample t-test, $P<0.01$) (Figure 3.15A). HOXA9 levels are also significantly higher in patients with low MN1 expression that develop AML subsequent to MDS (AML-MDS), and those that develop therapy-related AML (tAML) (Welch's two-sample t-test, $P<0.05$), suggesting that transcriptional pathways outside of MEIS1 play a role in MN1 leukemogenesis. In addition, there is a wider range of MEIS2 expression levels in patients with lower MN1 expression. Interestingly, there are specific patients with high MEIS2 expression that also showed lower levels of MEIS1 expression. However, the sample size is too small to determine if this correlation is statistically significant (Figure 3.15B).

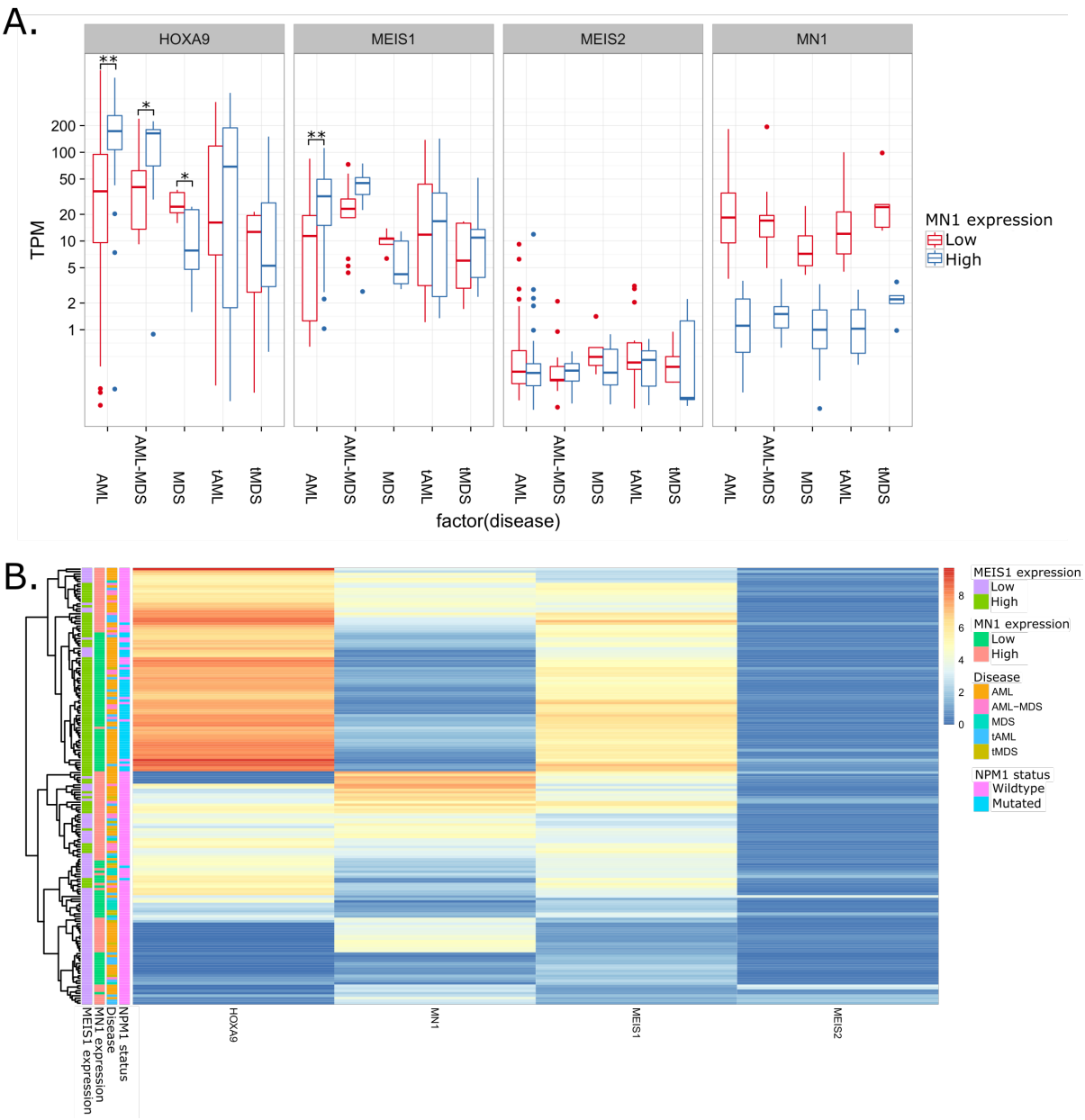

Figure 3.15 Gene expression from in-house patient MDS and AML dataset

(A) Distribution of HOXA9, MEIS1, MEIS2, and MN1 expression in patients with AML or MDS, categorized by MN1 expression level. *P<0.05, **P<0.01 (two-sided Welch's two-sample t-test). (B) Heat map of HOXA9, MN1, MEIS1, and MEIS2 expression from patients with AML or MDS, classified by MEIS1 and MN1 expression level and NPM1 status.

To access a larger patient dataset, I examined publicly available gene expression profiles of patients with AML. Gene expression data from Valk and colleagues[102] show no significant correlation between MEIS2 expression and inv(16) AML or MN1 high-expressing AML. (Table 3.4) However, across AML subtypes, MEIS1 and MEIS2 are inversely and significantly correlated (Pearson correlation, r=-0.224, -0.237, -0.245) (Table 3.5-3.7). As MEIS1 and MEIS2 share 85% amino acid sequence similarity (Figure 3.16), this may be sufficient to activate some shared downstream targets in the absence of signaling from their primary regulator. Interestingly, gene expression kinetics of primary MN1 subpopulations in *in vitro* culture show that low levels of Meis1 in the first 7-14 days in culture are accompanied by upregulation of Meis2 expression, which is then reversed as Meis1 levels increased after 14 days in culture (Figure 3.17), suggesting that expression levels of the family members are inversely correlated. Furthermore, knockdown of Meis2 in our leukemia-derived MN1 cell line results in an approximate 10-fold increase in Meis1 expression (unpaired t-test, n.s.), supporting the idea of some degree of compensatory expression between these family members (Figure 3.18).

Table 3.4 Correlation of MN1, MEIS1, MEIS2, and MEIS3 gene expression in patients with inv(16) AML

Pearson Correlations

		MN1	MEIS1_p1	MEIS1_p2	MEIS1_p3	MEIS2	MEIS3_p1	MEIS3_p2
MN1	Pearson Correlation	1	-.421*	-.537**	-.243	.081	.079	-.380
	Sig. (2-tailed)		.045	.008	.263	.712	.722	.074
	N	23	23	23	23	23	23	23
MEIS1_p1	Pearson Correlation	-.421*	1	.951**	.864**	.130	.125	.195
	Sig. (2-tailed)	.045		.000	.000	.555	.569	.373
	N	23	23	23	23	23	23	23
MEIS1_p2	Pearson Correlation	-.537**	.951**	1	.864**	.101	.095	.244
	Sig. (2-tailed)	.008	.000		.000	.648	.666	.262
	N	23	23	23	23	23	23	23
MEIS1_p3	Pearson Correlation	-.243	.864**	.864**	1	.119	.118	.139
	Sig. (2-tailed)	.263	.000	.000		.588	.591	.528
	N	23	23	23	23	23	23	23
MEIS2	Pearson Correlation	.081	.130	.101	.119	1	.999**	-.139
	Sig. (2-tailed)	.712	.555	.648	.588		.000	.526
	N	23	23	23	23	23	23	23
MEIS3_p1	Pearson Correlation	.079	.125	.095	.118	.999**	1	-.134
	Sig. (2-tailed)	.722	.569	.666	.591	.000		.542
	N	23	23	23	23	23	23	23
MEIS3_p2	Pearson Correlation	-.380	.195	.244	.139	-.139	-.134	1
	Sig. (2-tailed)	.074	.373	.262	.528	.526	.542	
	N	23	23	23	23	23	23	23

*. Correlation is significant at the 0.05 level (2-tailed).

**. Correlation is significant at the 0.01 level (2-tailed).

Table 3.5 Correlation of MN1, MEIS1, MEIS2, and MEIS3 gene expression in patients with AML

Pearson Correlations

		MN1	MEIS1_p1	MEIS1_p2	MEIS1_p3	MEIS2	MEIS3_p1	MEIS3_p2
MN1	Pearson Correlation	1	.091	.095	.041	-.062	.044	.061
	Sig. (2-tailed)		.292	.271	.637	.475	.610	.484
	N	135	135	135	135	135	135	135
MEIS1_p1	Pearson Correlation	.091	1	.967**	.912**	-.244**	.052	-.145
	Sig. (2-tailed)	.292		.000	.000	.004	.546	.094
	N	135	135	135	135	135	135	135
MEIS1_p2	Pearson Correlation	.095	.967**	1	.874**	-.237**	.080	-.158
	Sig. (2-tailed)	.271	.000		.000	.006	.356	.067
	N	135	135	135	135	135	135	135
MEIS1_p3	Pearson Correlation	.041	.912**	.874**	1	-.245**	.065	-.095
	Sig. (2-tailed)	.637	.000	.000		.004	.455	.273
	N	135	135	135	135	135	135	135
MEIS2	Pearson Correlation	-.062	-.244**	-.237**	-.245**	1	-.052	.102
	Sig. (2-tailed)	.475	.004	.006	.004		.549	.240
	N	135	135	135	135	135	135	135
MEIS3_p1	Pearson Correlation	.044	.052	.080	.065	-.052	1	-.081
	Sig. (2-tailed)	.610	.546	.356	.455	.549		.353
	N	135	135	135	135	135	135	135
MEIS3_p2	Pearson Correlation	.061	-.145	-.158	-.095	.102	-.081	1
	Sig. (2-tailed)	.484	.094	.067	.273	.240	.353	
	N	135	135	135	135	135	135	135

**. Correlation is significant at the 0.01 level (2-tailed).

Table 3.6 Correlation of MN1, MEIS1, MEIS2, and MEIS3 gene expression in patients with normal karyotype AML

Pearson Correlations

		MN1	MEIS1_p1	MEIS1_p2	MEIS1_p3	MEIS2	MEIS3_p1	MEIS3_p2
MN1	Pearson Correlation	1	.091	.095	.041	-.062	.044	.061
	Sig. (2-tailed)		.292	.271	.637	.475	.610	.484
	N	135	135	135	135	135	135	135
MEIS1_p1	Pearson Correlation	.091	1	.967**	.912**	-.244**	.052	-.145
	Sig. (2-tailed)	.292		.000	.000	.004	.546	.094
	N	135	135	135	135	135	135	135
MEIS1_p2	Pearson Correlation	.095	.967**	1	.874**	-.237**	.080	-.158
	Sig. (2-tailed)	.271	.000		.000	.006	.356	.067
	N	135	135	135	135	135	135	135
MEIS1_p3	Pearson Correlation	.041	.912**	.874**	1	-.245**	.065	-.095
	Sig. (2-tailed)	.637	.000	.000		.004	.455	.273
	N	135	135	135	135	135	135	135
MEIS2	Pearson Correlation	-.062	-.244**	-.237**	-.245**	1	-.052	.102
	Sig. (2-tailed)	.475	.004	.006	.004		.549	.240
	N	135	135	135	135	135	135	135
MEIS3_p1	Pearson Correlation	.044	.052	.080	.065	-.052	1	-.081
	Sig. (2-tailed)	.610	.546	.356	.455	.549		.353
	N	135	135	135	135	135	135	135
MEIS3_p2	Pearson Correlation	.061	-.145	-.158	-.095	.102	-.081	1
	Sig. (2-tailed)	.484	.094	.067	.273	.240	.353	
	N	135	135	135	135	135	135	135

**. Correlation is significant at the 0.01 level (2-tailed).

Table 3.7 Correlation of MN1, MEIS1, MEIS2, and MEIS3 gene expression in patients with AML with other karyotypes

Pearson Correlations

		MN1	MEIS1_p1	MEIS1_p2	MEIS1_p3	MEIS2	MEIS3_p1	MEIS3_p2
MN1	Pearson Correlation	1	.003	.033	-.044	.035	.104	-.139
	Sig. (2-tailed)		.974	.753	.676	.739	.325	.188
	N	91	91	91	91	91	91	91
MEIS1_p1	Pearson Correlation	.003	1	.980**	.940**	-.269**	-.011	-.141
	Sig. (2-tailed)	.974		.000	.000	.010	.914	.184
	N	91	91	91	91	91	91	91
MEIS1_p2	Pearson Correlation	.033	.980**	1	.922**	-.287**	.019	-.135
	Sig. (2-tailed)	.753	.000		.000	.006	.860	.203
	N	91	91	91	91	91	91	91
MEIS1_p3	Pearson Correlation	-.044	.940**	.922**	1	-.210*	-.016	-.116
	Sig. (2-tailed)	.676	.000	.000		.046	.878	.273
	N	91	91	91	91	91	91	91
MEIS2	Pearson Correlation	.035	-.269**	-.287**	-.210*	1	-.021	-.031
	Sig. (2-tailed)	.739	.010	.006	.046		.845	.771
	N	91	91	91	91	91	91	91
MEIS3_p1	Pearson Correlation	.104	-.011	.019	-.016	-.021	1	-.115
	Sig. (2-tailed)	.325	.914	.860	.878	.845		.279
	N	91	91	91	91	91	91	91
MEIS3_p2	Pearson Correlation	-.139	-.141	-.135	-.116	-.031	-.115	1
	Sig. (2-tailed)	.188	.184	.203	.273	.771	.279	
	N	91	91	91	91	91	91	91

**. Correlation is significant at the 0.01 level (2-tailed).

*. Correlation is significant at the 0.05 level (2-tailed).

Figure 3.16 Alignment of Meis2, Meis1a, and Meis1b amino acid sequences

Amino acids conserved between all three Meis members/isoforms listed in red; amino acids conserved between two isoforms listed in blue. DNA binding domain outlined in green; transcriptional activation domain outlined in magenta.

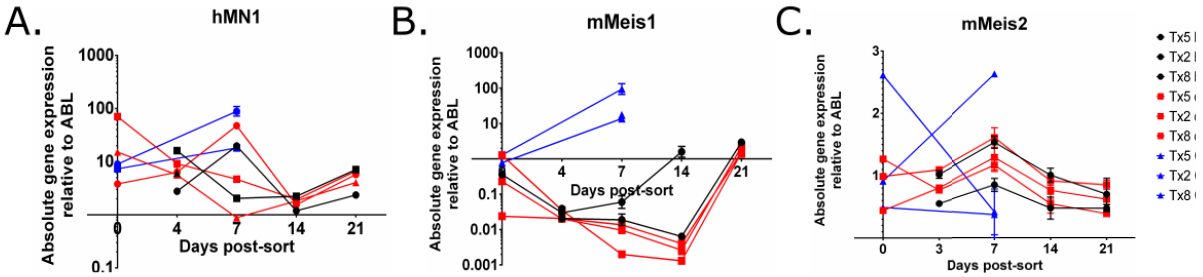

Figure 3.17 MN1, Meis1, and Meis2 gene expression kinetics of MN1 subpopulations *in vitro*

(A) MN1, (B) Meis1, and (C) Meis2 gene expression kinetics of primary MN1 mouse bone marrow cells sorted into MN1 bulk, cKit, and CD11b subpopulations and cultured *in vitro*. n=3 from three independent experiments. Error bars represent ± SD.

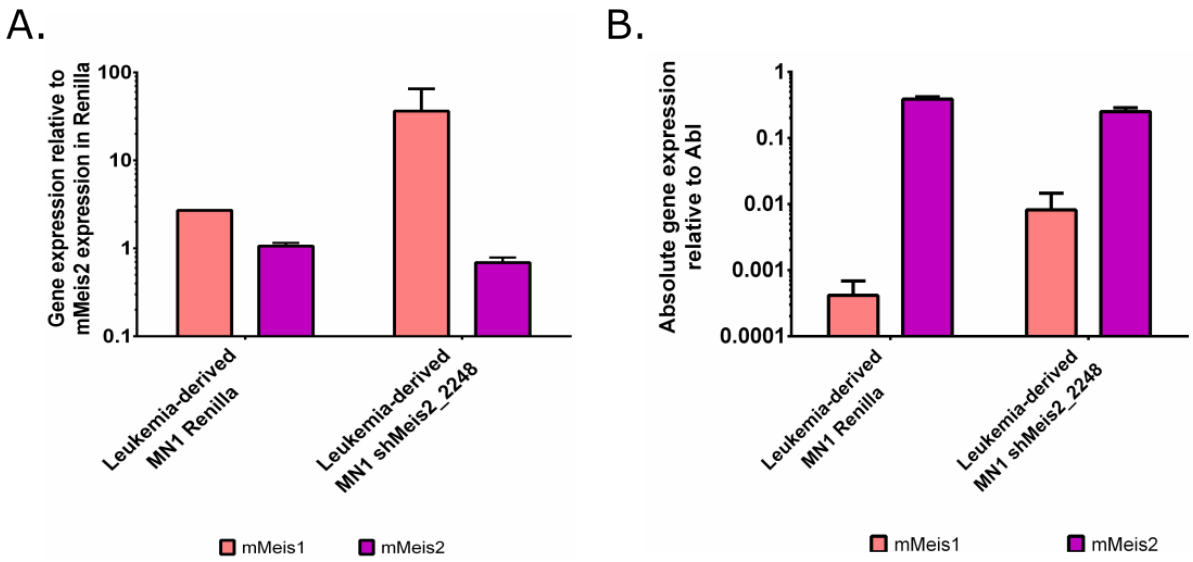

Figure 3.18 Relative gene expression of Meis1 and Meis2 upon knockdown of Meis2

Relative gene expression of mMeis1 and mMeis2 six days post-transduction in Renilla- or shMeis2_2248-transduced MN1 cells. Sorted meKO2$^+$ cells, n=3, two-sided t-test. Error bars represent ± SD; *P<0.05, **P<0.01.

3.4 Discussion

The data presented in this chapter identify and characterise key genes underlying MN1 leukemia. Functional studies demonstrate that the phenotypic heterogeneity of MN1 leukemic cells reflect a hierarchical model in which LSCs reside predominantly in the cKit subset and can regenerate the full spectrum of LIC-containing and LIC-depleted leukemic cells. Gene expression profiling of MN1 subpopulations, combined with comparisons of cells transduced with wildtype MN1 versus variants with differing leukemic activity, identified a shortlist of genes potentially critical to MN1 leukemogenesis. Knockdown of Hlf or HoxA9 significantly blunts leukemic cell growth and colony formation *in vitro*, demonstrating their critical roles in leukemia maintenance. Surprisingly, Meis1 knockdown has minimal effects on *in vitro* measures of leukemic activity. In

contrast, knockdown of Meis2 profoundly impairs *in vitro* proliferation and colony-forming ability, and partially restores myeloid differentiation, owing in part to increased apoptosis. Transplantation of shMeis2-transduced MN1 cells increases the latency of disease onset due to delayed engraftment kinetics and rapid depletion of shMeis2-expressing cells post-transplantation. Together, these data provide further support for the roles of HoxA9 and Meis1 in leukemia, demonstrate a functional role for Hlf in AML, and identify Meis2 as a novel essential player in MN1-induced leukemogenesis.

As previously described, immune regulation and response gene sets are enriched in the LIC-depleted CD11b subset. Interestingly, previous studies using MN1VP16 identified dysregulated immune regulation and response pathways in MN1 leukemia, tied to downregulation of Irf8 and its downstream target Ccl9[115]. Similarly, as described in Chapter 2 of this thesis, eosinophil cationic proteins (Ear1, Ear2, and Ear3), which play a role in neutrophil maturation, are among the most differentially upregulated genes between the more-mature leukemic MN1Δ7 and MN1 leukemic cells[131]. Together, these data suggest that suppression of immune pathways contribute to MN1 leukemic properties. Conversely, the limited downregulation of immune response pathways are more closely associated with the CD11b subfraction of MN1 leukemic cells and their reduced leukemogenic activity and more mature immunophenotype.

Among genes upregulated in the cKit subset are Hlf and members of the HoxA family and Meis1 transcription factors, the latter being well-known to play key roles in leukemic transformation, self-renewal, proliferation, and impairment of differentiation[39, 62-64, 77]. Overexpression of Hlf has established its role in HSC engraftment and apoptosis inhibition[183], and it has been tied to leukemia through the chromosomal translocation E2A-HLF in human B-cell acute lymphoblastic leukemia (B-ALL)[184]. However, the role of Hlf in AML has been largely unexplored, despite its

identification as a candidate gene for expansion and transformation of HSCs by NUP98-HOX fusion genes[185]. The work presented in this chapter provides new evidence that Hlf plays a role in the self-renewal and proliferative ability of MN1 AML cells. Additionally, data presented in this chapter reveals that shRNA-mediated knockdown of Hlf is associated with a significant decrease in HoxA9 expression. This previously unrecognized regulatory relationship between Hlf and HoxA9, and notably the possibility that Hlf is an upstream regulator of HoxA9 will be of interest to explore in future studies.

Previous work from our lab showed that MEIS1 is essential for MN1-induced transformation, as demonstrated by the inability of GMPs to be transformed by ectopic expression of MN1 in the absence of engineered co-overexpression of MEIS1 and HOXA9 or HOXA10[128]. However, it is unknown if upregulation of MEIS1 is required for MN1 leukemogenesis beyond the transformation event. Although MEIS1 contributes to the maintenance of AML in the MLL-AF9 model[86], studies evaluating its role in MN1 leukemic maintenance and progression are lacking. Surprisingly, knockdown of Meis1 has a minor impact on *in vitro* growth kinetics and short-term colony-forming ability of MN1 cells and no effect on *in vitro* competitive ability or myeloid differentiation block. This may reflect insufficient Meis1 knockdown, so further studies of a complete Meis1 knockout will be of interest. However, my findings are also consistent with a model in which upregulation of Meis1 is necessary for the initiation of MN1-induced leukemic transformation but not for maintenance of leukemic activity. Given the minimal effects of Meis1 knockdown on MN1 leukemic properties, closer examination of other Meis family members identified Meis2 as significantly upregulated in MN1 cells compared to MN1Δ1 or MN1VP16-transduced cells, and over 190-fold upregulated in MN1 leukemic cells over normal CMPs. Meis2 is typically associated with immature cells in embryonic development. High Meis2

expression plays a role in the proliferation and regulation of fate specification of retinal progenitor cells[186], and human cardiomyocyte cell proliferation as a reported target of miR-134[187, 188]. My data shows that Meis2 was expressed at substantially lower levels than Meis1 in all normal hematopoietic compartments tested, and its highest expression levels are found in the stem and progenitor cell compartments. Meis2 has only recently been implicated in malignant hematopoiesis, having been reported as upregulated in AML and ALL cell lines[189]. This is consistent with data in this chapter showing upregulation of Meis2 in primary murine MN1 leukemic bone marrow over normal CMPs and bulk bone marrow and in the LIC-containing over the LIC-depleted fraction in a human cord blood model of MN1-induced leukemia. Additionally, Meis2 is significantly upregulated in a murine model of AML driven by co-overexpression of HoxA9 and Meis1[12] and primary AML1-ETO-positive cells and human models[190]. Together, this data suggests that MEIS2 upregulation may occur in a subset of AMLs.

Expression of Meis2 in immature cells is tied to its role in differentiation. Meis2 is essential for cranial neural crest development. Meis2-deficient embryos exhibit defects in tissues derived from the neural crest, including abnormal heart outflow tract, cardiac and cranial nerves, cranial bones, and cartilage[191]. In addition, Meis2 plays a role in lens placode development[192-194], the production and retention of interdigital cells in the bat forelimb webbing[195], regulating embryonic stem cell differentiation into cardiac, neural, and retinal cell lineages[191], and spatial delineation in limb and digit development[196]. Similarly, Meis2 is expressed with Meis1, HoxA9, and HoxB4 in undifferentiated 32Dcl3 cells and downregulation of its expression is required for 32Dcl3 cell differentiation in the presence of IL3[197], supporting a role in the maintenance of immature cells in the hematopoietic system. This proposed role in differentiation is consistent with the observed knockdown of Meis2 significantly increasing CD11b expression in MN1 cells

in vitro, a phenotype that was also observed upon shRNA-mediated knockdown of MEIS2 in AML1-ETO-positive cells[190]. Although the increase in mature myeloid cell markers is minor, suggesting that other genes contribute to the block in myeloid differentiation, the largest increase in expression of donor-derived mature myeloid cells *in vivo* occurs within six weeks post-transplant, coinciding with the most marked delay in shMeis2-transduced cell engraftment.

Recent work by Vegi and colleagues demonstrated that MEIS2 is significantly upregulated in AML1-ETO leukemia and is critical for leukemogenesis[190]. Cell lines containing the AML1-ETO translocation show decreased proliferation and colony-forming ability, decreased cells in G0/G1 phase of cell cycle, and increased CD11b expression upon knockdown of MEIS2[190]. In contrast, retrovirally engineered co-expression of MEIS2 and AML1-ETO in murine progenitor cells increases colony formation in the colony-forming unit-spleen (CFU-S) assay and decreases the disease latency, with mice developing transplantable AML with high expression of the myeloid markers Gr-1 and CD11b, suggesting collaboration of these proteins[190]. In addition, MEIS2 strongly binds to AML1-ETO, leading to a loss of AML1-ETO binding at the YES1 promotor region and increased YES1 expression[190]. These data support a functional, critical role for Meis2 in MN1 leukemia, and prompt a further search for MEIS2 upregulation in other leukemic subtypes.

While Meis2 and retinoic acid (RA) are both key players in the induction of differentiation, the relationship between the two remains unclear. Early studies in P19 embryonic carcinoma cells showed that Meis2 expression could be induced by exogenous RA treatment[198]. In addition, HOXA1, PBX1 or PBX2, and MEIS2 form a trimeric complex that binds directly to a regulatory element of Raldh2, which is responsible for converting retinaldehyde to RA in the hindbrain.[199] Thus, these data are consistent with a model in which RA expression levels are regulated by the

Hox genes and their cofactors. However, recent studies in limb development show that Meis2 and RA may also operate independently, as both are expressed in bat wing membranes but have independent functions and mechanisms, with RA responsible for regulating interdigital webbing thinning and Meis2 regulating the formation and maintenance of interdigital cells.[195] Further study may elucidate the potential relationship between Meis2 and RA-induced signaling in leukemic cells.

As a master regulator of cell cycle expression, Meis2 is essential to maintain the expression of many cell cycle genes, including those involved in DNA replication, G2-M checkpoint control, and M phase progression in neuroblastoma cells[181]. In addition, FOXM1 is a direct target and required for MEIS2 to upregulate mitotic genes in neuroblastoma cells[181]. Similarly, Meis2 and Pbx1 homeodomains interact with Klf4 and promote expression of p15INK4a and E-cadherin expression, as evidenced by decreased p15 gene expression and increased S phase entry in HepG2 cells following knockdown of Meis2 or Pbx1 [182]. At the time these studies were initiated, the relationship between Meis2 and cell cycle in hematopoietic or AML cells was uncharacterised. BrdU analysis of shMeis2-transduced MN1 cells showed no effect on cell cycle. In contrast, shRNA-mediated suppression of MEIS2 in AML1-ETO-positive cell lines showed an increase in cells in G0/G1 phase[190]. However, unlike Vegi and colleagues, experiments described in this chapter did not include synchronization of cells prior to performing the BrdU assay[190]. Consequently, small shifts in cell cycle distribution upon Meis2 knockdown may have been masked by the well-documented proliferative ability of MN1 cells. In addition, conflicting reports as to the cell cycle stage(s) impacted by modulation of Meis2 expression in oncogenic contexts suggest that Meis2 has multiple cell cycle regulation targets, thus requiring further

study. Together, these data suggest that while Meis2 may play a role in regulating cell cycle progression, its contribution is likely minor in the context of MN1.

My data show that Meis2 knockdown in MN1 cells increases cells in early and late apoptosis, which is consistent with the impaired *in vitro* growth and *in vivo* engraftment and leukemogenesis observed, and suggests apoptosis as a mechanism contributing to the elimination of shMeis2-transduced MN1 cells from the population. Although the increased apoptosis may be linked to the increased myeloid differentiation observed upon knockdown of Meis2, given the relatively low absolute CD11b expression in shMeis2-transduced MN1 cells, it is likely that Meis2 knockdown confers decreased fitness to MN1 cells, resulting in increased apoptosis and a rapid depletion of these cells from the population. Noting the incomplete knockdown efficiency provided by the shRNAs, this suggests that the impairment in proliferation and increased apoptosis observed underestimates the impact of Meis2 knockdown, as the cells most affected by the shRNA are likely removed from the population more rapidly than detected at the timepoints analysed. These observations are consistent with examinations of embryonic lethal Meis2 knockout mice, which found large-scale cellular destruction and apoptosis, especially prominent in the liver[191]. Observations of apoptosis are also supported by work in numerous cancer models, as work in neuroblastoma cell lines show that ectopic MEIS2 overexpression enhances cell proliferation, anchorage-independent growth, and tumorigenicity, while its depletion leads to M-phase arrest and mitotic catastrophe[181]. Similarly, shRNA-mediated depletion of MEIS2 in AML1-ETO-positive cell lines also results in reduced proliferation and colony formation and a 38% decrease in cell viability upon siMEIS2 depletion in a primary human AML1-ETO sample[190]. Similarly, the rapid depletion of shMeis2-transduced MN1 cells shortly after transplantation supports the *in vitro* results, suggesting that MN1 cells expressing shMeis2 are

rapidly removed from the *in vivo* environment through a combination of apoptosis, differentiation, and inability to compete with untransduced MN1 cells. Together, this provides evidence that Meis2 upregulation in leukemia is a critical factor in dysregulation of apoptotic pathways and thus, contributes to the ability of leukemic cells to evade cell death.

As previously discussed, Meis1 and Meis2 share 85.7% identical amino acid sequence and nearly-identical DNA binding and transcriptional activation domains[198]. Consequently, the proteins may bind to similar DNA sequences and likely overlap in their target genes. Meis1 conditional knockout mice generate all hematopoietic compartments, albeit at lower cell numbers[81-83], suggesting that other transcriptional pathways can compensate for the loss of Meis1. As described in this chapter, absolute levels of Meis2 in LIC-containing MN1 subsets isolated from MN1 leukemic BM increased over the first seven days in culture, before returning to similar expression levels as at time of harvest. In contrast, MN1 and Meis1 expression levels decreased during the first 14 days after *in vitro* culture, after which they increased to levels seen at time of harvest. This inverse pattern of Meis1 and Meis2 gene expression suggests a degree of redundancy, such that upregulation of one Meis family member may be sufficient in leukemic contexts. This is supported by cell lines with substantial expression of MEIS2 compared to MEIS1, such as the ML2 line with 10-fold more MEIS2 than MEIS1, where knockdown of MEIS1 had no effect on *in vitro* clonogenic ability[86]. Similarly, in the MN1VP16 leukemia model, Meis2 is differentially regulated between MN1 and MN1VP16, despite similar Meis1 levels. Furthermore, data from the TCGA AML dataset shows that high MEIS2 expression is associated with improved overall survival. Consequently, while upregulation of Meis1 with or without Meis2 upregulation results in a more aggressive AML and occurs more frequently, Meis2 upregulation alone may also activate sufficient overlapping pathways to induce AML.

In the TCGA AML and Leukemia MILE datasets, MN1 and MEIS2 are upregulated in patients with inv(16) and complex AML, suggesting that there may be a subset of AMLs that show upregulation in both genes. However, the in-house dataset did not show a relationship between MEIS2 and MN1 expression in patients with de novo or therapy-related AML or MDS. Although this may be due to an insufficient sample size of patients with high MN1 expression, there is similarly no relationship between MEIS2 and MN1 in inv(16), MN1-high expressing, or across AMLs from the Valk dataset[102]. Interestingly, MEIS1 and MEIS2 are inversely and significantly correlated across AML subtypes[102]. This provides support for a compensatory relationship between MEIS1 and MEIS2 where AML may only require upregulation of one MEIS family member, typically MEIS1. Consistent with this idea, knockdown of Meis2 in our leukemia-derived MN1 cell line also shows upregulation of Meis1. This provides evidence that MEIS1 and MEIS2 can modulate their expression levels in response to activation of other family members, suggesting there may be mechanisms regulating the expression of these genes in relation to one another in leukemic cells.

These models provide a platform to identify and functionally assess genes critical to MN1 leukemic activity. Initial studies, described in this thesis, identify and characterize HoxA9, Hlf, and Meis2 as critical to leukemic properties. Furthermore, these models provide a platform to unravel the basis for the profound upregulation of Meis2 in MN1 leukemias, delineate potential functional differences between Meis2 and Meis1, and stimulate further study into the role of Meis2 in additional leukemic settings.

Chapter 4: Conclusions

4.1 Summary

Most acute leukemias are characterized by overexpression of HOX genes and the TALE family of cofactors[200]. Similarly, the oncogene MN1 is frequently upregulated in a wide range of leukemias. A growing body of data point to strong cooperative functions that link MN1 to Hox and Meis. The data presented in this thesis exploits a murine model of AML induced by overexpression of MN1 to explore the leukemogenic functions of MN1 and to identify potential genes, including HOX and MEIS family members, that are involved in its leukemic properties.

4.2 Significance of the work

4.2.1 MN1 structure-function analysis

HOX protein homeodomains have a high degree of sequence similarity, requiring additional sequence specificity to regulate the multiple downstream effects, often achieved through interaction with co-factors and collaborators[201, 202]. Current models suggest that TALE family co-factors such as MEIS1 bind at regulatory elements, increasing chromatin accessibility, followed by recruitment of HOX proteins like HOXA9[203], and recruitment of collaborators such as CREB and CBP[204] and lineage-specific transcription factors like PU.1 and C/EBPα to HOXA9 binding sites to increase chromatin accessibility, stabilize DNA binding and activate specific transcriptional programs[69, 205]. Among the many collaborators of MEIS1 and HOXA proteins is MN1, which requires their transcriptional programs for leukemic transformation[128].

The first significant contribution of my thesis is one of the first in-depth functional characterizations of the MN1 structure. Chapter 2 of this thesis describes the delineation and localization of specific regions of MN1 at a structural level to the leukemic properties of enhanced proliferation, self-renewal, impairments in erythroid, megakaryocyte, lymphoid, and myeloid cell differentiation ability, and resistance to ATRA. Comparisons of gene expression profiles of two MN1 variants, MN1Δ7 that generates a more mature AML than wildtype MN1 and MN1Δ1 which does not induce leukemia, to wildtype MN1 identified a subset of genes and pathways potentially relevant to these leukemic properties. The MN1Δ7 leukemic phenotype was later expanded upon by Sharma and colleagues, who also observed a more mature and less-aggressive AML from the fusion of the VP16 transactivation domain to MN1 and identified downregulation of immune regulation and immune response pathways, specifically Irf8 and its downstream target Ccl9, as critical targets of MN1-induced leukemia[115].

The discovery that the C-terminal 606 amino acids of MN1 regulate the myeloid-lymphoid phenotypic identity of MN1 leukemia stimulates questions surrounding regulation of lineage identity in leukemogenesis and transformation. Transplantation of MN1Δ5-7-transduced cells gives rise to T-ALL as opposed to the AML arising from wildtype MN1 overexpression. It is, however, unknown if this change in leukemic phenotypic identity arises from differences at the transformation event, such as a change in the target cell of transformation, changes that occur during leukemic progression due to differences in DNA binding, interacting proteins, or epigenetic regulation, or arise from differing target cells of transformation. Sorting and purification of HSCs, LMPPs, CMPs, and GMPs would facilitate investigation of the range of target cells susceptible to transformation by MN1Δ5-7 as compared to MN1Δ7 with a more mature myeloid phenotype, the non-leukemic MN1Δ1, and wildtype MN1. Additionally,

assessing properties including survival, proliferation, resistance to ATRA, and colony-forming ability *in vitro* and induction of leukemia *in vivo* would elucidate the range of hematopoietic stem and progenitor cells susceptible to transformation by each these MN1 mutants, and if varying the cell transformed impacts the phenotype that emerges. Of future interest, will be to exploit these MN1 variants using ChIP-Seq comparisons to elucidate differences in DNA binding locations compared to wildtype MN1 and subsequently provide insight into gene expression underlying the phenotype documented for each MN1 variant. Native ChIP-Seq and genome-wide DNA methylation analysis would provide further insight into regulation of gene expression at an epigenetic level. Examining the status of activating histone marks such as H3K27ac and methylation of H3K4 and repressive marks such as H3K27 and H3K9 methylation, combined with DNA methylation status across the genome would aid in correlating differences in gene expression with the specific phenotypes characteristic of wildtype MN1 and MN1 variants. Additionally, as few MN1-interacting proteins have been identified, mass spectrometry and other proteomic studies would be of great interest to identify proteins that contribute to the properties of wildtype MN1 compared to the MN1 variants.

The localisation of ATRA resistance to the MN1 C-terminus elegantly showcases the use of these MN1 variants for drug testing purposes, particularly against candidate differentiation-inducing treatments. Elucidating the modification status of known activating and repressing histone marks and DNA methylation by ChIP-Seq and genome-wide DNA methylation analysis, respectively, between wildtype MN1 and ATRA-sensitive variants would provide insight into genes that regulate the myeloid differentiation block and ATRA resistance characteristic of MN1. Furthermore, transcription factor chromatin immunoprecipitation and mass spectrometry of wildtype MN1 and the MN1 variants could aid in identifying locations of transcription factor

binding of MN1, and differing binding locations of its variants, as well as identifying members of the MN1 protein complex that bind at these sites. Together, these data would aid in identifying underlying differences between gene expression between wildtype MN1 and the MN1 variants, potentially modulated due to differing protein binding partners, and facilitate elucidation of their relationships to specific leukemic properties characterised by the MN1 variant phenotypes (Figure 4.1).

Figure 4.1 Model of protein complexes of MN1 variants.

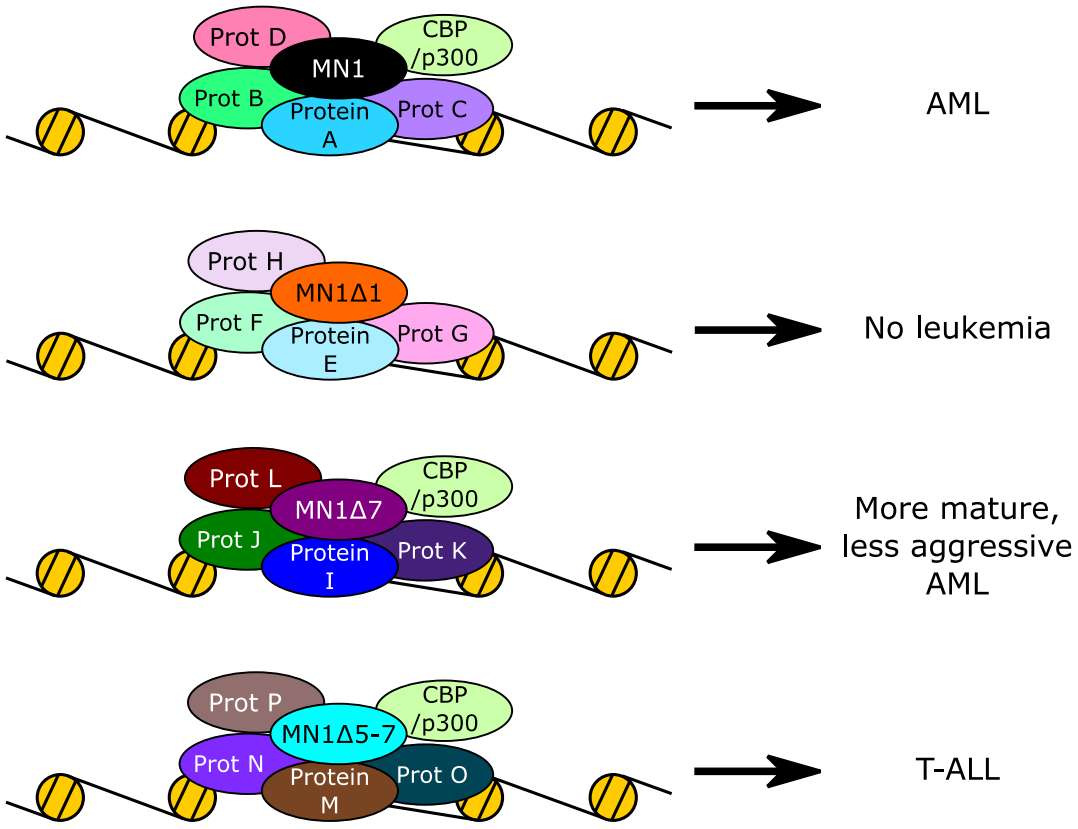

Identification of the different proteins interacting with MN1 and the MN1 variants generated and characterized in my thesis work may elucidate mechanisms by which their different phenotypes emerge.

Previous work has identified the MN1 N-terminus as a major source of transactivating activity[95], and co-expression of MN1 and p300 or RAC3 have been shown to synergistically activate transcriptional activity of RAR-RXR dimers in the presence of retinoic acid[95]. In addition, this region has been thought to potentially regulate myeloid cell growth and differentiation[93]. In support of this are the data presented in Chapter 2 identifying a role for the MN1 N-terminal 202 amino acids in proliferation, self-renewal, and blocking erythro-megakaryocyte differentiation in addition to leukemia initiation. Intriguingly, unsupervised hierarchical clustering of Affymetrix gene expression data demonstrates that despite its lack of leukemic activity, MN1Δ1 cells cluster more closely to full-length MN1 cells than mature myeloid cells, suggesting that MN1Δ1 represents a state primed for leukemia. Thus, genes differentially expressed between wildtype leukemic MN1 and MN1Δ1 are intriguing candidates for leukemic transformation. Mass spectrometry analysis of proteins that interact with wildtype MN1 and MN1Δ1 could aid in distinguishing the members of the MN1 protein complex that are critical for leukemic transformation compared to those that potentially contribute to erythro-megakaryocyte differentiation block or proliferation. Furthermore, these studies would further the understanding of how MN1 interacts with other proteins known to be dysregulated in leukemia, such as Meis1 and the HoxA family proteins, as well as providing further insight into the roles of these proteins in leukemogenesis.

4.2.2 Using gene expression comparisons of MN1 models to identify genes critical to leukemic activity

Gene expression comparisons between MN1Δ1 and wildtype MN1 provide insight into leukemic and non-leukemic MN1 models. Through examination of gene expression comparisons between leukemic versus non-leukemic MN1 models (MN1 vs MN1Δ1 described in Chapter 2, MN1 cKit versus MN1 CD11b subpopulations described in Chapter 3) and versus less-aggressive MN1 models (MN1VP16)[115], a subset of genes dysregulated in multiple comparisons were identified as intriguing potential targets and collaborators of MN1-induced leukemic activity. Among the validated genes not functionally assessed in this work are Gpr56, which was recently identified as a marker for cells with high repopulating potential in primary human AML cells[180], and Msi2, which is highly expressed in human AML cell lines and patients with AML, associated with aggressive disease and immature phenotype, and negatively associated with outcome in patients with AML[206, 207] Additionally, Sharma and colleagues previously described a role for immune response and regulation pathways in MN1 leukemia[115]. GSEA of the LIC-containing (cKit) and LIC-devoid (CD11b) MN1 subsets suggest that downregulation of the immune response and regulation pathways is characteristic of LIC-containing cells, providing support for this work and a crucial role for immune regulation in leukemogenesis. With growing recognition and interest in the role of the immune system in leukemogenesis and as a therapeutic target, particularly the early success of immunotherapy treatment in lymphomas, this represents an interesting avenue through which to further elucidate mechanisms of leukemogenesis.

Given the identification of a LIC-depleted subpopulation based on expression of two cell surface markers, cKit and CD11b, it is very likely that further work to identify more markers could further enrich MN1 cells for LSC activity and add power to identification of LSC-associated

genes. Furthermore, with sufficient enrichment, powerful single cell analyses of expression and epigenetic status could be applied, as recently described by the Göttgens lab[208, 209] and Rotem and colleagues[210], respectively. Nonetheless, initial analysis of the small subset of genes investigated in this thesis has already yielded important insights and novel observations.

Among these findings is the identification of Hlf as a new critical gene in MN1-induced leukemia while, surprisingly, knockdown of upregulated Meis1 does not have a significant effect on *in vitro* measures of leukemogenesis. Together, these data suggest that Meis1 is not required for MN1 maintenance or progression, that low levels of Meis1 expression are sufficient for MN1-induced leukemic activity, or that *in vitro* assessment of the impact of Meis1 knockdown on MN1 leukemia may be insufficient to capture the complexities of leukemogenic activity. To investigate these possibilities, MN1 transduction of Meis1 conditional knockout murine bone marrow could be performed prior to Meis1 deletion. Functional testing *in vitro* in the CFU assay and through *in vivo* transplantation assays, would assess the self-renewal and leukemogenicity of MN1 cells upon a complete loss of Meis1 expression both *in vitro* and *in vivo*.

4.2.3 A new appreciation for the role of MEIS2

The most striking finding from Chapter 3 of this thesis is the essential role of Meis2 for MN1 leukemic proliferation, survival, self-renewal, and *in vivo* leukemogenicity, providing evidence that it may be a novel key player in leukemia. The identification of Meis2 as upregulated in and critical to MN1 leukemic properties reported in this thesis, as well as the recent report of upregulated MEIS2 in AML1-ETO-positive leukemias[190] suggest that MEIS2 upregulation may be seen in other leukemic subtypes. Vegi and colleagues also demonstrated that the N-terminus

of Meis2 facilitates binding to AML1-ETO[190]. Similar studies could elucidate the protein regions of Meis2 responsible for binding to or forming complexes with other oncogenes, such as MN1, and identify these collaborating proteins.

The data presented in Chapter 3 suggests a degree of compensation exists between one or more Meis family members. Given the frequency of MEIS1 upregulation across multiple leukemia subtypes, particularly within AML[211], and the demonstrated requirement of Meis2 expression for MN1 leukemic activity, future studies provide an intriguing opportunity to elucidate the relationship between Meis1 and Meis2. The generation of model systems with the ability to measure Meis family member expression in real-time would facilitate such studies, allowing relative gene and protein expression to be tracked in response to perturbation of other family members and interacting proteins. In addition, comparisons of genes differentially regulated upon overexpression and knockdown of Meis1 and/or Meis2 compared to wildtype leukemic MN1 would aid in the identification of both common and unique targets of Meis1 and Meis2, respectively. Similarly, identification of Meis1 and Meis2 DNA binding sites by ChIP-Seq and protein interaction complexes by mass spectrometry would provide further insight into the ways Meis1 and Meis2 regulate target genes. Together, these studies would expand the current understanding of the manners in which the Meis family influence and modulate leukemogenesis, and potentially reveal a powerful therapeutic target.

4.2.4 Overall significance

The generation and functional characterization of the MN1 models with varying leukemic activity provides powerful models to better understand molecular events throughout

leukemogenesis. By combining the work described in Chapters 2 and 3, the MN1 variants could be used to track gene expression kinetics to identify early events in leukemic transformation, expanding and refining the subset of genes potentially critical to leukemic activity. However, the relative contributions of epigenetic regulation and protein binding in this leukemia model remain largely uncharacterised. Therefore, identification of interacting proteins – especially those that differ between MN1 and MN1Δ1 and thus, likely bind to the MN1 N-terminus – and differences in DNA binding between the MN1 wildtype and variants would provide further insight into genes critical to leukemic activity. Furthermore, these studies may also extend their investigation to other leukemic subtypes, supporting the use of MN1 overexpression as a model for AML.

The work presented in this thesis was performed exclusively in the mouse model. Murine models, however, do not always capture the complexities of the human system. The exciting results described in this thesis provide an impetus to move studies to a human context. MN1 and ND13 collaboration is sufficient to induce AML in the human cord blood model[126], and spurs questions if the MN1 mutant forms are also capable of collaboration with ND13 and if the leukemic phenotypes and identities shown to arise upon transformation of murine cells by MN1 variants also show differential effects in human cells. Furthermore, much like upregulation of MEIS2 was also seen in the LIC-containing $CD34^{+}GPR56^{+}$ fraction of the MN1+ND13 human cord blood model, future experiments in human contexts could also aid in the identification of candidate genes relevant to LSC activity.

4.3 Concluding remarks

Combined, these studies suggest that MN1 mediates its effects through a multifaceted approach, interacting with multiple proteins that, at present, have yet to be elucidated. Numerous MN1 models with varying structure and leukemogenic ability were generated and characterized, providing a useful series of models to explore multiple aspects of leukemic activity. Given the novel discovery of the ability of MN1 to collaborate with Meis2, adding to the established importance of such genes as HoxA9 and Meis1 in AML, expansion of current models, such as those initially proposed by Jay Hess[69], to include MN1 and Meis2 may be required (Figure 4.2).

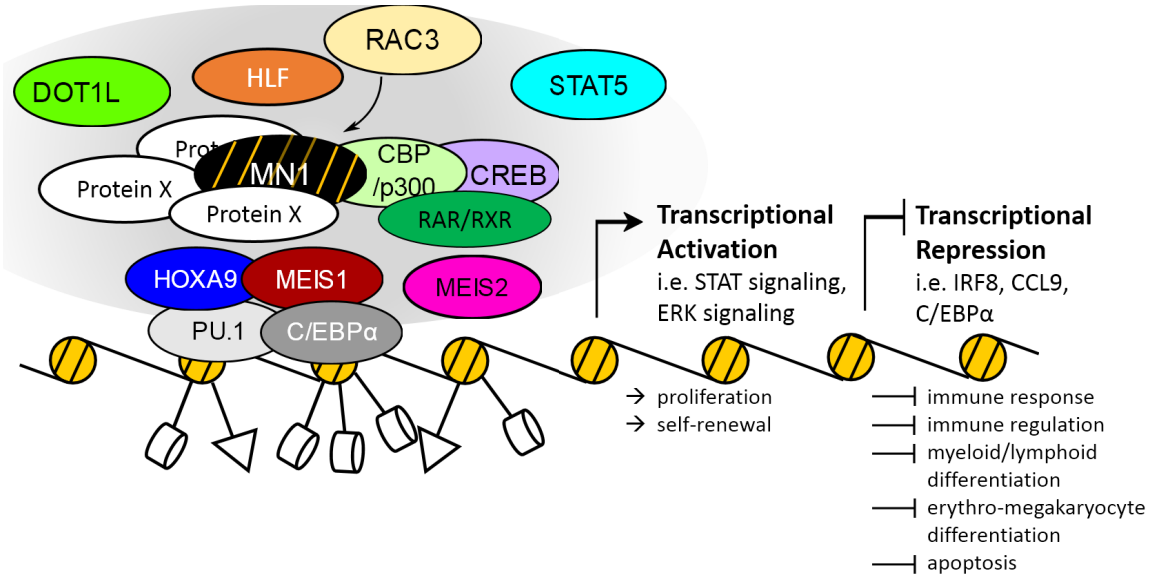

Figure 4.2 Model of MN1 as a protein complex member.

MN1 is a valuable tool for modeling leukemia, which continues to invite further exploitation. Overexpression of MN1 drives proliferation and self-renewal while blocking immune regulation and response, normal hematopoietic cell differentiation, and apoptosis. These phenotypes are driven through mechanisms of transcriptional activation and repression, some contributors of which, like STAT signaling, have been identified. Chapter 2 of my thesis describes the discovery of the structural basis of the multipartite functions of MN1, with leukemic properties (proliferation/self-renewal, block in differentiation) localised to distinct regions of the MN1 molecule – information

that can be used to probe further into molecular events governing leukemic transformation and progression, fate decisions, and identification of protein interactors and potential druggable targets. MN1 can bind throughout the genome, some sites of which overlap with HoxA9, Meis1, and RAR binding. Thus, MN1 may be part of a protein complex, initiated by pioneering factors like HoxA9 and Meis1, that interact with a number of proteins to exert its multifaceted effects. To this list of potential complex members, I can now add Hlf and Meis2 as critical players. This begs further resolution of these yet-unknown protein interactors (Protein X), as well as the epigenetic regulation governing their activity, which can provide valuable insight to our understanding of leukemogenesis,

References

1. Reya, T., S.J. Morrison, M.F. Clarke, and I.L. Weissman, *Stem cells, cancer, and cancer stem cells.* Nature, 2001. **414**(6859): p. 105-11.
2. Zuo, Z., J.M. Polski, A. Kasyan, and L.J. Medeiros, *Acute erythroid leukemia.* Arch Pathol Lab Med, 2010. **134**(9): p. 1261-70.
3. Hahn, A.W., B. Li, P. Prouet, S. Giri, R. Pathak, and M.G. Martin, *Acute megakaryocytic leukemia: What have we learned.* Blood Rev, 2016. **30**(1): p. 49-53.
4. Bruce, W.R. and H. Van Der Gaag, *A Quantitative Assay for the Number of Murine Lymphoma Cells Capable of Proliferation in Vivo.* Nature, 1963. **199**: p. 79-80.
5. Buick, R.N., J.E. Till, and E.A. McCulloch, *Colony assay for proliferative blast cells circulating in myeloblastic leukaemia.* Lancet, 1977. **1**(8016): p. 862-3.
6. Lapidot, T., C. Sirard, J. Vormoor, B. Murdoch, T. Hoang, J. Caceres-Cortes, M. Minden, B. Paterson, M.A. Caligiuri, and J.E. Dick, *A cell initiating human acute myeloid leukaemia after transplantation into SCID mice.* Nature, 1994. **367**(6464): p. 645-8.
7. Bonnet, D. and J.E. Dick, *Human acute myeloid leukemia is organized as a hierarchy that originates from a primitive hematopoietic cell.* Nat Med, 1997. **3**(7): p. 730-7.
8. Lane, S.W., D.T. Scadden, and D.G. Gilliland, *The leukemic stem cell niche: current concepts and therapeutic opportunities.* Blood, 2009. **114**(6): p. 1150-7.
9. Goardon, N., E. Marchi, A. Atzberger, L. Quek, A. Schuh, S. Soneji, P. Woll, A. Mead, K.A. Alford, R. Rout, S. Chaudhury, A. Gilkes, S. Knapper, K. Beldjord, S. Begum, S. Rose, N. Geddes, M. Griffiths, G. Standen, A. Sternberg, J. Cavenagh, H. Hunter, D. Bowen, S. Killick, L. Robinson, A. Price, E. Macintyre, P. Virgo, A. Burnett, C. Craddock, T. Enver, S.E. Jacobsen, C. Porcher, and P. Vyas, *Coexistence of LMPP-like and GMP-like leukemia stem cells in acute myeloid leukemia.* Cancer Cell, 2011. **19**(1): p. 138-52.
10. Eppert, K., K. Takenaka, E.R. Lechman, L. Waldron, B. Nilsson, P. van Galen, K.H. Metzeler, A. Poeppl, V. Ling, J. Beyene, A.J. Canty, J.S. Danska, S.K. Bohlander, C. Buske, M.D. Minden, T.R. Golub, I. Jurisica, B.L. Ebert, and J.E. Dick, *Stem cell gene expression programs influence clinical outcome in human leukemia.* Nat Med, 2011. **17**(9): p. 1086-93.
11. Somervaille, T.C. and M.L. Cleary, *Identification and characterization of leukemia stem cells in murine MLL-AF9 acute myeloid leukemia.* Cancer Cell, 2006. **10**(4): p. 257-68.
12. Mamo, A., J. Krosl, E. Kroon, J. Bijl, A. Thompson, N. Mayotte, S. Girard, R. Bisaillon, N. Beslu, M. Featherstone, and G. Sauvageau, *Molecular dissection of Meis1 reveals 2 domains required for leukemia induction and a key role for Hoxa gene activation.* Blood, 2006. **108**(2): p. 622-9.
13. Fialkow, P.J., R.J. Jacobson, and T. Papayannopoulou, *Chronic myelocytic leukemia: clonal origin in a stem cell common to the granulocyte, erythrocyte, platelet and monocyte/macrophage.* Am J Med, 1977. **63**(1): p. 125-30.
14. Yoffe, G., A.C. Chinault, M. Talpaz, M.B. Blick, H.M. Kantarjian, K. Taylor, and G. Spitzer, *Clonal nature of Philadelphia chromosome-positive and -negative chronic myelogenous leukemia by DNA hybridization analyses.* Exp Hematol, 1987. **15**(7): p. 725-8.

15. Takahashi, N., I. Miura, K. Saitoh, and A.B. Miura, *Lineage involvement of stem cells bearing the philadelphia chromosome in chronic myeloid leukemia in the chronic phase as shown by a combination of fluorescence-activated cell sorting and fluorescence in situ hybridization.* Blood, 1998. **92**(12): p. 4758-63.
16. Kovacic, B., A. Hoelbl, G. Litos, M. Alacakaptan, C. Schuster, K.M. Fischhuber, M.A. Kerenyi, G. Stengl, R. Moriggl, V. Sexl, and H. Beug, *Diverging fates of cells of origin in acute and chronic leukaemia.* EMBO Mol Med, 2012. **4**(4): p. 283-97.
17. Kirstetter, P., M.B. Schuster, O. Bereshchenko, S. Moore, H. Dvinge, E. Kurz, K. Theilgaard-Monch, R. Mansson, T.A. Pedersen, T. Pabst, E. Schrock, B.T. Porse, S.E. Jacobsen, P. Bertone, D.G. Tenen, and C. Nerlov, *Modeling of C/EBPalpha mutant acute myeloid leukemia reveals a common expression signature of committed myeloid leukemia-initiating cells.* Cancer Cell, 2008. **13**(4): p. 299-310.
18. Cozzio, A., E. Passegue, P.M. Ayton, H. Karsunky, M.L. Cleary, and I.L. Weissman, *Similar MLL-associated leukemias arising from self-renewing stem cells and short-lived myeloid progenitors.* Genes Dev, 2003. **17**(24): p. 3029-35.
19. Huntly, B.J., H. Shigematsu, K. Deguchi, B.H. Lee, S. Mizuno, N. Duclos, R. Rowan, S. Amaral, D. Curley, I.R. Williams, K. Akashi, and D.G. Gilliland, *MOZ-TIF2, but not BCR-ABL, confers properties of leukemic stem cells to committed murine hematopoietic progenitors.* Cancer Cell, 2004. **6**(6): p. 587-96.
20. Krivtsov, A.V., D. Twomey, Z. Feng, M.C. Stubbs, Y. Wang, J. Faber, J.E. Levine, J. Wang, W.C. Hahn, D.G. Gilliland, T.R. Golub, and S.A. Armstrong, *Transformation from committed progenitor to leukaemia stem cell initiated by MLL-AF9.* Nature, 2006. **442**(7104): p. 818-22.
21. Deshpande, A.J., M. Cusan, V.P. Rawat, H. Reuter, A. Krause, C. Pott, L. Quintanilla-Martinez, P. Kakadia, F. Kuchenbauer, F. Ahmed, E. Delabesse, M. Hahn, P. Lichter, M. Kneba, W. Hiddemann, E. Macintyre, C. Mecucci, W.D. Ludwig, R.K. Humphries, S.K. Bohlander, M. Feuring-Buske, and C. Buske, *Acute myeloid leukemia is propagated by a leukemic stem cell with lymphoid characteristics in a mouse model of CALM/AF10-positive leukemia.* Cancer Cell, 2006. **10**(5): p. 363-74.
22. Taussig, D.C., F. Miraki-Moud, F. Anjos-Afonso, D.J. Pearce, K. Allen, C. Ridler, D. Lillington, H. Oakervee, J. Cavenagh, S.G. Agrawal, T.A. Lister, J.G. Gribben, and D. Bonnet, *Anti-CD38 antibody-mediated clearance of human repopulating cells masks the heterogeneity of leukemia-initiating cells.* Blood, 2008. **112**(3): p. 568-75.
23. Jordan, C.T. and M.L. Guzman, *Mechanisms controlling pathogenesis and survival of leukemic stem cells.* Oncogene, 2004. **23**(43): p. 7178-87.
24. Rowley, J.D., *Chromosomes in leukemia and beyond: from irrelevant to central players.* Annu Rev Genomics Hum Genet, 2009. **10**: p. 1-18.
25. Rowley, J.D., *Letter: A new consistent chromosomal abnormality in chronic myelogenous leukaemia identified by quinacrine fluorescence and Giemsa staining.* Nature, 1973. **243**(5405): p. 290-3.
26. Daley, G.Q., R.A. Van Etten, and D. Baltimore, *Induction of chronic myelogenous leukemia in mice by the P210bcr/abl gene of the Philadelphia chromosome.* Science, 1990. **247**(4944): p. 824-30.
27. Lugo, T.G., A.M. Pendergast, A.J. Muller, and O.N. Witte, *Tyrosine kinase activity and transformation potency of bcr-abl oncogene products.* Science, 1990. **247**(4946): p. 1079-82.

28. Druker, B.J., S. Tamura, E. Buchdunger, S. Ohno, G.M. Segal, S. Fanning, J. Zimmermann, and N.B. Lydon, *Effects of a selective inhibitor of the Abl tyrosine kinase on the growth of Bcr-Abl positive cells.* Nat Med, 1996. **2**(5): p. 561-6.
29. Druker, B.J., C.L. Sawyers, H. Kantarjian, D.J. Resta, S.F. Reese, J.M. Ford, R. Capdeville, and M. Talpaz, *Activity of a specific inhibitor of the BCR-ABL tyrosine kinase in the blast crisis of chronic myeloid leukemia and acute lymphoblastic leukemia with the Philadelphia chromosome.* N Engl J Med, 2001. **344**(14): p. 1038-42.
30. Druker, B.J., M. Talpaz, D.J. Resta, B. Peng, E. Buchdunger, J.M. Ford, N.B. Lydon, H. Kantarjian, R. Capdeville, S. Ohno-Jones, and C.L. Sawyers, *Efficacy and safety of a specific inhibitor of the BCR-ABL tyrosine kinase in chronic myeloid leukemia.* N Engl J Med, 2001. **344**(14): p. 1031-7.
31. Sawyers, C.L., A. Hochhaus, E. Feldman, J.M. Goldman, C.B. Miller, O.G. Ottmann, C.A. Schiffer, M. Talpaz, F. Guilhot, M.W. Deininger, T. Fischer, S.G. O'Brien, R.M. Stone, C.B. Gambacorti-Passerini, N.H. Russell, J.J. Reiffers, T.C. Shea, B. Chapuis, S. Coutre, S. Tura, E. Morra, R.A. Larson, A. Saven, C. Peschel, A. Gratwohl, F. Mandelli, M. Ben-Am, I. Gathmann, R. Capdeville, R.L. Paquette, and B.J. Druker, *Imatinib induces hematologic and cytogenetic responses in patients with chronic myelogenous leukemia in myeloid blast crisis: results of a phase II study.* Blood, 2002. **99**(10): p. 3530-9.
32. Rowley, J.D., H.M. Golomb, and C. Dougherty, *15/17 translocation, a consistent chromosomal change in acute promyelocytic leukaemia.* Lancet, 1977. **1**(8010): p. 549-50.
33. Lo-Coco, F. and E. Ammatuna, *The biology of acute promyelocytic leukemia and its impact on diagnosis and treatment.* Hematology Am Soc Hematol Educ Program, 2006: p. 156-61, 514.
34. Zheng, P.Z., K.K. Wang, Q.Y. Zhang, Q.H. Huang, Y.Z. Du, Q.H. Zhang, D.K. Xiao, S.H. Shen, S. Imbeaud, E. Eveno, C.J. Zhao, Y.L. Chen, H.Y. Fan, S. Waxman, C. Auffray, G. Jin, S.J. Chen, Z. Chen, and J. Zhang, *Systems analysis of transcriptome and proteome in retinoic acid/arsenic trioxide-induced cell differentiation/apoptosis of promyelocytic leukemia.* Proc Natl Acad Sci U S A, 2005. **102**(21): p. 7653-8.
35. Meyer, C., E. Kowarz, J. Hofmann, A. Renneville, J. Zuna, J. Trka, R. Ben Abdelali, E. Macintyre, E. De Braekeleer, M. De Braekeleer, E. Delabesse, M.P. de Oliveira, H. Cave, E. Clappier, J.J. van Dongen, B.V. Balgobind, M.M. van den Heuvel-Eibrink, H.B. Beverloo, R. Panzer-Grumayer, A. Teigler-Schlegel, J. Harbott, E. Kjeldsen, S. Schnittger, U. Koehl, B. Gruhn, O. Heidenreich, L.C. Chan, S.F. Yip, M. Krzywinski, C. Eckert, A. Moricke, M. Schrappe, C.N. Alonso, B.W. Schafer, J. Krauter, D.A. Lee, U. Zur Stadt, G. Te Kronnie, R. Sutton, S. Izraeli, L. Trakhtenbrot, L. Lo Nigro, G. Tsaur, L. Fechina, T. Szczepanski, S. Strehl, D. Ilencikova, M. Molkentin, T. Burmeister, T. Dingermann, T. Klingebiel, and R. Marschalek, *New insights to the MLL recombinome of acute leukemias.* Leukemia, 2009. **23**(8): p. 1490-9.
36. Nguyen, T.T., L.N. Ma, M.L. Slovak, C.D. Bangs, A.M. Cherry, and D.A. Arber, *Identification of novel Runx1 (AML1) translocation partner genes SH3D19, YTHDf2, and ZNF687 in acute myeloid leukemia.* Genes Chromosomes Cancer, 2006. **45**(10): p. 918-32.
37. Takeda, A. and N.R. Yaseen, *Nucleoporins and nucleocytoplasmic transport in hematologic malignancies.* Semin Cancer Biol, 2014. **27**: p. 3-10.

38. Chibon, F., *Cancer gene expression signatures - the rise and fall?* Eur J Cancer, 2013. **49**(8): p. 2000-9.
39. Golub, T.R., D.K. Slonim, P. Tamayo, C. Huard, M. Gaasenbeek, J.P. Mesirov, H. Coller, M.L. Loh, J.R. Downing, M.A. Caligiuri, C.D. Bloomfield, and E.S. Lander, *Molecular classification of cancer: class discovery and class prediction by gene expression monitoring.* Science, 1999. **286**(5439): p. 531-7.
40. Krivtsov, A.V. and S.A. Armstrong, *MLL translocations, histone modifications and leukaemia stem-cell development.* Nat Rev Cancer, 2007. **7**(11): p. 823-33.
41. Kawagoe, H., R.K. Humphries, A. Blair, H.J. Sutherland, and D.E. Hogge, *Expression of HOX genes, HOX cofactors, and MLL in phenotypically and functionally defined subpopulations of leukemic and normal human hematopoietic cells.* Leukemia, 1999. **13**(5): p. 687-98.
42. Rozovskaia, T., E. Feinstein, O. Mor, R. Foa, J. Blechman, T. Nakamura, C.M. Croce, G. Cimino, and E. Canaani, *Upregulation of Meis1 and HoxA9 in acute lymphocytic leukemias with the t(4 : 11) abnormality.* Oncogene, 2001. **20**(7): p. 874-8.
43. Imamura, T., A. Morimoto, M. Takanashi, S. Hibi, T. Sugimoto, E. Ishii, and S. Imashuku, *Frequent co-expression of HoxA9 and Meis1 genes in infant acute lymphoblastic leukaemia with MLL rearrangement.* Br J Haematol, 2002. **119**(1): p. 119-21.
44. Grubach, L., C. Juhl-Christensen, A. Rethmeier, L.H. Olesen, A. Aggerholm, P. Hokland, and M. Ostergaard, *Gene expression profiling of Polycomb, Hox and Meis genes in patients with acute myeloid leukaemia.* Eur J Haematol, 2008. **81**(2): p. 112-22.
45. Heuser, M., G. Beutel, J. Krauter, K. Dohner, N. von Neuhoff, B. Schlegelberger, and A. Ganser, *High meningioma 1 (MN1) expression as a predictor for poor outcome in acute myeloid leukemia with normal cytogenetics.* Blood, 2006. **108**(12): p. 3898-905.
46. Takahashi, S., *Current findings for recurring mutations in acute myeloid leukemia.* J Hematol Oncol, 2011. **4**: p. 36.
47. Kihara, R., Y. Nagata, H. Kiyoi, T. Kato, E. Yamamoto, K. Suzuki, F. Chen, N. Asou, S. Ohtake, S. Miyawaki, Y. Miyazaki, T. Sakura, Y. Ozawa, N. Usui, H. Kanamori, T. Kiguchi, K. Imai, N. Uike, F. Kimura, K. Kitamura, C. Nakaseko, M. Onizuka, A. Takeshita, F. Ishida, H. Suzushima, Y. Kato, H. Miwa, Y. Shiraishi, K. Chiba, H. Tanaka, S. Miyano, S. Ogawa, and T. Naoe, *Comprehensive analysis of genetic alterations and their prognostic impacts in adult acute myeloid leukemia patients.* Leukemia, 2014. **28**(8): p. 1586-95.
48. Cancer Genome Atlas Research, N., *Genomic and epigenomic landscapes of adult de novo acute myeloid leukemia.* N Engl J Med, 2013. **368**(22): p. 2059-74.
49. Gehring, W.J., M. Affolter, and T. Burglin, *Homeodomain proteins.* Annu Rev Biochem, 1994. **63**: p. 487-526.
50. Lewis, E.B., *A gene complex controlling segmentation in Drosophila.* Nature, 1978. **276**(5688): p. 565-70.
51. Moretti, P., P. Simmons, P. Thomas, D. Haylock, P. Rathjen, M. Vadas, and R. D'Andrea, *Identification of homeobox genes expressed in human haemopoietic progenitor cells.* Gene, 1994. **144**(2): p. 213-9.
52. Sauvageau, G., P.M. Lansdorp, C.J. Eaves, D.E. Hogge, W.H. Dragowska, D.S. Reid, C. Largman, H.J. Lawrence, and R.K. Humphries, *Differential expression of homeobox*

genes in functionally distinct CD34+ subpopulations of human bone marrow cells. Proc Natl Acad Sci U S A, 1994. **91**(25): p. 12223-7.
53. Giampaolo, A., E. Pelosi, M. Valtieri, E. Montesoro, P. Sterpetti, P. Samoggia, A. Camagna, G. Mastroberardino, M. Gabbianelli, U. Testa, and et al., *HOXB gene expression and function in differentiating purified hematopoietic progenitors.* Stem Cells, 1995. **13 Suppl 1**: p. 90-105.
54. Pineault, N., C.D. Helgason, H.J. Lawrence, and R.K. Humphries, *Differential expression of Hox, Meis1, and Pbx1 genes in primitive cells throughout murine hematopoietic ontogeny.* Exp Hematol, 2002. **30**(1): p. 49-57.
55. Lawrence, H.J., C.D. Helgason, G. Sauvageau, S. Fong, D.J. Izon, R.K. Humphries, and C. Largman, *Mice bearing a targeted interruption of the homeobox gene HOXA9 have defects in myeloid, erythroid, and lymphoid hematopoiesis.* Blood, 1997. **89**(6): p. 1922-30.
56. Thorsteinsdottir, U., G. Sauvageau, and R.K. Humphries, *Hox homeobox genes as regulators of normal and leukemic hematopoiesis.* Hematol Oncol Clin North Am, 1997. **11**(6): p. 1221-37.
57. Lawrence, H.J., J. Christensen, S. Fong, Y.L. Hu, I. Weissman, G. Sauvageau, R.K. Humphries, and C. Largman, *Loss of expression of the Hoxa-9 homeobox gene impairs the proliferation and repopulating ability of hematopoietic stem cells.* Blood, 2005. **106**(12): p. 3988-94.
58. Antonchuk, J., G. Sauvageau, and R.K. Humphries, *HOXB4 overexpression mediates very rapid stem cell regeneration and competitive hematopoietic repopulation.* Exp Hematol, 2001. **29**(9): p. 1125-34.
59. Buske, C., M. Feuring-Buske, C. Abramovich, K. Spiekermann, C.J. Eaves, L. Coulombel, G. Sauvageau, D.E. Hogge, and R.K. Humphries, *Deregulated expression of HOXB4 enhances the primitive growth activity of human hematopoietic cells.* Blood, 2002. **100**(3): p. 862-8.
60. Sauvageau, G., U. Thorsteinsdottir, C.J. Eaves, H.J. Lawrence, C. Largman, P.M. Lansdorp, and R.K. Humphries, *Overexpression of HOXB4 in hematopoietic cells causes the selective expansion of more primitive populations in vitro and in vivo.* Genes Dev, 1995. **9**(14): p. 1753-65.
61. Kroon, E., U. Thorsteinsdottir, N. Mayotte, T. Nakamura, and G. Sauvageau, *NUP98-HOXA9 expression in hemopoietic stem cells induces chronic and acute myeloid leukemias in mice.* EMBO J, 2001. **20**(3): p. 350-61.
62. Thorsteinsdottir, U., E. Kroon, L. Jerome, F. Blasi, and G. Sauvageau, *Defining roles for HOX and MEIS1 genes in induction of acute myeloid leukemia.* Mol Cell Biol, 2001. **21**(1): p. 224-34.
63. Thorsteinsdottir, U., A. Mamo, E. Kroon, L. Jerome, J. Bijl, H.J. Lawrence, K. Humphries, and G. Sauvageau, *Overexpression of the myeloid leukemia-associated Hoxa9 gene in bone marrow cells induces stem cell expansion.* Blood, 2002. **99**(1): p. 121-9.
64. Ayton, P.M. and M.L. Cleary, *Transformation of myeloid progenitors by MLL oncoproteins is dependent on Hoxa7 and Hoxa9.* Genes Dev, 2003. **17**(18): p. 2298-307.
65. Drabkin, H.A., C. Parsy, K. Ferguson, F. Guilhot, L. Lacotte, L. Roy, C. Zeng, A. Baron, S.P. Hunger, M. Varella-Garcia, R. Gemmill, F. Brizard, A. Brizard, and J. Roche,

Quantitative HOX expression in chromosomally defined subsets of acute myelogenous leukemia. Leukemia, 2002. **16**(2): p. 186-95.
66. Milne, T.A., S.D. Briggs, H.W. Brock, M.E. Martin, D. Gibbs, C.D. Allis, and J.L. Hess, *MLL targets SET domain methyltransferase activity to Hox gene promoters.* Mol Cell, 2002. **10**(5): p. 1107-17.
67. Martin, M.E., T.A. Milne, S. Bloyer, K. Galoian, W. Shen, D. Gibbs, H.W. Brock, R. Slany, and J.L. Hess, *Dimerization of MLL fusion proteins immortalizes hematopoietic cells.* Cancer Cell, 2003. **4**(3): p. 197-207.
68. Zeisig, B.B., T. Milne, M.P. Garcia-Cuellar, S. Schreiner, M.E. Martin, U. Fuchs, A. Borkhardt, S.K. Chanda, J. Walker, R. Soden, J.L. Hess, and R.K. Slany, *Hoxa9 and Meis1 are key targets for MLL-ENL-mediated cellular immortalization.* Mol Cell Biol, 2004. **24**(2): p. 617-28.
69. Collins, C.T. and J.L. Hess, *Deregulation of the HOXA9/MEIS1 axis in acute leukemia.* Curr Opin Hematol, 2016. **23**(4): p. 354-61.
70. Argiropoulos, B. and R.K. Humphries, *Hox genes in hematopoiesis and leukemogenesis.* Oncogene, 2007. **26**(47): p. 6766-76.
71. Alharbi, R.A., R. Pettengell, H.S. Pandha, and R. Morgan, *The role of HOX genes in normal hematopoiesis and acute leukemia.* Leukemia, 2013. **27**(5): p. 1000-8.
72. Calvo, K.R., D.B. Sykes, M. Pasillas, and M.P. Kamps, *Hoxa9 immortalizes a granulocyte-macrophage colony-stimulating factor-dependent promyelocyte capable of biphenotypic differentiation to neutrophils or macrophages, independent of enforced meis expression.* Mol Cell Biol, 2000. **20**(9): p. 3274-85.
73. Buske, C., M. Feuring-Buske, J. Antonchuk, P. Rosten, D.E. Hogge, C.J. Eaves, and R.K. Humphries, *Overexpression of HOXA10 perturbs human lymphomyelopoiesis in vitro and in vivo.* Blood, 2001. **97**(8): p. 2286-92.
74. Calvo, K.R., D.B. Sykes, M.P. Pasillas, and M.P. Kamps, *Nup98-HoxA9 immortalizes myeloid progenitors, enforces expression of Hoxa9, Hoxa7 and Meis1, and alters cytokine-specific responses in a manner similar to that induced by retroviral co-expression of Hoxa9 and Meis1.* Oncogene, 2002. **21**(27): p. 4247-56.
75. Pineault, N., C. Buske, M. Feuring-Buske, C. Abramovich, P. Rosten, D.E. Hogge, P.D. Aplan, and R.K. Humphries, *Induction of acute myeloid leukemia in mice by the human leukemia-specific fusion gene NUP98-HOXD13 in concert with Meis1.* Blood, 2003. **101**(11): p. 4529-38.
76. Rawat, V.P., M. Cusan, A. Deshpande, W. Hiddemann, L. Quintanilla-Martinez, R.K. Humphries, S.K. Bohlander, M. Feuring-Buske, and C. Buske, *Ectopic expression of the homeobox gene Cdx2 is the transforming event in a mouse model of t(12;13)(p13;q12) acute myeloid leukemia.* Proc Natl Acad Sci U S A, 2004. **101**(3): p. 817-22.
77. Kroon, E., J. Krosl, U. Thorsteinsdottir, S. Baban, A.M. Buchberg, and G. Sauvageau, *Hoxa9 transforms primary bone marrow cells through specific collaboration with Meis1a but not Pbx1b.* EMBO J, 1998. **17**(13): p. 3714-25.
78. Calvo, K.R., P.S. Knoepfler, D.B. Sykes, M.P. Pasillas, and M.P. Kamps, *Meis1a suppresses differentiation by G-CSF and promotes proliferation by SCF: potential mechanisms of cooperativity with Hoxa9 in myeloid leukemia.* Proc Natl Acad Sci U S A, 2001. **98**(23): p. 13120-5.

79. Moskow, J.J., F. Bullrich, K. Huebner, I.O. Daar, and A.M. Buchberg, *Meis1, a PBX1-related homeobox gene involved in myeloid leukemia in BXH-2 mice.* Mol Cell Biol, 1995. **15**(10): p. 5434-43.
80. Hisa, T., S.E. Spence, R.A. Rachel, M. Fujita, T. Nakamura, J.M. Ward, D.E. Devor-Henneman, Y. Saiki, H. Kutsuna, L. Tessarollo, N.A. Jenkins, and N.G. Copeland, *Hematopoietic, angiogenic and eye defects in Meis1 mutant animals.* EMBO J, 2004. **23**(2): p. 450-9.
81. Kocabas, F., J. Zheng, S. Thet, N.G. Copeland, N.A. Jenkins, R.J. DeBerardinis, C. Zhang, and H.A. Sadek, *Meis1 regulates the metabolic phenotype and oxidant defense of hematopoietic stem cells.* Blood, 2012. **120**(25): p. 4963-72.
82. Unnisa, Z., J.P. Clark, J. Roychoudhury, E. Thomas, L. Tessarollo, N.G. Copeland, N.A. Jenkins, H.L. Grimes, and A.R. Kumar, *Meis1 preserves hematopoietic stem cells in mice by limiting oxidative stress.* Blood, 2012. **120**(25): p. 4973-81.
83. Miller, M.E., P. Rosten, M.E. Lemieux, C. Lai, and R.K. Humphries, *Meis1 Is Required for Adult Mouse Erythropoiesis, Megakaryopoiesis and Hematopoietic Stem Cell Expansion.* PLoS One, 2016. **11**(3): p. e0151584.
84. Wang, G.G., M.P. Pasillas, and M.P. Kamps, *Persistent transactivation by meis1 replaces hox function in myeloid leukemogenesis models: evidence for co-occupancy of meis1-pbx and hox-pbx complexes on promoters of leukemia-associated genes.* Mol Cell Biol, 2006. **26**(10): p. 3902-16.
85. Wang, G.G., M.P. Pasillas, and M.P. Kamps, *Meis1 programs transcription of FLT3 and cancer stem cell character, using a mechanism that requires interaction with Pbx and a novel function of the Meis1 C-terminus.* Blood, 2005. **106**(1): p. 254-64.
86. Wong, P., M. Iwasaki, T.C. Somervaille, C.W. So, and M.L. Cleary, *Meis1 is an essential and rate-limiting regulator of MLL leukemia stem cell potential.* Genes Dev, 2007. **21**(21): p. 2762-74.
87. Aspland, S.E., H.H. Bendall, and C. Murre, *The role of E2A-PBX1 in leukemogenesis.* Oncogene, 2001. **20**(40): p. 5708-17.
88. Shimabe, M., S. Goyama, N. Watanabe-Okochi, A. Yoshimi, M. Ichikawa, Y. Imai, and M. Kurokawa, *Pbx1 is a downstream target of Evi-1 in hematopoietic stem/progenitors and leukemic cells.* Oncogene, 2009. **28**(49): p. 4364-74.
89. Garcia-Cuellar, M.P., J. Steger, E. Fuller, K. Hetzner, and R.K. Slany, *Pbx3 and Meis1 cooperate through multiple mechanisms to support Hox-induced murine leukemia.* Haematologica, 2015. **100**(7): p. 905-13.
90. Lekanne Deprez, R.H., N.A. Groen, N.A. van Biezen, A. Hagemeijer, E. van Drunen, J.W. Koper, C.J. Avezaat, D. Bootsma, and E.C. Zwarthoff, *A t(4;22) in a meningioma points to the localization of a putative tumor-suppressor gene.* Am J Hum Genet, 1991. **48**(4): p. 783-90.
91. Buijs, A., S. Sherr, S. van Baal, S. van Bezouw, D. van der Plas, A. Geurts van Kessel, P. Riegman, R. Lekanne Deprez, E. Zwarthoff, A. Hagemeijer, and et al., *Translocation (12;22) (p13;q11) in myeloproliferative disorders results in fusion of the ETS-like TEL gene on 12p13 to the MN1 gene on 22q11.* Oncogene, 1995. **10**(8): p. 1511-9.
92. Buijs, A., L. van Rompaey, A.C. Molijn, J.N. Davis, A.C. Vertegaal, M.D. Potter, C. Adams, S. van Baal, E.C. Zwarthoff, M.F. Roussel, and G.C. Grosveld, *The MN1-TEL fusion protein, encoded by the translocation (12;22)(p13;q11) in myeloid leukemia, is a transcription factor with transforming activity.* Mol Cell Biol, 2000. **20**(24): p. 9281-93.

93. Grosveld, G.C., *MN1, a novel player in human AML.* Blood Cells Mol Dis, 2007. **39**(3): p. 336-9.
94. Lekanne Deprez, R.H., P.H. Riegman, N.A. Groen, U.L. Warringa, N.A. van Biezen, A.C. Molijn, D. Bootsma, P.J. de Jong, A.G. Menon, N.A. Kley, and et al., *Cloning and characterization of MN1, a gene from chromosome 22q11, which is disrupted by a balanced translocation in a meningioma.* Oncogene, 1995. **10**(8): p. 1521-8.
95. van Wely, K.H., A.C. Molijn, A. Buijs, M.A. Meester-Smoor, A.J. Aarnoudse, A. Hellemons, P. den Besten, G.C. Grosveld, and E.C. Zwarthoff, *The MN1 oncoprotein synergizes with coactivators RAC3 and p300 in RAR-RXR-mediated transcription.* Oncogene, 2003. **22**(5): p. 699-709.
96. Tanaka, M. and W. Herr, *Reconstitution of transcriptional activation domains by reiteration of short peptide segments reveals the modular organization of a glutamine-rich activation domain.* Mol Cell Biol, 1994. **14**(9): p. 6056-67.
97. Xiao, H. and K.T. Jeang, *Glutamine-rich domains activate transcription in yeast Saccharomyces cerevisiae.* J Biol Chem, 1998. **273**(36): p. 22873-6.
98. Gomes, I., W. Xiong, T. Miki, and M.R. Rosner, *A proline- and glutamine-rich protein promotes apoptosis in neuronal cells.* J Neurochem, 1999. **73**(2): p. 612-22.
99. Meester-Smoor, M.A., M.J. Janssen, G.C. Grosveld, A. de Klein, I.W.F. van, H. Douben, and E.C. Zwarthoff, *MN1 affects expression of genes involved in hematopoiesis and can enhance as well as inhibit RAR/RXR-induced gene expression.* Carcinogenesis, 2008. **29**(10): p. 2025-34.
100. Liu, P.P., A. Hajra, C. Wijmenga, and F.S. Collins, *Molecular pathogenesis of the chromosome 16 inversion in the M4Eo subtype of acute myeloid leukemia.* Blood, 1995. **85**(9): p. 2289-302.
101. Ross, M.E., R. Mahfouz, M. Onciu, H.C. Liu, X. Zhou, G. Song, S.A. Shurtleff, S. Pounds, C. Cheng, J. Ma, R.C. Ribeiro, J.E. Rubnitz, K. Girtman, W.K. Williams, S.C. Raimondi, D.C. Liang, L.Y. Shih, C.H. Pui, and J.R. Downing, *Gene expression profiling of pediatric acute myelogenous leukemia.* Blood, 2004. **104**(12): p. 3679-87.
102. Valk, P.J., R.G. Verhaak, M.A. Beijen, C.A. Erpelinck, S. Barjesteh van Waalwijk van Doorn-Khosrovani, J.M. Boer, H.B. Beverloo, M.J. Moorhouse, P.J. van der Spek, B. Lowenberg, and R. Delwel, *Prognostically useful gene-expression profiles in acute myeloid leukemia.* N Engl J Med, 2004. **350**(16): p. 1617-28.
103. Langer, C., G. Marcucci, K.B. Holland, M.D. Radmacher, K. Maharry, P. Paschka, S.P. Whitman, K. Mrozek, C.D. Baldus, R. Vij, B.L. Powell, A.J. Carroll, J.E. Kolitz, M.A. Caligiuri, R.A. Larson, and C.D. Bloomfield, *Prognostic importance of MN1 transcript levels, and biologic insights from MN1-associated gene and microRNA expression signatures in cytogenetically normal acute myeloid leukemia: a cancer and leukemia group B study.* J Clin Oncol, 2009. **27**(19): p. 3198-204.
104. Metzeler, K.H., A. Dufour, T. Benthaus, M. Hummel, M.C. Sauerland, A. Heinecke, W.E. Berdel, T. Buchner, B. Wormann, U. Mansmann, J. Braess, K. Spiekermann, W. Hiddemann, C. Buske, and S.K. Bohlander, *ERG expression is an independent prognostic factor and allows refined risk stratification in cytogenetically normal acute myeloid leukemia: a comprehensive analysis of ERG, MN1, and BAALC transcript levels using oligonucleotide microarrays.* J Clin Oncol, 2009. **27**(30): p. 5031-8.
105. Xiang, L., M. Li, Y. Liu, J. Cen, Z. Chen, X. Zhen, X. Xie, X. Cao, and W. Gu, *The clinical characteristics and prognostic significance of MN1 gene and MN1-associated*

microRNA expression in adult patients with de novo acute myeloid leukemia. Ann Hematol, 2013. **92**(8): p. 1063-9.
106. Carella, C., J. Bonten, S. Sirma, T.A. Kranenburg, S. Terranova, R. Klein-Geltink, S. Shurtleff, J.R. Downing, E.C. Zwarthoff, P.P. Liu, and G.C. Grosveld, *MN1 overexpression is an important step in the development of inv(16) AML.* Leukemia, 2007. **21**(8): p. 1679-90.
107. Schwind, S., G. Marcucci, J. Kohlschmidt, M.D. Radmacher, K. Mrozek, K. Maharry, H. Becker, K.H. Metzeler, S.P. Whitman, Y.Z. Wu, B.L. Powell, M.R. Baer, J.E. Kolitz, A.J. Carroll, R.A. Larson, M.A. Caligiuri, and C.D. Bloomfield, *Low expression of MN1 associates with better treatment response in older patients with de novo cytogenetically normal acute myeloid leukemia.* Blood, 2011. **118**(15): p. 4188-98.
108. Braun, C.J., K. Boztug, A. Paruzynski, M. Witzel, A. Schwarzer, M. Rothe, U. Modlich, R. Beier, G. Gohring, D. Steinemann, R. Fronza, C.R. Ball, R. Haemmerle, S. Naundorf, K. Kuhlcke, M. Rose, C. Fraser, L. Mathias, R. Ferrari, M.R. Abboud, W. Al-Herz, I. Kondratenko, L. Marodi, H. Glimm, B. Schlegelberger, A. Schambach, M.H. Albert, M. Schmidt, C. von Kalle, and C. Klein, *Gene therapy for Wiskott-Aldrich syndrome--long-term efficacy and genotoxicity.* Sci Transl Med, 2014. **6**(227): p. 227ra33.
109. Heuser, M., B. Argiropoulos, F. Kuchenbauer, E. Yung, J. Piper, S. Fung, R.F. Schlenk, K. Dohner, T. Hinrichsen, C. Rudolph, A. Schambach, C. Baum, B. Schlegelberger, H. Dohner, A. Ganser, and R.K. Humphries, *MN1 overexpression induces acute myeloid leukemia in mice and predicts ATRA resistance in patients with AML.* Blood, 2007. **110**(5): p. 1639-47.
110. Schroeder, T., A. Czibere, F. Zohren, M. Aivado, N. Gattermann, U. Germing, and R. Haas, *Meningioma 1 gene is differentially expressed in CD34 positive cells from bone marrow of patients with myelodysplastic syndromes with the highest expression in refractory anemia with excess of blasts and secondary acute myeloid leukemia.* Leuk Lymphoma, 2009. **50**(6): p. 1043-6.
111. Liu, W., Y. Lan, E. Pauws, M.A. Meester-Smoor, P. Stanier, E.C. Zwarthoff, and R. Jiang, *The Mn1 transcription factor acts upstream of Tbx22 and preferentially regulates posterior palate growth in mice.* Development, 2008. **135**(23): p. 3959-68.
112. Meester-Smoor, M.A., M. Vermeij, M.J. van Helmond, A.C. Molijn, K.H. van Wely, A.C. Hekman, C. Vermey-Keers, P.H. Riegman, and E.C. Zwarthoff, *Targeted disruption of the Mn1 oncogene results in severe defects in development of membranous bones of the cranial skeleton.* Mol Cell Biol, 2005. **25**(10): p. 4229-36.
113. Kandilci, A. and G.C. Grosveld, *Reintroduction of CEBPA in MN1-overexpressing hematopoietic cells prevents their hyperproliferation and restores myeloid differentiation.* Blood, 2009. **114**(8): p. 1596-606.
114. Liu, T., D. Jankovic, L. Brault, S. Ehret, F. Baty, V. Stavropoulou, V. Rossi, A. Biondi, and J. Schwaller, *Functional characterization of high levels of meningioma 1 as collaborating oncogene in acute leukemia.* Leukemia, 2010. **24**(3): p. 601-12.
115. Sharma, A., H. Yun, N. Jyotsana, A. Chaturvedi, A. Schwarzer, E. Yung, C.K. Lai, F. Kuchenbauer, B. Argiropoulos, K. Gorlich, A. Ganser, R.K. Humphries, and M. Heuser, *Constitutive IRF8 expression inhibits AML by activation of repressed immune response signaling.* Leukemia, 2015. **29**(1): p. 157-68.

116. Kawagoe, H. and G.C. Grosveld, *Conditional MN1-TEL knock-in mice develop acute myeloid leukemia in conjunction with overexpression of HOXA9.* Blood, 2005. **106**(13): p. 4269-77.
117. Carella, C., J. Bonten, J. Rehg, and G.C. Grosveld, *MN1-TEL, the product of the t(12;22) in human myeloid leukemia, immortalizes murine myeloid cells and causes myeloid malignancy in mice.* Leukemia, 2006. **20**(9): p. 1582-92.
118. Watanabe-Okochi, N., J. Kitaura, R. Ono, H. Harada, Y. Harada, Y. Komeno, H. Nakajima, T. Nosaka, T. Inaba, and T. Kitamura, *AML1 mutations induced MDS and MDS/AML in a mouse BMT model.* Blood, 2008. **111**(8): p. 4297-308.
119. Caudell, D., D.P. Harper, R.L. Novak, R.M. Pierce, C. Slape, L. Wolff, and P.D. Aplan, *Retroviral insertional mutagenesis identifies Zeb2 activation as a novel leukemogenic collaborating event in CALM-AF10 transgenic mice.* Blood, 2010. **115**(6): p. 1194-203.
120. Bergerson, R.J., L.S. Collier, A.L. Sarver, R.A. Been, S. Lugthart, M.D. Diers, J. Zuber, A.R. Rappaport, M.J. Nixon, K.A. Silverstein, D. Fan, A.F. Lamblin, L. Wolff, J.H. Kersey, R. Delwel, S.W. Lowe, M.G. O'Sullivan, S.C. Kogan, D.J. Adams, and D.A. Largaespada, *An insertional mutagenesis screen identifies genes that cooperate with Mll-AF9 in a murine leukemogenesis model.* Blood, 2012. **119**(19): p. 4512-23.
121. Raza-Egilmez, S.Z., S.N. Jani-Sait, M. Grossi, M.J. Higgins, T.B. Shows, and P.D. Aplan, *NUP98-HOXD13 gene fusion in therapy-related acute myelogenous leukemia.* Cancer Res, 1998. **58**(19): p. 4269-73.
122. Slape, C., H. Hartung, Y.W. Lin, J. Bies, L. Wolff, and P.D. Aplan, *Retroviral insertional mutagenesis identifies genes that collaborate with NUP98-HOXD13 during leukemic transformation.* Cancer Res, 2007. **67**(11): p. 5148-55.
123. Lin, Y.W., C. Slape, Z. Zhang, and P.D. Aplan, *NUP98-HOXD13 transgenic mice develop a highly penetrant, severe myelodysplastic syndrome that progresses to acute leukemia.* Blood, 2005. **106**(1): p. 287-95.
124. Pineault, N., C. Abramovich, and R.K. Humphries, *Transplantable cell lines generated with NUP98-Hox fusion genes undergo leukemic progression by Meis1 independent of its binding to DNA.* Leukemia, 2005. **19**(4): p. 636-43.
125. Heuser, M., L.M. Sly, B. Argiropoulos, F. Kuchenbauer, C. Lai, A. Weng, M. Leung, G. Lin, C. Brookes, S. Fung, P.J. Valk, R. Delwel, B. Lowenberg, G. Krystal, and R.K. Humphries, *Modeling the functional heterogeneity of leukemia stem cells: role of STAT5 in leukemia stem cell self-renewal.* Blood, 2009. **114**(19): p. 3983-93.
126. Imren, S., M. Heuser, M. Gasparetto, P.A. Beer, G.L. Norddahl, P. Xiang, L. Chen, T. Berg, G.W. Rhyasen, P. Rosten, G. Park, Y. Moon, A.P. Weng, C.J. Eaves, and R.K. Humphries, *Modeling de novo leukemogenesis from human cord blood with MN1 and NUP98HOXD13.* Blood, 2014. **124**(24): p. 3608-12.
127. Heuser, M., G. Park, Y. Moon, T. Berg, P. Xiang, F. Kuchenbauer, S. Vollett, C. Lai, and R.K. Humphries, *Extrinsic signals determine myeloid-erythroid lineage switch in MN1 leukemia.* Exp Hematol, 2010. **38**(3): p. 174-9.
128. Heuser, M., H. Yun, T. Berg, E. Yung, B. Argiropoulos, F. Kuchenbauer, G. Park, I. Hamwi, L. Palmqvist, C.K. Lai, M. Leung, G. Lin, A. Chaturvedi, B.K. Thakur, M. Iwasaki, M. Bilenky, N. Thiessen, G. Robertson, M. Hirst, D. Kent, N.K. Wilson, B. Gottgens, C. Eaves, M.L. Cleary, M. Marra, A. Ganser, and R.K. Humphries, *Cell of origin in AML: susceptibility to MN1-induced transformation is regulated by the MEIS1/AbdB-like HOX protein complex.* Cancer Cell, 2011. **20**(1): p. 39-52.

129. Riedel, S.S., J.N. Haladyna, M. Bezzant, B. Stevens, D.A. Pollyea, A.U. Sinha, S.A. Armstrong, Q. Wei, R.M. Pollock, S.R. Daigle, C.T. Jordan, P. Ernst, T. Neff, and K.M. Bernt, *MLL1 and DOT1L cooperate with meningioma-1 to induce acute myeloid leukemia.* J Clin Invest, 2016. **126**(4): p. 1438-50.
130. Bernt, K.M., N. Zhu, A.U. Sinha, S. Vempati, J. Faber, A.V. Krivtsov, Z. Feng, N. Punt, A. Daigle, L. Bullinger, R.M. Pollock, V.M. Richon, A.L. Kung, and S.A. Armstrong, *MLL-rearranged leukemia is dependent on aberrant H3K79 methylation by DOT1L.* Cancer Cell, 2011. **20**(1): p. 66-78.
131. Lai, C.K., Y. Moon, F. Kuchenbauer, D.T. Starzcynowski, B. Argiropoulos, E. Yung, P. Beer, A. Schwarzer, A. Sharma, G. Park, M. Leung, G. Lin, S. Vollett, S. Fung, C.J. Eaves, A. Karsan, A.P. Weng, R.K. Humphries, and M. Heuser, *Cell fate decisions in malignant hematopoiesis: leukemia phenotype is determined by distinct functional domains of the MN1 oncogene.* PLoS One, 2014. **9**(11): p. e112671.
132. Gilliland, D.G., *Hematologic malignancies.* Curr Opin Hematol, 2001. **8**(4): p. 189-91.
133. Dick, J.E., *Stem cell concepts renew cancer research.* Blood, 2008. **112**(13): p. 4793-807.
134. Thol, F., F. Damm, A. Ludeking, C. Winschel, K. Wagner, M. Morgan, H. Yun, G. Gohring, B. Schlegelberger, D. Hoelzer, M. Lubbert, L. Kanz, W. Fiedler, H. Kirchner, G. Heil, J. Krauter, A. Ganser, and M. Heuser, *Incidence and prognostic influence of DNMT3A mutations in acute myeloid leukemia.* J Clin Oncol, 2011. **29**(21): p. 2889-96.
135. Neumann, M., S. Heesch, C. Schlee, S. Schwartz, N. Gokbuget, D. Hoelzer, N.P. Konstandin, B. Ksienzyk, S. Vosberg, A. Graf, S. Krebs, H. Blum, T. Raff, M. Bruggemann, W.K. Hofmann, J. Hecht, S.K. Bohlander, P.A. Greif, and C.D. Baldus, *Whole-exome sequencing in adult ETP-ALL reveals a high rate of DNMT3A mutations.* Blood, 2013. **121**(23): p. 4749-52.
136. Vannucchi, A.M., T.L. Lasho, P. Guglielmelli, F. Biamonte, A. Pardanani, A. Pereira, C. Finke, J. Score, N. Gangat, C. Mannarelli, R.P. Ketterling, G. Rotunno, R.A. Knudson, M.C. Susini, R.R. Laborde, A. Spolverini, A. Pancrazzi, L. Pieri, R. Manfredini, E. Tagliafico, R. Zini, A. Jones, K. Zoi, A. Reiter, A. Duncombe, D. Pietra, E. Rumi, F. Cervantes, G. Barosi, M. Cazzola, N.C. Cross, and A. Tefferi, *Mutations and prognosis in primary myelofibrosis.* Leukemia, 2013. **27**(9): p. 1861-9.
137. Horton, S.J., J. Jaques, C. Woolthuis, J. van Dijk, M. Mesuraca, G. Huls, G. Morrone, E. Vellenga, and J.J. Schuringa, *MLL-AF9-mediated immortalization of human hematopoietic cells along different lineages changes during ontogeny.* Leukemia, 2013. **27**(5): p. 1116-26.
138. Wei, J., M. Wunderlich, C. Fox, S. Alvarez, J.C. Cigudosa, J.S. Wilhelm, Y. Zheng, J.A. Cancelas, Y. Gu, M. Jansen, J.F. Dimartino, and J.C. Mulloy, *Microenvironment determines lineage fate in a human model of MLL-AF9 leukemia.* Cancer Cell, 2008. **13**(6): p. 483-95.
139. Raaijmakers, M.H., S. Mukherjee, S. Guo, S. Zhang, T. Kobayashi, J.A. Schoonmaker, B.L. Ebert, F. Al-Shahrour, R.P. Hasserjian, E.O. Scadden, Z. Aung, M. Matza, M. Merkenschlager, C. Lin, J.M. Rommens, and D.T. Scadden, *Bone progenitor dysfunction induces myelodysplasia and secondary leukaemia.* Nature, 2010. **464**(7290): p. 852-7.
140. Morin, R.D., N.A. Johnson, T.M. Severson, A.J. Mungall, J. An, R. Goya, J.E. Paul, M. Boyle, B.W. Woolcock, F. Kuchenbauer, D. Yap, R.K. Humphries, O.L. Griffith, S. Shah, H. Zhu, M. Kimbara, P. Shashkin, J.F. Charlot, M. Tcherpakov, R. Corbett, A. Tam, R. Varhol, D. Smailus, M. Moksa, Y. Zhao, A. Delaney, H. Qian, I. Birol, J.

Schein, R. Moore, R. Holt, D.E. Horsman, J.M. Connors, S. Jones, S. Aparicio, M. Hirst, R.D. Gascoyne, and M.A. Marra, *Somatic mutations altering EZH2 (Tyr641) in follicular and diffuse large B-cell lymphomas of germinal-center origin.* Nat Genet, 2010. **42**(2): p. 181-5.

141. Ernst, T., A.J. Chase, J. Score, C.E. Hidalgo-Curtis, C. Bryant, A.V. Jones, K. Waghorn, K. Zoi, F.M. Ross, A. Reiter, A. Hochhaus, H.G. Drexler, A. Duncombe, F. Cervantes, D. Oscier, J. Boultwood, F.H. Grand, and N.C. Cross, *Inactivating mutations of the histone methyltransferase gene EZH2 in myeloid disorders.* Nat Genet, 2010. **42**(8): p. 722-6.
142. Haferlach, C., W. Kern, S. Schindela, A. Kohlmann, T. Alpermann, S. Schnittger, and T. Haferlach, *Gene expression of BAALC, CDKN1B, ERG, and MN1 adds independent prognostic information to cytogenetics and molecular mutations in adult acute myeloid leukemia.* Genes Chromosomes Cancer, 2012. **51**(3): p. 257-65.
143. Schambach, A., H. Wodrich, M. Hildinger, J. Bohne, H.G. Krausslich, and C. Baum, *Context dependence of different modules for posttranscriptional enhancement of gene expression from retroviral vectors.* Mol Ther, 2000. **2**(5): p. 435-45.
144. Antonchuk, J., G. Sauvageau, and R.K. Humphries, *HOXB4-induced expansion of adult hematopoietic stem cells ex vivo.* Cell, 2002. **109**(1): p. 39-45.
145. Gurevich, R.M., P.D. Aplan, and R.K. Humphries, *NUP98-topoisomerase I acute myeloid leukemia-associated fusion gene has potent leukemogenic activities independent of an engineered catalytic site mutation.* Blood, 2004. **104**(4): p. 1127-36.
146. Starczynowski, D.T., F. Kuchenbauer, B. Argiropoulos, S. Sung, R. Morin, A. Muranyi, M. Hirst, D. Hogge, M. Marra, R.A. Wells, R. Buckstein, W. Lam, R.K. Humphries, and A. Karsan, *Identification of miR-145 and miR-146a as mediators of the 5q- syndrome phenotype.* Nat Med, 2010. **16**(1): p. 49-58.
147. Heuser, M., D.B. Yap, M. Leung, T.R. de Algara, A. Tafech, S. McKinney, J. Dixon, R. Thresher, B. Colledge, M. Carlton, R.K. Humphries, and S.A. Aparicio, *Loss of MLL5 results in pleiotropic hematopoietic defects, reduced neutrophil immune function, and extreme sensitivity to DNA demethylation.* Blood, 2009. **113**(7): p. 1432-43.
148. Bruce, M.A. and M.J. Butte, *Real-time GPU-based 3D Deconvolution.* Opt Express, 2013. **21**(4): p. 4766-73.
149. Vonesch, C. and M. Unser, *A fast thresholded landweber algorithm for wavelet-regularized multidimensional deconvolution.* IEEE Trans Image Process, 2008. **17**(4): p. 539-49.
150. Gentleman, R.C., V.J. Carey, D.M. Bates, B. Bolstad, M. Dettling, S. Dudoit, B. Ellis, L. Gautier, Y. Ge, J. Gentry, K. Hornik, T. Hothorn, W. Huber, S. Iacus, R. Irizarry, F. Leisch, C. Li, M. Maechler, A.J. Rossini, G. Sawitzki, C. Smith, G. Smyth, L. Tierney, J.Y. Yang, and J. Zhang, *Bioconductor: open software development for computational biology and bioinformatics.* Genome Biol, 2004. **5**(10): p. R80.
151. Kauffmann, A., R. Gentleman, and W. Huber, *arrayQualityMetrics--a bioconductor package for quality assessment of microarray data.* Bioinformatics, 2009. **25**(3): p. 415-6.
152. Gautier, L., L. Cope, B.M. Bolstad, and R.A. Irizarry, *affy--analysis of Affymetrix GeneChip data at the probe level.* Bioinformatics, 2004. **20**(3): p. 307-15.

153. Smyth, G.K., J. Michaud, and H.S. Scott, *Use of within-array replicate spots for assessing differential expression in microarray experiments.* Bioinformatics, 2005. **21**(9): p. 2067-75.
154. Subramanian, A., P. Tamayo, V.K. Mootha, S. Mukherjee, B.L. Ebert, M.A. Gillette, A. Paulovich, S.L. Pomeroy, T.R. Golub, E.S. Lander, and J.P. Mesirov, *Gene set enrichment analysis: a knowledge-based approach for interpreting genome-wide expression profiles.* Proc Natl Acad Sci U S A, 2005. **102**(43): p. 15545-50.
155. Jacobs-Helber, S.M. and S.T. Sawyer, *Jun N-terminal kinase promotes proliferation of immature erythroid cells and erythropoietin-dependent cell lines.* Blood, 2004. **104**(3): p. 696-703.
156. Funnell, A.P., L.J. Norton, K.S. Mak, J. Burdach, C.M. Artuz, N.A. Twine, M.R. Wilkins, C.A. Power, T.T. Hung, J. Perdomo, P. Koh, K.S. Bell-Anderson, S.H. Orkin, S.T. Fraser, A.C. Perkins, R.C. Pearson, and M. Crossley, *The CACCC-binding protein KLF3/BKLF represses a subset of KLF1/EKLF target genes and is required for proper erythroid maturation in vivo.* Mol Cell Biol, 2012. **32**(16): p. 3281-92.
157. Kalra, I.S., M.M. Alam, P.K. Choudhary, and B.S. Pace, *Kruppel-like Factor 4 activates HBG gene expression in primary erythroid cells.* Br J Haematol, 2011. **154**(2): p. 248-59.
158. Marini, M.G., L. Porcu, I. Asunis, M.G. Loi, M.S. Ristaldi, S. Porcu, T. Ikuta, A. Cao, and P. Moi, *Regulation of the human HBA genes by KLF4 in erythroid cell lines.* Br J Haematol, 2010. **149**(5): p. 748-58.
159. Meester-Smoor, M.A., A.C. Molijn, Y. Zhao, N.A. Groen, C.A. Groffen, M. Boogaard, D. van Dalsum-Verbiest, G.C. Grosveld, and E.C. Zwarthoff, *The MN1 oncoprotein activates transcription of the IGFBP5 promoter through a CACCC-rich consensus sequence.* J Mol Endocrinol, 2007. **38**(1-2): p. 113-25.
160. Burnett, A.K., R.K. Hills, C. Green, S. Jenkinson, K. Koo, Y. Patel, C. Guy, A. Gilkes, D.W. Milligan, A.H. Goldstone, A.G. Prentice, K. Wheatley, D.C. Linch, and R.E. Gale, *The impact on outcome of the addition of all-trans retinoic acid to intensive chemotherapy in younger patients with nonacute promyelocytic acute myeloid leukemia: overall results and results in genotypic subgroups defined by mutations in NPM1, FLT3, and CEBPA.* Blood, 2010. **115**(5): p. 948-56.
161. Kandilci, A., J. Surtel, L. Janke, G. Neale, S. Terranova, and G.C. Grosveld, *Mapping of MN1 sequences necessary for myeloid transformation.* PLoS One, 2013. **8**(4): p. e61706.
162. Neumann, M., S. Heesch, N. Gokbuget, S. Schwartz, C. Schlee, O. Benlasfer, N. Farhadi-Sartangi, J. Thibaut, T. Burmeister, D. Hoelzer, W.K. Hofmann, E. Thiel, and C.D. Baldus, *Clinical and molecular characterization of early T-cell precursor leukemia: a high-risk subgroup in adult T-ALL with a high frequency of FLT3 mutations.* Blood Cancer J, 2012. **2**(1): p. e55.
163. Fellmann, C., T. Hoffmann, V. Sridhar, B. Hopfgartner, M. Muhar, M. Roth, D.Y. Lai, I.A. Barbosa, J.S. Kwon, Y. Guan, N. Sinha, and J. Zuber, *An optimized microRNA backbone for effective single-copy RNAi.* Cell Rep, 2013. **5**(6): p. 1704-13.
164. Maetzig, T., M.H. Brugman, S. Bartels, N. Heinz, O.S. Kustikova, U. Modlich, Z. Li, M. Galla, B. Schiedlmeier, A. Schambach, and C. Baum, *Polyclonal fluctuation of lentiviral vector-transduced and expanded murine hematopoietic stem cells.* Blood, 2011. **117**(11): p. 3053-64.

165. Hulsen, T., J. de Vlieg, and W. Alkema, *BioVenn - a web application for the comparison and visualization of biological lists using area-proportional Venn diagrams.* BMC Genomics, 2008. **9**: p. 488.
166. Patro, R., S.M. Mount, and C. Kingsford, *Sailfish enables alignment-free isoform quantification from RNA-seq reads using lightweight algorithms.* Nat Biotechnol, 2014. **32**(5): p. 462-4.
167. Koboldt, D.C., Q. Zhang, D.E. Larson, D. Shen, M.D. McLellan, L. Lin, C.A. Miller, E.R. Mardis, L. Ding, and R.K. Wilson, *VarScan 2: somatic mutation and copy number alteration discovery in cancer by exome sequencing.* Genome Res, 2012. **22**(3): p. 568-76.
168. Benjamini, Y. and Y. Hochberg, *Controlling the False Discovery Rate: A Practical and Powerful Approach to Multiple Testing.* Journal of the Royal Statistical Society. Series B (Methodological), 1995. **57**(1): p. 289-300.
169. Bagger, F.O., D. Sasivarevic, S.H. Sohi, L.G. Laursen, S. Pundhir, C.K. Sonderby, O. Winther, N. Rapin, and B.T. Porse, *BloodSpot: a database of gene expression profiles and transcriptional programs for healthy and malignant haematopoiesis.* Nucleic Acids Res, 2016. **44**(D1): p. D917-24.
170. Team, R.C. *R: A language and environment for statistical computing. R Foundation for Statistical Computing*. 2016 [cited 2016 December 19]; Available from: https://www.R-project.org/.
171. Fuller, J.F., J. McAdara, Y. Yaron, M. Sakaguchi, J.K. Fraser, and J.C. Gasson, *Characterization of HOX gene expression during myelopoiesis: role of HOX A5 in lineage commitment and maturation.* Blood, 1999. **93**(10): p. 3391-400.
172. So, C.W., H. Karsunky, P. Wong, I.L. Weissman, and M.L. Cleary, *Leukemic transformation of hematopoietic progenitors by MLL-GAS7 in the absence of Hoxa7 or Hoxa9.* Blood, 2004. **103**(8): p. 3192-9.
173. Afonja, O., J.E. Smith, Jr., D.M. Cheng, A.S. Goldenberg, E. Amorosi, T. Shimamoto, S. Nakamura, K. Ohyashiki, J. Ohyashiki, K. Toyama, and K. Takeshita, *MEIS1 and HOXA7 genes in human acute myeloid leukemia.* Leuk Res, 2000. **24**(10): p. 849-55.
174. Soulier, J., E. Clappier, J.M. Cayuela, A. Regnault, M. Garcia-Peydro, H. Dombret, A. Baruchel, M.L. Toribio, and F. Sigaux, *HOXA genes are included in genetic and biologic networks defining human acute T-cell leukemia (T-ALL).* Blood, 2005. **106**(1): p. 274-86.
175. Chowdhury, A.H., J.R. Ramroop, G. Upadhyay, A. Sengupta, A. Andrzejczyk, and S. Saleque, *Differential transcriptional regulation of meis1 by Gfi1b and its co-factors LSD1 and CoREST.* PLoS One, 2013. **8**(1): p. e53666.
176. Argiropoulos, B., L. Palmqvist, E. Yung, F. Kuchenbauer, M. Heuser, L.M. Sly, A. Wan, G. Krystal, and R.K. Humphries, *Linkage of Meis1 leukemogenic activity to multiple downstream effectors including Trib2 and Ccl3.* Exp Hematol, 2008. **36**(7): p. 845-59.
177. Moroy, T., L. Vassen, B. Wilkes, and C. Khandanpour, *From cytopenia to leukemia: the role of Gfi1 and Gfi1b in blood formation.* Blood, 2015. **126**(24): p. 2561-9.
178. Anguita, E., R. Gupta, V. Olariu, P.J. Valk, C. Peterson, R. Delwel, and T. Enver, *A somatic mutation of GFI1B identified in leukemia alters cell fate via a SPI1 (PU.1) centered genetic regulatory network.* Dev Biol, 2016. **411**(2): p. 277-86.
179. Kato, T., M. Sakata-Yanagimoto, H. Nishikii, M. Ueno, Y. Miyake, Y. Yokoyama, Y. Asabe, Y. Kamada, H. Muto, N. Obara, K. Suzukawa, Y. Hasegawa, I. Kitabayashi, K.

Uchida, A. Hirao, H. Yagita, R. Kageyama, and S. Chiba, *Hes1 suppresses acute myeloid leukemia development through FLT3 repression.* Leukemia, 2015. **29**(3): p. 576-85.
180. Pabst, C., A. Bergeron, V.P. Lavallee, J. Yeh, P. Gendron, G.L. Norddahl, J. Krosl, I. Boivin, E. Deneault, J. Simard, S. Imren, G. Boucher, K. Eppert, T. Herold, S.K. Bohlander, K. Humphries, S. Lemieux, J. Hebert, G. Sauvageau, and F. Barabe, *GPR56 identifies primary human acute myeloid leukemia cells with high repopulating potential in vivo.* Blood, 2016. **127**(16): p. 2018-27.
181. Zha, Y., Y. Xia, J. Ding, J.H. Choi, L. Yang, Z. Dong, C. Yan, S. Huang, and H.F. Ding, *MEIS2 is essential for neuroblastoma cell survival and proliferation by transcriptional control of M-phase progression.* Cell Death Dis, 2014. **5**: p. e1417.
182. Bjerke, G.A., C. Hyman-Walsh, and D. Wotton, *Cooperative transcriptional activation by Klf4, Meis2, and Pbx1.* Mol Cell Biol, 2011. **31**(18): p. 3723-33.
183. Shojaei, F., J. Trowbridge, L. Gallacher, L. Yuefei, D. Goodale, F. Karanu, K. Levac, and M. Bhatia, *Hierarchical and ontogenic positions serve to define the molecular basis of human hematopoietic stem cell behavior.* Dev Cell, 2005. **8**(5): p. 651-63.
184. Inaba, T., W.M. Roberts, L.H. Shapiro, K.W. Jolly, S.C. Raimondi, S.D. Smith, and A.T. Look, *Fusion of the leucine zipper gene HLF to the E2A gene in human acute B-lineage leukemia.* Science, 1992. **257**(5069): p. 531-4.
185. Palmqvist, L., N. Pineault, C. Wasslavik, and R.K. Humphries, *Candidate genes for expansion and transformation of hematopoietic stem cells by NUP98-HOX fusion genes.* PLoS One, 2007. **2**(8): p. e768.
186. Heine, P., E. Dohle, K. Bumsted-O'Brien, D. Engelkamp, and D. Schulte, *Evidence for an evolutionary conserved role of homothorax/Meis1/2 during vertebrate retina development.* Development, 2008. **135**(5): p. 805-11.
187. Louw, J.J., A. Corveleyn, Y. Jia, G. Hens, M. Gewillig, and K. Devriendt, *MEIS2 involvement in cardiac development, cleft palate, and intellectual disability.* Am J Med Genet A, 2015. **167A**(5): p. 1142-6.
188. Wu, Y.H., H. Zhao, L.P. Zhou, C.X. Zhao, Y.F. Wu, L.X. Zhen, J. Li, D.X. Ge, L. Xu, L. Lin, Y. Liu, D.D. Liang, and Y.H. Chen, *miR-134 Modulates the Proliferation of Human Cardiomyocyte Progenitor Cells by Targeting Meis2.* Int J Mol Sci, 2015. **16**(10): p. 25199-213.
189. Rosales-Avina, J.A., J. Torres-Flores, A. Aguilar-Lemarroy, C. Gurrola-Diaz, G. Hernandez-Flores, P.C. Ortiz-Lazareno, J.M. Lerma-Diaz, R. de Celis, O. Gonzalez-Ramella, E. Barrera-Chaires, A. Bravo-Cuellar, and L.F. Jave-Suarez, *MEIS1, PREP1, and PBX4 are differentially expressed in acute lymphoblastic leukemia: association of MEIS1 expression with higher proliferation and chemotherapy resistance.* J Exp Clin Cancer Res, 2011. **30**: p. 112.
190. Vegi, N.M., J. Klappacher, F. Oswald, M.A. Mulaw, A. Mandoli, V.N. Thiel, S. Bamezai, K. Feder, J.H. Martens, V.P. Rawat, T. Mandal, L. Quintanilla-Martinez, K. Spiekermann, W. Hiddemann, K. Dohner, H. Dohner, H.G. Stunnenberg, M. Feuring-Buske, and C. Buske, *MEIS2 Is an Oncogenic Partner in AML1-ETO-Positive AML.* Cell Rep, 2016. **16**(2): p. 498-507.
191. Machon, O., J. Masek, O. Machonova, S. Krauss, and Z. Kozmik, *Meis2 is essential for cranial and cardiac neural crest development.* BMC Dev Biol, 2015. **15**: p. 40.

192. Zhang, X., A. Friedman, S. Heaney, P. Purcell, and R.L. Maas, *Meis homeoproteins directly regulate Pax6 during vertebrate lens morphogenesis.* Genes Dev, 2002. **16**(16): p. 2097-107.
193. Conte, I., S. Carrella, R. Avellino, M. Karali, R. Marco-Ferreres, P. Bovolenta, and S. Banfi, *miR-204 is required for lens and retinal development via Meis2 targeting.* Proc Natl Acad Sci U S A, 2010. **107**(35): p. 15491-6.
194. Paylakhi, S.H., H. Moazzeni, S. Yazdani, P. Rassouli, E. Arefian, E. Jaberi, E.H. Arash, A.S. Gilani, J.B. Fan, C. April, S. Amin, F. Suri, and E. Elahi, *FOXC1 in human trabecular meshwork cells is involved in regulatory pathway that includes miR-204, MEIS2, and ITGbeta1.* Exp Eye Res, 2013. **111**: p. 112-21.
195. Mason, M.K., D. Hockman, L. Curry, T.J. Cunningham, G. Duester, M. Logan, D.S. Jacobs, and N. Illing, *Retinoic acid-independent expression of Meis2 during autopod patterning in the developing bat and mouse limb.* Evodevo, 2015. **6**: p. 6.
196. Capdevila, J., T. Tsukui, C. Rodriquez Esteban, V. Zappavigna, and J.C. Izpisua Belmonte, *Control of vertebrate limb outgrowth by the proximal factor Meis2 and distal antagonism of BMPs by Gremlin.* Mol Cell, 1999. **4**(5): p. 839-49.
197. Fujino, T., Y. Yamazaki, D.A. Largaespada, N.A. Jenkins, N.G. Copeland, K. Hirokawa, and T. Nakamura, *Inhibition of myeloid differentiation by Hoxa9, Hoxb8, and Meis homeobox genes.* Exp Hematol, 2001. **29**(7): p. 856-63.
198. Oulad-Abdelghani, M., C. Chazaud, P. Bouillet, V. Sapin, P. Chambon, and P. Dolle, *Meis2, a novel mouse Pbx-related homeobox gene induced by retinoic acid during differentiation of P19 embryonal carcinoma cells.* Dev Dyn, 1997. **210**(2): p. 173-83.
199. Vitobello, A., E. Ferretti, X. Lampe, N. Vilain, S. Ducret, M. Ori, J.F. Spetz, L. Selleri, and F.M. Rijli, *Hox and Pbx factors control retinoic acid synthesis during hindbrain segmentation.* Dev Cell, 2011. **20**(4): p. 469-82.
200. Eklund, E., *The role of Hox proteins in leukemogenesis: insights into key regulatory events in hematopoiesis.* Crit Rev Oncog, 2011. **16**(1-2): p. 65-76.
201. Collins, C.T. and J.L. Hess, *Role of HOXA9 in leukemia: dysregulation, cofactors and essential targets.* Oncogene, 2016. **35**(9): p. 1090-8.
202. Mann, R.S., K.M. Lelli, and R. Joshi, *Hox specificity unique roles for cofactors and collaborators.* Curr Top Dev Biol, 2009. **88**: p. 63-101.
203. Choe, S.K., F. Ladam, and C.G. Sagerstrom, *TALE factors poise promoters for activation by Hox proteins.* Dev Cell, 2014. **28**(2): p. 203-11.
204. Wang, Z., M. Iwasaki, F. Ficara, C. Lin, C. Matheny, S.H. Wong, K.S. Smith, and M.L. Cleary, *GSK-3 promotes conditional association of CREB and its coactivators with MEIS1 to facilitate HOX-mediated transcription and oncogenesis.* Cancer Cell, 2010. **17**(6): p. 597-608.
205. Merabet, S. and A. Dard, *Tracking context-specific transcription factors regulating hox activity.* Dev Dyn, 2014. **243**(1): p. 16-23.
206. Kharas, M.G., C.J. Lengner, F. Al-Shahrour, L. Bullinger, B. Ball, S. Zaidi, K. Morgan, W. Tam, M. Paktinat, R. Okabe, M. Gozo, W. Einhorn, S.W. Lane, C. Scholl, S. Frohling, M. Fleming, B.L. Ebert, D.G. Gilliland, R. Jaenisch, and G.Q. Daley, *Musashi-2 regulates normal hematopoiesis and promotes aggressive myeloid leukemia.* Nat Med, 2010. **16**(8): p. 903-8.

207. Byers, R.J., T. Currie, E. Tholouli, S.J. Rodig, and J.L. Kutok, *MSI2 protein expression predicts unfavorable outcome in acute myeloid leukemia.* Blood, 2011. **118**(10): p. 2857-67.
208. Nestorowa, S., F.K. Hamey, B. Pijuan Sala, E. Diamanti, M. Shepherd, E. Laurenti, N.K. Wilson, D.G. Kent, and B. Gottgens, *A single-cell resolution map of mouse hematopoietic stem and progenitor cell differentiation.* Blood, 2016. **128**(8): p. e20-31.
209. Moignard, V., S. Woodhouse, L. Haghverdi, A.J. Lilly, Y. Tanaka, A.C. Wilkinson, F. Buettner, I.C. Macaulay, W. Jawaid, E. Diamanti, S. Nishikawa, N. Piterman, V. Kouskoff, F.J. Theis, J. Fisher, and B. Gottgens, *Decoding the regulatory network of early blood development from single-cell gene expression measurements.* Nat Biotechnol, 2015. **33**(3): p. 269-76.
210. Rotem, A., O. Ram, N. Shoresh, R.A. Sperling, A. Goren, D.A. Weitz, and B.E. Bernstein, *Single-cell ChIP-seq reveals cell subpopulations defined by chromatin state.* Nat Biotechnol, 2015. **33**(11): p. 1165-72.
211. Lawrence, H.J., S. Rozenfeld, C. Cruz, K. Matsukuma, A. Kwong, L. Komuves, A.M. Buchberg, and C. Largman, *Frequent co-expression of the HOXA9 and MEIS1 homeobox genes in human myeloid leukemias.* Leukemia, 1999. **13**(12): p. 1993-9.